UNIVERSITAT DE BARCELONA

Some insights on theoretical reaction dynamics: Use of absorbing potentials and exact three-dimensional calculations.

Fermín Huarte Larrañaga

Some insights on theoretical reaction dynamics: use of absorbing potentials and exact three–dimensional calculations

Fermín Huarte Larrañaga
Departament de Química Física
Universitat de Barcelona

UNIVERSITAT DE BARCELONA

Some insights on theoretical reaction dynamics: use of absorbing potentials and exact three–dimensional calculations

Fermín Huarte Larrañaga
Departament de Química Física
Universitat de Barcelona

UNIVERSITAT DE BARCELONA

XAVIER GIMÉNEZ I FONT, Professor titular del Departament de Química Física de la Universitat de Barcelona, com a director

CERTIFICA: que el treball que es presenta, titulat *Some insights on theoretical reaction dynamics: use of absorbing potentials and exact three-dimensional calculations*, ha estat realitzat sota la seva direcció pel Llicenciat Fermín Huarte Larrañaga i constitueix la memòria de la seva Tesi Doctoral.

Xavier Giménez i Font

JOSEP MARIA LUCAS I ALCORTA, Professor titular del Departament de Química Física de la Universitat de Barcelona,

CERTIFICA: que ha estat tutor responsable dels estudis de doctorat del Llicenciat Fermín Huarte Larrañaga, dins el programa *Química Fonamental: Química Física* impartit pel mencionat departament i desenvolupat durant els cursos acadèmics 1995-1996 i 1996-1997.

Josep Maria Lucas Alcorta

CARLES MÜLLER JEVENOIS, Catedràtic i Director del Departament de Química Física de la Universitat de Barcelona,

CERTIFICA: que el treball que es presenta, titulat *Some insights on theoretical reaction dynamics: use of absorbing potentials and exact three-dimensional calculations*, ha estat realitzat sota la direcció del Dr. Xavier Giménez i Font i constitueix la memòria de la Tesi Doctoral del Llicenciat Fermín Huarte Larrañaga, autoritzant la seva presentació.
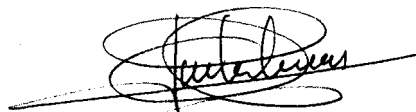
Carles Müller Jevenois

Barcelona, Maig de 1999

...Y tú para que quieres un barco, si puede saberse, fue lo que el rey preguntó cuando finalmente se dio por instalado con sufrible comodidad en la silla de la mujer de la limpieza, Para buscar la isla desconocida respondió el hombre, Qué isla desconocida, preguntó el rey, disimulando la risa, como si tuviese enfrente a un loco de atar, de los que tienen manías de navegaciones, a quien no sería bueno contrariar así de entrada, La isla desconocida, repitió el hombre, Hombre, ya no hay islas desconocidas, Quién te ha dicho rey, que ya no hay islas desconocidas, Están todas en los mapas, En los mapas están sólo las islas conocidas, Y qué isla desconocida es la que tú buscas, Si te lo pudiese decir, entonces no sería desconocida, A quién has oído hablar de ella, preguntó el rey ahora más serio, A nadie, En ese caso, por qué te empeñas en decir que ella existe, Simplemente porqué es imposible que no exista una isla desconocida, Y has venido aquí para pedirme un barco, Y tú quén eres para que yo te lo dé, Y tú quién eres para no darmelo, Soy el rey de este reino y los barcos me pertenecen todos, Más les perteneces tú a ellos que ellos a ti, Qué quieres decir, preguntó el rey inquieto, Que tú sin ellos nada eres, y que ellos sin ti, pueden navegar siempre. ...

José Saramago
El cuento de la isla desconocida.

- Ara que el tren s'ha aturat per un instants, em permet contemplar el panorama d'aquest viatge que he realitzat en els darrers quatre anys. El paissatge es mostra ample i difícil de descriure, en quatre anys passen moltes coses i persones, totes formen part del mosaic d'impressions, sensacions, experiències que em reflexa el mirall de l'experiència viscuda. Els miralls són sempre incòmodes perquè reflexen el que veuen, no coneixen la cortesia. El reflex del meu mirall, però, no és cruel, és més aviat agradable.

Si resumir quatre anys de feina ja em resulta una tasca feixuga, encara ho és més, agrair a tothom qui m'ha donat un cop de mà en aquest temps.

- El director del treball, en Xavi, a qui agraeixo la seva orientació mai autoritària i sempre respectuosa amb la meva opinió. A més, senta molt bé tenir un *dire* que de vegades et parli de coses alienes a la feina!

- L'Antonio, Margarita i Josep Maria, que en diferents moments i circumstàncies menys agradables han mirat de fer-me el major costat possible. En Jaume, que em va concedir dret a taça pròpia tot i no ser un habitual de l'hora del tè. L'Albert que, sense saber-ho ell, em va fer riure en algun que altre moment no tan alegre.

- Els meus companys del *Tugurio*. Les he passades de molt bones amb vosaltres i espero poder continuar essent un dels *fixes* al cafè de les 10. Entre vosaltres hi ha gent molt especial que portaré sempre molt aprop.

- A Perugia ho imparato tantissime cose (non soltanto scientifiche) "*dalle chiachere*" con tutti i "*freghi*" che ho conosciuto lí. Mi siete tutti tanto cari!

- Fora de la Facultat he passat moments d'allò més bons sobre tot amb els amics en majúscules dels partidets i les *farrikis* del dissabte, *sou mogollón d'entranyables*!

- La Rosanne, ningú coneix millor que ella els dies més amargs d'aquest treball.

- Els amics i companys són certament molt importants però l'origen de tot ha estat la família. Estic fermament convençut que els meus pares són els principals responsables d'aquest treball. Gracias Aitatxos!

Resum

La present memòria vol reflectir la tasca realitzada dins del projecte de recerca destinat a l'obtenció del Grau de Doctor en Química. El treball s'ha realitzat en el *Grup de Cinètica i Dinàmica de Reaccions elementals* de la Universitat de Barcelona. Per raons de conveniència, tot creient que així se'n facilita la seva difusió, l'autor d'aquest treball ha decidit redactar el mateix en llengua anglesa. Tanmateix, d'acord amb la normativa vigent per a la presentació de Tesis Doctorals a la nostra Universitat, i mostrant també una voluntat de difusió del nostre treball, de la manera més entenedora possible, dins la comunitat científica catalana, he redactat aquesta part del treball en català.

El treball es presenta en forma de compendi d'articles que descriuen el gruix de la feina realitzada. No obstant això, s'ha inclòs una minuciosa introducció dels diversos fonaments teòrics que hem estudiat i assimilat prèviament a la realització d'aquests treball. Hem considerat oportuna la presentació del compendi d'articles perquè crèiem que així es pot comprendre millor la unitat global de la nostra feina que ha estat, més que l'estudi dinàmic d'un sistema o d'una família de reaccions en concret, utilitzant metodologies ja existents, un estudi i aprofondiment en algunes de les metodologies que s'empren usualment a l'estudi de la dinàmica de reaccions, utilitzant com a exemples d'aplicació sistemes d'interès pràctic. Així, hem utilitzat tant tècniques mecanoquàntiques exactes i aproximades, com tècniques clàssiques, tot i que aquestes darreres només de manera col.lateral i per això no n'expliquem els seus fonaments. D'aquesta manera, els treballs es presenten en els darrers tres capítols de la memòria, com a tres unitats corresponents a la utilització de metodologia quàntica aproximada IOSA (capítol 7, articles 1, 2 i 3), al desenvolupament i aplicació d'un nou mètode aproximat (capítol 8, articles 4,5,6 i 7) i a l'estudi mitjançant metodologia mecanoquàntica exacta (capítol 9, article 8).

Considerem que les principals innovacions que aporta el nostre treball són les següents: a) el fet de detectar fenòmens de naturalesa quàntica en un sistema on es bescanvia un àtom pesat, com ara l'efecte túnel i les particularitats que mostra la distribució vibracional dels productes en la reacció $Mg + FH \rightarrow MgF + H$, b) el desenvolupament d'un nou mètode de tractament mecanoquàntic aproximat, basat en la implementació de potencials absorbents en la resolució propagativa del problema de dispersió reactiva, i c) l'estudi mecanoquàntic exacte del sistema $Ne + H_2^+ \rightarrow NeH^+ + H$, mitjançant el mètode hiperesfèric. La importància de la segona aportació recau bàsicament en l'eficiència i fiabilitat que ha mostrat el nou mètode, cosa que ha motivat crítiques molt positives per a alguns dels nostres treballs. Pel que fa a la tercera, la seva importància recau no només en el sistema reactiu en si, habitualment emprat en la física de plasmes, sinó també en el relativament escàs nombre de càlculs exactes que s'han realitzat fins el moment.

Introducció

Quan hom estudia una reacció química qualsevulga, habitualment té com a objectiu l'obtenció de dades quantitatives com ara la calor de reacció, el rendiment o, de manera més general, la influència de les diverses variables sobre el sistema. Aquests objectius s'assoleixen mitjançant dues disciplines de la Química: la termodinàmica i la cinètica. Per a qualsevol químic és ben conegut que la termodinàmica, tot i que és una eina bàsica a l'hora de conèixer la espontaneïtat d'una reacció, resulta incapaç de predir la velocitat amb que es donarà. Per tant, la informació proporcionada per la cinètica química resulta essencial per conèixer completament qualsevol procés químic.

Tanmateix, tant la cinètica com la termodinàmica, com a ciències basades en l'experimentació macroscòpica, resulten incapaces de proveir-nos d'una explicació del procés químic basada en primers principis i, per tant, la seva capacitat predictiva es veu restringida a correlacions empíriques. Resulta evident la necessitat d'una disciplina que estudiï els mecanismes íntims de la reacció química en el seu nivell més elemental. Aquesta és la tasca de la dinàmica de reaccions.

La dinàmica de reaccions és doncs una subdisciplina de la cinètica química i el seu objectiu és l'estudi dels mecanismes moleculars a través dels quals tenen lloc els processos químics. Per tant, es tracta d'una ciència que estudia les col.lisions intermoleculars i els moviments intramoleculars. D'ençà els seus inicis, al començament dels anys trenta, en els treballs de M. Polanyi, E. Wigner, H. Eyring, E. Pelzer i altres, l'estudi dels processos químics elementals ha esdevingut un camp d'importància creixent.

Des dels inicis de la dinàmica química fins avui en dia, s'han dut a terme nombrosos estudis de reacccions elementals en fase gasosa, importants tant per si mateixes com per les seves aplicacions posteriors. Aviat es va reconèixer que els experiments de feixos moleculars oferien els mitjans més directes per estudiar la dinàmica de les reaccions químiques elementals, permetent conèixer les principals característiques de la distribució de velocitat de productes, així com una sèrie de propietats inaccessibles a través dels mètodes cinètics tradicionals. Tot i això, com en un principi els experiments de dispersió químics eren escassos, degut a la dificultat que representava la seva realització, la interpretació dels resultats va haver d'esperar un ulterior desenvolupament i refinament tant dels aspectes experimentals com dels teòrics. Evidentment, a un mètode que depenia tan fortament de la tecnologia li calia un període d'evolució. Gràcies a la millora en les tecnologies de detecció de senyals, tècniques d'alt buit i l'us de computadores digitals en totes les fases de realització de l'experiment, així com al desenvolupament de nous mètodes teòrics per part del mon acadèmic, ha estat possible l'obtenció de resultats prou extensos com per poder establir generalitzacions en el comportament químic.

L'estudi d'una col.lisió simple és un problema físic especialment adaptat a les condicions d'un estudi teòric, degut a l'absència de forces perturbatives ex-

ternes al sistema. Això provoca que el nivell d'exigència que hom ha de tenir en la comparació de la teoria amb l'experiment sigui molt elevat. Els resultats experimentals han de valorar la capacitat predictiva dels models teòrics i a la vegada els resultats obtinguts per la teoria poden servir de guia per a la cerca de determinats fenòmens experimentals.

L'estudi teòric dels processos de col.lisió elemental, bé siguin reactius o no, es poden realitzar emprant diversos mètodes, la majoria dels quals tenen les seves arrels en el camp de la física atòmica o nuclear. Aquests mètodes es poden classificar genèricament en tres categories: mètodes clàssics, quàntics i semiclàssics. Aquesta classificació correspon a la manera en què els diferents mètodes resolen el moviment dels nuclis sotmesos a les forces exercides pel nuvol electrònic i la repulsió internuclear.

En els mètodes anomenats clàssics, s'assumeix que l'evolució dinàmica dels nuclis atòmics té lloc d'acord amb les lleis clàssiques del moviment, sobre una superfície d'energia potencial (PES) prèviament calculada, i ens permet treballar amb trajectòries associades a la reacció elemental. Habitualment es procedeix de manera que es calcula, resolent l'equació de Hamilton, un nombre suficient de trajectòries de manera que es reprodueixin les condicions inicials de l'experiment. Posteriorment es duu a terme un tractament estadístic sobre les trajectòries per tal d'obtenir els observables. Normalment, les equacions del moviment es resolen de manera que les condicions inicials siguin compatibles amb la descripció quàntica dels estats moleculars, en el que s'anomena l'aproximació *Quasiclàssica*. Tot i que els resultats obtinguts mitjançant la metodologia clàssica són generalment bons per a les quantitats promitjades, no es poden obviar les limitacions de la descripció clàssica de la natura i per tant hom no hauria d'esperar poder descriure correctament els fenòmens purament quàntics amb aquests mètodes.

Si el comportament microscòpic de la matèria només es pot reproduir rigorosament utilitzant la descripció de la natura que ens proporciona la mecànica quàntica, ha de ser aquesta la metodologia més adient per estudiar una col.lisió quan o bé es desitja una descripció molt acurada o bé els efectes quàntics són molt importants. En els mètodes *quàntics*, és l'equació de Schrödinger corresponent al moviment nuclear la que es resol sobre una SEP prèviament determinada. Malhauradament, la solució exacta de les equacions resultants només és possible des d'una perspectiva numèrica. El tractament mecano-quàntic de la reactivitat presenta bàsicament dues dificultats principals:

- les dificultats que provenen de la mateixa natura del procés reactiu, que no és sinó una reorganització de les partícules components del sistema. Tal procés de reordenament requereix una elecció molt acurada de les coordenades a utilitzar com a variables en la funció d'ona nuclear del sistema. En la pràctica, aquest problema es resol tractant de trobar un sistema de coordenades que sigui capaç de descriure tots els ordenaments possibles així com la regió de forta interacció.

- les dificultats que concerneixen essencialment els aspectes computacionals. El fet que una reacció química pugui involucrar un elevat nombre d'estats vibro-rotacionals tant de reactius com de productes fa que les dimensions del sistema d'equacions que s'ha de resoldre en la dinàmica s'incrementi fins el punt de impossibilitar el seu tractament exacte. Aquest fet ha motivat la relativa proliferació de models aproximats que redueixen la dimensionalitat del sistema d'equacions. Els recents avenços tecnològics, així com el desenvolupament de tècniques algebràiques i analítiques més recents han permès en els darrers deu anys la realització dels primers càlculs mecanoquàntics exactes sobre sistemes reactius.

La metodologia *semiclàssica* se situa entremig de les dues anteriors. Generalment utilitza una barreja d'ambdues, tractant clàssicament alguns graus de llibertat i altres quànticament. D'aquesta manera permet l'estudi de fenòmens quàntics i a la vegada permet relacionar-los amb imatges clàssiques.

Resultats i Conclusions

Estudis R-IOSA

Com ja hem dit, el sistema d'equacions diferencials acoblades a resoldre en el plantejament mecanoquàntic exacte és ben poques vegades resoluble de manera exacta, degut a l'elevat nombre d'estats assolibles pel sistema quan es treballa a les energies típiques de col.lisió. Així, per exemple, per al sistema $F + H_2$, calen un total de 150 estats rovibracionals i unes 30 ones parcials per obtenir càlculs, completament convergits, de la secció eficaç integral a cada energia. Això implica, com es veurà més endavant, resoldre per a cada valor del moment angular total i de l'energia un sistema de 150 equacions diferencials acoblades; no cal dir que per als sistemes que en aquest treball hem estudiat ($Mg + FH$ i $B + OH$), en ser molt més pesants, el nombre d'estats rovibracionals necessaris per convergir augmentaria considerablement.

Conseqüentment, una gran part dels esforços que s'han dut a terme en el camp de la dinàmica química han estat amb l'objectiu de desenvolupar simplificacions de les equacions exactes basades en criteris físics raonables. La primera aproximació consisteix en l'expansió de la funció d'ona en un conjunt de funcions de base corresponents a l'espectre discret de la molècula diatòmica, que generalment s'anomena *aproximació close coupling*. En un nivell inferior a aquesta aproximació es troba l'anomenada aproximació centrífuga sobtada (CS) que suposa que la col.lisió ve dominada pel potencial electrostàtic i oer la rotació molecular. Se suposa que, essencialment, el terme d'energia cinètica és prou gran com per a que el valor exacte del terme centrífug no sigui important. Segons aquesta aproximació els estats rotacionals encara es consideren de manera exacta i s'elimina

l'acoblament entre els diferents valors del moment angular orbital. Per a major detall, veure capítol 6.

En el següent nivell de teories aproximades trobem dues maneres de fer no només diferents sinó oposades. Ambdues aproximen el moviment rotacional del sistema, una de les aproximacions suposa que els períodes rotacionals són molt més grans que els vibracionals i utilitza una aproximació rotacional sobtada (ES) i l'altra aproximació es basa en que el moviment rotacional correlaciona amb una vibració de flexió en el camí de reacció i tracta adiabàticament el moviment de flexió. No anirem més enllà en la segona aproximació per que s'escaparia dels objectius introductoris d'aquesta part del treball.

L'aproximació utilitzada en aquest treball s'anomena *aproximació reactiva sobtada d'ordre infinit* (R-IOSA) (Reactive Infinite Order Sudden Approximation) i es basa en combinar les aproximacions CS i ES a partir de les equacions CC. Aquesta aproximació té com a principal conseqüència l'orientació fixada de l'arranjament àtom-diàtom. La vibració es tracta així de forma exacta, excepte per l'acoblament vibració-rotació i vibració-òrbita.

El mètode IOSA es va formular, en el seu origen, per al cas inelàstic amb la idea de reduir la complexitat que provoca l'existència d'un elevat nombre d'estats rotacionals per a cada nivell vibracional. Els bons resultats del mètode van fomentar la seva aplicació a la dispersió reactiva.

L'equació R-IOSA és de la forma:

$$\left[\frac{\partial^2}{\partial r_\lambda^2} + \frac{\partial^2}{\partial R_\lambda^2} - \frac{\bar{\ell}(\bar{\ell}+1)}{R_\lambda^2} - \frac{\bar{j}(\bar{j}+1)}{r_\lambda^2} \right] F_{J\bar{\ell}\bar{j}\,\bar{\Omega}_\lambda}^{\lambda}(r_\lambda, R_\lambda, \Theta_\lambda) = \qquad (1)$$

$$= \frac{2\mu}{\hbar^2} \left[V(r_\lambda, R_\lambda, \Theta_\lambda) - E \right] F_{J\bar{\ell}\bar{j}\,\bar{\Omega}_\lambda}^{\lambda}$$

on ℓ indica el canal d'ordenament i Θ_λ és un paràmetre que indica l'angle d'orientació àtom-diàtom en l'ordenament. El procés d'integració del sistema d'equacions es duu a terme, en el nostre cas, expressant el Hamiltonià segons l'anomenat sistema de coordenades circulars de col.lisió i fent servir el mètode de la matriu R per a resoldre la part radial de la solució. El mètode no s'explicarà amb més detall ja que ha estat exposat en anteriors treballs (veure capítol 6.1).

El notre grup de recerca ha treballat llargament amb aquest mètode aproximat i per tant creiem que tenim suficient experiència amb el mateix. Com en tots els mètodes aproximats, la clau per a emprar-los adientment és conèixer en profonditat les seves limitacions. El mètode R-IOSA s'ha mostrat com un mètode relativament fiable per a la majoria de sistemes estudiats en el nostre grup, i de manera especial quan l'efecte orientacional de la superfície és petit o es consideren energies elevades.

D'aquesta manera, en el capítol 7 de la memòria es presenten els artícles que hem publicat referents a l'estudi sobre dos sistemes reactius, $Mg + FH \rightarrow MgF + H$ i $B + OH \rightarrow BO + H$ utilitzant el mètode R-IOSA. En aquests

articles, es pot comprovar com a l'estudi del primer sistema ens vam concentrar en diferents aspectes de la seva dinàmica que es van traduir en dues publicacions. Pel que fa al segon sistema, vam trobar de prou interès l'estudi del patró de ressonàncies que presenta la reacció utilitzant un model reduït com ara el R-IOSA.

El sistema $Mg + FH \rightarrow MgF + H$.

El sistema presenta diverses característiques que van motivar el seu estudi. De fet, qualsevol sistema que, com aquest, es compongui de masses relativament elevades constitueix un repte per a un càlcul mecanoquàntic degut a l'increment en el nombre d'estats a considerar. Per altra banda, el sistema es mostra especialment adient per a un estudi IOS ja que les primeres inspeccions sobre la SEP van indicar una certa isotropia a la regió de l'estat de transició. Aquest fet afavoreix clarament un estudi del tipus IOS doncs la restricció d'orientació fixa perdrà relevància. Per tant, es va dur a terme un càlcul R-IOS extensiu per un total de 50 energies centrant-se principalment en la zona del llindar reactiu on es va emprar un espaiat energètic de fins a 0.01 eV.

Es van realitzar dos estudis a partir d'aquests resultats, centrant-se en aspectes més aviat diferents. En un d'ells ens vam concentrar en el llindar energètic per a la reacció i les peculiaritats que mostra la reactivitat a angle fixat. En el segon, vam realitzar un estudi més general sobre les distribucions vibracionals de productes (DVP) i els efectes de les masses isotòpiques. Per aquest segon treball, vam haver de realitzar un elevat nombre de trajectòries quasiclàssiques així com càlculs R-IOS addicionals per d les variants isotòpiques de la reacció, on se substituia l'àtom de hidrogen successivament per deuteri i triti.

La superfície de potencial emprada per realitzar els càlculs es va ajustar a punts *ab initio* utilitzant un funcional RBO. Sobre aquesta superfície, la reacció presenta una endoergicitat de 1.33 eV i una barrera endarrerida cap a productes de 1.83 eV on la geometria de l'estat de transició és clarament plegada amb un angle $Mg\hat{F}H$ d'uns 72°. A ,més d'aquestes característiques, la SEP presenta dos pous, un de col.lineal que es troba 0.34 eV per sota de l'assímptota de reactius i correspon al complex $MgFH$ i un segon pou d'uns 1.30 eV per sota de l'assímptota, de geometria altament plegada (al voltant de $\Theta = 35°$)que vam anomenar complex d'inserció. Aquest segon pou, tot i que és profund, només es pot assolir a través de la reorientació del sistema, de manera que serà intranscendent per a la reactivitat IOS, mentre que en el treball vam mostrar com juga un paper qualitativament important en la reactivitat que mostren les trajectòries quasiclàssiques. Diferents diagrames de contorn de potencial es mostren en la figura 7.1. Segons la nostra opinió, la importància d'aquests treballs recau en el fet que s'hagin trobat efectes quàntics notables en un sistema on és un atom pesat el que es transfereix.

- Energy mode effectiveness and tunnelling in triatomic reactions: the energy

threshold for the $Mg + FH \rightarrow MgF + H$ reaction. **Chemical Physics Letters 282 (1998) 91-99.**

En aquest article, es presentaven alguns dels resultats de l'estudi mecano-quàntic tridimensional aproximat sobre el sistema $Mg+FH$ per tal d'obtenir coneixement sobre el llindar de reactivitat i de com es veia afectat principalment per l'energia vibracional inicial de reactius. La reactivitat tridimensional global presentava un acusada selectivitat per al mode vibracional de l'energia, cosa que està d'acord amb les regles de Polanyi. Tal i com estableixen aquestes normes, per a reaccions amb barrera cap a productes, la reactivitat es veu fortament incrementada en augmentar l'energia vibracional inicial dels reactius. De totes maneres, a banda de les magnituds tridimensionals, es van explorar les seccions eficaces a angle fixat per tal d'obtenir alguna indicació addicional sobre el mecanisme de la reacció. Aquest va resultar ser més complex del que semblava a partir de les corbes tridimensionals. A partir d'aquest estudi a angle fixat vam poder establir dos tipus de comportament diferents en el sistema. D'una banda, per nivells vibracionals inicials de reactius baixos, la contribució més important a la seva reactivitat es troba per a angles propers al de la geometria de l'estat de transició. Per una altra banda, els nivells vibracionals més elevats de reactius tendeixen inesperadament cap a una reactivitat col.lineal. A més, d'ells corresponia a la corba per als reactius inicialment en el nivell vibracional $v = 3$ i un angle fixat a $\gamma = 180°$, llunyà de la geometria de l'estat de transició. Això s'assolia a través d'una important contribució de túnel. Es tractava doncs de dos aspectes més aviat sorprenents, atès que el punt més baix de la barrera de reacció es trobava per un angle tancat, allunyat de la col.linealitat.

Aquesta sèrie de fets, més aviat inusuals, els vam poder explicar gràcies a la representació dels camins de mínima energia a angle fixat, que són de fet els camins que "veuen" els càlculs IOS. En aquestes representacions vam poder veure com, tot i que l'alçada de la barrera augmentava en desplaçar-se cap a angles més oberts, el seu gruix disminuïa encara més significativament permetent d'aquesta manera un major efecte túnel. L'expressió analítica de la permeabilitat per a un model senzill de barrera quadrada, ens va permetre explicar el major efecte túnel per al nivell vibracional $v = 3$ per a una mateixa energia total.

- The influence of initial energy on product vibrational distributions and isotopic mass effects in endoergic reactions: the $Mg + FH$ case. **Physical Chemistry Chemical Physics, 1 (1999) 1133-1139.**
  En aquest segon treball, vam centrar la nostra atenció en un estudi detallat de la distribució vibracional de productes i una comparació extensiva de les seccions eficaces R-IOSA amb les corresponents obtingudes a través de trajectòries quasiclàssiques realitzades també per nosaltres mateixos. Per

aquest treball, a banda dels resultats que ja teniem, es van realitzar càlculs addicionals sobre les variacions isotòpiques D, T enlloc d'H, així com també les QCT corresponents, per tal de tenir un marc de comparació fiable.

Pel que fa a les DVPs, tot i que estan en acord general amb les regles de Polanyi, mostren comportaments qualitativament diferents, depenent no només de l'energia de col.lisió sinó també del nivell vibracional de reactius. Aquest és un camp que vam trobar interessant d'estudiar donat que podia aportar conclusions interessants pel que fa a la selectivitat d'estats de productes en les reaccions. D'aquesta manera, a energies de col.isió baixes la DVP pels nivells vibracionals inicials per sota de $v = 4$ són *estadístiques* mentre que la DVP corresponent al nivell $v = 4$ és més aviat adiabàtica. Quan hom es desplaça cap a energies més elevades, les DVP s'eixamplen, com era d'esperar, però a la vegada les distribucions corresponents a $v \leq 3$ tendeixen a desplaçar els seus màxims cap a valors més elevats del nivell vibracional final de productes (v') mentre que per $v = 4$ la distribució es comporta a la inversa, desplaçant-se cap a nivells vibracionals de productes menys excitats. Aquest comportament es va mirar de justificar en l'article a través del paper que juguen els diferents valors del moment angular orbital, representant les funcions opacitat.

A més a més, es van realitzar variacions isotòpiques sobre l'àtom lleuger (H, D, T) per tal d'assolir un millor coneixement del mecanisme de la reacció. D'acord amb la selectivitat de la reacció per al mode vibracional de l'energia, la secció eficaç per a una energia de col.lisió donada, per un mateix nivell vibracional inicial, disminueix a mesura que s'augmenta la massa de l'àtom lleuger. Per tal de tenir un marc de comparació pràctic, per comprovar la fiabilitat dels nostres resultats, es van realitzar càlculs QCT sobre el sistema així com les variacions isotòpiques. L'acord entre les dues metodologies va resultar satisfactori en general i el vam atribuir a una influència relativament baixa en la reactivitat tridimensional tant dels efectes quàntics com orientacionals.

El sistema $B + OH \rightarrow BO + H$.

- Cross sections exhibiting quantum ressonances: the $B+OH$ case. **Journal of Molecular Structure (Teochem) 463 (1999) 65-74**
Les ressonàncies són un dels efectes més notables que hom pot trobar en la dinàmica de reaccions. Les ressonàncies, que apareixen com pics lorentzians en la probabilitat de reacció, estan relacionades amb la formació de sistemes compostos metaestables i proporcionen informació extremadament acurada sobre l'estructura de la SEP. Aquest tipus de fenòmens són, doncs, quan són observables experimentalment, un marc de proves únic per a millorar els models teòrics. De totes formes, quan es prova de predir ressonàncies

teòricament a nivell de secció eficaç, hom es troba amb dues dificultats. El primer inconvenient està relacionat amb els temps de vida relativament curts dels complexos de col.lisió habituals, que porten a pics de probabilitat amples que fàcilment desapareixen en acumular els diferents moments angulars. Aquest problema pot ser, tanmateix, de menor importància si en el sistema reactiu es troben complexos relativament estables. La segona dificultat té a veure amb el cost computacional elevat d'un càlcul rigorós de dispersió reactiva; per tal de superar aquest contratemps hom pot emprar models de dimensionalitat reduïda, com ara el IOS, com a primera estimació de la importància del patró de ressonàncies d'un sistema reactiu.

En aquest context, vam considerar l'estudi aproximat del patró de ressonàncies presentat per al sistema $B + OH$. L'interès d'aquest sistema recau en la importància dels seus intermedis estables HBO i HOB, que podrien se importants en la formació d'estats ressonants. El complex HBO és conegut experimentalment i estudis teòrics han predit una geometria lineal per aquest mínim. La geometria del segon mínim HOB ha estat motiu de més controvèrsia, tot i que ajustant la SEP a una geometria col.lineal del mínim dóna una millor descripció de la reactivitat. Així doncs, es va utilitzar un ajust emprant un funcional Sorbie-Murrell, prenent una geometria col.lineal per a ambdós estats intermedis. Sobre aquesta SEP, la reacció resulta 3.60 eV exoèrgica i el seu canal alternatiu es va poder negligir a les energies de treball, doncs resulta 1.75 eV endoergic. L'energia del complex BOH es troba 6.4 eV per sota de l'assímptota de reactius i es troba en la zona de reactius. Seguint el camí de mínima energia, una barrera de 1.21 eV connecta aquest mínim amb el de HBO, d'energia uns 4.9 eV per sota de l'assímptota de productes.

En aquesta publicació vam mostrar com la component ressonant de la reactivitat global era prou significativa pel sistema en estudi. La representació gràfica de les funcions opacitat i seccions eficaces diferencials van confirmar aquest fet mostrant funcions opacitat accentuadament estructurades i seccions eficaces diferencials molt simètriques. La significativa estructura que *sobreviu* en la secció eficaç integral indica que la seva mesura experimental podria resultar molt útil per al refinament del potencial d'interacció per aquest sistema.

Implementació dels NIPs a la solució propagativa del problema reactiu.

En aquesta part de la memòria es presenten els articles publicats respecte del nostre treball en la implementació de la tècnica dels Potencial Negatius Imaginaris (NIP, acrònim de l'anglès) en un esquema propagatiu, en concret del tipus *invariant embedding* i específicament l'anomenat mètode de propagació de la matriu

R. Alhora es va presentar la aplicació d'aquesta nova metodologia a una família de sistemes reactius que cobreixen un ampli interval de casos possibles. Aques treball s'ha reflectit, fins ara, en tres articles i una comunicació, tots ells cobrint diferents aspectes del desenvolupament i l'aplicació del mètode.

- On the accuracy of reactive scattering calculations with absorbing potentials: a new implementation based on a generalized R-matrix propagation. **Chemical Physics Letters 291 (1998) 346-350**
  En aquest treball, la nostra intenció era notificar l'èxit de la implementació dels potencials absorbents a un mètode de propagacio *invariant embedding*, centrant-nos en la seva factibilitat i les bones prestacions del codi numèric.

  La idea, com s'explica en la secció 2.7, consisteix bàsicament en reduir un problema de dispersió reactiva en un d'inelàstic introduint convenientment un potencial complex. Com s'explica a la memòria i a l'article, coneixent la capacitat del NIP d'absorbir el flux associat a la funció d'ona, si hom col.loca tal potencial absorbent més enllà de la regió de l'estat de transició, on s'assumeix que les interaccions reactives ja ja han tingut lloc, hom pot aleshores atribuir la pèrdua de flux que provoca el NIP a la component reactiva. Per tant, introduint un NIP i realitzant un càlcul inelàstic, que en principi resulta més senzill, hom pot obtenir probabilitats reactives globals. Naturalment, l'esquema de propagació va haver de ser modificat per tal de tenir en compte la naturalesa complexa de les matrius d'interacció, cosa que es va explicar en una altra publicació.

  Enlloc de comprovar el nou mètode amb reaccions prototípiques, vam trobar que seria més interessant l'estudi col.lineal de la reacció de bescanvi $Cl + HCl \rightarrow ClH + Cl$, reacció per a la que disposavem de resultats exactes que havien estat prèviament publicats per altres autors. Els nostres resultats van coincidir plenament amb els publicats, fins i tot en comparar les fines estructures ressonants que presenta el sistema. A més a més, la implementació es mostrava més eficient que els nostres càlculs previs utilitzant una propagació estàndard de la matriu R, és a dir sense la introducció del NIP.

- Comment in the 110 Faraday Discussion on Chemical Reaction Theory. General Discussion. **Faraday Discussion 110 (1998) 236-238**
  En aquesta comunicació es presenta el comentari que vam aportar en la Discusió General de la 110 Faraday Discussion. El nostre comentari feia referència a un article presentat per Peng[69] en el que desacoblaven reactius i productes. Vàrem creure que era interessant esmentar en aquest contexte la implementació dels NIP sobre la propagació de la matriu R, que haviem desenvolupat. En concret, vàrem mostrar els resultats obtinguts per al càlcul de la secció eficaç del sistema $Ne + H_2^+ \rightarrow NeH^+ + H$ per unes

200 energies entre 0.7 i 1.1 eV. Aquests resultats evidencien una reactivitat molt estructurada.

- The application of complex absorbing potentials to an invariant embedding scattering method: I. Theory and computational details. **Journal of Chemical Physics 109 (1998) 5761-5769**
  En el citat article desenvolupem en detall l'extensió que vam realitzar dels mètodes mecano-quàntics basats en el mètode de propagació de la matriu R per tal de poder incorporar potencials complexos absorbents. Partint de la base que no erem pioners en l'ús de potencials òptics, sí que ho hem estat en implementar-los en un esquema propagatiu, i l'article mira de donar primerament una revisió de l'us històric i desenvolupament dels potencials òptics. El principal objectiu del treball publicat era descriure en detall els aspectes claus que havien estat modificats a l'esquema de propagació de la matriu R, de manera que pogués tenir en compte una matriu d'interacció de naturalesa complexa. Com ja s'explica en les seccions 2.7 i 8.1 de la memòria, mitjançant la introducció d'un potencial negatiu imaginari (NIP) hom pot reduir el problema de dispersió reactiva en el que nosaltres vam anomenar problema *pseudo-inelàstic*. Aleshores, es pot dur a terme un càlcul com si només es donés dispersió inelàstica, que és molt més senzilla de tractar, i després assignar la pèrdua de flux al flux reactiu. Aquest potencial absorbent és, en el nostre cas, una rampa lineal negativa que depèn de les coordenades físiques del sistema. La introducció de tal potencial imaginari provoca que la matriu d'interacció esdevingui complexa. El mètode propagació de la matriu R assumeix, tal i com es va formular originàriament, que la matriu d'interacció és real i simètrica, cosa que ja no és el cas. Les modificacions van implicar essencialment un generalització de les solucions per al problema de potencial constant a cada sector, passant a un quocient de funcions exponencials enlloc de les funcions trigonomètriques i hiperbòliques habituals així com la inversió explícita d'algunes matrius de transformació que ja no són real simètriques. L'assignació assimptòtica es va realitzar d'acord amb la propagació estàndar de la matriu R pel cas inelàstic i després es van calcular les probabilitats inelàstiques estat-a-estat.

Una vegada el mètode de la matriu R havia estat generalitzat, vam emprar un Hamiltonià d'ordre infinit (IOS) (veure més amunt i secció 6.1) per tal d'obtenir una expressió més explícita de la matriu d'interacció. A més, com que disposàvem de resultats previs utilitzant la metodologia tradicional R-IOS, propagant la matriu R en les regions de productes i reactius, vam pensar que seria una bona prova per a les prestacions del nou mètode. Així doncs, vam fer diversos càlculs del codi NIP-IOS desenvolupat sobre la reacció de bescanvi $Cl + HCl \rightarrow ClH + Cl$. La fiabilitat dels nostres resultats ja havia estat comprovada en la comunicació presentada anteriorment. En aquest article vam mostrar l'estabilitat del mètode, no només pel que fa

als paràmetres del NIP sinó tambe els paràmetres propis de la propagació, que resulten en unes prestacions superiors del NIP-IOS respecte el R-IOS.

- The application of complex absorbing potentials ot an invariant embedding scattering method: II. Applications. **Journal of Chemical Physics (in press)**
La publicació de l'anterior treball ha estat seguida per la publicació d'un altre treball en el que s'aplica la nova implementació a l'estudi dels sistemes $Li + FH$, $Mg + FH$ i $H + F_2$. Amb l'estudi d'aquestes reaccions es cobreixen diferents ergicitats i nivells de complexitat en la SEP, així com diferents combinacions de masses. Aquest estudi el vam realitzar ja que, tot i que les primeres aplicacions del mètode semblaven indicar una millora en el càlcul de magnituds globals respecte l'anterior tècnica R-IOS, vam pensar que seria interessant disposar d'una prova addicional que establís de manera definitiva el nivell de prestació del mètode. A més de provar els NIPs per diverses condicions, preteniem aprofitar-nos d'un mètode computacionalment barat per tal d'aprofondir en la dinàmica d'alguna de les reaccions mencionades anteriorment.

Tot i que en principi, en el tractament IOS, hom hauria de necessitar diferents paràmetres del NIP per cada angle d'orientació diferent, a la pràctica això no és el cas habitual i hem estat capaços d'utilitzar un únic conjunt de paràmetres NIP per a totes les orientacions, excepte per les SEP altament anisotròpiques, com ara la del $H + F_2$, on vam haver d'utlitzar dos conjunts de paràmetres. Aquest fet, conjuntament amb la relativa facilitat amb què es troben els paràmetres òptims del NIP, mostra que el temps consumit en obtenir el NIP convenient és negligible en comparació amb el temps estalviat.

La comparació de les prestacions del mètodes R-IOS i NIP-IOS va evidenciar clarament el menor esforç computacional del segon. Generalment, el nombre de sectors translacionals es redueix a la meitat i la dimensió de la base vibracional es veu significativament reduïda. Ambdues reduccions es tradueixen en un estalvi de temps de CPU. Mentre la reducció de temps és lineal amb la reducció de sectors, com el procés de propagació implica la inversió explícita d'una matriu, l'estalvi de temps en la reducció de la base és proporcional a N^3.

Tot i que en el treball publicat fins ara els mètodes NIP-IOS i R-IOS mostren un bon grau d'acord, hom no hauria d'esperar a priori una coincidència exacte dels resultats, ja que no es tracta de mètodes totalment equivalents. Creiem que cal recalcar que el NIP-IOS només restringeix el moviment pel que fa a l'orientació fixada de reactius. No hi ha restriccions addicionals més enllà de la zona de l'estat de transició on s'absorbeix el flux. Això no és així pel R-IOS on la solució s'ha de propagar també en la regió de

productes i per tant també es restringeix el seu moviment.

La relativament bona eficiència i fiabilitat del codi ens va empènyer a realitzar alguns càlculs addicionals en els que vam obtenir satisfactòriament probabilitats cumulatives de reacció amb un estalvi significatiu de temps. La idea consistia en, dins un càlcul NIP-IOS normal, realitzar l'assignació assimptòtica poc després de la zona de forta interacció on, tot i que les interaccions inelàstiques encara són importants, les reactives ja es poden negligir. Això condueix, òbviament, a probabilitats inelàstiques estat-a-estat errònies però si l'objectiu és una magnitud global com ara la constant de velocitat, la probabilitat cumulativa de reacció és tot el que necessitem.

Càlculs hiperesfèrics exactes.

- Exact quantum 3D cross sections for the $Ne+H_2^+ \rightarrow NeH^+ + H$ reaction by the hyperspherical method. Comparison with approximate quantum mechanical and classical results. **Physical Chemistry Chemical Physics 1 (1999) 1125-1132**
  En aquest article vam publicar els primers resultats de l'estudi mecanoquàntic exacte del sistema $Ne+H_2^+ \rightarrow NeH^+ + H$ utilitzant el mètode hiperesfèric, tal i com està explicat en la secció 5.1. El relativament recent desenvolupament tecnològic, així com l'aparició dels primers codis numèrics realment pràctics ha donat un nou impuls al càlcul mecanoquàntic exacte de la dispersió reactiva. Tanmateix, encara pocs mètodes s'han mostrat capaços de realitzar càlculs en condicions acceptables, pel que fa a recursos computacionals. Un dels mètodes més eficients i àmpliament utilitzat és el desenvolupat per Launay i LeDorneuf, que nosaltres hem emprat en el treball descrit en la publicació.

  En concret, hem estudiat un membre de la família de sistemes $X + H_2^+$, on $X = He, Ne, Ar$, per la qual hi ha una quantitat considerable de dades experimentals. A més, la reacció en concret és pot trobar habitualment en el camp de la física de plasmes on els àtoms de Ne són introduïts en plasmes de H_2 per a refredar-los desactivant el H_2^+. Les característiques que fan aquesta reacció mereixedora d'estudi són principalment dues: l'important increment en la reactivitat que pateix el sistema amb l'excitació vibracional dels reactius i l'elevada estructura que mostra la probabilitat de reacció, reveladora d'un probable espectre dens de ressonàncies. Disposàvem de resultats preliminars prèviament publicats que ens van estar de gran utilitat a l'hora de trobar els paràmetres de convergència, un pas més aviat crític en qualsevol càlcul numèric.

  Es va descriure a l'article, doncs, amb relatiu detall la cerca dels paràmetres òptims de convergència. El procés de convergència va ser comprovat sobre la probabilitat de reacció per moment angular total nul ($J = 0$) utilitzant fins

a 800 energies en un interval de 0.4 eV. El principals paràmetres convergits van ser el valor màxim (assimptòtic) de l'hiperradi, el nombre de sectors i el tamany de la base interna. En concret, es va tenir especial cura a la determinació de ρ_{max} i els nostres resultats van confirmar els publicats anteriorment. A continuació es van establir les condicions de convergència per al càlcul de la secció eficaç, en concret del màxim valor del moment angular total (J) que contribueix a la reactivitat així com el nombre de projeccions de J que s'ha d'incloure en la propagació.

Els resultats obtinguts van confirmar la important efectivitat del mode vibracional de l'energia. La destacable estructura ressonant sembla que sigui causa de complexes de llarga vida, més que d'efectes de la barrera centrífuga. Vam comparar també els nostres resultats exactes amb altres mètodes aproximats com CS, R-IOS i QCT amb diferents nivells d'acord. Mentre, com era d'esperar, els resultats CS eren els més propers als exactes, els resultats obtinguts per QCT eren inespereradament equivocats, probablement degut a una violació sistemàtica de la regla de conservació de l'energia del punt zero i a una contribució molt important dels estats ressonants.

Contents

CONTENTS

Chapter 1

Introduction

Contents

Probably, one of the main goals when studying chemical reactions is the acquaintance of quantitative data, such as the reaction heat, the reaction yield or, more generally, the influence of relevant variables on the behaviour of the reacting system. This goal is usually achieved under the framework of two chemistry disciplines, thermodynamics and kinetics.

In general terms, thermodynamics provides us information about the sense in which the reaction will take place. The well-known general criterion for spontaneity is that the free energy variation between reactants and products has to be negative. It is worth pointing out that this measure is expressed by means of state functions; therefore their variation associated to the process depends only on the initial and final state features. However, since thermodynamics cannot provide information about the rate with which the reaction will occur, there can be the case where a spontaneous process will not appreciably occur. It can therefore be said that, for the complete study of a chemical process, one needs as well the information given by chemical kinetics, as the branch of science that studies the rate of chemical reactions.

The thermodynamic and kinetic characterization of chemical processes is known to be of great technological importance. It is also true, however, that both disciplines, as sciences based on macroscopic experimentation, are not capable of providing an explanation of the chemical process based on first principles, and therefore their predictive capability remains constrained to empirical correlations. Given the enormous variety of behaviours that can be found in the *chemical world*, an effort to extract the fundamental trends that characterize it appears as essential. These trends have to be obtained from the microscopic study of the

1

chemical species and the further connection to the macroscopically measurable information through statistical mechanics, including both equilibrium (partition functions, etc.) and non-equilibrium disciplines (microcanonical and canonical rate constants, correlation functions, etc.).

Being more specific, chemical kinetics gives us an initial path to find out the connection between the experimental behaviour, macroscopically observed, and the corresponding microscopical foundings. Thus, a very usual result one obtains, from a macroscopic kinetics study of a particular reaction, is the plot of the concentration variation with time, for each of the chemical species taking part in the process. The study of these variations leads to establishing empirically the rate equation, that for a process such as:

$$aA + bB + cC + \cdots \rightarrow mM + nN + \cdots$$
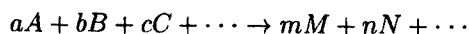
has the general form:

$$v = k(T)[A]^{\alpha}[B]^{\beta}[M]^{\mu}[N]^{\nu} \cdots$$

where $k(T)$ is the rate constant -usually T-dependent- specific for each reaction, and $\alpha, \beta, \ldots$ are generally positive or negative, integer or half-integer exponents. For some other complicated cases, the rate equation can be more involved and contain summations and/or other algebraic terms. Using this macroscopic rate equation, a mechanism able to explain the whole process can be inferred. Actually, most of the processes usually formulated by a single chemical equation are the global outcome of a series of elementary stages, some of them acting successively and others simultaneously, in which intermediate species happen to occur and disappear.

The study of the concentration profiles, establishing the rate equation and the mechanism, as well as the study of the influence of temperature and other variables on the rate constant constitute the domains of the *formal chemical kinetics*, macroscopic branch of chemical kinetics.

The main characteristic of the rate equations, corresponding to each of the elementary stages of any mechanism, is that their mathematical form corresponds to a simple case, since only reactants concentrations appear in them and their exponents coincide with their respective stoichiometric coefficients. This allows us to deduce that the reaction rate is due to a common factor, non intrinsic to the system, namely concentrations, and an intrinsic factor, the rate constant. If there would be no rate constant in the rate equation, the rate of all elementary reactions with identical stoichiometry would be the same, disregarding the nature of the chemical species undertaking the reaction. Nevertheless, experience tells us the contrary, for if the concentration term plays the role of modifying the number of collisions in a unit of time, the rate constant is found to characterize the effectivity of these collisions.

The explicit quantification of how different factors modify the value of the rate constant requires a microscopic explanation of the collisions between the chemical species. These are the domains of molecular dynamics.

1.1 Molecular Dynamics

The scope of molecular dynamics is then the study of the molecular mechanisms through which chemical and physical processes take place. It is, therefore, related to the intermolecular collisions and the intramolecular motions. The understanding of the dynamical behaviour of a system at a molecular level will then be the clue for the interpretation of its macroscopic kinetics. This has been generally accepted ever since the *kinetic theory of gases* stated that intermolecular collisions are the microscopic mechanism of all phenomena in which velocity is a relevant magnitude. On the other hand, it is not far the time in which the development of both theoretical and experimental techniques has allowed the first studies of kinetic processes at a molecular level. Nowadays, the most intimate details of a physical change or a chemical reaction are beginning to be experimentally observed, as the result of a 75-year experience.

The first studies on *elementary chemical processes* can be dated on the publication of several works by M. Polanyi, E. Wigner, H. Eyring, E. Pelzer and others in the beginning of the thirties. Molecular dynamics has become since then a new aspect of science by itself and chemical dynamics appears as its most important branch. This provides not only the foundings for macroscopic chemical kinetics, but an important source of knowledge on the basic phenomena involved in the elementary chemical event.

We can then say that the main goal of molecular dynamics is the study of elementary chemical processes, i.e., the study of what goes on in a single collision between reacting species. The fact we are studying a single collision will affect the conditions under which the experimental measures will take place and make the subject specially adapted to be treated from the theoretical point of view.

1.2 Interaction between experiment and theory

Since we are interested in simple collisions, the experiment will generally be free of those factors that usually prevent the experimental results from being directly comparable to the theoretical ones. Therefore, we will not care, in principle, about external influences on the collision process and neither will we consider the cooperative phenomena between species occurring in the condensed phase. Experiments in the field of molecular dynamics basically concern the development of *molecular beams* techniques, although other experimental techniques have also provided some detailed information on elementary reactive processes

-chemiluminiscence, photoionization, ion-imaging, photoelectron spectroscopy, femtosecond laser spectroscopy , etc.-.

The fact that the experimental environment can be described in a relatively simple way does not mean that the information to be extracted, or the corresponding theoretical calculations, have to be simple as well. Nevertheless, the absence of external disturbing factors makes that, wishing to have theory and experiment at the same level, the theoretical methodology and the experimental technique become complicated to really high limits. When this is achieved, the theoretical treatments can predict the experimental behaviour and advances in the experiment can confirm or discard the validity of these theoretical models. On the other hand, when the acquaintance of experimental data is complicated, theory can appear as a valuable *ab initio* source of data.

This mutual interaction can only be found in those fields of science where theory and experiment are at comparable levels, being this the case in many of the molecular dynamics applications.

1.3 Theoretical methods

The theoretical study of elementary collision processes that imply atomic and/or molecular systems, reactive or not, can be carried away using several methodologies that find their origin in the field of atomic or nuclear physics. The many methodologies nowadays available are usually classified in three main categories: classical, quantum and semiclassical. These refer to the way in which the motion associated to the atomic nuclei, under the forces exerted by the the electronic cloud and the internuclear repulsion, is solved.

In classical methods, it is assumed that the dynamical evolution of the atomic nuclei occurs according to the classical laws of motion, over a previously calculated potential energy surface (PES), and allows us to deal with trajectories associated to an elementary reaction. Solving the Hamilton equations, a number of trajectories, sampling the set of initial conditions which are found to match the experimentally controllable initial states, can be calculated. After a statistical treatment of a large enough number of trajectories, the relevant observables can be obtained. Usually, the equations of motion are solved in a way that the initial conditions are compatible with the quantum description of molecular states, leading to the *Quasiclassical approach*. Although the results obtained are generally satisfactory for averaged quantities, one has to be aware of the classical mechanics limitations; therefore one should not expect purely quantum phenomena to be treated correctly using this methodology.

Since the microscopic behaviour of matter can only be rigorously reproduced using the description provided by quantum mechanics, this methodology must be the most convenient for studying an elementary collision whenever high accuracy is important or quantum effects dominate the reaction outcome. The Schrödinger

equation corresponding to the nuclear motion over a previously determined PES, is the one to be solved in that case. However, the exact solution of the resulting equation is hard to be obtained even from a purely numerical perspective. This has hindered its application for a long time, even for the simplest chemical systems. The quantum-mechanical treatment of reaction dynamics has historically presented two main difficulties:

- firstly, difficulties arising from the fact that the nature of a rearrangement process demands a careful selection of the coordinates to be used, in order to describe the nuclear wavefunction of the system. Unlike elastic and inelastic processes, where, for instance, a three-body process can be described as an *effective 2-body problem*, a rearrangement event forces the study to remain under the three-body optics. In practice, this problem yields major difficulties in the choice of the most appropriate coordinate system, i.e. that capable of describing all the possible asymptotic arrangements and at the same time capable of describing the close-interaction regions where the triatomic ensemble is found.

- a second difficulty concerns essentially computational aspects and arises from the fact that a chemical reaction can involve a large number of vibro-rotational states of both reagents and products. This increases dramatically the dimension of the coupled set of differential equations into which the initial Schrödinger equation is usually transformed. This has caused efforts to be put for a long time on the development of approximations that would reduce the number of states involved and therefore ease the solution of the nuclear equation. Fortunately, relatively recent technological developments as well as new analytical and algebraic advances have provided us with powerful calculating tools, which have made feasible rigorous reactive scattering calculations.

The semiclassical methodology finds its spot in the middle of the classical and the purely quantum mechanics. In some approaches, it employs a mixture of both, treating classically some degrees of freedom and others quantally. This allows the study of quantum phenomena and relates them to classical pictures. Other well-known methodologies are the *JWKB semiclassical approach* (Marcus) and the *Path Integral* which yields the classical-limit approach to the S-matrix (Miller).

Chapter 2

Quantum mechanical formalism

Contents

In this chapter, a brief description of the collision processes, based essentially on the formal aspects of the operator theory, is presented, since it provides a solid theoretical framework on which the different methodologies have been developed. Basically, the theory consists in an adaptation to the field of bimolecular elementary reactions of the particle dispersion formal theory. In the following, a general overview of the formalism will be given. Firstly, the simple case of a structureless and spinless particle under a scattering potential is discussed. This will be a way to introduce the concepts of bound and scattering states, being the last responsible for the reactive event. Next, the key operator to the quantum treatment of scattering will be defined, the scattering operator. It will be proven how this operator relates linearly the initial and final states of a collision process. Following, the time-independent treatment will be introduced through the stationary scattering states. It will be seen how the use of a stationary treatment essentially saves one dimension (time) and modifies the boundary conditions of the problem. Within this stationary frame the case of elastic scattering will be treated as an example and used to introduce the concept of the partial wave expansion. We will then proceed to describe the generalization of the scattering fundamentals

to the case of more complex systems with more than two particles and therefore with several different arrangement possibilities between its components. In this context the central equation of the quantum mechanical treatment of elementary reactivity, the *close coupling equation set*, can be developed.

2.1 Scattering operator for a single particle.

In this section, a brief description to most of the essential concepts that can be found in scattering problems, such as the scattering operator, the Möller wave operators or the cross section for the potential scattering will be given. We will point out how the free motion of a particle prior to the collision can be related directly to its free motion after the collision has taken place, through the unitary scattering operator, S.

Let $|\psi_t>$ be the state vector of a particle satisfying the time-dependent Schrödinger equation

$$i\frac{d}{dt}|\psi_t> = \hat{H}|\psi_t> \tag{2.1}$$

The solution to this equation will be of the form $|\psi_t> = \hat{U}(t)|\psi> = e^{-i\hat{H}t}|\psi>$, as it can be proven by direct substitution on 2.1, where $\hat{U}(t) \equiv e^{-i\hat{H}t}$ is the so called time evolution operator and $|\psi>$ is a vector belonging to the spinless particle Hilbert space. Each orbit, as we will call hereinafter $\hat{U}(t)|\psi>$, is univocally labeled by the $|\psi>$ vector, which is the state vector for the system at time $t = 0$. Let's suppose the particle is under a scattering potential so that $H = H^0 + V$, where H^0 is the free particle Hamiltonian and V is a finite range scattering potential. Considering that the orbit describes a scattering experiment, if we would then follow it back to a time long before collision, this orbit would represent a wavepacket localized far away from the scattering center.

$$\hat{U}(t)|\psi> \xrightarrow{t \to -\infty} \hat{U}^0(t)|\psi_{in}> \tag{2.2}$$

where $\hat{U}^0(t)$ is the time evolution operator associated to the free Hamiltonian H^0. Similarly, if we would follow the orbit evolution forward in time for the scattering experiment, we would find as well a wavepacket localized far from the scattering center

$$\hat{U}(t)|\psi> \xrightarrow{t \to +\infty} \hat{U}^0(t)|\psi_{out}> \tag{2.3}$$

$|\psi_{in}>$ and $|\psi_{out}>$ are called, respectively, the incoming and outgoing asymptotes for the $|\psi>$ scattering state.

Of course, one should not expect all orbits to have asymptotes, for there will be some orbits that will have asymptotes, and will correspond to *scattering states*, and there will some other that will not and will correspond to *bound states*. In this sense, the *asymptotic condition* establishes that, for any vector $|\psi_{in}> \in \mathcal{H}$, there is a solution to the Schrödinger equation that is asymptotic to the free orbit

2.1. Scattering operator for a single particle.

$\hat{U}^0(t)|\psi_{in}>$ when $t \to -\infty$, and similarly for any $|\psi_{out}>$ when $t \to +\infty$. This indicates that any incoming (and outgoing) asymptotic state is linearly related to a scattering state. Thus, it can be written

$$\hat{U}(t)|\psi> -\hat{U}^0(t)|\psi_{in}> \overset{t \to -\infty}{\longrightarrow} 0$$

since $\hat{U}$ is unitary,

$$|\psi> -\hat{U}(t)^T\hat{U}^0(t)|\psi_{in}> \overset{t \to -\infty}{\longrightarrow} 0$$

then

$$|\psi> = \lim_{t \to -\infty} \hat{U}(t)^T\hat{U}^0(t)|\psi_{in}> \equiv \hat{\Omega}_+|\psi_{in}> \qquad (2.4)$$

and analogously

$$|\psi> = \lim_{t \to +\infty} \hat{U}(t)^T\hat{U}^0(t)|\psi_{out}> \equiv \hat{\Omega}_-|\psi_{out}> \qquad (2.5)$$

where $\hat{\Omega}_+$ and $\hat{\Omega}_-$ are called the Möller wave operators and are isometric operators, i.e., their domain and range are not the same space. In other words, they operate over the whole Hilbert space but their image is only found in the scattering states subspace.

Next, two principles will be stated but they will not be proven, for a rigorous proof see [1]. The *orthogonality theorem* establishes that the bound states space, $\mathcal{B}$, is orthogonal to the space formed by states that have an incoming asymptote, $\mathcal{R}_+$, and to the space formed by those having an outgoing asymptote, $\mathcal{R}_-$.

$$\mathcal{B} \perp \mathcal{R}_+$$
$$\mathcal{B} \perp \mathcal{R}_-$$

The *asymptotic completeness theorem* establishes that the space of those states with incoming asymptote and that of those with outgoing asymptote are actually the same, $\mathcal{R}_+ = \mathcal{R}_- = \mathcal{R}$. Thus, the Hilbert space ($\mathcal{H}$) for a particle under a potential can be divided in two orthogonal subspaces, $\mathcal{B}$ expanding the bound states and $\mathcal{R}$ the scattering states.

$$\mathcal{H} = \mathcal{B} \oplus \mathcal{R}$$

According to the asymptotic completeness theorem, any scattering state has an incoming and outgoing asymptote, and so these can be related:

$$|\psi> = \hat{\Omega}_+|\psi_{in}> \qquad ; \qquad |\psi> = \hat{\Omega}_-|\psi_{out}>$$
$$|\psi_{out}> = \hat{\Omega}_-^T|\psi> = \hat{\Omega}_-^T\hat{\Omega}_+|\psi_{in}> \quad ; \quad \hat{S} \equiv \hat{\Omega}_-^T\hat{\Omega}_+$$

it is the usually written:

$$|\psi_{out}> = \hat{S}|\psi_{in}> \qquad (2.6)$$

Thus, we call *scattering operator* ($\hat{S}$) the operator relating the asymptotic states of a particular scattering state. Since only the asymptotic states are observable in the experiment, this magnitude will provide us with all the information necessary in order to express the experimental measurable quantities in terms of more fundamental ones.

2.2 The S-matrix.

As it has been shown, the S operator relates the motion of a free particle leaving a collision to its initial asymptotic state. For large values of time, once the interaction is over, a state $|\psi_{out}>$ is obtained belonging to the Hilbert space of the free Hamiltonian $(\hat{H}^0)$ eigenvectors, but does not have to be necessarily an eigenfunction:

$$|\psi_{out}> = \sum_{n=1}^{\infty} |\varphi_i> < \varphi_i|\psi_{out}>$$

Taking into account equation 2.6 the expression can be rewritten in terms of the incoming asymptotic states:

$$|\psi_{out}> = \sum_{n=1}^{\infty} |\varphi_i> < \varphi_i|\hat{S}|\psi_{in}>$$

Then, the probability for obtaining the state $|\varphi_i>$ as a consequence of the interaction, starting from the $|\psi_{in}>$ state (for this, we can choose an eigenvector of $\hat{H}^0$) is:

$$\omega\left(\varphi_i \leftarrow \psi_{in}\right) = \left|< \varphi_i|\hat{S}|\psi_{in}>\right|^2$$

Unfortunately, although those details that refer to the orbit state at time $t = 0$, labeled as the instant of the collision, have been eliminated, this quantity cannot still be experimentally measured. This is due to the fact that the $|\varphi_i>$ and $|\psi_{in}>$ wavepackets cannot be univocally identified in practice. Only position and momentum can be relatively known for $|\psi_{in}>$, but not univocally. Regarding the final state, generally the state is only detected in the experiment if the direction of the outgoing motion is within the solid angle element, $d\Omega$, around a particular direction. Thus, instead of calculating the $\omega\left(\varphi_i \leftarrow \psi_{in}\right)$ probability, one should calculate $\omega\left(d\Omega \leftarrow \psi_{in}\right)$, which is the probability for, starting from an initial free asymptotic state, the outgoing direction to be within the $d\Omega$ element. The fact that the precise incoming asymptotic is ignored, will just imply an averaging of this probability over all the relevant $|\psi_{in}>$ states. This averaging process will lead to the *cross section* concept.

As it has been stated in the previous section, the scattering operator is a unitary operator, combination of two isometric operators, that acts and projects onto the whole Hilbert space. One of the most important properties of this operator is that it is energy conserving, as expected, since we are only considering internal forces. For a time independent Hamiltonian the system is conservative and therefore the expected energy value for any orbit is constant. Since the S operator relates the free asymptotic states, one would expect it to commute with $\hat{H}^0$ rather than with $\hat{H}$. Using the intertwining relation[2] of the Möller operators, which states $\hat{H}\Omega_{\pm} = \Omega_{\pm}\hat{H}^0$, it can be seen that:

$$\hat{S}\hat{H}^0 = \Omega_-^T\Omega_+\hat{H}^0 = \Omega_-^T\hat{H}\Omega_+ = \hat{H}^0\Omega_-^T\Omega_+ = \hat{H}^0\hat{S}$$

and therefore:

$$\left[\hat{S}, \hat{H}^0\right] = 0 \tag{2.7}$$

and consequently energy is conserved, $< \psi_{in}|\hat{H}^0|\psi_{in} > = < \psi_{out}|\hat{H}^0|\psi_{out} >$. Since the free Hamiltonian and the scattering operator commute, a complete orthonormal eigenfunction set common to both operators, can be constructed. Derived from the wavepacket treatment, it has been considered as convenient to choose the momentum representation,

$$|\vec{p}> \quad so\,that \quad \begin{array}{ll} \hat{H}^0|\vec{p}> = \frac{\vec{p}^2}{2m}|\vec{p}> = E_p|\vec{p}> & ; \quad E_p = \frac{p^2}{2m} \\ < \vec{x}|\vec{p}> = \frac{1}{(2\pi)^{3/2}}e^{i\vec{p}\cdot\vec{x}} & ; \quad < \vec{p}'|\vec{p}> = \delta_3\left(\vec{p}' - \vec{p}\right) \end{array}$$

Thus, we can express the matrix representation of the S operator in the momentum representation. Using the latter commutation relation 2.7, we can establish that:

$$0 = \left\langle \vec{p}'\right| \left[\hat{H}^0, \hat{S}\right] \left|\vec{p}\right\rangle = (E_{p'} - E_p) < \vec{p}'|\hat{S}|\vec{p}> \tag{2.8}$$

and then the matrix element is zero unless the energy of both states is the same. We can then write that:

$$< \vec{p}'|\hat{S}|\vec{p}> = \delta(E_{p'} - E_p) \times other\,terms$$

After some manipulations[3] of the expression in order to factorise elastic scattering one obtains:

$$< \vec{p}'|\hat{S}|\vec{p}> = \delta_3\left(\vec{p}' - \vec{p}\right) + \frac{i}{2\pi m}\delta(E_{p'} - E_p)f(\vec{p}' \leftarrow \vec{p}) \tag{2.9}$$

where $f(\vec{p}' \leftarrow \vec{p})$ is called the *scattering amplitude* and is a smooth function, i.e., does not vary abruptly as the previous Dirac function. Its physical interpretation will be given later on when dealing with the stationary treatment (see section 2.3).

Once the general characteristics of the scattering operator and its matrix representation, the S matrix, have been stated, we are now ready to define the cross section, probably the most important quantity in reaction dynamics. Let's consider a scattering state with asymptotes, $\psi_{in}(p)$ and $\psi_{out}(p)$. The probability for this state to emerge with linear momentum within the solid angle $d\Omega$ around a particular direction $d\hat{p}$ is:

$$\omega\left(d\Omega \leftarrow \psi_{in}\right) = d\Omega \int p^2\,dp\,|\psi_{out}(\vec{p})|^2 \tag{2.10}$$

We will assume that $\psi_{in}(p)$ is a well localized function over a particular momentum, $\vec{p}_0$. Imagine a series of experiments where the incoming asymptotic state is $|\psi_{in}> = |\varphi_\rho>$ where $|\varphi_\rho>$ is obtained through random rigid shiftings of the

$|\varphi>$ state (localized over $\vec{p}_0$) along r. This means that φ_ρ is a function of the same shape as φ but its maximum probability peak is shifted by ρ.

$$\varphi_\rho(\vec{p}) = e^{-i\vec{p}\cdot\vec{\rho}}\varphi(\vec{p})$$

Suppose a whole series of experiments all with different small shiftings, the total number of scattered orbits within the solid angle element $d\Omega$ around $\vec{p}$ will be,

$$N_{sc}(d\Omega) = \int d^2\rho\, n_{inc}\omega\, (d\Omega \leftarrow \varphi_\rho)$$

where n_{inc} is the density of incident states and can be considered as constant for a random distribution. We then write:

$$N_{sc}(d\Omega) = n_{inc}\int d^2\rho\, \omega(d\Omega \leftarrow \varphi_\rho) \equiv n_{inc}\, \sigma(d\Omega \leftarrow \varphi) \qquad (2.11)$$

From this expression one obtains the differential cross section as,

$$\sigma(d\Omega \leftarrow \varphi) \equiv \int d^2\rho\, \omega(d\Omega \leftarrow \varphi_\rho) \qquad (2.12)$$

taking into account equation 2.10, one can write

$$\sigma(d\Omega \leftarrow \varphi) = \int d^2\rho\, d\Omega \int p^2\, dp\, |\psi_{out}(\vec{p})|^2 \qquad (2.13)$$

and given that $|\psi_{out}> = \hat{S}|\psi_{in}>$, which written in the momentum representation takes the form,

$$\psi_{out}(\vec{p}) = \int d^3p'\, <\vec{p}|\hat{S}|\vec{p}'>\psi_{in}(\vec{p}')$$

considering 2.9 and substituting in 2.13, after some modifications where it is assumed that the incoming wavefunction $\varphi(p)$ is well localized over $\vec{p}_0$ and that the measure is carried away far from the $\vec{p}_0$, allows us to derive the differential cross section expression:

$$\sigma(d\Omega \leftarrow \varphi) = d\Omega\, |f(\vec{p} \leftarrow \vec{p}_0)|^2 \qquad (2.14)$$

and $\sigma(\varphi) = \int_\Omega \sigma(d\Omega \leftarrow \varphi)d\Omega$ is the expression for the integral cross section.

2.3 Stationary scattering states.

In the previous sections we have followed a time dependent description of the collision processes. First we have described collisions in terms of the scattering operator, then we have decomposed the S matrix elements in terms of the scattering amplitude, and we have finally seen the expression for the cross section. However, for time-independent Hamiltonians it is possible to perform an equivalent treatment based on the time-independent Schrödinger equation. This

2.3. Stationary scattering states.

implies working with wavefunctions of definite energy, and therefore extended over the whole configuration space, as well as considering the proper boundary conditions, as it will be seen later on. The methods employed in the present work follow a time independent treatment. The formalism is built on the basis of the stationary scattering states $|p\pm>$ that we will briefly describe next.

Let's define the following $|\varphi+>$ and $|\varphi->$ states at time $t=0$ corresponding to the to the incoming and outgoing asymptote $|\varphi>$ so that,

$$|\varphi+>=\Omega_+|\varphi> \; ; \; |\varphi->=\Omega_-|\varphi>$$

if the $|\varphi>$ state is expanded in the momentum representation,

$$|\varphi>=\int d^3p\,\varphi(\vec{p})\,|\vec{p}> \qquad (2.15)$$

we can proceed analogously for the state vector at $t=0$

$$|\varphi+>=\Omega_+|\varphi>=\int d^3p\,\varphi(\vec{p})\,\Omega_+|\vec{p}>\equiv\int d^3p\,\varphi(\vec{p})\,|\vec{p}+> \qquad (2.16)$$

We can then get to write the following linear relation:

$$|\vec{p}+>=\Omega_+|\vec{p}> \qquad (2.17)$$

An immediate interpretation of the latter is that the $|\varphi+>$ state at $t=0$ has the same expansion in terms of $|\vec{p}+>$ as the asymptotic $|\varphi>$ state in terms of $|\vec{p}>$. If the $|\vec{p}>$ state is an eigenvector of the free Hamiltonian with corresponding eigenvalue E_p, then $|\vec{p}+>$ is an eigenvector as well, with the same eigenvalue, but corresponding this time to the complete Hamiltonian.

$$\hat{H}|\vec{p}+>=\hat{H}\Omega_+|\vec{p}>=\Omega_+\hat{H}^0|\vec{p}>=E_p|\vec{p}+>$$
$$\hat{U}(t)|\vec{p}+>=e^{\frac{-iE_pt}{\hbar}}|\vec{p}+>$$

$|\vec{p}+>$ is, thus, a *stationary state*. We then have that, since $\{|\vec{p}>\}$ is an orthonormal basis of $\mathcal{H}$, according to 2.17 $\{|\vec{p}+>\}$ will be an orthonormal basis of $\mathcal{R}$. We then have a state vector basis for the scattering states and if we add to it a basis for the bound states subspace we will have a basis set for the whole Hilbert space,

$$1=\int|p><p|d^3p=\int d^3|p+><p+|+\sum_n|n><n|$$
$$=\int d^3|p-><p-|+\sum_n|n><n| \qquad (2.18)$$

It can be proven that these stationary states have the following asymptotic form, in the position representation, as the distance between the colliding species becomes infinity (or large with respect to the scattering center dimensions),

$$<\vec{x}|\vec{p}+>\rightarrow\frac{1}{(2\pi)^{3/2}}\left[e^{i\vec{p}\cdot\vec{x}}+f\left(p\hat{x}\leftarrow\vec{p}\right)\frac{e^{ipr}}{r}\right] \qquad (2.19)$$

where we find once more the scattering amplitude, $f(p\hat{x} \leftarrow \vec{p})$. It can be seen that $< \vec{x}|\vec{p}+ >$ represents at the same time an incident beam and an infinite and spherically scattered particle beam. It is on this boundary conditions that the stationary treatment does actually reflect, since we are imposing, at an infinite distance, the state of the system to be represented by an incident beam and, at the same time, a spherically scattered beam. It can be seen as well that $< \vec{x}|\vec{p}- >$ represents a plane wave and another wave that collapses spherically and therefore has no direct physical meaning. Here we can clearly introduce the physical interpretation of the scattering amplitude, $f(p\hat{x} \leftarrow \vec{p})$, as the anisotropic angular factor on the scattered beam.

It can be easily shown that the differential cross section of a collision process, in its stationary interpretation, is defined as the quotient between the emitted particle flux through a unit solid angle and the incident flux. The integral cross section is correspondingly defined as the integration of the differential cross section with respect to the solid angle. The different geometry of the reference surface at which the flux is measured for each beam, a plane wave for the incident and a spherical one for the emergent, causes the cross section to have dimensions of area.

2.4 Scattering by a center of force. Stationary treatment

In this section, the simplest collision process will be studied, the elastic scattering between two spinless particles.

An elastic collision is one in which there is no change in the internal energies of the colliding species. The collision process of two atoms, without changing their respective electronic states, is the most important and simple example of such processes from the theoretical point of view. Elastic scattering can be found as well in molecular collisions, even if it is usually of secondary interest, since the inelastic collisions, where there is change in molecular rotational and vibrational energies, are much more frequent.

Adopting the center-of-mass coordinate system, the elastic process between two species, atoms hereinafter, produces a change in the direction of the relative velocity vector $(\vec{v})$ but does not alter its magnitude. Therefore the scattering is univocally determined by the change in the orientation of $\vec{v}$ and the two-particle collision is formally reduced to the motion of a single particle with reduced mass μ under a potential $V(\vec{r})$, where $\vec{r}$ is the interparticle vector. Since we have assumed we are dealing with atoms, the potential energy depends only on their separation $V(r)$ and so we have a central force problem.

This central force problem is formally identical to the well-known case of the electronic energy levels of the hydrogen atoms, the single but crucial difference

2.4. Scattering by a center of force. Stationary treatment

relying on the boundary conditions, as we will see. As in the hydrogen atom, the Schrödinger equation for this system is most easily solved using polar spherical coordinates and factorising the wavefunction into a product of angular functions (spherical harmonics) and radial functions.

As we have already said, the difference between our case and that of the hydrogen atom spectrum lies not in the form of the Schrödinger equation but in the boundary conditions applied to the solutions. For bound-state problems, the wavefunction approaches to zero as r tends to infinity and this boundary condition causes the quantization of the energy levels. As we have stated in the stationary treatment of the scattering problem, our wavefunction will not decay at infinity; rather we will have a wavefunction representing at the same time atoms coming together initially along straight lines and departing from one another in some angular pattern determined by the scattering amplitude.

Let's start by considering the wavefunction that represents initially the stream of particles moving with momentum $k\hbar$ in the positive direction of z.

$$e^{ikz}$$

This plane wave describes the incident beam in the idealized crossed beam experiment. Once the collision has taken place and the atoms are away from the collision region, we will have particles moving with the same velocity as the incident beam but in all directions. If the particles were moving isotropically, this would be represented by a wavefunction

$$\frac{e^{ikr}}{r}$$

i.e., a spherical wave. In the previous section we have seen that the scattering amplitude $f(\theta)$ introduces the anisotropic character of the scattering experiment, so we represent the situation after the collision by:

$$\frac{f(\theta)e^{ikr}}{r}$$

Note that for the scattering amplitude only one angular variable is needed since we are dealing with a central force problem and therefore the wavefunction is independent of the polar angle ϕ, due to the cylindrical symmetry of the problem about the z axis.

We can now establish the boundary conditions as:

$$\Psi \sim e^{ikz} + \frac{f(\theta)e^{ikr}}{r} \ , \ r \to \infty \qquad (2.20)$$

The form of the wavefunction remains unknown in the interaction region and to find it out we must solve the Schrödinger equation with this boundary condition.

Let's formulate then the equation for a system of reduced mass μ under a central potential $V(r)$

$$\left[\frac{-\hbar^2}{2\mu}\nabla_{\vec{r}}^2 + V(r)\right]\Psi(\vec{r}) = E\Psi(\vec{r}) \tag{2.21}$$

We can simplify this expression introducing the variables

$$k^2 = \frac{2\mu E}{\hbar^2}, \quad U(r) = \frac{2\mu V(r)}{\hbar^2} \tag{2.22}$$

then,

$$\left[\nabla_{\vec{r}}^2 + k^2 - U(\vec{r})\right]\Psi(\vec{r}) = 0 \tag{2.23}$$

We can obtain a completely general solution of this equation taking an expansion of the wavefunction in spherical harmonics functions, because this is a complete set of functions for the description of any analytic function of the polar angles:

$$\Psi(\vec{r}) = \sum_{\ell=0}^{\infty}\sum_{m=-\ell}^{\ell} R_{\ell m}(r)Y_{\ell m}(\theta,\phi) \tag{2.24}$$

However, as we have already said, because of the cylindric symmetry around the z axis, there is no ϕ dependence in the wavefunction and only $m = 0$ terms contribute to the expansion. The functions $Y_{\ell 0}$ are, apart from a multiplying factor, the Legendre $P_\ell(\cos\theta)$ functions. The expansion is therefore usually written as

$$\Psi(\vec{r}) = \frac{1}{r}\sum_{\ell=0}^{\infty} A_\ell \psi_\ell(r) P_\ell(\cos\theta) \tag{2.25}$$

which is called the *partial wave expansion*. The $\frac{1}{r}$ term is introduced in order to get rid of the first derivative term of the radial Laplacian. Although mathematically convenient, this expansion is not always highly convergent.

If one substitutes the expansion 2.25 into 2.23, using the orthogonality of the Legendre functions, one finds that the radial wavefunction $\psi_\ell(r)$ is the solution of the radial equation

$$\left[\frac{d^2}{dr^2} + k^2 - U_\ell(r)\right]\psi_\ell(r) = 0 \tag{2.26}$$

where $U_\ell(r)$, called the effective potential, combines the actual potential and the centrifugal barrier:

$$U_\ell(r) = U(r) + \frac{\ell(\ell+1)}{r^2} \tag{2.27}$$

Since equation 2.26 is a second-order differential equation, there will be two linearly independent solutions for each value of k^2 and ℓ. However, these will be physically acceptable only if they are regular at the origin, this is, the solution being zero when $r = 0$.

2.4. Scattering by a center of force. Stationary treatment

It is relatively easy to find solutions of 2.26 for any potential $U_\ell(r)$ by numerical integration, starting the wavefunction with zero amplitude at $r = 0$ and integrating outwards to a value of r large enough for $U_\ell(r)$ to be taken as zero. When r reaches such a value the equation becomes

$$\left(\frac{d^2}{dr^2} + k^2\right)\psi(r) = 0 \tag{2.28}$$

and its general solutions can be written in the form

$$\sin(kr + \eta_\ell) \tag{2.29}$$

where η_ℓ is a phase which depends on k, ℓ and the form of the potential.

We have already seen in the previous sections that our interest is the asymptotic form of the function at $r = \infty$, since it is from by which we obtain the cross section. In this region the only feature that depends on the potential is the phase η_ℓ. We therefore see how important this phase is in the theory of elastic scattering. However, its value depends not only on the actual potential $U(r)$ but on the centrifugal barrier as well (see equation 2.27), and it is therefore usually convenient to take as a reference value the phase that is obtained by the centrifugal potential by itself, that is, the phase for a constant null potential $U(r) = 0$.

$$\left[\frac{d^2}{dr^2} + k^2 - \frac{\ell(\ell+1)}{r^2}\right]\psi_\ell(r) = 0 \tag{2.30}$$

The solutions for this equation are well known[4] and related to the spherical Bessel functions $j_\ell(r)$ by the expression

$$\psi_\ell(r) = kr j_\ell(kr) \tag{2.31}$$

which has the asymptotic form

$$\psi_\ell \sim \sin\left(kr - \frac{\ell\pi}{2}\right) \tag{2.32}$$

Therefore, the asymptotic form of the solutions of equation 2.26 can be then defined to be

$$\psi_\ell \sim \sin\left(kr - \frac{\ell\pi}{2} + \delta_\ell\right) \tag{2.33}$$

where $\delta_\ell = \eta_\ell + \frac{\ell\pi}{2}$ is called the *phase shift*. Note that for some potentials, such as the Coulomb potential, the formula does not apply, since the potentials fall more slowly than the centrifugal barrier and therefore cannot be neglected. The dependence of δ_ℓ on ℓ is very interesting and reflects features of the potential.

The relationship between the scattering amplitude and the phase shift can be derived comparing the asymptotic expression obtained from substitution of 2.33 in 2.25,

$$\Psi(r) \sim \frac{1}{r} \sum_{\ell=0}^{\infty} A_\ell \sin\left(kr - \frac{\ell\pi}{2} + \delta_\ell\right) P_\ell(\cos\theta) \tag{2.34}$$

and the asymptotic expression 2.20. The result of this comparison[4] is known as the partial wave expansion of the scattering amplitude:

$$f(\theta) = \frac{1}{2ik} \sum_{\ell=0}^{\infty} (2\ell + 1)(e^{2i\delta_\ell} - 1) P_\ell(\cos\theta) \tag{2.35}$$

From the two terms of the central factor of the expression, the first, $e^{2i\delta_\ell}$, is due to the interatomic potential and the second, (-1), to the contribution from the unscattered incident plane wave.

We can deduce the scattering cross section in its stationary interpretation from the amplitudes of the incident and scattered waves in the asymptotic wavefunction expression. In the incident beam, the flux across unit area is proportional to

$$|e^{ikz}|^2 = 1 \tag{2.36}$$

and in the scattered beam the flux across the unit solid angle is proportional to

$$r^2 |\frac{f(\theta)e^{ikr}}{r}|^2 = |f(\theta)|^2 \tag{2.37}$$

Since we are dealing with elastic phenomena, the momenta of the particles are the same in the incident and the scattered beams and therefore the proportionality constants in the respective fluxes coincide. We have defined the stationary differential cross section as the ratio of the scattered flux per unit solid angle to the the incident flux per unit area and we therefore have:

$$\sigma(\theta) = |f(\theta)|^2 \tag{2.38}$$

If we replace the scattering amplitude by its partial wave expansion 2.35 we obtain the following expression:

$$\sigma(\Theta) = \frac{1}{4k^2} \sum_{\ell=0}^{\infty} \sum_{\ell'=0}^{\infty} (2\ell+1)(2\ell'+1)(e^{-2i\delta_\ell} - 1)(e^{2i\delta_{\ell'}} - 1) P_\ell(\cos\theta) P_{\ell'}(\cos\theta) \tag{2.39}$$

Note that there are interference terms between ℓ and ℓ' partial waves. On the other hand, the expression for the corresponding integral cross section will be rather simple, benefiting from the orthogonality properties of the Legendre polynomials, so that only $\ell = \ell'$ will perdure after integration over θ:

$$\sigma = \frac{\pi}{k^2} \sum_{\ell=0}^{\infty} (2\ell + 1)(e^{-2i\delta_\ell} - 1)(e^{2i\delta_\ell} - 1) \tag{2.40}$$

$$= \frac{4\pi}{k^2} \sum_{\ell=0}^{\infty} (2\ell + 1) \sin^2 \delta_\ell \tag{2.41}$$

2.5 Multichannel Scattering

Until now we have only dealt with processes that involved structureless particles. Now let's return to the more formal presentation of the scattering event but let's take a step forward as well in the complexity of the problem. From now on we will consider inelastic and rearrangement processes, i.e. collisions between particles with an internal structure. In this section a description will be given on how the generalization of the latter expressions is obtained and a formal expression will be obtained for the *close coupling equations*, which are the central equations for the multichannel collisions treatment under a target states expansion.

Let's consider a simple case where three spinless particles a, b and c are forced to move on a line, so that they can only lead to ac and bc bound systems, which are usually called arrangements. For each arrangement the bound systems can support several different states, called *channels*. Suppose that, at a given collision energy, only the (bc), $(bc)^*$ and (ac) cases are possible, being $(bc)^*$ an excited internal state of the bc arrangement. A table of the available channels for a collision process will look like this:

channel	0	1	2	3
	a + b + c	a + (bc)	a + (bc)*	b + (ac)

The system Hamiltonian will therefore be of the form,

$$\hat{H} = \frac{\hat{p}_a^2}{2m_a} + \frac{\hat{p}_b^2}{2m_b} + \frac{\hat{p}_c^2}{2m_c} + \hat{V}_{ab}(x_{ab}) + \hat{V}_{ac}(x_{ac}) + \hat{V}_{bc}(x_{bc}) = \hat{H}^0 + \hat{V} \qquad (2.42)$$

where x_{ab}, x_{bc}, x_{ac} are the interatomic distances in the collinear arrangement. Let's consider the 0 channel, if one follows the orbit back to a time long before the collision, one finds three infinitely separated particles

$$e^{-i\hat{H}t}|\psi> \overset{t \to -\infty}{\longrightarrow} e^{-i\hat{H}^0 t}|\psi_{in}>$$

and the corresponding asymptotic states wavefunction is of the form $< x|\psi_{in} >= \chi(x_a, x_b, x_c) \in \mathcal{S}_0$, where $\mathcal{S}_0$ is the subspace of those asymptotic functions that can label incoming or outgoing asymptotes in the 0 channel, i.e., the dissociation channel.

In channel 1, following the same procedure, one would find particle a infinitely separated from the system bc which is in the bound state (bc),

$$e^{-i\hat{H}t}|\psi> \overset{t \to -\infty}{\longrightarrow} e^{-i\hat{H}^1 t}|\psi_{in}>$$

and therefore the Hamiltonian can be factorised as $\hat{H} = \hat{H}^1 + \hat{V}^1$, where $\hat{V}^1$ is the channel potential containing the V_{ab} and V_{ac} potentials that become zero as a goes away from bc and the system evolves into channel 1:

$$\hat{H}^1 = \frac{\hat{p}_a^2}{2m_a} + \frac{\hat{p}_b^2}{2m_b} + \frac{\hat{p}_c^2}{2m_c} + \hat{V}_{bc}(x_{bc}) \quad ; \quad \hat{V}^1 = \hat{V}_{ab}(x_{ab}) + \hat{V}_{ac}(x_{ac})$$

The asymptotic state wavefunction would be $< x|\psi_{in} > = \chi(x_a, x_{bc})\varphi_{(bc)}(x_{bc}) \in \mathcal{S}_1$, where $\mathcal{S}_1$ is the subspace of those asymptotic functions labeling incoming or outgoing asymptotes in channel 1, i.e., the channel in which b and c form together the fundamental bound state and a moves freely.

For the other channels one would proceed in a similar way, defining a partition as $\hat{H} = \hat{H}^\lambda + \hat{V}^\lambda$ so that $\hat{V}^\lambda$ is a potential that becomes zero as the system evolves asymptotically into channel λ.

The asymptotic condition is generalized for the multichannel case establishing that, for any function belonging to the $\mathcal{S}_\alpha$ asymptotic functions subspace, there is a corresponding scattering state given by the corresponding Möller operator:

$$\forall \, |\psi_{in} > \in \mathcal{S}_\alpha \; \exists |\psi > \;\; | \; e^{-i\hat{H}t}|\psi > \to e^{-i\hat{H}^\alpha t}|\psi_{in} >$$
$$|\psi > = \Omega_+^\alpha |\psi_{in} >$$

These new Möller operators are, as the former, isometric operators that map the $\mathcal{S}_\alpha$ functions onto the scattering states space.

Concerning the orthogonality, it can be proven that all the subspaces of scattering states with incoming asymptotes belonging to different channels are orthogonal and, at the same time, are orthogonal as well to the bound states subspace.

$$\mathcal{B} \perp \mathcal{R}_+^\alpha \perp \mathcal{R}_+^{\alpha'}$$

The generalization of the asymptotic completeness theorem establishes that the direct sum of all the spaces of states with incoming asymptote belonging to any channel is coincident with that of the spaces of states with outgoing asymptote belonging to any channel. Furthermore, the sum of this subspace to that of the bound states generates the whole Hilbert space.

$$\mathcal{R} = \mathcal{R}_{1+} \oplus \cdots \oplus \mathcal{R}_{n+} = \mathcal{R}_{1-} \oplus \cdots \oplus \mathcal{R}_{n-} \; ; \; \mathcal{H} = \mathcal{B} \oplus \mathcal{R}$$

For the most general case of multichannel scattering, an orbit ought to be considered so that its incoming asymptote would be a linear combination of all the n channels asymptotic functions,

$$|\psi_{in} > = \left\{|\psi_{in}^0 >, ..., |\psi_{in}^n > \right\} \; ; \; |\psi_{in} > \in \mathcal{H}_{as} = \mathcal{S}^0 \oplus \cdots \oplus \mathcal{S}^n$$

the state at $t = 0$ would then be expressed as:

$$|\psi > = \Omega_+^0 |\psi_{in}^0 > + ... + \Omega_+^n |\psi_{in}^n >$$

In practice, however, initial conditions are selected so that there is only a single asymptote on a channel and only the scattering on a single channel is measured resulting

$$|\psi_{in} > = \{0, ..., |\varphi >, ..., 0\} \;\;\; ; \;\; |\varphi > \in \mathcal{S}_\alpha$$
$$|\psi_{out} > = \{0, ..., |\varphi' >, ..., 0\} \;\;\; ; \;\; |\varphi' > \in \mathcal{S}_{\alpha'}$$

2.5. Multichannel Scattering

The scattering state is then written as $|\psi> = \Omega_+^\alpha |\varphi>$ and $|\psi> = \Omega_-^{\alpha'} |\varphi'>$ and the probability for the system to evolve from a φ asymptote in channel α to a φ' asymptote in channel α' is:

$$\omega\left(\varphi'\alpha' \leftarrow \varphi\alpha\right) = \left|<\varphi'|\left(\Omega_-^{\alpha'}\right)^T \Omega_+^\alpha |\varphi>\right|^2 \tag{2.43}$$

Since $\mathcal{H}_{as}$ is the direct sum of each channel asymptotic functions subspaces, $\mathcal{S}_\alpha$, we can obtain a basis set for this space combining the basis sets of each subspace. Thus, since the $|\vec{p}, \alpha>$ vectors are an orthonormal basis set for $\mathcal{S}_\alpha$, then the set of vectors

$$\{0, ..., 0, |\mathbf{p}, \alpha>, 0, ...0\} \quad \alpha = 0, ..., n \; ; \; \forall \mathbf{p}$$

is an orthonormal momentum basis set for $\mathcal{H}_{as}$. From now on we will assume the following abbreviation:

$$\{0, ..., 0, |\mathbf{p}, \alpha>, 0, ...0\} \equiv |\mathbf{p}, \alpha> \quad , \quad <\mathbf{p}, \alpha|\mathbf{p}', \alpha'> = \delta_{\alpha\alpha'}\delta(\mathbf{p} - \mathbf{p}')$$

It can be seen[3] that the S matrix under this representation is of the form:

$$<\mathbf{p}', \alpha|S|\mathbf{p}, \alpha> = \delta_{\alpha\alpha'}\delta(\mathbf{p}'-\mathbf{p}) - \frac{i}{2\pi m}\delta(E-E')\delta_3(P'-P)f\left(\vec{p}'\alpha' \leftarrow \vec{p}\alpha\right) \tag{2.44}$$

where $\mathbf{p}$ represents the n_α linear momenta, P is the center of mass linear momentum and $\vec{p}$ represents the $n_\alpha - 1$ relative linear momenta.

The stationary scattering states are obtained for the multichannel case in a similar way as performed previously (see section 2.3):

$$\begin{aligned}
|\vec{p}\alpha\pm> &= \Omega_\pm^\alpha |\vec{p}\alpha> \\
\hat{H}|\vec{p}\alpha\pm> &= \hat{H}\Omega_\pm^\alpha |\vec{p}\alpha> = \Omega_\pm^\alpha \hat{H}^\alpha |\vec{p}\alpha> = E_p^\alpha |\vec{p}\alpha\pm>
\end{aligned} \tag{2.45}$$

For the elastic and inelastics collisions, the stationary states wavefunction is usually expanded in terms of target states, $\varphi_\alpha(x_{tar})$. As an example let's consider the channel 1 of the above example. The Hamiltonian can be then partitioned as $\hat{H} = \hat{H}^1 + \hat{V}^1$, where

$$\hat{H}^1 = \frac{\hat{\vec{p}}_a^2}{2m_a} + \hat{H}_{(bc)}$$

From this expression, where the Hamiltonian contains two independent terms, it appears clearly that the following products can be used as eigenfunctions of $\hat{H}^1$,

$$\frac{1}{(2\pi)^{3/2}}e^{i\vec{p}\vec{x}_a}\varphi_\alpha(x_b)$$

where $\varphi_\alpha(x_b)$ labels any eigenfunction of $\hat{H}_{(bc)}$ with corresponding eigenvalue, E_α. These states can be of two types, for there will be n bound states, and also the continuum states, where the diatomic bc molecule dissociates. So, for a general

channel λ, the stationary states wavefunction can be expanded in the following form:

$$< \vec{x}, x_{tar} | \vec{p}, \lambda+ >= \int_\alpha \sum_\alpha \eta_\alpha(\vec{x}) \varphi_\alpha(x_{tar}) \tag{2.46}$$

where the summation and integral signs indicate that their combination includes all the bound and continuum target states and where η_α is responsible for the asymptotic form when r becomes infinity:

$$\eta_\alpha \to \frac{1}{(2\pi)^{3/2}} \left[e^{i\vec{p}\cdot\vec{x}} \delta_{\alpha 1} + f(p_\alpha \hat{x} \leftarrow p1) \frac{e^{ip_\alpha r}}{r} \right] \tag{2.47}$$

taking into account the Hamiltonian factorization ($\hat{H} = \hat{H}^\lambda + \hat{V}^\lambda$), substituting 2.46 into the Schrödinger equation , multiplying by $\varphi_\alpha^*(x_{tar})$ and integrating over all internal coordinates one obtains:

$$\frac{-\nabla^2}{2m} \eta_\alpha(\vec{x}) + \int_\alpha \sum_\alpha \overline{V}_{\alpha\alpha'}(\vec{x}) \eta_{\alpha'}(\vec{x}) = (E - E_\alpha) \eta_\alpha(\vec{x}) \tag{2.48}$$

where $\overline{V}_{\alpha\alpha'}(\vec{x}) = \int dx_{tar} \varphi_\alpha^*(x_{tar}) V^\lambda(\vec{x}, x_{tar}) \varphi_{\alpha'}(x_{tar})$.

An infinite and continuous set of coupled integrodifferential equations is obtained. If one eliminates the continuum target states from the expansion, one obtains the *close coupling (CC) equations*. This approximation is valid for energies below the diatomic dissociation limit, which is always the case, for the present work:

$$\left[\frac{-\nabla^2}{2m} + \overline{V}_{\alpha\alpha} - (E - E_\alpha) \right] \eta_\alpha(\vec{x}) = - \sum_{\alpha' \neq \alpha} \overline{V}_{\alpha\alpha'}(\vec{x}) \eta_{\alpha'}(\vec{x}) \tag{2.49}$$

Each of the so-called radial functions η_α satisfies a single-body Schrödinger equation in which the potential term couples all solutions together.

Briefly, the close coupling equations then have been established in a formal rather than practical way. The goal of the following sections will be to establish a more practical formulation of these equations for the triatomic case, where an atom collides with a diatomic molecule. This will be achieved exploiting firstly the fact that total angular momentum of the system is conserved. This will allow us to expand the wavefunction in terms of the $\hat{J}^2$ operator eigenfunctions, where $\vec{J}$ is the total angular momentum. This will lead to a *partial wave expansion* similar to that obtained in section 2.4. Then, an expansion in terms of the target bound eigenstates of the diatomic molecule will render a more practical formulation of the close coupling equations. Let's begin then by expressing the conservation of the total angular momentum as the commutation of its operator with the system Hamiltonian:

$$\left[\hat{H}, \hat{J}^2 \right] = 0 \tag{2.50}$$

so that the global wavefunction can be expressed as:

$$\Psi(\vec{x}, x_{tar}) = \sum_{J=0}^{\infty} c_J \psi_J(\vec{x}, x_{tar}) \qquad (2.51)$$

However, in order to build an expression of the close coupling equations that can be numerically solved, we will need to express the wavefunction and the Hamiltonian in an adequate coordinate system. This will be the subject of the following chapters, although we will first consider some other cases which will prove of interest later on.

2.6 Collinear inelastic scattering

The practical formulation of the close-coupling equations can be a cumbersome task when considered in its full dimensionality, even for the atom+diatom case. For this reason, we begin by considering a reduced dimensionality treatment, which nevertheless contains all the essentials that we need[4]. This reduction in dimensionality is obtained by forcing the system to move exclusively along the axis defined by the diatomic molecule, i.e. considering only collinear geometries.

The collinear collision for an atom and a diatomic molecule was studied by Jackson and Mott, as early as 1932, as a model for the exchange of energy in the collision between an atom and a solid surface. A landmark paper in 1966 by Secrest and Johnson provided the first exact quantum mechanical results for inelastic collisions and allowed comparison with earlier classical, semi-classical and approximate quantum mechanical results. In this section we will give a brief outline on the Secrest-Johnson treatment.

In this model it is assumed that an atom A interacts along the x axis with a harmonic diatomic oscillator BC of force constant k. The corresponding Hamiltonian, under the collinear restriction, is as follows:

$$\hat{H} = -\frac{\hbar^2}{2m_A}\frac{\partial^2}{\partial x_A^2} - \frac{\hbar^2}{2m_B}\frac{\partial^2}{\partial x_B^2} - \frac{\hbar^2}{2m_C}\frac{\partial^2}{\partial x_C^2} + \frac{k}{2}(x_{BC} - x_{BC}^0)^2 + V_{A-BC} \qquad (2.52)$$

where $x_{BC} = x_B - x_C$, and x_{BC}^0 is the equilibrium bond length of BC. By transferring to a center-of-mass coordinate system, where:

$$
\begin{aligned}
X_{CM} &= \frac{x_A m_A + x_B m_B + x_C m_C}{M} \\
X &= x_A - \frac{x_B m_B + x_C m_C}{m_B + m_C} \\
Y &= x_B + x_C \\
M &= m_A + m_B + m_C
\end{aligned}
\qquad (2.53)
$$

the Hamiltonian becomes

$$\hat{H} = \frac{-\hbar^2}{2M}\frac{\partial^2}{\partial X_{CM}^2} - \frac{-\hbar^2}{2\mu}\frac{\partial^2}{\partial X^2} - \frac{-\hbar^2}{2\mu_{BC}}\frac{\partial^2}{\partial Y^2} + \frac{k}{2}(Y - Y^0)^2 + V_{A-BC} \qquad (2.54)$$

where

$$\mu = \frac{m_A(m_B + m_C)}{M}, \quad \mu_{BC} = \frac{m_B m_C}{m_B + m_C} \qquad (2.55)$$

Since the center of mass motion is conserved, one can neglect the first term in 2.54. On the other hand, the interaction potential V_{A-BC} couples the X and Y motions. Moreover, if this was a function only of X, then even the X and Y motions would be uncoupled. More realistically, for the case of an atom A colliding collinearly to a an AB diatom from the B side, the interaction potential can be viewed as a function, by now still undetermined, of the $A - B$ distance. This latter distance, in terms of the relative X and Y coordinates, is:

$$x_A - x_B = X - \frac{m_C Y}{m_B + m_C} \qquad (2.56)$$

The diabatic basis expansion, in terms of the target states, that will lead to the corresponding close coupling equations, can be done using the harmonic oscillator eigenfunctions

$$\Psi(X, Y) = \sum_j \psi_j(X)\chi_j(Y) \qquad (2.57)$$

where

$$\chi_j(Y) = \left[\frac{k^{1/4}\mu_{BC}^{1/4}}{\hbar^{1/2}\pi^{1/2}2^j j!}\right]^{1/2} H_j(Q)e^{-Q^2/2} \qquad (2.58)$$

and

$$Q = \left(\frac{k\mu_{BC}}{\hbar^2}\right)^{1/4}(Y - Y^0) \qquad (2.59)$$

being $H_i(Q)$ the Hermite polynomials. The basis set eigenvalues are

$$E_j^0 = \left(\frac{\hbar^2 k}{\mu_{BC}}\right)^{1/2}\left(j + \frac{1}{2}\right) \qquad (2.60)$$

The close coupling equations using this basis take the form

$$\left[-\frac{\hbar^2}{2\mu}\frac{d^2}{dX^2} + E_i^0 - E + V_{ii}(X)\right]\psi_i(X) + \sum_{j \neq i} V_{ij}(X)\psi_j(X) = 0 \qquad (2.61)$$

where

$$V_{ij}(X) = \frac{1}{(2^{i+j}\pi i! j!^{1/2})} \times \qquad (2.62)$$

$$\times \int_{-\infty}^{\infty} H_i(Q)H_j(Q)e^{-Q^2}V\left(X - \frac{m_C Y^0}{m_B + m_C} - \epsilon Q\right)dQ$$

and

$$\epsilon = \frac{m_C}{m_B + m_C} \left(\frac{\hbar^2}{k\mu_{BC}}\right)^{1/2} \tag{2.63}$$

The coupled set of second-order differential equations in 2.61 depend only on one variable and can therefore be solved using the standard numerical techniques available for the ordinary differential equations. These are usually propagative techniques which involve integration outwards from $X = 0$ or, in practice, a value of X where the $A - BC$ repulsive potential energy is high enough for all the channel wavefunctions to be considered as zero. To start this integration one must specify initial values for the derivatives $\psi_i'(0)$.

The multichannel equations must be integrated outwards to a large enough value of X so that all elements of the potential energy matrix can be neglected, which means that the potential V dies off at sufficiently large distances. At this point the equations have the form

$$\left(-\frac{\hbar^2}{2\mu}\frac{d^2}{dX^2} + E_i^0 - E\right)\psi_i(X) = 0 \tag{2.64}$$

The general solutions of these equations, which are therefore the asymptotic solutions to 2.61, can be derived analytically:

$$\psi_i(X) \sim A_i e^{ik_i X} + B_i e^{-ik_i X} \tag{2.65}$$

where

$$k_i = \left[\frac{2\mu(E - E_i^0)}{\hbar^2}\right] \tag{2.66}$$

are called channel wave numbers. From 2.66 we see that if $E > E_i^0$, the channel wave numbers are real and it is possible for the system to emerge from the scattering event in the i channel; these are called *open channels*. On the other hand, whenever $E < E_i^0$ the corresponding channel wave number is positive (by convention) imaginary and the system is not physically capable of emerging in the i channel; we say these are *closed channels*.

Thus, for the closed channels one must impose a $B_i = 0$ boundary condition, otherwise the asymptotic form 2.65 would be an exponentially increasing function of X. This must be imposed to ensure that closed channels are not present at the asymptotic limit.

If we are looking for a wavefunction that, under the stationary states framework, represents the system in an initial internal state i, emerging in final states j (open channels), we then write the jth component of the wavefunction as

$$\psi_j(X) \sim \delta_{ij} e^{-ik_i X} - S_{ji}\left(\frac{k_i}{k_j}\right)^{1/2} e^{ik_j X} \tag{2.67}$$

where the coefficients S_{ij} are the elements of the S-matrix and its square modulus represents the probability density for the system entering collision with incoming asymptote ψ_i to leave the collision with outgoing asymptote ψ_j. Introducing the factors $\left(\frac{k_i}{k_j}\right)^{1/2}$ this probability is converted to a flux. The S_{ij} are evidently related to the coefficients in 2.65 (see Appendix A).

2.7 The Optical Potential.

In section 2.5 we have seen that an expansion of the full wavefunction of the collision process in terms of target eigenstates as

$$\int \sum_{\alpha} \eta_{\alpha}(x)\phi_{\alpha}(x_{tar}) \qquad (2.68)$$

converts the original many-body problem into an infinite set of coupled one-body equations. In the same section we have seen that it is a generally valid approximation to retain the first N terms of this expansion, which correspond to the first N eigenstates of the target's discrete spectrum. However, it could be the case where we would be interested in a certain subset of N' (obviously $N > N'$) channels, where it would no longer be a good approximation to simply ignore all the other η_{α} to which our subset is coupled.

In this section we shall outline how, for any given choice of N' channels, it is formally possible to define an operator V_{opt}, called the *optical potential*, so that the N' wavefunctions $\eta_{\alpha}(x)$ exactly satisfy N' coupled equations with a potential matrix given by V_{opt} (for proof see Appendix B or, alternatively, [5]). This will establish the formal basis to introduce the complex absorbing potentials which are one of the main scopes of the body of the work presented, particularly its implementation in an invariant embedding propagation technique.

As an example, let's consider the case of $N = 1$; that is, we consider just the wavefunction $\eta_1(x)$ which will then describe the elastic scattering in channel 1. One can define a one-particle operator[3], V_{opt} so that $\eta_1(x)$ exactly satisfies the following one-particle equation:

$$\left(\frac{\hbar}{2\mu}\nabla^2 + V_{opt}\right)\eta_1(x) = (E - E_1)\eta_1(x) \qquad (2.69)$$

with the corresponding one-channel boundary condition,

$$\eta_1(x) \to \frac{1}{2\pi}^{3/2}\left(e^{i\mathbf{k}\cdot\mathbf{r}} + f_{11}\frac{e^{ikr}}{r}\right) \qquad (2.70)$$

and the inelastic scattering is exactly reduced to an equivalent one-channel problem.

Obviously, such an astonishing simplification of the multichannel problem must have a price to pay. The price is the knowledge of the optical potential which is a generally extremely complicated operator. In particular, it is nonlocal, energy-dependent, and, for energies above the first inelastic threshold, it is not Hermitian. This last characteristic is what one should expect ; if the Hamiltonian were Hermitian, the corresponding evolution operator would be unitary. This would mean that solutions of the corresponding time dependent Schrödinger equation would have constant norm or, equivalently, that the stationary wavefunction would have equal incoming or outgoing fluxes. This situation would not allow for loss of flux due to inelastic processes. Nevertheless, if inelastic processes occur (i.e. if E is above the inelastic threshold) and we are describing only the elastic scattering using an optical potential, then the Hamiltonian has to be non-Hermitian.

One can actually take profit from this property since, by calculating the flux loss in the elastic calculation, one can indirectly obtain the flux towards inelastic scattering. So, if one would be interested in knowing the inelastic flux regardless of the specific outgoing state and the corresponding V_{opt} would be at hand, it would be a particular advantageous thing to do, to perform just the elastic scattering calculation and attribute the loss of flux to the inelastic process. It has to be stressed that this would lead to a state-to-all information of the inelastic process. This, which might seem rather excentric for the inelastic case, could be, on the other hand, of great advantage for reactive processes in which one would just be interested in state-to-all magnitudes (e.g. cross sections) or directly the rate constant. For such processes one would be able to constrain the calculation to a much simpler inelastic (and elastic) scattering one by means of a non-hermitian Hamiltonian where the V_{opt} would have been included and assign finally the flux loss to the reactive event.

We would like to point out that this methodology could perfectly be included in the family of effective potential methods, not necessarily complex. To this family belong very well-known methods as Hartree-Fock or Kohn-Sham, for the calculation of molecular systems electronic structure, where non local potentials appear explicitly.

2.7.1 Approaches to the calculation of V_{opt}

Unfortunately, the optical potential is in practice far too complicated for an exact calculation of it. Rather, the importance of what we have shown lies in the knowledge of its existence, since it provides a reliable basis for the development of approximate calculations of these optical potentials.

The first estimations of optical potentials were performed in the field of Nuclear Physics in the 50s[6]. They dealt essentially with the elastic scattering at energies where inelastic and/or reactive channels were as well accessible. Concerning its application to scattering processes in molecular systems, two rather

well different stages might be distinguished.

The first, covers approximately a period from 1965 to 1985, and focused its activity in elastic processes, this is, solving the close coupling equations for a single term[7, 8].

On one hand, formal developments dealt with well-known problems associated with the use of NIPs as, for instance, the non-locality of the potential[9]. Adiabatic and decoupling approximations were also taken into account to simplify the dimensionality of the problem[10]. Among other relevant works, that of Wolken[11] can be pointed out, who devised a procedure for, given a numerically solved problem, extracting that optical potential which allowed reproducing a desired S-matrix subset. This method was subsequently used by Truhlar and coworkers[12] to study electron-atom collisions. The main results found were that the sharp variations of the optical potential, found when the radial wavefunction has a node, could be smoothed without significantly altering the results. On the other hand, phenomenological approaches were also adopted for the form of the NIP. Different *ad hoc* functional forms with adjustable parameters were used by Marriot and Micha[13], Micha and Rotenberg[14] and Ross and cols.[15], to successfully reproduce experimental information on elastic data by means of parameterizing the absorption as a function of the orbital angular momentum. Although some insights on the elastic behaviour of collisions in the presence of inelastic and reactive phenomena were obtained, no systematic procedure became available and the use of adjustable parameters limited its predictive capability.

The second stage which we distinguish in the development of the optical potentials application to molecular systems begins in 1986, when Kosloff and coworkers[16] considered the problem of artificial back-reflection of wavepackets. This back-reflection usually takes place at the boundaries of the point grid defined on the configuration space for time-dependent wavepacket propagations. They proposed the use of empirical forms of negative imaginary potentials (NIP) to solve this problem. In fact, it can be actually proven that a purely imaginary potential absorbs or creates flux associated to a stationary wavefunction according to whether this potential is negative or positive (see appendix C). This idea was adopted by Neuhauser and Baer[17], and they used it to propose a linear NIP ramp as a functional form that would allow perfect absorption conditions of the wavepacket.

Shortly after, an extension of this idea allowed a wide spreading of the imaginary potentials on the study of chemical reactivity. The authors[18, 19] proposed to place the NIP, not at the limits of the grid but *right after the transition state region, at the beginning of the products arrangement channel.* This change in the NIP position allowed to consider that all the absorbed flux was that flowing towards products. As the authors claim in their article, one has to consider that the probability flux that yields purely reactive transitions is that measured once well crossed the transition state region. If this is accomplished, we are able to have just the inelastic (and elastic) component of the scattered wavefunction treated

2.7. The Optical Potential.

exactly using a local, less energy- and system- dependent imaginary potential. This results therefore in a rather simple and easy to implement approximation to the optical potential.

The characteristic that differentiates the present approach from the previous phenomenological derivations of optical potentials is that, in principle, the reactive flux is completely apart from the inelastic and elastic ones, i.e., it takes place in a different region of configuration space. So, a complex potential as a function of physical coordinates will be able to select the reactive component from the rest in the total flux. We can then study the reactive collision as a distorted inelastic process where the NIP is placed in the products rearrangement entrance. Like this, using inelastic scattering propagative techniques, generalized to take complex valued interaction matrices into account (see section 4.4 and chapter 8), the corresponding inelastic probabilities are calculated and subtracting the sum of these to unity one obtains reactive state-to-all probabilities. We stress the fact that these are global probabilities, this means only state-to-all magnitudes can be obtained through this methodology, as presently formulated.

The major methodological improvement of this approach relies on the fact that almost no attention must be paid to the products arrangement characteristics. This turns into a much simpler choice of coordinates and therefore the possibility of using much simpler Hamiltonians. Moreover, the configuration space is approximately halved with the corresponding saving in integration time. On the other hand the technique presents basically two disadvantages: Firstly, as it has been derived here, the method is not capable of yielding state-to-state reaction probabilities. Secondly, the calculation becomes involved from the numerical point of view, because of the complex valued nature of the potential instead of being real-valued, as usual. Nevertheless, we claim the advantages of the application clearly overcome its disadvantages when dealing with the calculation of global magnitudes such as state-to-all integral cross sections and, to a major extent, reaction rates.

Different methods employing NIPs have recently proposed in the literature. Among them, we would like to point out that by Manthe, Seideman and Miller[20], that calculates the cumulative reaction probability using NIPs on both reactants and products arrangement channels. The total flux is then obtained averaging according to a Boltzmann distribution to yield directly the reaction rate. The main advantage of this method is that rate constants are readily obtained sampling a comparatively small part of configuration space. In particular, just a small portion before and after the transition state has to be included to achieve rate constant (i.e. cumulative reaction probability) convergence.

Baer and coworkers have continued developing the method originally proposed by them. In particular, they have extended it to the calculation of state-to-state probabilities[17] by means of a generalized variational procedure.

Chapter 3

The accurate description of the Reactive System

Contents

In the previous chapter we have settled the basis for the quantum mechanical description of the reactive event. Finally, a rather practical formulation of the *close coupling* equations has been presented, but still in terms of two general variables, $\vec{x}$ and x_{tar}. It is now turn to give these variables an expression, to choose the coordinate system in which we will express the wavefunction and the Hamiltonian.

3.1 Electrons - nuclei system

The Quantum Mechanical study of collision processes essentially consists in the description of an n-electron and N-nuclei system. Such system will be univocally

described at a given instant t by its associated wavefunction, Ψ. The evolution of the system will be governed by the corresponding time-dependent Schrödinger equation :

$$\hat{H}\Psi(\mathbf{r},\mathbf{R},t) = i\hbar\frac{\partial}{\partial t}\Psi(\mathbf{r},\mathbf{R},t) \qquad (3.1)$$

where the wavefunction is a function of all electronic ($\mathbf{r}$) and nuclear coordinates ($\mathbf{R}$) as well as time. If one does not consider relativistic effects, one can write the system Hamiltonian ($\hat{H}$) as the sum of the nuclear and electronic kinetic energy operators and the operators describing the interaction between them. Therefore, the corresponding time independent Schrödinger equation will be

$$[T_N(\mathbf{R}) + T_e(\mathbf{r}) + V_{NN}(\mathbf{R}) + V_{Ne}(\mathbf{R},\mathbf{r}) + V_{ee}(\mathbf{r})]\,\Psi(\mathbf{R},\mathbf{r}) = E\Psi(\mathbf{R},\mathbf{r}) \qquad (3.2)$$

where $T_N(\mathbf{R})$, $T_e(\mathbf{r})$ are respectively the nuclear and electronic kinetic energy operators, $V_{NN}(\mathbf{R})$ is the electrostatic repulsion between the nuclei, $V_{Ne}(\mathbf{R},\mathbf{r})$ represents the electron - nuclei interaction and $V_{ee}(\mathbf{r})$ is the electronic repulsion.

The fact that the Hamiltonian contains a Coulombic interaction term between nuclei and electrons, therefore mixing nuclear and electronic coordinates,

$$V_{Ne} = \sum_{i=1}^{n}\sum_{k=1}^{N}\frac{z_k}{|r_i - R_k|} \qquad (3.3)$$

does not allow the construction of a global wavefunction as the product of two functions, each one depending on either one or the other type of coordinates.

However, attempts have been made to express the global wavefunction on a basis that differentiates electronic and nuclear functions.

3.1.1   Adiabatic representation. Born - Oppenheimer App.

The common concept of a Potential Energy Surface arises from the recognition that in a molecule the motion of electrons is much faster than that of the nuclei since masses are so different but charges much more comparable, and therefore these two types of motion can be in a fairly accurate way separated. We could think of the electrons as being subject to a electrostatic field created by stationary nuclei. On the other hand, the nuclei would be subject to a potential which is the sum of the nuclear repulsion and the average field due to the electrons.

It is a strictly rigorous approach to expand the system global wavefunction as the linear combination of direct products of a complete basis of electronic functions, $\{\varphi_j(\mathbf{r})\}$ and a nuclear functions basis set:

$$\Psi(\mathbf{R},\mathbf{r}) = \sum_{ij}\chi_i(\mathbf{R})\varphi_j(\mathbf{r}) \qquad (3.4)$$

However, this would not be very efficient, since a much higher number of electronic functions would be needed than if we would use another electronic functions basis

3.1. Electrons - nuclei system

set $\{\Phi_j(\mathbf{r}; \mathbf{R})\}$, this parametrically dependent on the nuclear coordinates and the nuclear wavefunction, χ.

$$\Psi(\mathbf{R}, \mathbf{r}) = \sum_j \chi_j(\mathbf{R})\Phi_j(\mathbf{R}, \mathbf{r}) \tag{3.5}$$

The parametric introduction of the nuclear coordinates in the electronic functions allows to optimize the basis size even if it then implies a different, in principle, electronic basis set for each nuclear configuration. These functions $\Phi_j(\mathbf{R}, \mathbf{r})$ are solution of the electronic Schrödinger equation :

$$[T_e(\mathbf{r}) + V_{Ne}(\mathbf{R}, \mathbf{r}) + V_{ee}(\mathbf{r})]\Phi_j(\mathbf{R}, \mathbf{r}) = W_j(\mathbf{R})\Phi_j(\mathbf{R}, \mathbf{r}) \tag{3.6}$$

This equation describes the motion of the electronic system for a given nuclear configuration, $\mathbf{R}$. Introducing the expansion 3.5 into equation 3.2, considering 3.6, pre-multiplying by Φ_i and integrating over all electronic coordinates leads to the following expression[21]:

$$[T_N + U_i(\mathbf{R}) - E]\chi_i(\mathbf{R}) + \sum_j c_{ij}(\mathbf{R}, \mathbf{P})\chi_j(\mathbf{R}) = 0 \tag{3.7}$$

where $U_i = W_i + V_{NN}$ is the potential energy function for the i state and the so called *non adiabatic coupling terms*, c_{ij} are

$$c_{ij}(\mathbf{R}, \mathbf{P}) = \sum_k \frac{1}{M_k}\left(A_{ij}^{(k)} \cdot \mathbf{P}_k + B_{ij}^{(k)}\right) \tag{3.8}$$

The operator $\mathbf{P}_k$ is the nuclear momentum operator, M_k the mass of each nuclei and the terms A_{ij}, B_{ij} represent

$$A_{ij}^{(k)}(\mathbf{R}) = \int \Phi_i^\star(\mathbf{R}, \mathbf{r})\left(\frac{-ih}{2\pi}\nabla_k\right)\Phi_j^\star(\mathbf{R}, \mathbf{r})d\tau_{el} \tag{3.9}$$

$$B_{ij}^{(k)}(\mathbf{R}) = \int \Phi_i^\star(\mathbf{R}, \mathbf{r})\left(\frac{-h^2}{8\pi^2}\nabla_k^2\right)\Phi_j^\star(\mathbf{R}, \mathbf{r})d\tau_{el} \tag{3.10}$$

For a stationary state the electronic wavefunction can be chosen as a real function and therefore the diagonal A_{ii} term can be set to zero and equation 3.7 is then rewritten:

$$[T_N + U_i(\mathbf{R}) + B_{ii}(\mathbf{R}) - E]\chi_i(\mathbf{R}) = -\sum_{j \neq i} c_{ij}(\mathbf{R}, \mathbf{P})\chi_j(\mathbf{R}) \tag{3.11}$$

Generally the coupling terms are only important between a small group of states $\{\Phi_j\}$, so that the expansion can be then truncated to a smaller electronic basis. It can then be said that equation 3.11 is the nuclear Schrödinger equation .

In the *adiabatic approximation*, the coupling terms c_{ij} are taken as zero and then equation 3.11 turns into

$$[T_N + U_i(\mathbf{R}) + B_{ii}(\mathbf{R}) - E]\chi_i(\mathbf{R}) = 0 \tag{3.12}$$

Chapter 3. The accurate description of the Reactive System

The Born-Oppenheimer Approximation

The well-known and commonly used *Born-Oppenheimer approximation* is a particular case of this adiabatic approximation. Consider the Schrödinger equation for the global electrons-nuclei system (3.2). The Born-Oppenheimer approximation goes a step further in the adiabatic representation and the wavefunction, Ψ, is rewritten as the product of *one* electronic wavefunction depending parametrically on the nuclear configuration and another nuclear wavefunction:

$$\Psi_i(\mathbf{R},\mathbf{r}) = \chi_i(\mathbf{R})\Phi_i(\mathbf{R},\mathbf{r}) \tag{3.13}$$

Note the difference between this approximation and the rigorous basis expansion of the adiabatic representation in equation 3.5, this arises from the fact of expressing the wavefunction as a *single* product instead of the former adiabatic basis expansion. As in the previous case, the electronic wavefunction is solution of 3.6, the electronic Schrödinger equation. At its turn, $\chi_i(\mathbf{R})$ will be the solution of:

$$[T_N + U_i(\mathbf{R}) - E]\chi_i(\mathbf{R}) = 0 \tag{3.14}$$

where $U_i(\mathbf{R}) = V_{NN}\mathbf{R}) + W_i(\mathbf{R})$ is known as the *Potential Energy Surface (PES)*. Notice that 3.14 differs from 3.12 only in the small adiabatic correction term, $B_{ii}(\mathbf{R})$.

To realize to which extent the assumption in 3.13 is valid, let's introduce the expression into 3.2 (the index i being dropped for the sake of clarity):

$$[T_N(\mathbf{R}) + T_e(\mathbf{r}) + V_{NN}(\mathbf{R}) + V_{Ne}(\mathbf{R},\mathbf{r}) + Vee(\mathbf{r})]\,\Phi(\mathbf{R},\mathbf{r})\chi(\mathbf{R}) = \tag{3.15}$$
$$= E\Phi(\mathbf{R},\mathbf{r})\chi(\mathbf{R})$$

Considering the form of the nuclear kinetic energy operators:

$$T_N(\mathbf{R}) = \frac{-\hbar^2}{8\pi^2}\sum_k \frac{1}{M_k}\nabla_k^2 \tag{3.16}$$

where k runs over all nuclei. The application of operator 3.16 to the previous expression of the wavefunction yields:

$$T_N(\mathbf{R})\Phi(\mathbf{R},\mathbf{r})\chi(\mathbf{R}) = \Phi(\mathbf{R},\mathbf{r})\left[\frac{-\hbar^2}{8\pi^2}\sum_k \frac{1}{M_k}\nabla_k^2\chi(\mathbf{R})\right] \tag{3.17}$$
$$+\chi(\mathbf{R})\left[\frac{-\hbar^2}{8\pi^2}\sum_k \frac{1}{M_k}\nabla_k^2\Phi(\mathbf{R},\mathbf{r})\right]$$
$$-\frac{-\hbar^2}{8\pi^2}\sum_k \frac{1}{M_k}\{\nabla_k\Phi(\mathbf{R},\mathbf{r})\}\{\nabla_k\chi(\mathbf{R})\}$$

Considering this expression in 3.6, it can be seen[21] that equation 3.15 transforms into 3.14 only when

$$\chi(\mathbf{R})\left[\frac{-\hbar^2}{8\pi^2}\sum_k \frac{1}{M_k}\nabla_k^2\Phi(\mathbf{R},\mathbf{r})\right] - \frac{-\hbar^2}{8\pi^2}\sum_k \frac{1}{M_k}\{\nabla_k\Phi(\mathbf{R},\mathbf{r})\}\{\nabla_k\chi(\mathbf{R})\} = 0 \tag{3.18}$$

Usually this terms can be neglected and therefore the approximation is valid. For example, the first term contains the second derivatives of Φ with respect to the nuclear coordinates. These will be of the same order of magnitude as the derivative with respect to the electronic ones. However, while the $T_e\Phi$ is of the same order of magnitude as the energy of one of the electrons, this term will then be of the order of $\frac{m}{M_k}$ and therefore negligible (m being the mass of the electron).

Among the work being done recently on non adiabatic transitions, i.e., processes where the Born Oppenheimer approximation breaks down, stress has been put on lately on those transitions caused by spin-orbit coupling. These have appeared to be of a greater relevance than expected since, for instance, reaction barriers had to be modified, when including the spin orbit interaction, in very accurate calculations on both the PES and the dynamics of the $F + H_2 \rightarrow FH + H$ system[22].

3.1.2 Diabatic representation

Let's return to the complete basis expansion in 3.5. Whatever linear combination of the adiabatic basis functions is used, it would not lead to any alteration of the global wavefunction, Ψ. Consider then a basis change that eliminates the A_{ij}, B_{ij} (equations 3.9 and 3.10) couplings between electronic states. Such a process is known as diabatization and the resulting basis set is correspondingly called *diabatic basis*. Obviously, the electronic Hamiltonian would not longer be diagonal under this representation and its off-diagonal terms would represent the new couplings.

3.2 Jacobi coordinates

From here on, we will assume the validity of the Born-Oppenheimer approximation. We are going to study then the nuclear Schrödinger equation, so we therefore need to specify the set of nuclear coordinates$\{\mathbf{R}\}$ on which the nuclear wavefunction depends. The number of coordinates needed for the complete description of a N-particle system is $3N$. Considering that our study will concern the motion and rearrangement of 3 nuclei ($A + BC$ case), we can specify the position of the three particles A, B and C using three position vectors of common origin in a laboratory fixed frame, $\vec{r}_A$, $\vec{r}_B$ and $\vec{r}_C$.

A first rigorous simplification can be performed by separating the motion of the center of mass from the relative motion between the particles. This is done introducing the vector:

$$\vec{CM} = \frac{m_A\vec{r}_A + m_B\vec{r}_B + m_C\vec{r}_C}{m_A + m_B + m_C} \qquad (3.19)$$
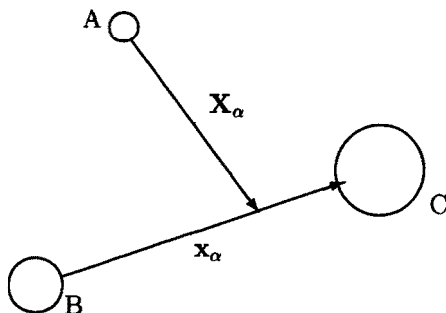
Figure 3.1: Mass-scaled Jacobi coordinate for the α arrangement

Thus, the nuclear wavefunction can be factorised in a part depending exclusively on $\vec{CM}$, which is simply a free particle wavefunction, and another part depending on all the other internal degrees of freedom. This last part could be expressed, for example, in terms of internuclear distances. However, this choice would lead to a non-diagonal kinetic energy tensor and therefore great complications in the calculations.

The Jacobi vectors[23] show up to be a proper choice to overcome the problem of the mixed derivative, being as well still tightly related the physical situation of the process and therefore have become a coordinate set of great relevance.

Let's consider the Jacobi vectors for a three particle-system (A,B,C) and in particular, those related to the arrangement $\alpha = A + BC$ (figure 3.1):

$$\vec{X}_\alpha = \vec{r}_A - \frac{m_B \vec{r}_B + m_C \vec{r}_C}{m_B + m_C} \tag{3.20}$$

$$\vec{x}_\alpha = \vec{r}_C - \vec{r}_B \tag{3.21}$$

where α indicates the particular arrangement, $\vec{x}_\alpha$ is the internuclear vector joining B and C, and $\vec{X}_\alpha$ is the vector joining the center of mass of the molecule BC to atom A. Note that this procedure is completely general for the n-particle case since the internal coordinates of n bodies can always be expressed in terms of $n-1$ Jacobi vectors. As it has been said before, the Jacobi vectors allow not only the separation of the center of mass motion but also enable an expression of the kinetic part of the nuclear Hamiltonian where no mixed derivative terms appear. For example, for the latter α arrangement the Kinetic Energy Operator reads:

$$\hat{T} = -\frac{\hbar^2}{2\mu_{A,BC}} \hat{\nabla}^2_{\vec{X}_\alpha} - \frac{\hbar^2}{2\mu_{BC}} \hat{\nabla}^2_{\vec{x}_\alpha} \tag{3.22}$$

Note that the kinetic energy operator expression on 3.22 depends explicitly on two different reduced masses, $\mu_{BC} = \frac{m_B m_B C}{m_B + m_C}$ and $\mu_{A,BC} = \frac{m_A (m_B + m_C)}{m_A + m_B + m_C}$. It can

be shown that, for the other two possible arrangements, $AB + C$ and $A + BC$ (usually denoted by β and γ) two other different reduced masses appear respectively, yielding six different reduced masses when considering the whole ensemble. A remarkable reduction and simplification can be achieved by mass-scaling the Jacobi vectors. The mass-scaled Jacobi coordinates relate to the unscaled ones by a dimensionless factor:

$$d_\tau = \left[\frac{m_\tau}{\mu} \left(1 - \frac{m_\tau}{M} \right) \right]^{1/2} \qquad (3.23)$$

where τ labels the particular arrangement (so that $\tau = \alpha, \beta, \gamma$ and $m_\alpha = \frac{m_A(m_B+m_C)}{m_A+m_B+m_C}$ and so on) and μ is the three-body reduced mass,

$$\mu = \left[\frac{m_A m_B m_C}{M} \right]^{1/2} \qquad (3.24)$$

Employing these scaled coordinates the kinetic energy operator takes the following form:

$$\hat{T} = -\frac{\hbar}{2\mu} \left(\nabla^2_{\mathbf{R}_\tau} + \nabla^2_{\mathbf{r}_\tau} \right) \qquad \tau = \alpha, \beta, \gamma \qquad (3.25)$$

where only a single reduced mass appears and therefore the expression is valid for all three possible arrangements (the only changes are the transformation equations to the center of mass position vectors).

3.2.1 Kinematic rotations

It can be shown that transformations between different sets of scaled Jacobi coordinates (usually corresponding to other possible arrangements) are the so-called *kinematic rotations*,

$$\begin{pmatrix} \mathbf{R}_\xi \\ \mathbf{r}_\xi \end{pmatrix} = \mathbf{T}(\chi_{\xi\tau}) \begin{pmatrix} \mathbf{R}_\tau \\ \mathbf{r}_\tau \end{pmatrix} \qquad (3.26)$$

where $\mathbf{T}$ is the 6×6 matrix:

$$\mathbf{T}(\chi_{\xi\tau}) = \begin{pmatrix} \cos\chi_{\xi\tau}\mathbf{1} & \sin\chi_{\xi\tau}\mathbf{1} \\ -\sin\chi_{\xi\tau}\mathbf{1} & \cos\chi_{\xi\tau}\mathbf{1} \end{pmatrix} \qquad (3.27)$$

These rotations involve terms depending only on the masses of the colliding partners. The kinematic angles $\chi_{\tau+1,\tau}$, for a cyclic order (i.e. when $\tau = \alpha$, $\tau+1 = \beta$, $\tau+2 = \gamma$, but if $\tau = \beta$, $\tau+1 = \gamma$, $\tau+2 = \alpha$), are the *negative, obtuse* angles defined by:

$$\cos\chi_{\tau+1,\tau} = \frac{\mu}{d_\tau d_{\tau+1} m_{\tau+2}} \qquad (3.28)$$

and

$$\sin\chi_{\tau+1,\tau} = \frac{-1}{d_\tau d_{\tau+1}} \qquad (3.29)$$

3.2.2 Spatial rotations. Body Fixed Jacobi Coordinates.

Besides kinematic rotations, which mix the Jacobi vectors, we will need several Body Frame (BF) axes systems, and therefore ordinary spatial rotations must be introduced. Consider the rotation $\mathcal{R}(2 \leftarrow 1)$ that carries some axes set 1 into axes set 2,

$$\mathcal{R}(2 \leftarrow 1) = \begin{pmatrix} \mathbf{R} & \mathbf{0} \\ \mathbf{0} & \mathbf{R} \end{pmatrix} \quad ; \quad \begin{pmatrix} \mathbf{R}_\tau^2 \\ \mathbf{r}_\tau^2 \end{pmatrix} = \mathcal{R}(2 \leftarrow 1) \begin{pmatrix} \mathbf{R}_\tau^1 \\ \mathbf{r}_\tau^1 \end{pmatrix} \tag{3.30}$$

where $\mathbf{0}$ is the 3×3 null matrix, 1 and 2 superindexes denote the vector components on the two different axes set and $\mathbf{R}$ is a 3×3 matrix of Euler angles:

$$\mathbf{R} = \begin{pmatrix} \cos\alpha\cos\beta\cos\gamma - \sin\alpha\sin\gamma & \sin\alpha\cos\beta\cos\gamma + \cos\alpha\sin\gamma & -\sin\beta\cos\gamma \\ -\sin\alpha\cos\beta\sin\gamma - \sin\alpha\cos\gamma & -\sin\alpha\cos\beta\cos\gamma + \cos\alpha\cos\gamma & \sin\beta\cos\gamma \\ \cos\alpha\sin\beta & \sin\alpha\cos\beta & \cos\beta \end{pmatrix}$$

where $\alpha = \alpha_{21}, \beta = \beta_{21}$ and $\gamma = \gamma_{21}$ are the Euler angles that carry axes system 1 into axes system 2.

Of particular interest is the case when 1 is the space-frame (SF) and 2 is the BF_τ system (see figure 3.2) in which the BF z axis points along R_τ. This leads to $\alpha_{21} = \alpha_\tau = \varphi_{R_\tau}$ and $\beta_{21} = \beta_\tau = \vartheta_{R_\tau}$, i.e., the spherical polar coordinates of $\mathbf{R}_\tau$ in the SF system, but leaves $\gamma_{21} = \gamma_\tau$ arbitrary. It is often convenient to choose the third Euler angle γ_τ so as to make r_τ lie in the BF_τ xz plane with a nonnegative x component, therefore the vector in the new frame is expressed as:

$$R_\tau^\tau = \begin{pmatrix} 0 \\ 0 \\ R_\tau \end{pmatrix} \tag{3.31}$$

$$r_\tau^\tau = \begin{pmatrix} x_\tau^\tau \\ 0 \\ z_\tau^\tau \end{pmatrix} = \begin{pmatrix} r_\tau \sin\Theta_\tau \\ 0 \\ r_\tau \cos\Theta_\tau \end{pmatrix} \tag{3.32}$$

where Θ_τ is the angle between the two Jacobi vectors.

Thus, the body-frames for $\tau = A, B$ and C all have a common y axis, and one can transform from one to another by rotating about this common axis.

3.2.3 Close Coupling equations.

In this section we will derive the explicit expression of the close coupling equations, introduced in section 2.5, in the Jacobi coordinate system, firstly for the inelastic scattering case and later for the reactive process.
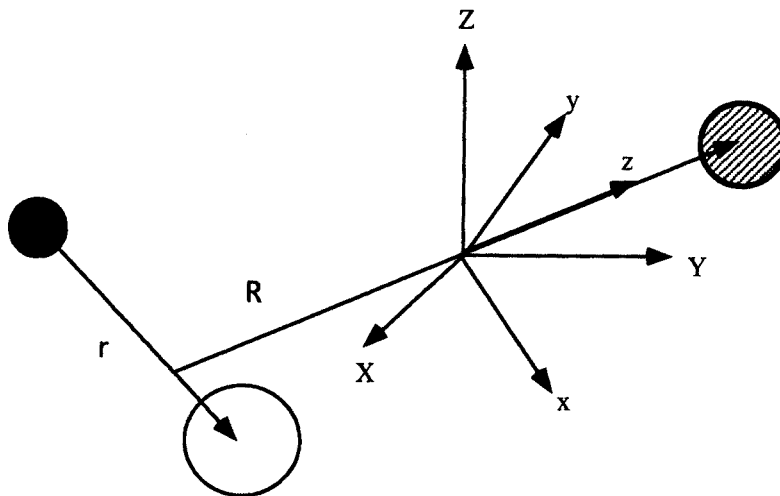
Figure 3.2: Space fixed (X,Y,Z) and body fixed (x,y,z) axis frames

Inelastic scattering.

Let's assume we are dealing with an inelastic process within the $A + BC$ arrangement. Jacobi coordinates are particularly adequate for describing this process, the Hamiltonian being a function of $\mathbf{R}_\tau$ and $\mathbf{r}_\tau$. Subscripts labeling the particular arrangement will be omitted throughout the section. One can clearly see how adequate are the $B - C$ distance and the distance from A to the BC center of mass, as variables to describe the inelastic process and specially for the target states basis expansion, since we will have functions for the target states that will depend just on one vector, $\mathbf{r}$ (three variables). For the moment we will consider we are using a Space Fixed reference frame and later we will transform to the Body Fixed. The factorization of the system Hamiltonian that allows a target basis set expansion in this arrangement has the form:

$$\hat{H} = \frac{-\hbar^2}{2\mu}\nabla_{\mathbf{R}}^2 + \hat{H}_{BC}(\vec{r}) + V(R, r, \Theta) \qquad (3.33)$$

where, as explained in section 2.5, $\hat{H}_{BC}$ represents the BC system Hamiltonian (assuming a Σ electronic state)

$$\hat{H}_{BC} = \frac{-\hbar^2}{2\mu_{BC}}\nabla_{\mathbf{r}}^2 + V_{BC}(r) \qquad (3.34)$$

$$= \frac{-\hbar^2}{2\mu_{BC}}\frac{1}{r^2}\frac{\partial}{\partial r}r^2\frac{\partial}{\partial r} + \frac{j_{\hat{r}}^2}{2\mu_{BC}r^2} + V_{BC}(r)$$

where $j_{\hat{r}}^2$ is the BC system rotational angular momentum, whose eigenfunctions are hyperspherical harmonics depending on the angular components of $\mathbf{r}$, i.e.

Chapter 3. The accurate description of the Reactive System

$\hat{r} = (\vartheta_r, \varphi_r)$ in the SF frame. The target eigenstates satisfy the Schrödinger equation :

$$\hat{H}_{BC}\Phi_{jv}(r,\hat{r}) = \epsilon_{jv}\Phi_{jv}(r,\hat{r}) \tag{3.35}$$

and since we know the angular part eigenfunctions we can further decompose the eigenstates as a product of radial and angular functions:

$$\left(\hat{H}_{BC} - \epsilon_{jv}\right)\phi(r)_{jv}Y_{jm_j}(\hat{r}) = 0 \tag{3.36}$$

The kinetic energy operator for the *translational* Jacobi coordinate, **R** can undertake a similar transformation if we express it in a radial and angular part:

$$\frac{-\hbar^2}{2\mu}\nabla_{\mathbf{R}}^2 = \frac{-\hbar^2}{2\mu}\frac{1}{R^2}\frac{\partial}{\partial r}R^2\frac{\partial}{\partial R} + \frac{\ell_{\hat{R}}^2}{2\mu R^2} \tag{3.37}$$

where ℓ denotes the orbital angular momentum of A around BC. Similarly to the rotational angular momentum case, eigenfunctions for the $\hat{\ell}^2$ that depend only on the angular components of **R** can be found in the spherical harmonics that, in this case, will be $Y_{\ell m_\ell}(\hat{R})$, with $\hat{R} = (\vartheta_R, \varphi_R)$. One can now couple the two angular functions basis sets to build a basis set for the whole angular part of 3.33. One will be then coupling the two angular momenta to obtain the total angular momentum, $\mathbf{J} = \mathbf{j} + \boldsymbol{\ell}$. This is achieved by means of the Clebsch-Gordan coefficients:

$$Y_{j\ell}^{JM} = \sum_{m_j=-j}^{j}\sum_{m_\ell=-\ell}^{\ell} C(j\ell J; m_j m_\ell M)Y_{jm_j}(\hat{r})Y_{\ell m_\ell}(\hat{R}) \tag{3.38}$$

As it has been said at the end of section 2.5, since the total angular momentum is conserved all along the process, its corresponding operator commutes with the total Hamiltonian. One can therefore find a common eigenfunction basis set $\{\psi^{JM}\}$ and build our wavefunction as their linear combination in what it is called *partial wave expansion*

$$\Psi = \sum_{J=0}^{\infty}\psi^{JM} \tag{3.39}$$

Each of these functions satisfies

$$\hat{H}\psi^{JM} = E\psi^{JM} \tag{3.40}$$

These functions will be the product of the angular function, eigenstate of the total momentum operator and its Z-axis projection in the SF frame, and two radial functions, one which is the target *vibrational* function and the other which will depend on the translational radial component.

$$\psi^{JM} = \sum_{j}\sum_{\ell}\sum_{v}\frac{1}{R}G_{j\ell v}^{J}(R)\phi_{jv}(r)Y_{j\ell}^{JM}(\hat{R},\hat{r}) \tag{3.41}$$

3.2. Jacobi coordinates

Here we have written $\frac{1}{R}G_{j\ell v}^{J}(R)$ for convenience, since a simpler expression for the equations will be obtained. We identify the summation over v as the target expansion explained in section 2.5. Substituting 3.41 into 3.33 and premultiplying the resulting equation by

$$\frac{1}{r}\psi_{j'v'}^{*}(r)Y_{j'\ell'}^{JM*}(\hat{R},\hat{r}),$$

integrating over r and the angular components of R and r, and benefiting from the orthogonality properties of the spherical harmonics and the Clebsch-Gordan coefficients, we obtain the following expression for the close coupling equations using SF Jacobi coordinates:

$$\left[\frac{d^2}{dR^2} + \left(\frac{2\mu}{\hbar^2}\right)(E - \epsilon_{j'v'}) - \frac{\ell'(\ell'+1)}{R^2}\right]G_{j'\ell'v'}^{J}(R) = \tag{3.42}$$

$$= \left(\frac{2\mu}{\hbar^2}\right)\sum_{j}\sum_{\ell}\sum_{v}\langle j'\ell'v'\,|V|\,j\ell v\rangle\, G_{j\ell v}^{J}(R)$$

where

$$\langle j'\ell'v'\,|V|\,j\ell v\rangle = \int_0^{\infty} r^2 dr \int \frac{1}{r}\psi_{j'v'}^{*}(r)Y_{j'\ell'}^{JM*}(\hat{R},\hat{r}) \times \tag{3.43}$$

$$\times V(R,r,\Theta)Y_{j\ell}^{JM}(\hat{R},\hat{r})\phi_{jv}(r)d\hat{R}d\hat{r}$$

Next, we will derive the expression of this equation set using Jacobi coordinates as well, but this time under a Body Fixed frame, whose quantization axis follows **R** along the rearrangement process. All there is to do is to perform the rotation described in section 3.2.2 from the SF to the BF frames along polar and azimuthal Euler angles of **R** in the SF frame. The orbital angular momentum components in this axis frame will then be

$$\ell_x = -(p_R)_y R \tag{3.44}$$

$$\ell_y = -(p_R)_x R \tag{3.45}$$

$$\ell_z = 0 \tag{3.46}$$

The Hamiltonian operator in BF Jacobi coordinates is written as:

$$\hat{H} = \frac{1}{2\mu}\left[\frac{-\hbar^2}{R}\frac{\partial^2}{\partial R^2}R + \frac{\hat{\ell}^2}{R^2}\right] + \hat{H}_{BC}(\mathbf{r}) + V(R,r,\Theta) \tag{3.47}$$

where the rotor angular momentum, $\hat{\mathbf{j}}_\tau$, is included in the BC Hamiltonian and $\hat{\ell}_\tau$ the orbital angular momentum of atom τ about the diatom. Remember that the subscript labeling the particular arrangement is being omitted in this section.

If one now expresses the orbital angular momentum as the difference between the total and rotational angular momenta:

$$\boldsymbol{\ell} = \mathbf{J} - \mathbf{j} \tag{3.48}$$

Chapter 3. The accurate description of the Reactive System

equation 3.47 may be rewritten as:

$$\hat{H} = \frac{1}{2\mu} \left[\frac{-\hbar^2}{R} \frac{\partial^2}{\partial R^2} R + \frac{(\hat{J}_x - \hat{j}_x)^2}{R^2} + \frac{(\hat{J}_y - \hat{j}_y)^2}{R^2} \right] + \hat{H}_{BC}(\mathbf{r}) + V(R, r, \Theta) \quad (3.49)$$

One can conveniently introduce the ladder operators $\hat{j}_\pm = \hat{j}_x \pm i\hat{j}_y$ (and correspondingly for $\hat{J}_\pm$) and transform 3.34, knowing that $J_z = j_z$, into:

$$\hat{H} = \frac{1}{2\mu} \left[\frac{-\hbar^2}{R} \frac{\partial^2}{\partial R^2} R + \frac{1}{R^2} \left(\hat{J}^2 + \hat{j}^2 - 2\hat{J} - \hat{J}_+\hat{j}_- - \hat{J}_-\hat{j}_+ \right) \right] + \quad (3.50)$$

$$+ \hat{H}_{BC}(\mathbf{r}) + V(R, r, \Theta)$$

To derive the close coupling equations in their BF Jacobi coordinates formulation, one has to see the effect of a $SF \rightarrow BF$ rotation on the SF partial wave wavefunction, $\psi_{j\ell v}^{JM}$. In the literature[25, 26], this is expressed as:

$$\Phi_{j\ell v\Omega}^{JM}(\mathbf{R}, \mathbf{r}) = R\psi_{j\ell v}^{JM} = \sum_{\Omega'=-J}^{J} D_{M\Omega'}^{J\star} \chi_{\Omega'}^{Jj\ell v\Omega}(R, \mathbf{r}) \quad (3.51)$$

where Ω is the projection of the total angular momentum on the BF quantization axis, z. Hereinafter, we will express the $j\ell v$ set as β. Substituting 3.51 into 3.50 and after some manipulations, the equation set becomes:

$$H_{\Omega,\Omega-1}\chi_{\Omega-1}^{J\beta\Omega} + H_{\Omega,\Omega}\chi_{\Omega}^{J\beta\Omega} + H_{\Omega,\Omega+1}\chi_{\Omega+1}^{J\beta\Omega} = 0 \quad (3.52)$$

where

$$H_{\Omega\Omega} = -\frac{\hbar^2}{2\mu} \left(\frac{1}{r} \frac{\partial^2}{\partial r^2} r + \frac{1}{R} \frac{\partial^2}{\partial R^2} R \right) + \frac{\hat{j}^2}{2\mu r^2} + \quad (3.53)$$

$$+ \frac{1}{2\mu R^2} \left[J(J+1)\hbar^2 - 2\Omega\hbar\hat{j}_x + \hat{j}^2 \right] + V(r, R, \Theta)$$

$$H_{\Omega\Omega\pm 1} = -\frac{\hbar^2}{2\mu R^2} \sqrt{J(J+1) - \Omega(\Omega \pm 1)\hat{j}_\pm} \quad (3.54)$$

If one then performs the target basis set expansion:

$$\chi_{\Omega'}^{J\beta\Omega}(R, \mathbf{r}) = \sum_{\beta'} \frac{1}{R} u_{\beta'\Omega'}^{J\beta\Omega}(R)\Phi_{\beta'\Omega'}(\mathbf{r}) \quad (3.55)$$

where

$$\Phi_{\beta'\Omega'}(\mathbf{r}) = \frac{1}{r}\phi_{\beta'}(r)Y_{j'\Omega'}(\hat{r}) \quad (3.56)$$

substituting equations 3.55 and 3.56 into 3.52, multiplying by $\left(\frac{2\mu}{\hbar^2} \right) \Phi_{\beta'\Omega'}^*$ and integrating over $\mathbf{r}$, we finally obtain the close coupling equations, using Jacobi coordinates, under a BF reference frame:

$$h_{\Omega',\Omega'-1}^{\beta'} u_{\beta'\Omega}^{J\beta\Omega'-1}(R) + h_{\Omega',\Omega'}^{\beta'} u_{\beta'\Omega}^{J\beta\Omega'}(R) + h_{\Omega',\Omega'+1}^{\beta'} u_{\beta'\Omega}^{J\beta\Omega'+1}(R) = \quad (3.57)$$

$$= \sum_{\beta'} \langle \beta\Omega' |U| \beta'\Omega \rangle$$

where,

$$
h_{\Omega'\Omega'}^{\beta} = \frac{d^2}{dr^2} + k_\beta^2 - \left[J(J+1) + j(j+1) - 2\Omega'^2 \right] \frac{1}{R^2} \tag{3.58}
$$

$$
h_{\Omega'\Omega'\pm 1}^{\beta} = \left\{ J(J+1) - \Omega'^2 \right\}^{1/2} \left\{ j(j+1) - \Omega'(\Omega \pm 1) \right\}^{1/2} \frac{1}{R^2} \tag{3.59}
$$

and

$$
\langle \beta\Omega' | U | \beta'\Omega \rangle = \frac{2\mu}{\hbar^2} \int \phi_\beta(r) Y_{j\Omega'}^*(\hat{r}) V(R,r,\Theta) \phi_{\beta'}(r) Y_{j'\Omega'}^*(\hat{r}) dr d\hat{r} \tag{3.60}
$$

Reactive scattering.

To develop the close coupling equations for the reactive event in Jacobi coordinates we will continue on the BF frame, and the treatment will be, in principle, completely analogous to that of the inelastic scattering. Attention should be paid now to the fact that we will be having as many BF frames as different arrangements involved in the rearrangement process. Since we have to distinguish between arrangements, the subindex labeling them has to be put once again and therefore the nuclear Schrödinger equation:

$$
\left[\frac{1}{2\mu} \left(\frac{-\hbar^2}{R_\lambda} \frac{\partial^2}{\partial R_\lambda^2} R_\lambda - \frac{\hbar^2}{r_\lambda} \frac{\partial^2}{\partial r_\lambda^2} r_\lambda + \frac{\hat{j}_\lambda^2}{r_\lambda^2} + \frac{\hat{\ell}_\lambda^2}{R_\lambda^2} \right) + \right. \tag{3.61}
$$
$$
\left. + \hat{H}_{tar}(\mathbf{r}_\lambda) + V(R,r,\Theta) - E \right] \Psi^\lambda(\mathbf{R}_\lambda, \mathbf{r}_\lambda) = 0
$$

will be the Schrödinger equation expressed in Jacobi coordinates for a given arrangement λ. As in the inelastic case, the *partial wave expansion* can be performed (the rearrangement obviously does not alter the conservation of total angular momentum). Each SF partial wave can expressed in terms of Wigner rotation matrices and BF_λ wavefunctions(note the arrangement subscript labeling the $Ox_\lambda y z_\lambda$ axis system),

$$
\psi_{JM}^\lambda(\mathbf{R}_\lambda, \mathbf{r}_\lambda) = \sum_{\Omega_\lambda=-J}^{J} D_{M\Omega_\lambda}^J \chi_{J\Omega_\lambda}^\lambda \tag{3.62}
$$

where the quantum number Ω_λ specifies the projection of **J** on the z_λ axis, or equivalently on $\mathbf{R}_\lambda$. This number will therefore depend on the specific arrangement channel considered. Due to a treatment analogous to that for the inelastic scattering, the BF close coupling equations can be obtained as:

$$
\left(t_{\Omega_\lambda\Omega_\lambda}^{J\lambda j_\lambda} - E \right) F_{J j_\lambda \Omega_\lambda}^\lambda(R_\lambda, r_\lambda) + t_{\Omega_\lambda\Omega_\lambda+1}^{J\lambda j_\lambda} F_{J j_\lambda \Omega_\lambda+1}^\lambda(R_\lambda, r_\lambda) + \tag{3.63}
$$
$$
+ t_{\Omega_\lambda\Omega_\lambda-1}^{J\lambda j_\lambda} F_{J j_\lambda \Omega_\lambda-1}^\lambda(R_\lambda, r_\lambda) + \sum_{j_\lambda=|\Omega_\lambda|}^{\infty} V_{j_\lambda j_\lambda'}^{\lambda\Omega_\lambda} F_{J j_\lambda' \Omega_\lambda-1}^\lambda(R_\lambda, r_\lambda) = 0
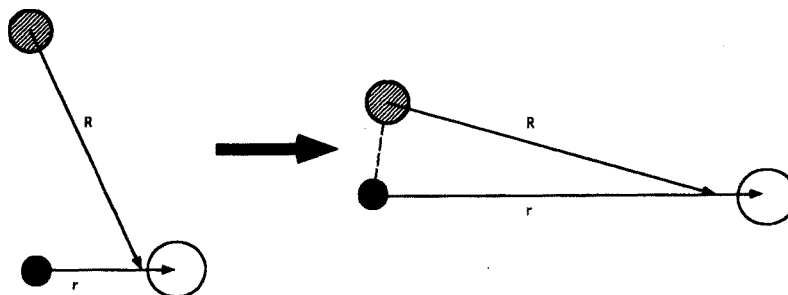$$

Figure 3.3: The reactive event clearly evidences two radically different physical situations

$$J = 0, 1, 2, \ldots \quad \Omega_\lambda = -J, -J+1, \ldots, J \quad j_\lambda = |\Omega_\lambda|, |\Omega_\lambda| + 1$$

where $F^\lambda_{Jj_\lambda \Omega_\lambda}(R_\lambda, r_\lambda)$ are the functions depending on the radial components of both Jacobi vectors. For derivation of the equations and explicit form of the $t^{J\lambda j_\lambda}_{\Omega_\lambda \Omega'_\lambda}$ terms refer to [26].

Note that the resulting equations have been expressed so that their solution is a function that depends on both radial coordinates r_λ, R_λ. This means that no expansion of the total wavefunction has been carried away on the target's vibrational eigenfunctions. This is done so because this would result in a rather inefficient formulation whenever dealing with a rearrangement process. As an example, consider the particular case of a $A + BC$ reactive process. One would solve the problem integrating the Schrödinger equation from the strong interaction region to the reactants and products region. Suppose we want to express the total wavefunction in terms of eigenstates in r_α, the vibrational α-arrangement Jacobi coordinate. The Schrödinger equation ought to be the integrated from 0 to a given value R^{max}_α, of the corresponding translational Jacobi coordinate. From figure 3.3 appears clearly evident that a large number of eigenstates in r_α will be necessary to accurately describe the wavefunction for β-product arrangement configurations, since now motion along r corresponds to a translation rather than a vibration. This means that one attempts to describe a translational motion through an expansion in terms of vibrational eigenstates, which is the main source of inefficiency. There would appear also difficulties in describing the strong interaction region (there is a shift in the vibrational baricenter).

Several attempts have been made (some of them quite successful) to overcome this problem remaining in Jacobi coordinates. In particular, in the present work, Jacobi coordinates have been used for the study of reactive scattering under an *Infinite Order Sudden Approximation* (see section 6.1 and chapters 7 and 8). There, the close coupling equations are solved employing the R-matrix method of section 4.4. The problem is formulated in Jacobi reactant coordinates when propagating in the reactants valley and in the corresponding Jacobi products coordinates when in the products valley. In the strong interaction region a rela-

tion between both sets of coordinates is established so that the equations can be transformed from one set to the other[27].

However, nowadays it is commonly accepted that Jacobi coordinates, as here formulated, are not efficient enough to describe the reactive event and several alternative coordinate systems have been developed.

3.3   Hyperspherical coordinates

The application of hyperspherical coordinates[28], introduced in Atomic Physics around the thirties, and adopted in Molecular Physics and Kinetics in the beginning of the sixties, has spreaded rapidly and successfully in the last twenty years, showing up to be a powerful tool for the solution of the reactive problem. Although it is by no means the only possible approach for the description of a reactive process, it is undoubtly one of the most powerful and has already been successfully tested.

Essentially, the hyperspherical description aims to transform the problem of the three particles moving in a three-dimensional space into that of a single particle evolving in a N-dimensional space. For the atom-diatom reactive process, for example, the reactive event can be described (after CM motion separation) in terms of a 6-dimensional hypersphere. Such a description, is capable of fully describing the collective motion of the three atoms, even though it can give rise to numerical difficulties, in terms of convergence, for the asymptotic situations.

Remembering how inefficient the particular Jacobi coordinates set of a given arrangement was to describe the physical situation in a different arrangement, it can be concluded that a general variable that cuts both valleys perpendicularly is convenient for a good convergence. The people who developed the hyperspherical coordinates found in curvilinear coordinates a good candidate and among them the polar coordinates are the most simple choice,

$$\rho = \sqrt{R_\gamma^2 + r_\gamma^2} \tag{3.64}$$

$$\chi_\gamma = \arctan R_\gamma^2 / r_\gamma^2 \tag{3.65}$$

Generalization of these equations to the tridimensional processes leads to the hyperspherical coordinates. In the d-dimensional space ($d = 3(N - 1)$) of the mass-scaled vectors, the hyperradius (corner stone of the whole hyperspherical approach) has the meaning of the radius of a hypersphere:

$$\rho^2 = \sum_{i=1}^{n-1} |x_i|^2 \tag{3.66}$$

$$D = 2 \rightarrow \rho = x^2 \quad ; D = 3 \rightarrow \rho = x^2 + y^2$$

For our case ($N = 3$), we can derive an expression in terms of the Jacobi vectors

$$\rho = \sqrt{R_\alpha^2 + r_\alpha^2} = \sqrt{R_\beta^2 + r_\beta^2} = \sqrt{R_\gamma^2 + r_\gamma^2} \tag{3.67}$$

Probably the most important characteristic of this quantity is that it is universal, i.e. invariant with respect to the Jacobi set considered. This makes the hyperradius an ideal variable to follow the reaction evolution. Low values of ρ label strong interaction situations while large values describe asymptotic (either reactants or products) ones.

Another very important characteristics of the hyperradius is that it is an almost separable variable. This means that separating the motion in the hyperradial coordinate from the rest of motions is a considerably good approximation, having enabled considerable advances. This will be very helpful, for instance, for propagative techniques, since we will be able to divide our integration region into fixed ρ sectors where we will solve the Schrödinger equation for all the other variables without significant loss of accuracy. We still lack, however, $d - 1$ other variables to cover the full d-dimensional space and thus completely specify the motion of the internal system. These variables are usually parameterized as the hyperangles covering the hypersphere's surface. There are many different parameterizations of these hyperangles. It can be shown that the many possible choices correspond to different angular momenta coupling schemes. The key works in this subject were performed by Smith[29, 30], who generalized the angular momentum to the hypersphere and thoroughly studied the motion of three particles in a plane.

3.3.1 Asymmetric Parameterization. Fock coordinates.

One possible choice for the hyperangles corresponds to the so-called asymmetric parameterization, which was introduced in the thirties and later Fock[31] gave an ultimate impulse. In order to define the five hyperangular variables, let's refer to a mass-scaled Jacobi vector set, keeping in mind that these coordinates allow the separation of the center of mass motion. We can then represent $\mathbf{R}, \mathbf{r}$ in a reference frame centered on the center of mass and its axes parallel to the space-fixed frame.

Let's define $\mathbf{x}$ as the 3×2 matrix containing the 6 cartesian components of the Jacobi vectors for a given arrangement α and, alternatively, their expressions in terms of spherical coordinates:

$$\mathbf{x} = \begin{pmatrix} r_{X\alpha} & R_{X\alpha} \\ r_{Y\alpha} & R_{Y\alpha} \\ r_{Z\alpha} & R_{Z\alpha} \end{pmatrix} = \begin{pmatrix} r_\alpha \sin\vartheta_{r_\alpha} \cos\varphi_{r_\alpha} & R_\alpha \sin\vartheta_{R_\alpha} \cos\varphi_{R_\alpha} \\ r_\alpha \sin\vartheta_{r_\alpha} \sin\varphi_{r_\alpha} & R_\alpha \sin\vartheta_{R_\alpha} \sin\varphi_{R_\alpha} \\ r_\alpha \cos\vartheta_{r_\alpha} & R_\alpha \cos\vartheta_{R_\alpha} \end{pmatrix} \tag{3.68}$$

The fifth hyperangle is chosen from a direct extension of the polar coordinates:

$$\chi_\alpha = \arctan \frac{|\mathbf{R}_\alpha|}{|\mathbf{r}_\alpha|} \tag{3.69}$$

3.3. Hyperspherical coordinates

and consequently χ_α ranges from 0 to $\pi/2$.

Although this set of coordinates has almost direct physical interpretation, has the important disadvantage that all angles depend explicitly on the considered Jacobi set. However, this set allows a simple description of the three-atom spatial rotation, and an almost immediate construction of the nuclear angular momentum eigenfunctions. On the other hand, an additional coordinate transformation has to be introduced since the potential energy depends only on ρ, χ and Θ_α, being Θ_τ is the angle formed between the two Jacobi vectors of the corresponding arrangement:

$$\cos \Theta_\alpha = \cos \vartheta_{r_\alpha} \cos \vartheta_{R_\alpha} + \sin \vartheta_{r_\alpha} \sin \vartheta_{R_\alpha} \cos(\varphi_{R_\alpha} - \varphi_{r_\alpha}) \qquad (3.70)$$

These difficulties can be overcome using a rotating frame whose origin is common to the preceding fixed frame. In order to specify the orientation of the rotating system in space one needs the three Euler angles α, β, γ, which are defined in a form which is dependent on the choice taken for the orientation of the rotating axes. Schematically, the above rotation can be expressed as:

$$XYZ \xrightarrow{(\alpha,\beta,\gamma)} xyz \qquad (3.71)$$

For this case, z coincides with $\mathbf{R}$ while $\mathbf{r}$ lies on the xz plane. Therefore the new 3×2 matrix $\mathbf{x}'$ containing the cartesian components is now:

$$\mathbf{x}' = \begin{pmatrix} r_x & 0 \\ 0 & 0 \\ r_z & R \end{pmatrix} \qquad (3.72)$$

and relates to $\mathbf{x}$ so that

$$\mathbf{x} = D(\alpha, \beta, \gamma)\mathbf{x}' \qquad (3.73)$$

this is,

$$\begin{pmatrix} r_X & R_X \\ r_Y & R_Y \\ r_Z & R_Z \end{pmatrix} = \begin{pmatrix} \cos\alpha & -\sin\alpha & 0 \\ \sin\alpha & \cos\alpha & 0 \\ 0 & 0 & 1 \end{pmatrix} \begin{pmatrix} \cos\beta & 0 & \sin\beta \\ 0 & 1 & 0 \\ -\sin\beta & 0 & \cos\beta \end{pmatrix} \qquad (3.74)$$
$$\begin{pmatrix} \cos\gamma & -\sin\gamma & 0 \\ \sin\gamma & \cos\gamma & 0 \\ 0 & 0 & 1 \end{pmatrix} \begin{pmatrix} r_x & 0 \\ 0 & 0 \\ r_z & R \end{pmatrix}$$

Introducing $r_x = r \sin \Theta$ and $r_z = r \cos \Theta$ and performing the matrix multiplications, it can be verified that:

$$\alpha = \varphi_{R_\alpha} \qquad (3.75)$$

$$\beta = \vartheta_{R_\alpha} \qquad (3.76)$$

To this point the asymmetric hyperangular parameterization can be considered as completed. The six internal coordinates of the triatomic system have been factorised in terms of the product of a rotation matrix function of external coordinates (Euler angles $\varphi_{R_\alpha}, \vartheta_{R_\alpha}, \gamma$) and a term which is function of the internal coordinates, ρ, χ (from polar coordinates) and Θ (keep in mind that it is the angle between the Jacobi vectors, whose range is $[0, \pi]$).

3.3.2 Symmetric Parameterization. Smith coordinates.

One set of hyperangles which yields a coordinate system non-dependent on the particular arrangement is that developed by Felix Smith for both the planar (1962) and tridimensional (1967) cases[29, 30]. A later formal modification (1980) by Johnson[32] is quite often used.

This coordinate set is defined as well on a rotating frame. In order to understand as best as possible the path leading to these coordinates, let's start from the three-body inertia tensor[25]. This tensor is defined as

$$\mathbf{I} = \mathbf{1} tr(\mathbf{Z}) - \mathbf{Z} \tag{3.77}$$

where $\mathbf{Z} = \mathbf{x}\bar{\mathbf{x}}$ and $\mathbf{x}$, as in 3.68 is the cartesian components matrix of the Jacobi vectors, with $\bar{\mathbf{x}}$ its transpose. It can be seen that:

$$tr(\mathbf{Z}) = \rho^2 \tag{3.78}$$

The inertia tensor is then a 3×3 matrix that has all its components different from zero in the center of mass fixed frame:

$$\mathbf{I} = \begin{pmatrix} \rho^2 - r_X^2 - R_X^2 & -(r_X r_Y + R_X R_Y) & -(r_X r_Z + R_X R_Z) \\ -(r_Y r_X + R_Y R_X) & \rho^2 - r_Y^2 - R_Y^2 & -(r_Y r_Z + R_Y R_Z) \\ -(r_Z r_X + R_Z R_X) & -(r_Z r_Y + R_Z R_Y) & \rho^2 - r_Z^2 - R_Z^2 \end{pmatrix} \tag{3.79}$$

Now, let's introduce here as well the same rotating reference frame defined in equation 3.73. Since the rotating system x, y, z is related to the preceding by a rotation function of the Euler angles, we can write,

$$\mathbf{Z} = \mathbf{x}\bar{\mathbf{x}} = \mathbf{D}\mathbf{x}'\bar{\mathbf{x}}'\tilde{\mathbf{D}} = \mathbf{D}\mathbf{Z}'\tilde{\mathbf{D}} \tag{3.80}$$

Keeping in mind that $\mathbf{D}$ is an orthogonal rotation matrix, we can obtain the tensor of inertia in the rotating system with its z-axis along $\mathbf{R}$:

$$\mathbf{I}' = \tilde{\mathbf{D}}\mathbf{I}\mathbf{D} = \begin{pmatrix} \rho^2 - r_x^2 & 0 & -r_x r_z \\ 0 & \rho^2 & 0 \\ -r_x r_z & 0 & \rho^2 - R^2 \end{pmatrix} \tag{3.81}$$

We can then choose a rotating reference frame in which the inertia tensor becomes diagonal, finding the appropriate Euler angles $\alpha_I, \beta_I, \gamma_I$ for which the matrix

3.3. Hyperspherical coordinates

product $\tilde{\mathbf{D}}(\alpha_I, \beta_I, \gamma_I)\mathbf{ID}(\alpha_I, \beta_I, \gamma_I)$ is diagonal. This is a crucial choice since we are choosing a BF frame oriented along the principal axes of inertia. Since we are dealing with a non-rigid body, these evolve in a natural way with the reaction, changing from the initial arrangement to the final one, and so will do our reference frame.

Also in this case, we can express in a compact form the relationship between the cartesian components of the Jacobi vectors in the center of mass and those of the new frame

$$
\begin{pmatrix} r_X & R_X \\ r_Y & R_Y \\ r_Z & R_Z \end{pmatrix} = \tilde{\mathbf{D}}(\alpha_I, \beta_I, \gamma_I) \begin{pmatrix} r_\xi & R_\xi \\ 0 & 0 \\ r_\zeta & R_\zeta \end{pmatrix} \tag{3.82}
$$

being ξ and ζ the labels for the new reference frame. We therefore have,

$$
\tilde{\mathbf{D}}\mathbf{ID} = \rho^2 \mathbf{1} - \tilde{\mathbf{D}}\mathbf{ZD} \tag{3.83}
$$

where

$$
\tilde{\mathbf{D}}\mathbf{ZD} = \begin{pmatrix} r_\xi & R_\xi \\ 0 & 0 \\ r_\zeta & R_\zeta \end{pmatrix} \begin{pmatrix} r_\xi & 0 & r_\zeta \\ R_\xi & 0 & R_\zeta \end{pmatrix} = \tag{3.84}
$$

$$
= \begin{pmatrix} r_\xi^2 + R_\xi^2 & 0 & r_\xi r_\zeta + R_\xi R_\zeta \\ 0 & 0 & 0 \\ r_\xi r_\zeta + R_\xi R_\zeta & 0 & r_\zeta^2 + R_\zeta^2 \end{pmatrix}
$$

This, to be diagonal, requires: $r_\xi r_\zeta + R_\xi R_\zeta = 0$. This condition is immediately satisfied defining:

$$
r_\xi = \rho \sin\Theta \cos\Phi \qquad r_\zeta = \rho \cos\Theta \sin\Phi \tag{3.85}
$$

$$
R_\xi = \rho \sin\Theta \sin\Phi \qquad R_\zeta = -\rho \cos\Theta \cos\Phi \tag{3.86}
$$

which leads to the following transformed $\mathbf{Z}'$ matrix:

$$
\mathbf{Z}' = \begin{pmatrix} \rho^2 \sin^2\Theta & 0 & 0 \\ 0 & 0 & 0 \\ 0 & 0 & \rho^2 \cos^2\Theta \end{pmatrix} \tag{3.87}
$$

and the tensor of inertia is

$$
\mathbf{I}' = \mathbf{1}tr\mathbf{Z} - \mathbf{Z}' = \begin{pmatrix} \rho^2 \cos^2\Theta & 0 & 0 \\ 0 & \rho^2 & 0 \\ 0 & 0 & \rho^2 \sin^2\Theta \end{pmatrix} = \begin{pmatrix} I_1 & 0 & 0 \\ 0 & I_2 & 0 \\ 0 & 0 & I_3 \end{pmatrix} \tag{3.88}
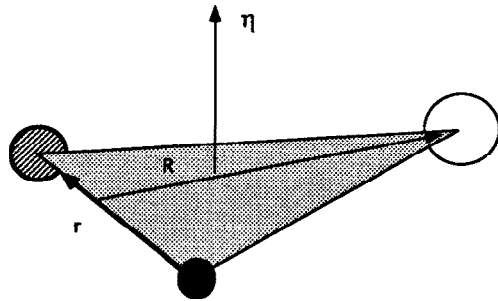$$

these eigenvalues represent the principal moments of inertia of the system. Note that $\sum I_i = 2\rho^2$; this relation allows us to establish the square of the hyperradius

as a measure of the total inertia of the system. Furthermore, see that since the three atoms evidently lie on a plane $I_2 = I_1 + I_3$, and since Θ ranges in the physical space from 0 to $\pi/4$[29], I_3 is always smaller than I_1. Therefore, in this reference frame τ and ξ are respectively the maximum and minimum inertia axes.

We can find a physical meaning as well for the two internal angles (Θ, Φ) of the symmetric parameterization. It is evident that, since one can express Θ in terms of ρ and the moments of Inertia (see 3.88), the variable is therefore not altered if the set of Jacobi vectors is changed. In fact, we can easily verify that Θ is tightly bound to the area (A) of the triatomic triangle.

$$A = |\vec{\eta}| \;=\; \frac{\mathbf{R} \times \mathbf{r}}{2} \qquad (3.89)$$
$$= \frac{r_\xi R_\zeta - r_\zeta R_\xi}{2}$$
$$= \frac{\rho^2 \sin 2\Theta}{4}$$

Representation of the relationship
between the Θ hyperangular
coordinate and the area of the
triatomic triangle

At the same time, Φ (ranging $[0, 2\pi]$ see [29, 30]) labels the different forms of the triangle with the same moment of inertia, i.e. distinguishes the different possible arrangements.

In conclusion, the coordinates for the hyperspherical symmetric parameterization of a reactive collision process are composed of three external variables, such as the $\alpha_I, \beta_I, \gamma_I$ Euler angles, and the internal variables ρ, Θ, Φ.

3.3.3 Hamiltonian.

In this section we will show the expression of the Hamiltonian using hyperspherical coordinates. In these coordinates the kinetic energy operator may be written as

$$\hat{K} = \frac{-\hbar^2}{2\mu} \left[\rho^{-(d-1)} \frac{\partial}{\partial \rho} \rho^{(d-1)} \frac{\partial}{\partial \rho} + \rho^{-2} \Lambda^2(\Omega_{d-1}) \right] \qquad (3.90)$$

where we do not introduce the explicit form of the hyperangular coordinates. Therefore this expression applies to both previous parameterizations. Let's consider the tridimensional atom-diatom collision where we explicitly distinguish between the external and internal hyperangles of the six-dimensional hypersphere

by denoting $\Omega_5 = (\varpi, \varpi_E)$ and let's write the system Hamiltonian taking into account that, in the absence of external forces, the potential will depend only on the internal hyperangles ϖ,

$$\hat{H} = \frac{-\hbar^2}{2\mu} \left[\rho^{-5} \frac{\partial}{\partial \rho} \rho^5 \frac{\partial}{\partial \rho} + \rho^{-2} \Lambda^2(\Omega_5) \right] + V(\rho, \varpi) \qquad (3.91)$$

Now, all that remains to know in order to write more explicitly the form of the Hamiltonian is to introduce the hyperangular parameterization one is using. This will not affect the hyperradial part of the kinetic energy operator, but will definitely have an effect on $\Lambda^2(\Omega_5)$, known as the Casimir operator.

Asymmetric Parameterization.

The form of the Casimir operator for the six-dimensional hypersphere, $\Lambda^2(\Omega_5)$, can be found in the literature[33] as:

$$\Lambda(\Omega_5) = -\frac{1}{\sin^2 2\chi} \frac{\partial}{\partial \chi} \sin^2 2\chi \frac{\partial}{\partial \chi} + \frac{\hat{j}^2(\varphi_r, \vartheta_r)}{\cos^2 \chi} + \frac{\hat{\ell}^2(\varphi_R, \vartheta_R)}{\sin^2 \chi} \qquad (3.92)$$

where χ is the polar angle defined in 3.69 and $\hat{j}$ and $\hat{\ell}$ are, respectively, the rotational and orbital angular momenta.

The eigenvalue equation for this operator read[34]:

$$\Lambda^2 Y_{\lambda j\ell}(\Omega_5) = -\lambda(\lambda + 4) Y_{\lambda j\ell}(\Omega_5) \qquad (3.93)$$

where λ is called the grand angular quantum number and takes the values

$$\lambda = 2n + j + \ell \qquad (3.94)$$

where n takes all the integer values from zero to infinity and j and ℓ all the integer values from zero to λ.

The eigenfunctions of this operator are the hyperspherical harmonics[33, 34] and in the asymmetric parameterization have the following explicit form:

$$Y_{\lambda j\ell}(\chi, \varphi_R, \vartheta_R, \varphi_r, \vartheta_r) = |\chi; \lambda; j; \ell> Y_{jm_j}(\varphi_r, \vartheta_r) Y_{\ell m_\ell}(\varphi_R, \vartheta_R) \qquad (3.95)$$

where $|\chi; \lambda; j; \ell>$ is a Jacobi polynomial of order n conveniently weighted and normalized[33].

Symmetric Parameterization.

Let's now turn to the six-dimensional Hamiltonian in the symmetric parameterization which is the one we will be solving. In the corresponding section we have seen how this parameterization corresponds to using hyperspherical coordinates

in a reference frame which is parallel to the principal axes of inertia. This would explain why Pack and coworkers[28] named these coordinates Adiabatically Adjusting Principal Axis Hyperspherical (APH) coordinates. In section 3.3.2 we have derived the expression for these coordinates considering the orientation of the solidary axis system, so that the z axis is oriented along the least inertia principal axis, but we could have chosen alternatively z to be oriented along the most inertia principal axis, i.e. that going out from the triatomic plane. Next we will write down the expression of the Casimir operator for the two possible choices.

If we consider the orientation in which z lies along the least inertia principal axis, the Casimir operator can be written as[28]

$$\Lambda^2(\Omega_5) = -\frac{1}{\sin 4\Theta}\frac{\partial}{\partial\Theta}\sin 4\Theta\frac{\partial}{\partial\Theta} - \frac{1}{\cos^2 2\Theta}\frac{\partial^2}{\partial\Phi^2} \tag{3.96}$$
$$-\frac{2i\sin 2\Theta}{cos^2 2\Theta}\hat{J}_y\frac{\partial}{\partial\Phi} + \frac{\hat{J}_x^2}{\sin^2\Theta} + \frac{\hat{J}_y^2}{\cos^2 2\Theta} + \frac{\hat{J}_z^2}{\cos^2\Theta}$$

According to Pack[28], it is often convenient to write this expression as a sum of a hyperradial, rotational and Coriolis term:

$$\hat{\Lambda}^2 = \hat{\Lambda}_h^2 + \hat{\Lambda}_r^2 + \hat{\Lambda}_c^2 \tag{3.97}$$

where,

$$\hat{\Lambda}_h = -\frac{1}{\sin 4\Theta}\frac{\partial}{\partial\Theta}\sin 4\Theta\frac{\partial}{\partial\Theta} - \frac{1}{\cos^2 2\Theta}\frac{\partial^2}{\partial\Phi^2} \tag{3.98}$$

$$\hat{\Lambda}_r = \frac{\hat{J}_x^2}{\sin^2\Theta} + \frac{\hat{J}_y^2}{\cos^2 2\Theta} + \frac{\hat{J}_z^2}{\cos^2\Theta} \tag{3.99}$$

$$\hat{\Lambda}_c = -\frac{2i\sin 2\Theta}{cos^2 2\Theta}\hat{J}_y\frac{\partial}{\partial\Phi} \tag{3.100}$$

where the Coriolis term typically couples the internal and global rotation motion through a mixed derivative. This choice of orientation of the solidary BF frame leads to a minimization of the Coriolis couplings[35]. Note that $\hat{\Lambda}_h$ represents the Casimir operator for the case of null total angular momentum.

On the other hand, choosing the BF z axis oriented along the maximum inertia axis leads to a simpler expression of the Coriolis term in the Casimir operator:

$$\Lambda^2(\Omega_5) = -\frac{1}{\sin 4\Theta}\frac{\partial}{\partial\Theta}\sin 4\Theta\frac{\partial}{\partial\Theta} - \frac{1}{\cos^2 2\Theta}\frac{\partial^2}{\partial\Phi^2} - \tag{3.101}$$
$$-\frac{2i\sin 2\Theta}{cos^2 2\Theta}\hat{J}_z\frac{\partial}{\partial\Phi} + \frac{\hat{J}_x^2}{\sin^2\Theta} + \frac{\hat{J}_y^2}{\cos^2\Theta} + \frac{\hat{J}_z^2}{\cos^2 2\Theta}$$

The expression for the Coriolis coupling is simpler because it includes $\hat{J}_z$ instead of $\hat{J}_y$, and the first has a much simpler expression:

$$\hat{J}_z = -i\frac{\partial}{\partial\gamma_I} \tag{3.102}$$

3.3. Hyperspherical coordinates

Unfortunately, unlike the asymmetric parameterization case, the eigenfunctions of the Casimir operator in this parameterization are not known for the case of total angular momentum greater than zero. Thus, in applications it is commonly used an expansion as:

$$Y_{\lambda\sigma}^{JM}(\Theta, \Phi, \alpha_I, \beta_I, \gamma_I) = \sum_{\Omega=-J}^{J} Y_{\lambda\sigma\Omega}(\Theta, \Phi) D_{M\Omega}^{J}(\alpha_I, \beta_I, \gamma_I) \qquad (3.103)$$

where Ω is the projection of J on the principal axis frame and the form of the $Y_{\lambda\sigma\Omega}(\Theta, \Phi) D_{M\Omega}^{J}(\alpha_I, \beta_I, \gamma_I)$ functions will be shown in another section (see section 5.1).

Chapter 4

Solution of the CC Equations. The propagative approach

Contents

Among all the methods that can be used for solving the close coupling (CC) equations, in this work we have always used the propagative approach for the time-independent Schrödinger equation associated to the nuclear motion. Propagation essentially consists in solving the properly formulated close-coupling equations by dividing the scattering coordinate in several, small partitions, called sectors. Within each sector, solutions for the internal problem, parametrically dependent on the scattering coordinate, are obtained. This leads to an adiabatic basis treatment throughout the sectors. Inside each sector, instead, the same basis is used to express the scattering part of the solution at one end in terms of that obtained in the previous end. Thus, within a given sector, a diabatic approach is used. The global procedure is sometimes termed as adiabatic intersector diabatic intrasector. A common problem one encounters when trying to propagate the whole set of close-coupling equations is that, as originally formulated, they are what is called a *stiff* set of equations. The stiffness arises as a consequence of the inclusion of closed channel solutions of the internal problem, necessary to ensure the proper convergence of the numerical solution. The resulting instability originated from the exponentially growing nature of the closed channel solutions,

56

Chapter 4. Solution of the CC Equations. The propagative approach

which tend to dominate the whole solution -and destroy linear independence-, is a consequence of the finite precision of the numerical solution algorithms.
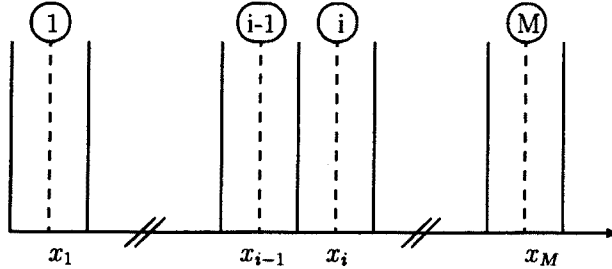

Figure 4.1: Sectorization of the propagation region. The scattering (propagation) coordinate is divided into small intervals where an internal eigenvalue problem will be solved. Its solutions will serve as a basis for propagation.

Several procedures have been proposed to overcome these difficulties, which are reviewed in the following sections. We shall pay special attention to the specific methods used in the present work.

4.1 General formulation of the propagation. The Cauchy propagators

Let's consider the most general form of the scattering equations

$$\left[\frac{d^2}{dx^2} + \mathbf{A}(x) + \mathbf{B}(x) \right] \psi(x) = 0 \tag{4.1}$$

where x is the scattering coordinate and the matrices correspond to the target states expansion. The problem is usually formulated so that $\mathbf{A}=0$. The solution is obtained at an asymptotic value by propagating its value starting from an initial value. By propagating, we understand the obtention of a function value at a given point given the corresponding value at a preceding point.

The propagator of a function in an interval $[x', x'']$ is defined as a $2N \times 2N$ block matrix that connects values of any solution of 4.1, ψ, and its derivative, ψ', at the endpoints x' and x''. Such a propagator is called a *Cauchy propagator*[36]

$$\Omega = \left(\begin{array}{cc} \Omega_1 & \Omega_2 \\ \Omega_3 & \Omega_4 \end{array} \right)$$

for which the defining relation takes the form

$$\left(\begin{array}{c} \psi(x'') \\ \psi'(x'') \end{array} \right) = \left(\begin{array}{cc} \Omega_1(x'', x') & \Omega_2(x'', x') \\ \Omega_3(x'', x') & \Omega_4(x'', x') \end{array} \right) \left(\begin{array}{c} \psi(x') \\ \psi'(x') \end{array} \right) \tag{4.2}$$

4.2. Invariant embedding type propagators.

The existence of such propagators is guaranteed in all the intervals $[x', x'']$ where the matrices $\mathbf{A}(r)$ and $\mathbf{B}(r)$ are continuous functions of x. The basic properties of the Cauchy propagators are[36]:

$$\Omega(x'', x') = \Omega(x'', y)\Omega(y, x') \; for \; y \in [x', x''] \tag{4.3}$$

$$\Omega(x', x') = 1 \tag{4.4}$$

In order to determine the expression of $\Omega(x'', x')$ one needs to solve an appropriate number of initial value problems for the system of equations 4.1.

4.2 Invariant embedding type propagators.

Besides the Cauchy propagators, there is a number of other types of propagators which are involved with boundary value problems rather than initial value ones. These are called *invariant embedding* propagators. The invariant embedding technique consists in solving a series of simple problems embedded in the space of the complete problem. The inherent stability of these methods derives from the fact that the *bounded* scattering amplitude is propagated through space, rather than the wavefunction for the entire system. The so called *reflection* $(Y^{\pm})$ and *transmission* $(Z^{\pm})$ matrices form the propagator originally formulated in ref.[36] that satisfies the following relation for any solution ψ:

$$\begin{pmatrix} \psi(x') \\ \psi(x'') \end{pmatrix} = \begin{pmatrix} Y^+(x', x'') & Z^-(x', x'') \\ Z^+(x', x'') & Y^-(x', x'') \end{pmatrix} \begin{pmatrix} \psi'(x') \\ \psi'(x'') \end{pmatrix} \tag{4.5}$$

Other types of invariant embedding propagators can be formulated such as the R-matrix or the log-derivative method, which we will see in the following sections. For example, let's consider an alternative expression of 4.5 where:

$$\begin{pmatrix} \psi'(x') \\ \psi'(x'') \end{pmatrix} = \begin{pmatrix} L^{(1)}(x', x'') & L^{(2)}(x', x'') \\ L^{(3)}(x', x'') & L^{(4)}(x', x'') \end{pmatrix} \begin{pmatrix} \psi(x') \\ \psi(x'') \end{pmatrix} \tag{4.6}$$

The specific form of the boundary value problems can be established in the following form. Let's call ψ^+, ψ^- the two solutions of 4.1 and impose:

$$\psi^{\pm}(x') = \begin{cases} 1 \\ 0 \end{cases} , \quad \psi^{\pm}(x'') = \begin{cases} 0 \\ 1 \end{cases} \tag{4.7}$$

Substituting in 4.6 we obtain:

$$\begin{pmatrix} \psi^{+\prime}(x') \\ \psi^{+\prime}(x'') \end{pmatrix} = \begin{pmatrix} L^{(1)} & L^{(2)} \\ L^{(3)} & L^{(4)} \end{pmatrix} \begin{pmatrix} 1 \\ 0 \end{pmatrix} \tag{4.8}$$

$$\begin{pmatrix} \psi^{-\prime}(x') \\ \psi^{-\prime}(x'') \end{pmatrix} = \begin{pmatrix} L^{(1)} & L^{(2)} \\ L^{(3)} & L^{(4)} \end{pmatrix} \begin{pmatrix} 0 \\ 1 \end{pmatrix} \tag{4.9}$$

Chapter 4. Solution of the CC Equations. The propagative approach

and therefore,

$$
\begin{aligned}
L^{(1)} &= \psi^{+'}(x') & L^{(2)} &= \psi^{-'}(x') \\
L^{(3)} &= \psi^{+'}(x'') & L^{(4)} &= \psi^{-'}(x'')
\end{aligned}
\tag{4.10}
$$

Since solutions to particular boundary values do not always exist, all invariant embedding type propagators fail to exist for some intervals $[x', x'']$. This difficulty can be however overcome.

Obviously these invariant embedding propagators are related to one another as well as to the Cauchy operators. Consequently, the basic properties of the standard Cauchy propagator can be expressed in terms of the properties of the of any other propagator. In this way, the recurrence relations of the invariant embedding propagators can be derived[36]:

$$
L(x', x'') = \hat{L}\left[\Omega(x''.x')\right]
\tag{4.11}
$$

where $\hat{L}$ acts on a $2N \times 2N$ block matrix

$$
\mathbf{C} = \begin{pmatrix} C_1 & C_2 \\ C_3 & C_4 \end{pmatrix}
\tag{4.12}
$$

so that

$$
\hat{L}\left[\mathbf{C}\right] = \begin{pmatrix} -C_2^{-1}C_1 & C_2^{-1} \\ -C_4C_2^{-1}C_1 + C_3 & C_4C_2^{-1} \end{pmatrix}
\tag{4.13}
$$

acting on both sides of 4.3

$$
L(x', x'') = \hat{L}\left[\Omega(x''.x')\right] = \hat{L}\left\{\hat{L}^{-1}[L(y, x'')]\hat{L}^{-1}[L(x', y)]\right\}
\tag{4.14}
$$

after performing the necessary matrix operations[36]:

$$
\begin{aligned}
L^{(1)}(x', x'') &= L^{(1)}(x', y) - L^{(2)}(x', y) \times \\
&\quad \underbrace{\left[L^{(4)}(x', y) - L^{(1)}(v, x'')\right]^{-1}}_{\mathbf{1}(x', y, x'')} L^{(3)}(x', y)
\end{aligned}
\tag{4.15}
$$

$$
L^{(2)}(x', x'') = L^{(2)}(x', y)\mathbf{1}(x', y, x'')L^{(2)}(y, x'')
\tag{4.16}
$$

$$
L^{(3)}(x', x'') = -L^{(3)}(y, x'')\mathbf{1}(x', y, x'')L^{(3)}(x', y)
\tag{4.17}
$$

$$
L^{(4)}(x', x'') = L^{(4)}(y, x'') + L^{(3)}(y, x'')\mathbf{1}(x', y, x'')L^{(2)}(y, x'')
\tag{4.18}
$$

This recurrence relations can be converted to the following differential form[36] in the $(x'' - y) \to 0$ limit:

$$
\frac{d}{dy}L^{(1)}(x', y) = -L^{(2)}(x', y)A_2(y)L^{(3)}(x', y)
\tag{4.19}
$$

$$
\frac{d}{dy}L^{(2)}(x', y) = -L^{(2)}(x', y)\left[A_1(y) + A_2(y)L^{(4)}(x', y)\right]
\tag{4.20}
$$

$$\frac{d}{dy}L^{(3)}(x',y) = \left[A_4(y) - L^{(4)}(x',y)A_2(y)\right]L^{(3)}(x',y) \qquad (4.21)$$

$$\frac{d}{dy}L^{(4)}(x',y) = A_3(y) + A_4(y)L^{(4)}(x',y) - L^{(4)}(x',y)A_1(y) \qquad (4.22)$$

$$-L^{(4)}(x',y)A_2(y)L^{(4)}(x',y)$$

The A_i, $i = 1, 2, 3, 4$ denote blocks of the coupling matrix in the system of first order differential equations equivalent to the system 4.1:

$$\left(\begin{array}{cc} A_1 & A_2 \\ A_3 & A_4 \end{array} \right) = \left(\begin{array}{cc} 0 & 1 \\ -B & -A \end{array} \right) \qquad (4.23)$$

Let's take a step forward and point out that the propagator whose properties we have been developing is an extension of what is usually called a log-derivative matrix L_D, which is defined by the relation

$$\overline{\psi}'(x) = L_D\overline{\psi}(x)$$

where $\overline{\psi}$ is a solution of 4.1 satisfying the initial $\overline{\psi}(x) = 0$ condition. Indeed, substituting $\overline{\psi}$ into 4.6 it can be seen that $L_D = L^{(4)}$, which is enough for inelastic scattering. This particular method of propagation will be developed from a slightly different point of view in the next section.

4.3   The log-derivative method

In 1973, B.R. Johnson briefly presented his, at that time, new method for propagatively solving the *multichannel equations*[37]. The method is relatively popular, although no really transparent derivation of its algorithm was fully published by the author. However, two different derivations of the method can be found in the literature. One was published by Mrugala and Secrest[36], which has already proven useful as a basis for several improvements[38], which will be later on outlined, and extensions [39, 40] to the original algortihm. However, this derivation relies on a highly sofisticated form of invariant embedding, whose introductory lines have been developed in the preceding section, and it is therefore quite complicated to describe. Another simpler and more understandable derivation, based only on finite difference approximations, has been published by D.E. Manolopoulos[38, 41].

In this section we will follow basically the derivation of the Johnson's log-derivative method from [38], since it will provide us a clearer introduction to the Johnson-Manolopoulos method used in our work.

Let's write the close coupling equations in matrix notation as

$$\Psi(x) = \mathbf{W}(x)\Psi(x), \qquad (4.24)$$

Chapter 4. Solution of the CC Equations. The propagative approach

where x is the propagation coordinate and

$$\mathbf{W}(x) = \frac{2\mu}{\hbar^2}\mathbf{V}(x) - \mathbf{k}^2 \tag{4.25}$$

The centrifugal term is assumed to be included in the potential energy matrix, decaying as x tends to infinity. μ is the collision reduced mass, and $\mathbf{k}$ is a diagonal matrix of asymptotic channel wave vectors. The wavefunction $\mathbf{\Psi}(x)$ is a square matrix where each column is a linearly independent solution of the problem. In principle, the expansion is infinite, but in practice it is always truncated at some finite value, N. The log-derivative matrix is defined as:

$$\mathbf{Y}(x) = \mathbf{\Psi}'(x)\mathbf{\Psi}^{-1}(x) \tag{4.26}$$

In the different log-derivative methods it is this matrix that is propagated, rather than the wavefunction itself and its derivative. This eliminates the stability problems arising whenever the integration is started deep inside the classically forbidden region.

Differentiating 4.26 and using 4.24 to get rid of the second derivative we obtain

$$\mathbf{Y}'(x) = \mathbf{W}(x) - \mathbf{Y}^2(x) \tag{4.27}$$

which is a Riccati matrix equation. In most inelastic scattering problems $\mathbf{W}$ is a real and symmetric coupling matrix. Transposing this equation throughout, one then finds that $\mathbf{Y}'(x)$ is also a solution of the same first order differential equation, as $\mathbf{Y}(x)$. Since its initial value will be symmetric and the solution is unique, the log-derivative matrix will be symmetric for all x. This symmetry is not essential but has computational advantages, particularly for matrix inversion.

From its definition in 4.26, it can be seen that the log-derivative matrix becomes undefined whenever the wavefunction determinant becomes zero. This causes the standard numerical techniques of integration not to be applicable. However, the log-derivative matrix may be safely propagated using a special form of invariant embedding technique (section 4.2). Let's define an embedding type propagator, $\mathcal{Y}$, on a interval $[x', x'']$ by

$$\begin{bmatrix} \mathbf{\Psi}'(x') \\ \mathbf{\Psi}'(x'') \end{bmatrix} = \begin{bmatrix} \mathcal{Y}_1(x', x'') & \mathcal{Y}_2(x', x'') \\ \mathcal{Y}_3(x', x'') & \mathcal{Y}_4(x', x'') \end{bmatrix} \begin{bmatrix} -\mathbf{\Psi}(x') \\ \mathbf{\Psi}(x'') \end{bmatrix} \tag{4.28}$$

The blocks of this propagator are obtained solving appropriate boundary value problems on the interval $[x', x'']$. It is well known that solutions to particular boundary value problems do not always exist, so $\mathcal{Y}$ can also be undefined on some intervals, this, however, does not cause any practical difficulties.

A recursion relation for the log-derivative matrix can be obtained post-multiplying the upper part of the matrix equation in 4.28 by $\mathbf{\Psi}^{-1}(x')$ and the lower part by $\mathbf{\Psi}^{-1}(x'')$ and then eliminating $\mathbf{\Psi}(x')\mathbf{\Psi}^{-1}(x'')$ One obtains:

$$\mathbf{Y}(x'') = \mathcal{Y}_4(x', x'') - \mathcal{Y}_3(x', x'')\left[\mathbf{Y}(x') + \mathcal{Y}_1(x', x'')\right]^{-1}\mathcal{Y}_2(x', x'') \tag{4.29}$$

This recursion relation forms the basis of the log-derivative method. The integration range will be partitioned into a series of small intervals, as it has already been explained, the propagator matrix $\mathcal{Y}$ constructed for each sector and the log-derivative matrix propagated by recursive application of 4.29.

4.3.1   The Johnson-Manolopoulos method

. First published by D.E. Manolopoulos[38], the method is based on the log derivative method 4.3 of Johnson and it has widely proven to be highly competitive for the majority of atomic and molecular collision problems. In particular, we have employed this propagation method in our work for the exact solution of the close coupling equations with the Hyperspherical method presented in chapter 9. The method, as it will be seen, basically differs from the previous one formulated by Johnson in the way in which the sector propagators are constructed.

The algorithm is presented as a means by which the log-derivative matrix can be propagated across a single sector, $[a, b]$. The original sector is divided into two half-sectors. It is then convenient to define the mid point c and step size h by

$$c = \frac{b + a}{2}, \quad h = \frac{b-a}{2} \tag{4.30}$$

In what follows we shall use as well $[x', x'']$ to denote both half-sectors $[a, c]$ and $[c, b]$. Then another basic step is introduced. Prior to obtaining the solution of the complete CC equations, one solves first a simpler homogeneous problem, inside each sector, defining a simple reference potential. This leads to propagators for the homogeneous solutions. The global solution (and the global propagator) is then obtained through the Green's function method, as it will be explained below. Let's start by constructing the analytical solutions to a simple homogeneous problem on the interval $[a, b]$. The equation has the form

$$\Phi''(x) = \mathbf{W}_{ref}(x)\Phi(x) \tag{4.31}$$

where the reference potential $\mathbf{W}_{ref}(x)$ is continuous throughout the sector. In the original log-derivative method $\mathbf{W}_{ref}(x)$ was set to zero, but Manolopoulos introduced instead a piecewise constant diagonal reference potential,

$$\mathbf{W}_{ref}(x)_{ij} = \delta_{ij}p_j^2, \quad r \in [a, b]. \tag{4.32}$$

Homogeneous equation 4.31 is easily solved analytically using this reference potential. One can then define a propagator matrix y corresponding to the homogeneous solutions $\Phi(x)$ analogously to 4.28. The blocks of this propagator for the half-sectors $[x', x'']$ are also easily obtained as,

$$y_1(x', x'')_{ij} = y_4(x', x'')_{ij} = \delta_{ij} \left\{ \begin{array}{ll} |p_j| \coth |p_j| h, & p_j^2 \geq 0, \\ p_j| \cot |p_j| h, & p_j^2 \leq 0, \end{array} \right. \tag{4.33}$$

62

Chapter 4. Solution of the CC Equations. The propagative approach

$$y_2(x', x'')_{ij} = y_3(x', x'')_{ij} = \delta_{ij} \begin{cases} |p_j|csch|p_j|h, & p_j^2 \geq 0, \\ p_j| \csc |p_j|h, & p_j^2 \leq 0. \end{cases}$$

These become undefined whenever its argument approaches an integer multiple of π in a classically allowed region ($p_j^2 \leq 0$). However, the step size h is usually small enough for this situation not to arise.

Equation 4.24 can be reformulated as an integral equation, through the use of the Green's function method[36] on the interval $[a, b]$, with the homogeneous part given by 4.31. Manolopoulos' algorithm consists of discretizing the integral equation using the same quadrature as in the original log-derivative method. The residual coupling matrix is defined as,

$$\mathbf{U}(x) = \mathbf{W}(x) - \mathbf{W}_{ref}(x) \tag{4.34}$$

which is the difference, at each sector end, between the true and the reference potential. Then the quadrature contributions from the three grid points are given by

$$\begin{aligned} \mathbf{Q}(a) &= \frac{h}{3}\mathbf{U}(a) \\ \mathbf{Q}(c) &= \frac{1}{2}\left[\mathbf{I} - \frac{h^2}{6}\mathbf{U}(c)\right]^{-1} \frac{4h}{3}\mathbf{U}(c) \\ &= \frac{4}{h}\left[\mathbf{I} - \frac{h^2}{6}\mathbf{U}(c)\right]^{-1} - \frac{4}{h}\mathbf{I}(c) \\ \mathbf{Q}(b) &= \frac{h}{3}\mathbf{U}(b), \end{aligned} \tag{4.35}$$

where the weights introduced are identical to those used in Simpson's rule integration. To obtain the quadrature contributions from the original log-derivative method one simply has to set $\mathbf{W}_{ref} = 0$ in 4.34.

Finally, the half-sector propagators for the solution of 4.24, $\hat{\mathcal{Y}}(x', x'')$, may be obtained. These contain both analytical contributions from the reference potential and quadrature contributions from the residual potential, which combine in the following way:

$$\begin{aligned} \hat{\mathcal{Y}}_1(x', x'') &= y_1(x', x'') + Q(x'), \\ \hat{\mathcal{Y}}_2(x', x'') &= y_2(x', x''), \\ \hat{\mathcal{Y}}_3(x', x'') &= y_3(x', x''), \\ \hat{\mathcal{Y}}_4(x', x'') &= y_4(x', x'') + Q(x''). \end{aligned} \tag{4.36}$$

The log-derivative matrix is propagated from a to b across the sector by repeated application of the recursion relation,

$$\hat{Y}(x'') = \hat{\mathcal{Y}}_4(x', x'') - \hat{\mathcal{Y}}_3(x', x'')\left[\hat{Y}(x') + \hat{\mathcal{Y}}_1(x', x'')\right]^{-1} \hat{\mathcal{Y}}_2(x', x'') \tag{4.37}$$

where $\hat{Y}(a) = \mathbf{Y}(a)$ and yields the log-derivative value at the end of the particular sector

$$\hat{Y}(b) = \mathbf{Y}(b) + O(h^4).$$

The authors call $\hat{y}(x', x'')$ *effective* propagators because the matrix $\hat{Y}(c)$ defined when 4.37 is first applied, i.e. in the $[x', x''] = [a, c]$, is *not* directly related to $Y(c)$, the log-derivative matrix evaluated at the center of the sector, a quite simple explanation for this can be found in [38].

Once the recursion relation has been established, all that is left is to choose the diagonal reference potential. Manolopoulos and his coworkers have usually used the diagonal of the coupling matrix evaluated at the midpoint c:

$$p_j^2 = \mathbf{W}(c)_{jj} \qquad (4.38)$$

Such a simple to implement choice has proven to give rapidly convergent results with respect to the sector width. Since the reference potential changes from sector to sector, the algorithm is somehow a *function approach* [36, 42] propagative method, especially in regions where the coupling matrix is nearly diagonal. The authors claim that improvement in convergence over the original method (purely *potential approach*[36, 42]) relies on the improved homogeneous solutions in each sector.

The log-derivative matrix may be propagated across any desired interval, $[x_{min}, x_{max}]$, dividing the interval into a series of sectors. Usually x_{min} is chosen to be deep inside the classically forbidden region, and then a diagonal approximation to the **WKB** initial value is used:

$$Y(x_{min})_{ij} = \delta_{ij}\mathbf{W}(x_{min})_{jj}^{1/2} \qquad (4.39)$$

x_{max} will be some large value of the propagation coordinate, beyond which the interaction potential can be neglected. Once this region is reached, the asymptotic log-derivative matrix will be used to calculate the scattering S matrix.

4.3.2   Asymptotic analysis.

The propagation of the log-derivative matrix instead of the wavefunction itself, is found to ease as well the evaluation of the relevant asymptotic quantities. It is so, due to fact that one can write the S-matrix (or, equivalently, the K-matrix) directly in terms of Bessel and Neuman functions and the asymptotic log-derivative. So, once one has obtained the asymptotic log-derivative matrix, an expression can be derived for extracting the scattering matrix from it. To do so, let's first write the wavefunction considering the scattering coordinate is large enough for all potential interactions, but the centrifugal; to be neglected:

$$\psi(x) = \mathbf{J}(x) + \mathbf{N}(x)\mathbf{K}, \quad x \to \infty \qquad (4.40)$$

64

Chapter 4. Solution of the CC Equations. The propagative approach

being $\mathbf{J}(x)$ and $\mathbf{N}(x)$ diagonal. For the open channels these matrix elements will be the Riccati-Bessel functions,

$$[\mathbf{J}(x)]_{ij} = \delta_{ij} k_j^{-1/2} \hat{j}_{l_j}(k_j x), \tag{4.41}$$

$$[\mathbf{N}(x)]_{ij} = \delta_{ij} k_j^{-1/2} \hat{n}_{l_j}(k_j x), \tag{4.42}$$

and for the closed channels these are modified spherical Bessel functions of the first and third kinds

$$[\mathbf{J}(x)]_{ij} = \delta_{ij}(k j x)^{-1/2} I_{l_j+1/2}(k_j x), \tag{4.43}$$

$$[\mathbf{N}(x)]_{ij} = \delta_{ij}(k_j x)^{-1/2} K_{l_j+1/2}(k_j x), \tag{4.44}$$

where k_j is the channel wave number. Performing the log-derivative on 4.40, this is, differentiating with respect to x and post-multiplying by the inverse, we get (setting $x = x_{as}$):

$$\mathbf{K} = -[\mathbf{y}(x_{as})\mathbf{N}(x_{as}) - \mathbf{N}'(x_{as})]^{-1} \times [\mathbf{y}(x_{as})\mathbf{J}(x_{as}) - \mathbf{J}'(x_{as})] \tag{4.45}$$

This matrix $\mathbf{K}$ is the so called reaction matrix and contains elements connecting closed and open channels. It can be shown that it can be factorised as into open-open, open-closed, closed-open and closed-closed submatrices:

$$\mathbf{K} = \begin{pmatrix} \mathbf{K}_{OO} & \mathbf{K}_{OC} \\ \mathbf{K}_{CO} & \mathbf{K}_{CC} \end{pmatrix} \tag{4.46}$$

The scattering matrix can be obtained from the open-open submatrix using the formula[37]:

$$\mathbf{S} = -(\mathbf{I} + i\mathbf{K}_{OO})^{-1} \times (\mathbf{I} - i\mathbf{K}_{OO}) \tag{4.47}$$

The solution corresponding to the closed channels is an exponentially increasing function (equation 4.44) and an exponentially decreasing function (equation 4.44). These, specially the first, can cause numerical trouble when evaluating 4.45. Johnson[37] proposed to eliminate this problem by the replacement of the closed channel matrix elements by:

$$[\mathbf{J}(x_N)]_{ii} \rightarrow 1, \tag{4.48}$$

$$[\mathbf{J}(x_N)]_{ii} \rightarrow [\mathbf{J}'(x_N)]_{ii} \times [\mathbf{J}(x_N)]_{ii}^{-1} \tag{4.49}$$

Expressions for $\mathbf{N}$ are obtained by substitution. Quite clearly, this leaves the open-open submatrix $\mathbf{K}_{OO}$ unchanged.

4.4 The R-matrix method

In 1976, J.C. Light, D.J. Zvijac and R.B. Walker presented in two consecutive articles[44, 43] their new approach to the solution of close coupling equations by using the R-matrix method, originally presented by E.P. Wigner and

4.4. The R-matrix method

L. Eisenbud[45]. The method is based upon a division of the dynamically accessible regions of configuration space into smaller regions (sectors), in each of which a local matrix of the inverse log-derivative, called R-matrix, is determined analytically. Then, these sector R-matrices are assembled recursively and yield a R-matrix for the whole integration region. The scattering matrix can be obtained from this global matrix.

Unlike the Johnson-Manolopoulos method, which we have just employed as originally formulated by the authors, during this work we have got to work quite deeply with this propagation method. So, we have generalized the formulation of the approach in order to take complex potentials into account. This derivated from the problems arisen when a complex absorbing potential was placed so as to absorb all the flux towards products (see sections 2.7 and chapter 8). Due to the use of this potential, a reactive problem was reduced to an inelastic one but paying the price of a complex interaction matrix to be used for the propagation. Then, the R-matrix propagation method had to be adapted in order to consider complex valued interaction matrices. Details of the theory are fully given in the next sections (see specifically section 8.3).

Chapter 5

The Hyperspherical Method

Contents

5.1   The method of Launay and LeDourneuf

In the late 80s and beginning of the 90s, J.M Launay, M. LeDourneuf and coworkers published a series of papers which, in our opinion, caused a major impulse in the development of exact cross-section calculations of reactive systems. Relevance of this work relies on the particularly intelligent partition of the Hamiltonian which allowed the practical calculation of reactive cross-sections, as we will show later on.

5.1.1   The Hamiltonian.

Let's consider we are studying an atom-diatom reactive collision using symmetric hyperspherical coordinates, under a BF rotating solidary frame, whose z lies along the least inertia principal axis. These have been called by some authors APH coordinates[28] (see section 3.3.2). In constructing the APH Hamiltonian, one minimizes the couplings due to rotation of the body frame at linear or near-linear configurations.

The expression of the Kinetic energy operator in APH coordinates, following ref.[46], is:

$$H = -\frac{1}{2\mu\rho^5}\frac{\partial}{\partial\rho}\rho^5\frac{\partial}{\partial\rho} + \frac{\Lambda^2}{2\mu\rho^2} + V(\rho,\varpi) \tag{5.1}$$

where V is the interaction potential and Λ^2, the Casimir operator, is the square root of the grand angular momentum. Following Launay's derivation we replace the original Smith-Whitten hyperangle Θ by θ, which is its double, to allow a familiar $[0, \pi/2]$ range of variation, 0 corresponding to linear configurations and $\pi/2$ to symmetric top configurations. The Casimir operator in 3.96 transforms then into:

$$\Lambda^2(\Omega_5) = -\frac{4}{\sin 2\theta}\frac{\partial}{\partial\theta}\sin 2\theta\frac{\partial}{\partial\theta} - \frac{1}{\cos^2\theta}\frac{\partial^2}{\partial\phi^2} - \frac{2i\sin\theta}{cos^2\theta}\hat{J}_y\frac{\partial}{\partial\phi} + \tag{5.2}$$
$$\frac{2\hat{J}_x^2}{1-\cos\theta} + \frac{\hat{J}_y^2}{\cos^2\theta} + \frac{2\hat{J}_z^2}{1+\cos\theta}$$

This choice of the reference frame allowed Launay to introduce the following partition of the Casimir operator:

$$\Lambda^2 = {\Lambda^2}_0 + \frac{4J_z^2}{\sin^2\theta} + \mathcal{R} \tag{5.3}$$

where ${\Lambda^2}_0$ and $\mathcal{R}$, which contains a part of the rotational kinetic energy and Coriolis coupling, are given by

$${\Lambda^2}_0 = -\frac{4}{\sin 2\theta}\frac{\partial}{\partial\theta}\sin 2\theta\frac{\partial}{\partial\theta} - \frac{1}{\cos^2\theta}\frac{\partial^2}{\partial\chi^2} \tag{5.4}$$

$$\mathcal{R} = \frac{J_{\bar{x}}^2 - J_{\bar{z}}^2}{\cos^2\frac{1}{2}\theta} + \frac{J_{\bar{y}}^2}{\cos^2\theta} - \frac{2i\sin\theta J_{\bar{y}}}{\cos^2\theta}\frac{\partial}{\partial\chi} \tag{5.5}$$

${\Lambda^2}_0$ is the square of the grand angular momentum operator for $J = 0$ in the principal axis frame.

For the sake of simplicity, from now on we will label globally the hyperangular variables, the internal as $\bar{\omega}$ (θ, ϕ) and the external as $\bar{\omega}_E$ (the Euler angles). One may then consider a (parametrically) ρ-dependent basis of five-dimensional functions,

$$\Phi_{k\Omega}^{JM\epsilon_I\epsilon_P}(\rho;\bar{\omega},\bar{\omega}_E) = \varphi_k^{\epsilon_I\epsilon_P\Omega}(\rho;\bar{\omega})N_\Omega^{JM\epsilon_I}(\bar{\omega}_E) \tag{5.6}$$

where the symmetric top wavefunctions $N_\Omega^{JM\epsilon_I}(\bar{\omega}_E)$ of definite parity $\epsilon_I = \pm 1$ are linear combinations of Wigner rotation matrices:

$$N_\Omega^{JM\epsilon_I}(\bar{\omega}_E) = \sqrt{\frac{2J+1}{16\pi^2(1+\delta_{\Omega 0})}}\left[D_{M\Omega}^{J*}(\bar{\omega}_E) + \epsilon_I(-1)^{J+\Omega}D_{M-\Omega}^{J*}(\bar{\omega}_E)\right] \tag{5.7}$$

Here, J is the total angular momentum and M its projection on the space-frame z axis, while $\Omega \geq 0$ is the absolute magnitude of its projection onto the body-frame z axis. The index ϵ_P in (5.6) labels the symmetry of the wavefunction with respect to the permutation of two identical atoms (or even more).

The functions $\varphi_k^{\epsilon_I \epsilon_P \Omega}$, also called surface states, are Ω- and ρ-dependent solutions of a two-dimensional Schrödinger equation at fixed hyperradius ρ:

$$H^\Omega(\rho;\varpi)\varphi_k^{\epsilon_I \epsilon_P \Omega}(\rho;\varpi) = \epsilon_k^{\epsilon_I \epsilon_P \Omega}\varphi_k^{\epsilon_I \epsilon_P \Omega}(\rho;\varpi) \tag{5.8}$$

$$H^\Omega(\rho;\varpi) = \frac{1}{2\mu\rho^2}\left(\Lambda_0^2 + \frac{4\Omega^2}{\sin^2\theta}\right) + V(\rho;\varpi) \tag{5.9}$$

The consideration of a ρ-dependent basis will be very useful thanks to the near separability of the hyperradius. Equation 5.8 can be solved within a $\{\epsilon_I, \epsilon_p, \Omega\}$ symmetry block, following Launay's approach, by variational expansion over a primitive basis of orthogonal eigenfunctions $\{\mathcal{Y}\}$ (pseudoharmonics), see appendix D.

5.1.2   Coupled hyperradial equations

Taking profit from the fact that the hyperradius is a near-separable variable and that a parametrically ρ- and Ω-dependent basis for a part of the Hamiltonian has been obtained, the Schrödinger equation is solved using the diabatic-by-sector method[47], in which the range of integration along ρ is divided into smaller sectors $[\rho_{p-1/2}, \rho_{p+1/2}]$ centered around ρ_p. In each sector, the total wavefunction is expanded on the basis defined at ρ_p,

$$\Psi^{JM\epsilon_I \epsilon_P}(\rho;\varpi,\varpi_E) = \frac{1}{\rho^{5/2}}\sum_{k\Omega}\Phi_{k\Omega}^{JM\epsilon_I \epsilon_P}(\rho_p;\varpi,\varpi_E)f_{k\Omega}^{J\epsilon_I \epsilon_P}(\rho_p;\rho) \tag{5.10}$$

In practice, the expansion of the wavefunction is finite. In particular, we can vary separately the number of k and Ω components in the linear combination 5.10. For instance, the maximum value of Ω in the expansion will be denoted by Ω_m. The functions $f_{k\Omega}^{J\epsilon_I \epsilon_P}(\rho_p;\rho)$, called hyperradial functions, are solutions of the following set of coupled second-order differential equations,

$$\left(-\frac{1}{2\mu}\frac{d^2}{d\rho^2} + \frac{15}{8\mu\rho^2} + \epsilon_k^{\epsilon_I \epsilon_P \Omega}(\rho_p) - E\right)f_{k\Omega}^{J\epsilon_I \epsilon_P}(\rho_p;\rho) \quad *$$

$$+ \sum_{k'}V_{kk'}^{\epsilon_I \epsilon_P \Omega}(\rho_p;\rho)f_{k'\Omega}^{J\epsilon_I \epsilon_P}(\rho_p;\rho) \quad + \tag{5.11}$$

$$+ \frac{1}{2\mu^2}\sum_{k'\Omega'}\mathcal{R}_{k\Omega,k'\Omega'}^{J\epsilon_I \epsilon_P}(\rho_p)f_{k'\Omega'}^{J\epsilon_I \epsilon_P}(\rho_p;\rho) = 0,$$

where the coupling matrix elements are given by (taking into account (5.6)):

$$V_{kk'}^{\epsilon_I \epsilon_P \Omega}(\rho_p;\rho) = <\varphi_k^{\epsilon_I \epsilon_P \Omega}(\rho_p;\varpi)|V(\rho,\varpi)|\varphi_{k'}^{\epsilon_I \epsilon_P \Omega}(\rho_p;\varpi)>_\varpi \tag{5.12}$$

$$\mathcal{R}_{k\Omega,k'\Omega'}^{J\epsilon_I \epsilon_P}(\rho_p) = <\Phi_{k\Omega}^{JM\epsilon_I \epsilon_P}(\rho_p;\varpi,\varpi_E)|\mathcal{R}|\Phi_{k'\Omega'}^{JM\epsilon_I \epsilon_P}(\rho_p;\varpi,\varpi_E)>_{\varpi,\varpi_E} \tag{5.13}$$

The evaluation of these matrix elements is relatively easy since the basis functions $\Phi_{k\Omega}^{JM\epsilon_I \epsilon_P}$ are factorized in 5.6 into an internal part $\varphi_k^{\epsilon_I \epsilon_P \Omega}$, which is

independent of the total angular momentum J, and an external part. Firstly, the potential energy coupling matrix V is independent of the total angular momentum and connects states with the same projection Ω. Therefore, the interaction matrix elements are computed at the boundaries and the middle of each sector and further evaluated inside each sector interpolating by means of a three-point Lagrange interpolation scheme. Secondly, to what the $\mathcal{R}$ matrix elements concerns, integrals over the θ, χ coordinates are independent of J while J-dependent integrals over the Euler angles, ϖ_E can be performed analytically. The authors indicate that $\mathcal{R}$ is smooth and well behaved for linear configurations ($\theta = 0$) and can evaluated just at the middle of each sector, but diverges dramatically for symmetric top configurations ($\theta = \pi/2$). Further comment has to made to point out that $\mathcal{R}$ connects states with $\Delta\Omega = 0, \pm 1, \pm 2$. Therefore, the kinetic coupling leads to a pentadiagonal $\mathcal{R}$ matrix which will be propagated throughout the configuration space. The $\Delta\Omega = 0, \pm 1$ terms arise from Coriolis couplings while those with $\Delta\Omega = \pm 2$ from rotational couplings.

The logarithmic derivative linearly independent solutions of the coupled equations (5.11) are propagated outwards in each sector using the Johnson[37] - Manolopoulos[38] algorithm (see section 4.3). When the boundary of each sector $\rho_{p+1/2}$ is reached, a transformation to the basis of the next sector computed at ρ_{p+1}, is performed. This is repeatedly performed from the first sector until the last one (ρ_q), this corresponding to the asymptotic region. The sector width is an important parameter for controlling the accuracy and efficiency of the calculations.

5.1.3 Asymptotic matching

As the hyperradius ρ increases, the functions φ_k whose energy is lower than the potential ridge tend to concentrate into the arrangement valleys, whereas the atom-diatom interaction potential tends to zero, i.e. the system approaches the asymptotic situation. The behaviour of the φ_k functions then becomes simple, very close to the rovibrational target states into which we have expanded the wavefunction in section 2.6. But this cannot be easily seen from (5.8), since the Smith-Whitten coordinates there used are not suited to describe the atom-diatom fragmentation region (they lead to the well-known *large-ρ shrinkage problem*[48]). On the other hand, Fock asymmetric hyperspherical coordinates provide an optimal parametrization of the system at large hyperradius. It is therefore convenient, once one has got to the asymptotic hyperradius, to rewrite the Hamiltonian (5.9) in Fock internal coordinates ([31] and section 3.3.1). For a given arrangement λ the two Fock angles ($\chi_\lambda, \Theta_\lambda$) are the hyperradial correlation angle $\chi_\lambda = \arctan r_\lambda / R_\lambda$ and the bending angle $\Theta_\lambda = \arccos(\hat{\mathbf{r}}_\lambda \cdot \hat{\mathbf{R}}_\lambda)$. Using these

5.1. The method of Launay and LeDourneuf

coordinates, the Hamiltonian becomes

$$
\begin{aligned}
H^{\Omega}(\rho; \chi_\lambda, \Theta_\lambda) \;=\; & \frac{1}{2\mu\rho^2}\left(-\frac{1}{\sin^2 2\chi_\lambda}\frac{\partial}{\partial\chi_\lambda}\sin^2 2\chi_\lambda\frac{\partial}{\partial\chi_\lambda}\right) + \\
& + \frac{1}{2\mu\rho^2}\frac{4}{\sin^2 2\chi_\lambda}\left(-\frac{1}{\sin\Theta_\lambda}\frac{\partial}{\partial\Theta_\lambda}\sin\Theta_\lambda\frac{\partial}{\partial\Theta_\lambda}+\frac{\Omega^2}{\sin^2\Theta_\lambda}\right) + \\
& + V(\rho;\chi_\lambda,\Theta_\lambda)
\end{aligned}
\tag{5.14}
$$

Moreover, inside each λ-arrangement valley and at large enough hyperradius, the potential becomes independent of the bending angle η_λ and therefore can be written as $V_\lambda(\rho,\chi_\lambda)$. Knowing this, it can be stated that the coupled equations become separable in $(\chi_\lambda,\Theta_\lambda)$ coordinates. Thus, the $\varphi_k^{\epsilon_I \epsilon_P \Omega}$ functions converge to a rovibrational function vj in each arrangement λ, separable in χ_λ and Θ_λ,

$$
\varphi_k^{\epsilon_I \epsilon_P \Omega} \to \chi_{\lambda vj}(\rho;\chi_\lambda)P_j^{\Omega}(\Theta_\lambda).
\tag{5.15}
$$

This separation can be seen as a factorization of the vibration ($\chi_{\lambda vj}(\rho;\chi_\lambda)$) and the rotation ($P_j^{\Omega}(\Theta_\lambda)$) motions. The $P_j^{\Omega}(\Theta_\lambda)$ are associated Legendre functions and the $\chi_{\lambda vj}$ are the solutions of the one-dimensional equation

$$
\left[\frac{1}{2\mu\rho^2}\left(-\frac{1}{\sin^2 2\chi_\lambda}\frac{d}{d\chi_\lambda}\sin^2 2\chi_\lambda\frac{d}{d\chi_\lambda}+\frac{4j(j+1)}{\sin^2 2\chi_\lambda}\right)+V_\lambda(\rho,\chi_\lambda)\right]\chi_{\lambda vj}(\rho;\chi_\lambda)=
\tag{5.16}
$$
$$
\epsilon_{\lambda vj}(\rho)\chi_{\lambda vj}(\rho;\chi_\lambda)
$$

where $V_\lambda(\rho,\chi_\lambda)$ is the asymptotic potential in arrangement λ.

After determination of the fragmentation vj quantum numbers, the total wavefunction is projected onto the space-fixed basis functions, which can be written as $\chi_{\lambda vj}(\rho_q;\chi_\lambda)Y_{jl}^{JM}(\hat{r}_\lambda,\hat{R}_\lambda)$ of each arrangement in order to obtain its hyperradial components $f_{\lambda vjl}^{J\epsilon_I\epsilon_P}(\rho_q,\rho_{as})$ and normal derivatives in that basis. This projection involves two steps:

- firstly, a transformation that reorients the principal axis $\bar{z}$ along $\hat{R}_\lambda$, the atom-diatom vector of arrangement λ. This involves two-dimensional quadratures in the $(\chi_\lambda,\Theta_\lambda)$ coordinates.

- secondly, a standard body-frame to space-frame projection is made using analytical methods.

Regular and irregular asymptotic channel functions are expressed as spherical Bessel functions of the radial variable R_λ. The matching of the components $f_{\lambda vjl}^{J\epsilon_I\epsilon_P}(\rho_q,\rho_{as})$ and of their normal derivatives to these asymptotic functions on the $\rho = \rho_{as}$ hypersphere yields the reactance K and the scattering S matrix, as shown in chapter 2.

Chapter 6

Approximate Close-Coupling Methods

Contents

Given the difficulty for obtaining reactive quantities from an exact quantum mechanical description, a lot of effort has been historically put, and still is, on the development of approximate methodologies and theories that may produce in a reliable but much simpler way the desired results. The goal is then to develop simplifications to the exact equations based on reasonable physical criteria. The development of any approximate method demands a great deepening in the understanding of the physical phenomena, involved in chemical reactions in our case, since it is the understanding of the dependence on all factors that will give the clues to individualize these factors and single out the role they play.

Thus, many approximate methods for the study of reactive scattering, based on different levels of accuracy, can be found in the literature. Most of them are checked with the exchange $H + H_2 \rightarrow H_2 + H$ reaction which, although being a chemically unrelevant reaction, was until recently the only reaction for which one had relevant exact close coupling results at hand. However, many other methods have been developed to study quite different reactions, i.e. non collinearly dominated, and therefore comparison to experimental results has to be carried. But in this case great care has to be taken in their interpretation, since discrepancies could arise as well from inaccuracies in the potential energy surface.

One of the principal difficulties in solving exactly the close coupling equations is the high dimensionality of the resulting equation set. Knowing the great number of approximate theories that can be found in the bibliography, it is by no means the intention of this chapter to give a detailed description to all of

them. Nevertheless, we intend to give a brief description to some of them and describe in more detail the particular approach that has been used in our work , the *Infinite Order Sudden* (IOS) approximation.

Actually, working under the close-coupling (CC) framework, we have already assumed a first approximation, since the CC expansion is not complete strictly speaking (as discussed in section 2.5, the states belonging to the dissociation continuum are excluded from the expansion) although generally acceptable when working below the dissociation threshold. Assuming this approximation, the most general one that is usually made is the so-called *Centrifugal Sudden* (CS) approximation, that supposes the collision to be dominated by the electrostatic potential and the molecular rotation. Essentially, this turns into assuming that the relative kinetic energy term is large enough so that one can consider that the orbital angular momentum to be constant along the collision. In this way, the $\hat{\ell}$ operator can be substituted by a fixed value $\bar{\ell}(\bar{\ell}+1)$ and the Coriolis coupling is diagonalized. Thus, the CS approximation still treats the rotational states exactly and therefore it is often called j_z *conserving* or *helicity conserving* approximation. To see how the CC equations simplify under this approximation let's rewrite the BF Jacobi coordinate CC equations:

$$\left(t^{J\lambda j_\lambda}_{\Omega_\lambda\Omega_\lambda} - E\right) F^\lambda_{Jj_\lambda\Omega_\lambda}(R_\lambda,r_\lambda) + t^{J\lambda j_\lambda}_{\Omega_\lambda\Omega_\lambda+1} F^\lambda_{Jj_\lambda\Omega_\lambda+1}(R_\lambda,r_\lambda) + \tag{6.1}$$

$$+t^{J\lambda j_\lambda}_{\Omega_\lambda\Omega_\lambda-1} F^\lambda_{Jj_\lambda\Omega_\lambda-1}(R_\lambda,r_\lambda) + \sum_{j_\lambda=|\Omega_\lambda|}^{\infty} V^{\lambda\Omega_\lambda}_{j_\lambda j'_\lambda} F^\lambda_{Jj'_\lambda\Omega_\lambda-1}(R_\lambda,r_\lambda) = 0$$

$$J = 0,1,2,\ldots \quad \Omega_\lambda = -J,-J+1,\ldots,J \quad j_\lambda = |\Omega_\lambda|,|\Omega_\lambda|+1$$

Neglection of the Coriolis coupling corresponds to setting the Ω-off-diagonal blocks to zero:

$$t^{J\lambda j_\lambda}_{\Omega_\lambda\Omega_\lambda\pm1} = 0 \tag{6.2}$$

and in the Ω-diagonal term the orbital angular momentum operator is substituted by a fixed value. We therefore obtain a CS-CC equation set:

$$\left(\bar{t}^{J\lambda j_\lambda}_{\Omega_\lambda\Omega_\lambda} - E\right) F^\lambda_{Jj_\lambda\Omega_\lambda}(R_\lambda,r_\lambda) \sum_{j_\lambda=|\Omega_\lambda|}^{\infty} V^{\lambda\Omega_\lambda}_{j_\lambda j'_\lambda} F^\lambda_{Jj'_\lambda\Omega_\lambda-1}(R_\lambda,r_\lambda) = 0 \tag{6.3}$$

where

$$\bar{t}^{J\lambda j_\lambda}_{\Omega_\lambda\Omega_\lambda} = -\frac{\hbar}{2\mu}\left(\frac{\partial^2}{\partial R_\lambda^2} + \frac{\partial^2}{\partial r_\lambda^2}\right) + \frac{\hbar^2 \hat{j}_\lambda}{2\mu r_\lambda^2} + \frac{\hbar^2 \ell(\ell+1)}{2\mu R_\lambda^2} \tag{6.4}$$

Although this approximation eliminates the coupling between different values of Ω_λ, it still treats all rotational channels exactly and therefore the dimensionality of the equation set is still high.

Quite evidently, to move on further from the CS approximation, one must establish approximations on the rotational motion of the target, since it is usually

the source of the largest increase in the number of states of the close-coupling expansion. We would like to distinguish in the next level of approximation between two different approaches, depending on how the rotational motion is treated. On one hand, it is argued that since rotational periods are large in comparison to vibrational periods, it is reasonable to use what is called a *sudden rotational* or *energy sudden* (ES) approximation, for which the atom-diatom orientation remains fixed for the motions in both reactants and products channels. On the other hand, it could be argued that, since the rotational motion correlates with a flexion-vibration along the reaction path, this flexion motion can be treated adiabatically and correlate it statistically to the asymptotic rotational levels.

The first approximation is what is called *Infinite Order Sudden* (IOS) approximation and it has been the approach employed in some of the calculations of this work. Since it will be described in the following section, in particular its application to reactive scattering, here we will just point out that the IOS approximation reflects, in the BF Jacobi coordinates CC equations, as a parametrization of the Jacobi orientation angle. Thus, the number of variables is reduced to two (R_λ, r_λ) and the third becomes a parameter (Θ_λ), the equation set is then solved for each value of Θ_λ, for a wide enough range of angles, to cover the whole reaction window.

The second approximation for the treatment of rotation in the scattering event (once under the CS approximation) englobes a variety of methods which are called generally *Reduced Dimensionality Exact Quantum* (RDEQ) approaches. The different approaches differ from one another in the different degree of adiabaticity with which the flexion motion is considered as well as other approximations to the treatment of the centrifugal potentials. Full description of these methods can be widely found in the literature[26].

The real behaviour observed in most of the systems is obviously a mixture of both assumptions, sudden and adiabatic. The flexion dynamics for energies near the threshold, is in fact adiabatic but at energies well above the system clearly tends to a sudden behaviour.

There exist as well other approximate methods arising from rather different assumptions than what we have seen up to now. One of them is based on the *distorted wave* (DW) theory, which considers the reactive event as a small perturbation on the non-reactive collision dynamics. This consideration is based on the fact that cross sections for inelastic or elastic processes are usually of some orders of magnitude greater than the reactive ones. Thus, the reactive scattering matrix can be approximated as a matrix element of a perturbative Hamiltonian operator, using non-reactive wavefunctions of the reactants and products states.

Practical results using the DW theory showed that reaction is usually a perturbation much larger than first order, so that most of these methods were abandoned. However, more recently, Baer and coworkers set up a method which shares some characteristics with the DW approach. It is based on dividing both the Hamiltonian and the scattering solution in a reference problem plus a per-

turbative part. The reference portion is defined so as to have a simpler solution (elastic, average angle inelastic, complete inelastic or even average reactive collisions have been taken as reference problems), while the perturbation, which is included completely (not through perturbative methods), considers the remaining interaction. Approximations are then flexibly built into the method, since it can be considered separately both in the reference and the perturbation parts. The solution to the whole problem is obtained by means of a generalized-Lagrange-multiplier variational approach. The inclusion of absorbing potentials inside the method gave a major impulse to it, so that it has been widely applied for the approximate treatment of three-, four- and five-atom reactions[49].

6.1 R-IOSA

The IOS approach, initially formulated for the inelastic case, was introduced with the aim of reducing the complexity that the great number of rotational states for each vibrational state causes. Historically, the first works on this approximation date from the middle 50s to the middle 60s[50, 51], but their formulations resulted rather involved and not so easy to interpret. Curtiss[52], Pack[53] and Secrest[54] extended the formulation and gave an almost ultimate practical form. This development allowed Pack to perform the first applications[55]. Since then, the method has been confronted with exact CC or other approximate results with generally satisfactory conclusions.

The considerable good agreement found encouraged its application to reactive scattering by three research groups almost simultaneously. The first article published was a communication on the preliminary results by Bowman and Lee[56] for the $H + H_2$. Then followed the theoretical works by Khare, Kouri and Baer[57, 58, 59] (KKB), Barg and Drolshagen[60] (BD) as well as that of Bowman and Lee[61] (BL). Formulations by KKB and BL and essentially identical, since both are based on the explicit use of the orbital angular momentum, while BD formulated their own approximation based on the total angular momentum.

Major differences can be found, anyway, in how these approaches perform the matching process between both rearrangement channels and how do they relate the IOS parameters for reactants with those of products. In particular, since, as we will see, the IOS motion is based on a constant atom-diatom orientation angle along the collision, a criterion for a reactants-products orientation angle correspondence must be established. To do this, the approaches of BL and BD must introduce additional simplifications, while the KKB formulation is able to base the whole matching process on a parameter $B_{\nu\lambda}$.

The KKB theory defines a surface to match both channels so that:

$$r_\nu = B_{\nu\lambda} r_\lambda$$

where the parameter allows to take into account the possible asymmetry of the

two channels involved in the rearrangement process. On the other hand, BL must introduce the approximation of centrifugal potential conservation in the reactants to products transition which permits to write $\Theta_\nu = \pi - \Theta_\lambda$. At their turn, BD obtain the reactive equations only for the limiting case in which the central atom mass can be considered as infinite. In the approach here followed we have used the matching parameter of KKB and we have set this parameter so that transition between both arrangement coordinate sets is done on the potential ridge, the region where the reactive transition probability is a maximum[62].

As usual, the first applications of the method were performed on the $H + H_2 \rightarrow H_2 + H$ system[62, 63, 64]. Results were compared to exact data available on the reaction and some of them appeared to be in rather good agreement, the cross section not differing in more than 25%. On the other hand, in some other rather sensible quantities as the differential cross section or the opacity function, greater discrepancies were found.

The first application to a more asymmetrical system was done by Clary and Drolshagen[65] on the $D + HCl \rightarrow DH + Cl$ system, in the context of the Light-Heavy-Light (LHL) limiting case of an infinite central mass. Results were in good agreement with those obtained by a less approximated technique[66], mostly at high energies for both global and more detailed quantities. However, no comparison was performed of this results with experimental or less approximated data for this reaction nor the $H(D) + HBr \rightarrow H(D)Br + H$ studied later by Clary[67] as well.

The IOS approach has been widely used in our research group[68] as well as in the work presented here. We have used both the reactive and inelastic applications of the IOS approximation. The first calculations were performed using the R-IOS code as developed by Giménez et al.[26] on the $Mg + FH \rightarrow MgF + H$, with the purpose of studying the dynamics of this reaction. The code propagates a IOS solution of the nuclear Schrödinger equation using the R-matrix propagation method. Other R-IOS calculations have been recently carried away in the group as well on the $B + OH \rightarrow BO + H$, in which we did some calculations. Next, once the R-matrix was generalized to take complex values of the interaction matrix into account, we were able to introduce Negative Imaginary Potentials in our problem and formulate the reactive problem as a pseudo-inelastic one (see 2.7); the R-IOS was modified to a NIP-IOS code which resulted of the same accuracy of the previous code and generally of better efficiency. The new implementation was tested on a wide range of systems showing a rich variety of scattering dynamics, since they were characterized by heavy masses, varied ergicities, involved PESs, ...

6.1.1 R-IOS Approximation equations.

As we have already said, the IOS approximation assumes that a possible form of simplifying the rotational motion arises from the consideration that rotational

periods are usually considerably large when compared to vibrational periods. It is then reasonable to think that, as a limiting case, the orientation between the atom and the diatomic molecule remains fixed in both rearrangement channels. However, we must point out that, technically, this is not an assumption but rather a consequence of how the approximation is constructed.

The IOS approximation is obtained by imposing simultaneously the centrifugal sudden (CS) and energy sudden (ES) restrictions, which in practical terms can be written as:

$$\hat{\ell}^2 \;\to\; \overline{\ell}(\overline{\ell}+1) \tag{6.5}$$

$$\hat{j}^2 \;\to\; \overline{j}(\overline{j}+1) \tag{6.6}$$

i.e., both angular momentum operators are substituted by fixed constant values.

In the expression we have derived for the Jacobi coordinates in the BF frame, the rotational angular momentum j is found explicitly, but not the orbital angular momentum ℓ . This leaves two possibilities: a) to find the condition equivalent to 6.6 in the BF formulation or, b) change the representation frame so that the centrifugal frame appears explicitly. We will refer to the first case as the J-labeled IOS formulation and in the second to the ℓ-labeled IOS.

The J-labeled formulation was developed by Barg and Drolshagen[60] and translates the 6.6 condition into the following approximations in the equation set 6.1:

$$\Omega'_\lambda \to \overline{\Omega}_\lambda \tag{6.7}$$

$$t^{J\lambda j'_\lambda}_{\Omega'_\lambda \Omega'_\lambda \pm 1} \to 0 \tag{6.8}$$

However, this J-labeled formulation has proven to undergo some difficulties in inelastic scattering[57]. In particular, when the potential is spherically symmetrical, physically senseless transitions are found between different levels m_j. On the other hand, the ℓ-labeled formulation is exact at this limit.

It is therefore convenient to derive the R-IOS equations in their ℓ-labeled formulation. A direct way of doing this would be to employ the Jacobi SF close coupling equations. However, transformation between different rearrangement channels would still be much clearer under a BF frame, for which the procedure followed[26] could be to integrate the SF equations in each channels and transform them to the BF frame once it gets to matching both arrangements.

Both representations are related by the following unitary transformation:

$$F^\lambda_{Jj'_\lambda \ell'_\lambda}(r_\lambda, R_\lambda) = \sum_{\Omega'_\lambda} \left(\frac{2\ell'_\lambda + 1}{2J + 1}\right)^{1/2} \langle \ell'_\lambda 0 j'_\lambda \Omega'_\lambda | J\Omega'_\lambda \rangle \, F^\lambda_{Jj'_\lambda \Omega'_\lambda}(r_\lambda, R_\lambda) \tag{6.9}$$

and the inverse transformation will be given by:

$$F^\lambda_{Jj'_\lambda \Omega'_\lambda}(r_\lambda, R_\lambda) = \sum_{\ell'_\lambda} \left(\frac{2\ell'_\lambda + 1}{2J + 1}\right)^{1/2} \langle \ell'_\lambda 0 j'_\lambda \Omega'_\lambda | J\Omega'_\lambda \rangle \, F^\lambda_{Jj'_\lambda \ell'_\lambda}(r_\lambda, R_\lambda) \tag{6.10}$$

If one substitutes 6.10 into the Schrödinger equation 6.1, one obtains after some manipulations and neglecting the Coriolis couplings:

$$\left[\left(\frac{\partial^2}{\partial R_\lambda^2} + \frac{\partial^2}{\partial r_\lambda^2}\right) + \frac{2\mu E}{\hbar^2} - \frac{\ell_\lambda'(\ell_\lambda'+1)}{R_\lambda^2} - \frac{j_\lambda'(j_\lambda'+1)}{r_\lambda^2}\right] F_{Jj_\lambda'\ell_\lambda'}^\lambda(r_\lambda, R_\lambda) = \quad (6.11)$$

$$\frac{2\mu}{\hbar^2}\sum_{\ell_\lambda''}\sum_{j_\lambda''}\left\langle \ell_\lambda' j_\lambda'|V^J|\ell_\lambda'' j_\lambda''\right\rangle F_{Jj_\lambda''\ell_\lambda''}^\lambda(r_\lambda, R_\lambda)$$

where now the kinetic energy term is diagonal and does not depend on J. On the other hand the potential energy term contains much more coupling than in the BF case:

$$\left\langle \ell_\lambda' j_\lambda'|V^J|\ell_\lambda'' j_\lambda''\right\rangle = \sum_{\Omega_\lambda'} \frac{\sqrt{(2\ell_\lambda'+1)(2\ell_\lambda''+1)}}{(2J+1)}\left\langle \ell_\lambda' 0 j_\lambda'\Omega_\lambda'|J\Omega_\lambda'\right\rangle \quad (6.12)$$

$$\left\langle \ell_\lambda'' 0 j_\lambda''\Omega_\lambda'|J\Omega_\lambda'\right\rangle 2\pi \int_0^\pi Y_{j_\lambda'\Omega_\lambda'}^*(\Theta_\lambda, 0)V(r_\lambda, R_\lambda, \Theta_\lambda)Y_{j_\lambda''\Omega_\lambda'}(\Theta_\lambda, 0)\sin\Theta_\lambda d\Theta_\lambda$$

Note that this term depends explicitly on J. This equation can be simplified if one introduces the following transformation:

$$F_{J\bar{\ell}\bar{j}\bar{\Omega}_\lambda}^\lambda(r_\lambda, R_\lambda, \Theta_\lambda) = \sum_{\ell_\lambda' j_\lambda'} \sqrt{\frac{2\ell_\lambda'+1}{2J+1}}\left\langle \ell_\lambda' 0 j_\lambda'\bar{\Omega}_\lambda|J\bar{\Omega}_\lambda\right\rangle \quad (6.13)$$

$$Y_{j_\lambda'\bar{\Omega}_\lambda}(\Theta_\lambda, 0)F_{Jj_\lambda'\ell_\lambda'}^\lambda(r_\lambda, R_\lambda, \Theta_\lambda)$$

this allows us as well to define the function $F_{J\ell j\Omega_\lambda}^\lambda(r_\lambda, R_\lambda, \Theta_\lambda)$ parametrically depending on the angle Θ_λ. Substituting 6.13 into 6.11, one obtains:

$$\left[\frac{\partial^2}{\partial r_\lambda^2} + \frac{\partial^2}{\partial R_\lambda^2} - \frac{\bar{\ell}(\bar{\ell}+1)}{R_\lambda^2} - \frac{\bar{j}(\bar{j}+1)}{r_\lambda^2}\right] F_{J\bar{\ell}\bar{j}\bar{\Omega}_\lambda}^\lambda(r_\lambda, R_\lambda, \Theta_\lambda) = \quad (6.14)$$

$$= \frac{2\mu}{\hbar^2}\left[V(r_\lambda, R_\lambda, \Theta_\lambda) - E\right]F_{J\bar{\ell}\bar{j}\bar{\Omega}_\lambda}^\lambda$$

This equation is known as the IOS Schrödinger equation since it gives the radial solution for each value of the atom - diatom orientation angle. Note that the terms in 6.14 still contain the λ superindex labeling the arrangement. This is to remind that, for rearrangement processes, we will have an equation as 6.14 for each possible arrangement channel ($\lambda = \alpha, \beta, \gamma$). The solution of these equations can be performed in many ways, but at a certain moment a matching procedure must be carried away between the solutions from the different regions of the configuration space. This matching procedure, as well as the asymptotic boundary conditions, characterize the reactive process with respect to that elastic or inelastic.

In this work, as well as in other works published by our research group, the integration of the IOS coupled equations at each value of the orientation angle

will be carried away employing natural circular coordinates and the R-matrix propagation method. For the derivation of the IOS coupled equations using these coordinates, see [26].

Chapter 7

R-IOS studies.

Contents

In this chapter we will englobe the works we have done employing the R-IOS approximate methodology. Our research group has worked for a long time using this approach and we believe we have earned relative experience on it. As in all approximate methods the clue to their adequacy is the knowledge in depth of their restrictions. R-IOS has shown up to be a relatively reliable method for most of the systems studied in our group[68], specially when the orientational effect of the surface was small or when high collision energies were considered.

So, in this context we present the articles we have published concerning our work on two reactive systems, namely $Mg + FH \rightarrow MgF + H$ and $B + OH \rightarrow BO + H$, employing the R-IOS code we had at hand as developed by ref.[26]. As it will be seen, the study on the first system was carried away rather thoroughly on many aspects and led to the publication of two articles, each of them focusing on a different aspect we found interesting. Concerning the second system, we found it worth studying the rather involved resonance pattern presented by the system even at the three-dimensional level (cross section) employing a reduced dimensionality model.

7.1   The $Mg + FH \rightarrow MgF + H$ system.

The system presents many interesting characteristics that motivated its study. Any system composed by relatively high masses constitutes a challenge for a quantum mechanical study due to the increase in the number of states that have to be considered. Moreover, the present system evolves through a non collinear transition state and this is not the usual case in the reactions commonly studied. Besides, the system showed to be properly suited for a IOS study since simple studies on the potential energy surface used proved that the transition state region was rather isotropic as a function of the orientation angle. This fact clearly enfavours a simpler IOS study where its fixed orientation restriction will loose relevance. An extensive R-IOS calculation was thus carried away on the title reaction calculating a total of 50 energy points, specially focusing on the threshold region using an energy grid of up to 0.01 eV.

Two rather differenced studies were carried from these results, in one of them we focused mainly on the energy threshold to reactivity and the curious characteristics showed by the fixed angle reactivity. In the second a wider study was performed concerning the product vibrational distribution (PVD) and the isotopic mass effect. For this second study, extensive quasiclassical trajectories calculation were run as well as additional R-IOS calculations for the title reaction and their isotopic variations.

The potential energy surface employed for the calculations was fitted to *ab initio* points using a **RBO** functional form. The reaction presents a 1.33 eV endoergicity and a late barrier of 1.83 eV whose transition state geometry is clearly bent with a $Mg\hat{F}H$ angle of 72°. Besides these characteristics, two wells characterize the surface, a collinear well 0.34 eV below reactants' asymptote corresponding to the $MgFH$ complex and a second well 1.30 eV below reactants' asymptote corresponding to a highly bent geometry (around $\Theta = 35°$) which we shall call *insertion* complex. This second well, although deep, can only be reached through reorientation since the barrier for the fixed geometry is to high and will therefore be unrelevant for the IOS reactivity while it will play a qualitatively significant role in quasiclassical trajectories reactivity. Relevance of the works presented relies, mainly, in our opinion, on the fact of having found noticeable quantum effects in a system where a heavy atom is transferred. General features of the PES here described can be observed in the contour plots of figure 7.1.

7.1.1   Energy mode effectiveness and tunneling in triatomic reactions: the energy threshold for the $Mg + FH \rightarrow MgF + H$ reaction.

Chemical Physics Letters 282 (1998) 91-99.

In this paper, a three-dimensional approximate quantum mechanical calcula-
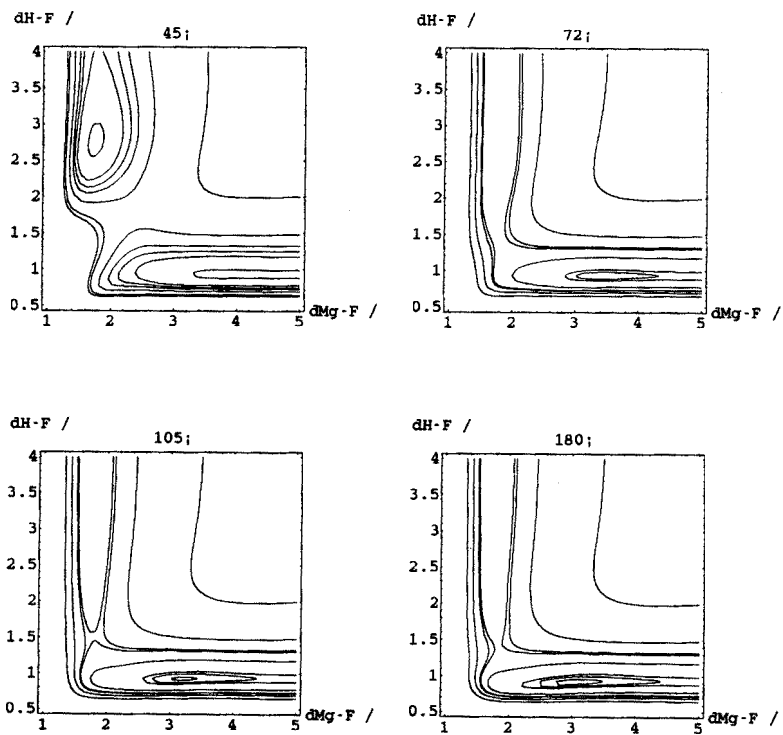
7.1. The $Mg + FH \rightarrow MgF + H$ **system.**

Figure 7.1: PES contour levels at four different relevant atom - diatom orientation angles. Upper-left panel corresponds to $\Theta = 45°$ and shows the insertion well, upper-right panel to $\Theta = 72°$, which is the transition state geometry, lower-left to $\Theta = 105°$, which is an intermediate angle and lower-right to collinearity showing the collinear well.

tion on the $Mg + FH$ system was presented in order to get some insights on the effects on the reactivity threshold and how it was affected mainly by the reactants initial vibrational energy. The global three-dimensional cross section presented a marked selectivity towards the vibrational energy mode, in agreement with the Polanyi rules. So, accordingly to what these rules state for a late barrier, reactivity was drastically enhanced by an increasing in the initial vibrational energy of reactants. However, rather than the tridimensional magnitudes, the fixed angle cross sections were explored in order to get some indications on the reaction mechanism which showed up to be more complex than it appeared from the 3D curves. From this fixed angle study two well differentiated behaviours were stated. On one hand, for low initial vibrational levels significant reactivity was found only for angles close to that of the transition state geometry. On the other hand, higher vibrational levels tended quite unexpectedly to collinear reactivity. Moreover, studying the reactivity threshold we found that the lowest energy threshold to reactivity was given by the $v = 3$ reactants initial vibrational level at a fixed angle of $\Theta = 180°$, far from the TS geometry. This was achieved by the system through a significant tunneling contribution. These were two rather surprising facts since the lowest point of the reaction barrier was located at a bent angle, far from collinearity.

The key to the explanation of this rather unusual behavior was given by the plots of the fixed angle Minimum Energy Paths (MEPs) where it could be seen how, even if the barrier increased when moving towards open angles, its width decreased even more significantly allowing then for a greater tunneling probability. The analytic formula for permeability of a simple square barrier model justified the higher tunneling effect for the $v = 3$ vibrational level, at the same total energy.

Energy mode effectiveness and tunnelling in triatomic reactions: the energy threshold for the Mg + FH → MgF + H reaction

Fermín Huarte-Larrañaga [a], Xavier Giménez [a], Margarita Albertí [a],
Antonio Aguilar [a], Antonio Laganà [b], José Maria Alvariño [b,1]

[a] Departament de Química Física, Universitat de Barcelona, Martí i Franquès 1, 08028 Barcelona, Spain
[b] Dipartimento di Chimica, Università di Perugia, Via Elce di Sotto 8, 06130 Perugia, Italy

Abstract

An approximate three-dimensional quantum approach has been adopted to investigate threshold effects for the Mg + FH → MgF + H reaction and their dependence upon reactants' vibrational energy. The main results are: (a) vibrational energy is the most effective mode (however, this switches from vibration at open angles to translation at bent angles); (b) although a fairly heavy atom is transferred, the threshold is determined by the tunneling region, being dominant orientation angles significantly differing from that of the saddle; (c) the threshold moves to lower energy values as the reactant vibrational level increases. A rationale is given in terms of fixed orientation-angle minimum potential-energy profiles. © 1998 Elsevier Science B.V.

1. Introduction

The accurate determination of reactive thresholds is of key importance in studies of reaction dynamics and chemical kinetics [1–3]. As an example, the value of the rate constant of gas-phase elementary reactions with a positive activation energy are, in the usual temperature ranges, mainly controlled by the amount of reactivity around the threshold. The value of the threshold temperature is usually linked to the value of some key structural parameters (like the height of the barrier to reaction of the potential energy surface (PES)) via the calculation of the cross section (σ) from which rate constants can be evalu-

ated by integrating over energy. Most often, the calculation of the rate constant is performed using a simple classical transition state treatment (TST) [1,4], which assumes reactions occur only at energies higher than the saddle. Tunneling corrections, if any, are in general introduced in a one-dimensional fashion along the minimum energy path (MEP) of the PES [1]. Only rarely, corner-cutting corrections are introduced [5]. To include the dependence of reactivity on the collision angle (γ), one can make use of a fixed γ TST treatment. As a result, one obtains a fixed γ contribution $\sigma(\gamma)$ to the cross section and a fixed γ threshold energy (E_{th}), whose dependence on the collision angle has the same shape as the window to reaction of the PES. This is in general also found when performing a reactive infinite-order sudden (RIOS) [6–8] calculation. Such a finding implies that

tunneling effects do not change significantly with the collision angle, as has been found previously in calculations on a wide variety of atom–diatom systems [9–14]. However, this is not the case for the Mg + FH reaction; for this reaction, the peculiar features characterizing the PES of the system make the value of γ at which threshold energy is lowest differ significantly from the one at which the potential energy barrier is minimal.

The well known Polanyi rules [2] state that the reactivity of endothermic processes which have a late barrier (i.e. a barrier displaced into the exit valley) is more efficiently enhanced by vibrational energy than by translational energy. This is also found for the title reaction. However, factors similar to those which lead to the different contribution of tunneling to reactivity, as the collision angle varies, also alter the relative importance of the various energetic modes, resulting in a much more complex picture of the reaction outcome as a function of the collision angle.

The Mg + FH reaction has alread_ been investigated theoretically. A reliable PES was developed and three-dimensional (3D) quasiclassical trajectory (QCT) calculations were performed on it [15–18]. The present quantum study focuses on some features of the corresponding quantum results.

The Letter is organised as follows: in Section 2 the potential energy surface is briefly illustrated by pointing out the features of the PES useful for understanding tunneling effects. Section 3 describes the main results obtained. In Section 4 the factors determining both the enhancement of reactivity with vibration and the amount of tunneling for the different initial conditions are analyzed. Finally, in Section 5, the main conclusions are presented.

2. Potential energy surface and calculation method

As mentioned above, we used the Mg + FH → MgF + H PES of Ref. [15], fitted to ab initio potential energy values using an RBO functional. The PES is 1.33 eV endoergic and has a late barrier located well inside the product channel, which is 1.826 eV higher than the reactants' asymptote for the bent ($\gamma = 72°$) transition state geometry. In the strong interaction region the MEP shows two minima: one,

collinear ($\gamma = 180°$), 0.34 eV deeper than the reactants' asymptote, is located just before the reaction barrier and the other, 1.30 eV deeper than the reactants' asymptote, is located late in the products channel. The second minimum corresponds to a highly bent configuration ($\gamma = 35°$) that can only be reached through reorientation, since at $\gamma = 35°$ the barrier interposed between the reactant asymptote and the well is high. The two minima are separated by a large barrier. Another important feature of this PES (see solid line of Fig. 1) is that the fixed angle barrier to reaction (that, as already noted, has a minimum at $\gamma = 72°$) rises sharply on moving to smaller values of γ (more bent geometries) while it rises slightly (about 0.2 eV in the range $74° \leq \gamma \leq 115°$ and about zero from $\gamma = 115°$ to $\gamma = 180°$) moving to larger values of the collision angle. As a support to a TST rationalization of the angular dependence of E_{th}, we also plot in the same figure (dotted line) the fixed γ zero-point energy at the
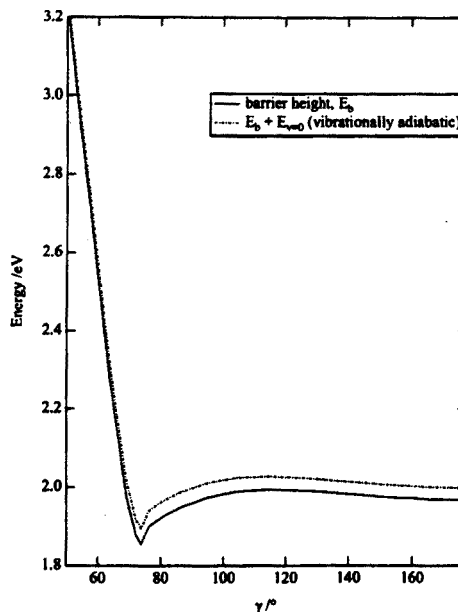

Fig. 1. Value of the fixed γ barriers to reaction plotted as a function of the collision angle γ. Continuous line: potential energy values. Dotted line: potential energy plus zero-point energy (effective barrier).

7.1. The $Mg + FH \rightarrow MgF + H$ system.

barrier (effective barrier) obtained from a RIOS treatment.

As already mentioned, a program based on the RIOS approximation was used for the calculations of 3D quantum reaction probabilities. For a detailed description of the methodology, see [6–14]. A total of 50 energy points were considered by paying particular attention to the threshold region, for which a grid spacing of 0.01 eV was adopted. The computational parameters [9–14] leading to optimum convergence are the following: 35 vibrational basis functions, 390 sectors (240 for the reactants channel and 150 for the products channel), 16 values of the orientation angle γ (ranging from 45° to 180°) and up to 200 angular momentum partial waves. The calculation of the energy-independent part (potential profiles, vibrational eigenvalues and eigenfunctions and potential matrix elements for each sector and overlaps between sectors) took approximately 25 s, while propagation along the translational sectors, by means of a standard invariant embedding R-matrix method [19,20], for all relevant partial waves and all orientation angles necessary to get converged 3D cross sections, took an average of 15000 s, per energy, on a single processor (R8000) Silicon Graphics Power Challenge L Workstation.
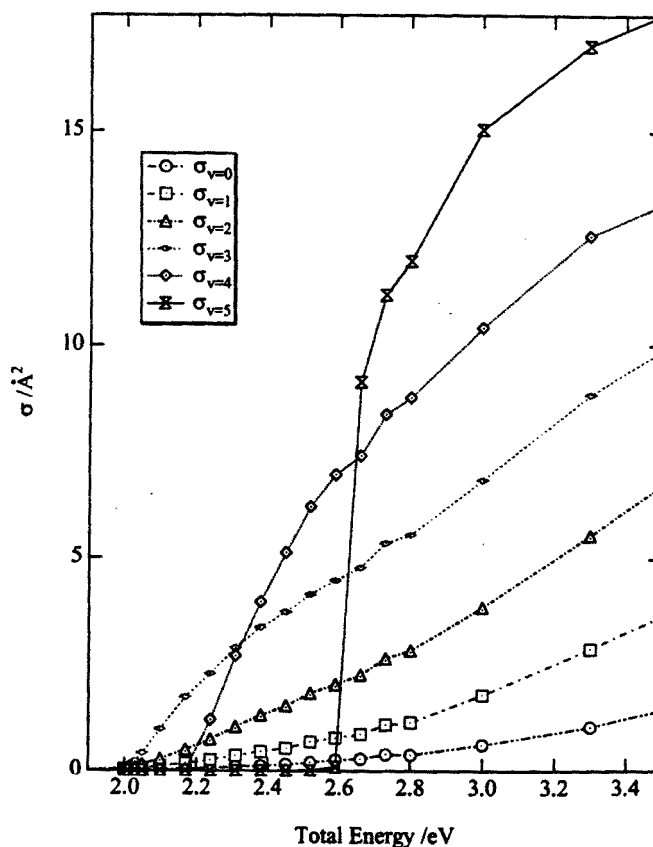

Fig. 2. Vibrational state specific cross sections plotted as a function of total energy for the first six reactant vibrational levels.

3. Main features of the results

Vibrational state-specific cross sections (the rotational state is always set equal to zero, in our study, taking advantage of the fact that rotations are decoupled in the RIOS treatment) are plotted in Fig. 2, as a function of total energy, for the first six reactant vibrational levels. A first indication given by the plots shown in the figure is that vibrational energy is effective in promoting reaction, as expected from the late location of the reaction barrier on the fixed γ MEPs. The reactive cross section becomes, in fact, larger when v, the reactant quantum vibrational number, increases (saturation is observed only at much

higher energies). The effectiveness of vibrational energy in promoting reaction is confirmed also by the dependence of the E_{th} values on v, as shown by the different curves plotted in Fig. 2: for reactant vibrational levels asymptotically lying below the reaction barrier ($v = 0$, 1, 2 and 3), the threshold is located basically at the same energy value (1.89 eV). This means that for $v = 0$, 1, 2 and 3 the coupling of different degrees of freedom is adequate (although in a different way) to allow reaction. Therefore, any energy increase (either in translation or in internal degrees of freedom) actively contributes to the overtaking of the barrier, though with different effectiveness. In other words, motions along all degrees of
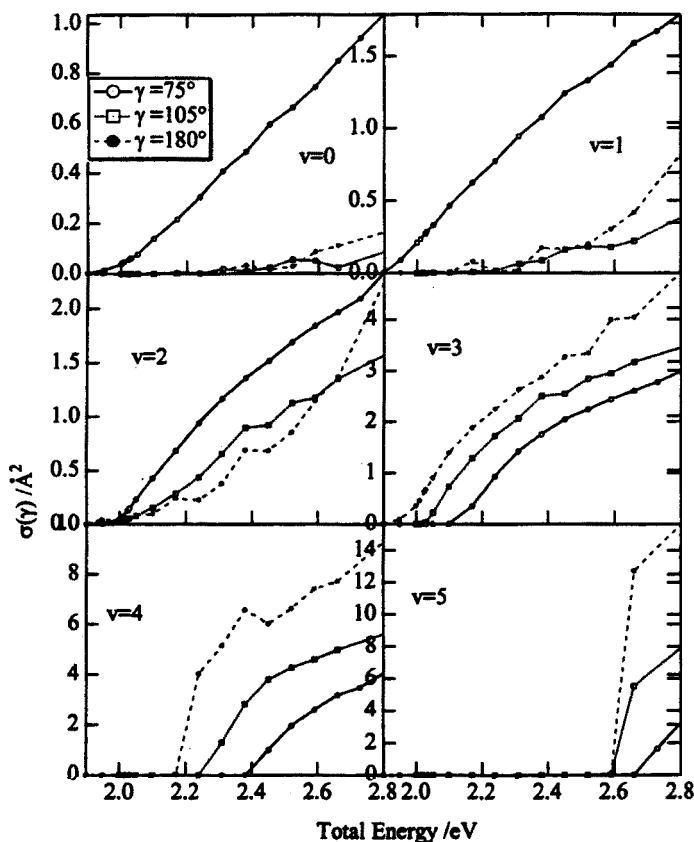

Fig. 3. Fixed-γ vibrational state specific contributions to the cross sections plotted as a function of total energy for $\gamma = 75°$ (continuous line and open circles), $\gamma = 105°$ (dotted line and open squares), $\gamma = 180°$ (dashed line and full circles).

7.1. The $Mg + FH \rightarrow MgF + H$ system.

freedom are open to reaction. For $v = 4$ or larger, the threshold energy coincides with the reactant vibrational energy (2.09 eV at $v = 4$, 2.50 eV at $v = 5$, ...) since the energy at which the channel opens is higher than the reaction barrier. In addition, no effective barriers due, for instance, to vibrational adiabaticity, come into play.

Although these results seem to indicate that the reactivity determining feature of the PES is the height of the effective barrier, that at $\gamma = 72°$ amounts to 1.866 eV (see Fig. 1), fixed angle RIOS calculations provide a more complex picture of the reaction

mechanism. A decisive argument is offered by the value of fixed-angle cross sections, plotted in Figs. 3 and 4 as a function of total energy, at initial vibrational states ranging from $v = 0$ to $v = 5$ and $\gamma = 75$, 105, and 180°. In Fig. 3, the curves are given for an interval of total energy going from 1.8 to 2.8 eV at three values of γ relevant to reaction. In Fig. 4, an enlargement of these curves over the threshold region is given by including also the cases of $\gamma = 72°$ and $\gamma = 95°$. Plots of the two figures related to $v = 0$ and 1 clearly show that, at low vibrational energy, the most important contribution to the reactive cross
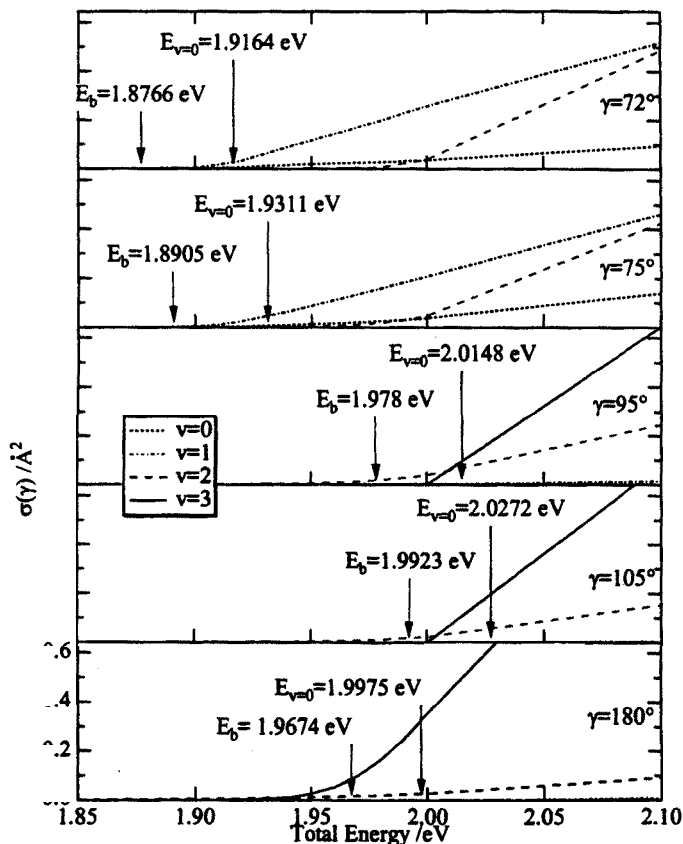

Fig. 4. Fixed-angle contributions to the cross section plotted as a function of total energy, in the threshold energy region, at several reactant vibrational levels and γ values. $E_{r=0}$ and E_b indicate the vibrationally adiabatic $v = 0$ and barrier height energy, respectively (see also Fig. 1).

section (top row of Fig. 3) comes from the γ value of the transition-state; it also determines the energy value of the threshold (E_{th} is 1.900 eV for $v = 0$ and $E_{th} = 1.896$ eV for $v = 1$). This is not clearly so at $v = 2$, while it definitely does not apply to $v = 3$. In fact, at $v = 2$, although the largest contribution to the cross section (central lhs panel of Fig. 3) comes from $\gamma = 75°$, the threshold energy is now determined by the $\gamma = 180°$ contribution (as shown in Fig. 4, $E_{th} = 1.880$ eV for $\gamma = 180°$, $E_{th} = 1.950$ eV for $\gamma = 105°$ and $E_{th} = 1.950$ eV for $\gamma = 75°$). The central rhs panel of Fig. 3 also shows that at $v = 3$, the orientational angle contributing most to the overall reactivity is $\gamma = 180°$, ($\sigma(180°) > \sigma(105°) > \sigma(75°)$). Related calculated energy thresholds are: $E_{th}(180°) = 1.922 < E_{th}(105°) = 2.000 < E_{th}(75°) = 2.10$ eV. Results at higher v values are similar to those at $v = 3$. However, the threshold energies are in this case higher since they are determined by the opening of the asymptotic energy levels.

In summary, the above data indicate that:

(1) the effectiveness of the reactants' energy in promoting product formation decreases when moving from open to bent collision angles. In relative terms, translation is more effective at bent angles while vibration is more effective at open angles.

(2) threshold energy decreases as both γ and v increase thanks also to non-classical (tunneling) contributions.

4. Discussion

The first comment will be addressed to the effect of varying the allocation of energy into the different molecular modes of the reactants. It is, in fact, generally true that for this reaction vibration enhances reactivity, as usual for processes having a late barrier (MEPs of Fig. 5 evidence a late position of the barrier at all values of the collision angle). At the same time it is also true that, for bent orientation angles (e.g. $\gamma = 75°$), reaction is clearly favoured by high translational energy, with initial vibrational energy being less effective than for open angle collisions (although, absolutely speaking, vibration is more effective than translation at all values of the orientation angle). In contrast, at open orientation angles reactivity is increasingly enhanced as vibra-
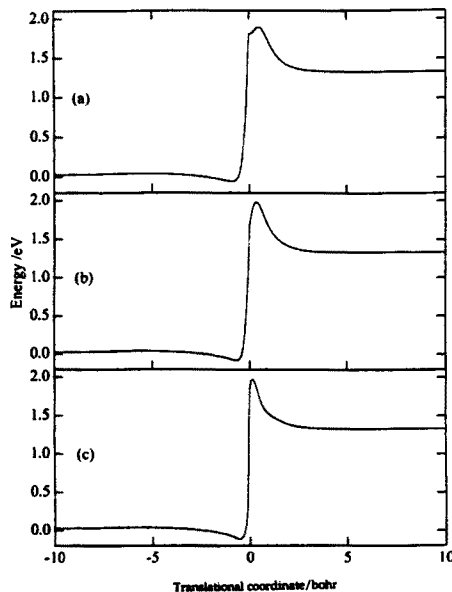

Fig. 5. Potential energy minimum energy path, as a function of the (translational) circular collision coordinate of Ref. [10], at different values of γ (top panel $\gamma = 75°$, central panel $\gamma = 105°$, bottom panel $\gamma = 180°$).

tional energy increases. The above features indicate that, in relative terms, insertion-like collisions (small γ values) are favoured by translational energy, while abstraction-like collisions (large γ values) are favoured by vibrational energy.

This can be rationalized as follows: in insertion-like collisions, translational energy produces both the effect of displacing H and bringing Mg closer to F. Besides that, insertions are made more difficult by high vibration since, in this case, the incoming atom meets, on average, a large number of repulsive diatomic configurations as a result of the higher frequency of the H-atom motion and of the strong endothermicity of the MgH channel (4.692 eV). In contrast, in collinear-like collisions the H-atom motion is less disturbing, for geometrical reasons and, since the collision is gradually oriented towards the F-atom end, it becomes benefited from the larger F-atom kinetic energy as vibration is increased.

As a result, the overall reactive behaviour is determined by the relative importance of the two

mechanisms as the orientational angle is varied, in agreement to what was found in previous studies of triatomic reactions with a bent transition state and following complex dynamics [9–14,21]. It is important to emphasize here that the overall behaviour of the Mg + FH reaction is more characterized by open angle configurations than closed ones, contrary to what one usually expects (i.e. that reactive collisions are strongly characterized by the nature of the saddle configuration). This is due to the "anomalous" feature of the saddle point of this system that allows less reactive flux than the higher barriers of more open configurations do.

A second reactive feature analyzed here is the threshold location on the energy scale. Since thresholds are in general associated with tunneling region effects, one might found their analysis on one dimensional (fixed γ MEP) transition state models and rationalize the observed behaviour in terms of tunneling through the barrier of the fixed γ MEP. However, as it has been commented before, such an analysis would lead to the wrong conclusion that the lowest fixed angle threshold is associated with the γ value of the transition state. This is not the case for the Mg + FH reaction, since the main contributors to the energy threshold (Fig. 4) are γ values much larger than that of the saddle point. Such a shortcoming of the one dimensional tunneling model could be eliminated by introducing a higher dimensionality tunneling treatment. It is well-known, however, that higher dimensionality tunneling models are rather involved and difficult to implement [3,4]. For this reason we choose here an approximate two-dimensional analysis that includes the contribution of the degree of freedom orthogonal to the reaction coordinate (adiabat) in an step-wise fashion. To illustrate the approach we first show in Fig. 5 the lowest adiabat of the Mg + FH reaction as a function of the (translational) circular collision coordinate [19,20] at three values of the angle γ. The plots evidence shows two important features: (a) in agreement with data shown in Fig. 1, the adiabatic barrier height varies little with the orientation angle; (b) the barrier *width narrows as the orientation angle becomes larger*. This implies that tunneling may become larger as collisions tend to collinearity. The model adopted allows us to work out a more quantitative estimate of the tunneling contribution. By fitting a rectangular

Table 1

$G_v(E)$: barrier permeabilities for the square-potential problem (see text for definition) given as a function of the total energy E and the initial vibrational level v, at total energies corresponding to the threshold regions. The square potential features have been fitted so as to match as closely as possible the potential energy profiles corresponding to $\gamma = 72°$ ($E_{\text{barrier}} = 1.8766$ eV and $\Delta u = 1.2$ bohr) and $\gamma = 180°$ ($E_{\text{barrier}} = 1.9674$ eV and $\Delta u = 0.7$ bohr), shown in columns (a) and (b), respectively

E_{tot} (eV)	(a) $\gamma = 72°$		(b) $\gamma = 180°$	
	$v = 0$	$v = 3$	$v = 0$	$v = 3$
1.86	0.19	0.39	0.34	0.51
1.90	0.24	0.47	0.37	0.56
1.94	0.28	0.55	0.40	0.61

barrier to each adiabat, a simple analytic expression can be given for the barrier permeability $G_v(E)$ [3]:

$$G = (4k_{C_v}/k_{A_v})\Big[(1 + k_{C_v}/k_{A_v})^2 \cos^2(k_{B_v}\Delta u)$$
$$+ (k_{B_v}/k_{A_v} + k_{C_v}/k_{A_v})^2 \sin^2(k_{B_v}\Delta u)\Big]^{-1},$$

where Δu is the barrier width and k_{A_v}, k_{B_v} and k_{C_v} are the wavevectors associated with the entrance (before the square barrier), intermediate (over the barrier) and exit section (after the barrier), respectively, of the reaction profile. Results for several threshold energies and vibrational levels are given in Table 1. Values reported in the table give a quantitative grounding to the qualitative considerations previously described. In addition, using the same model it is possible to illustrate why E_{th} shifts to lower positions as the initial vibrational number v increases from 0 to 3. In fact, since when varying the kinetic energy (comparisons are made at constant total energy), the permeability is approximately proportional to k_{C_v}/k_{A_v} (k_{C_v} is the wavevector associated to the asymptote past the collision (in our case, the products region) and k_{A_v} the wavevector associated with the reactants region [3]), k_{A_v} diminishes as v is increased, so that tunneling will be larger at larger initial vibrational energy, as observed in our calculations.

5. Conclusions

In this work, a RIOS study of the Mg + FH → MgF + H reaction has been carried out, as a function

of initial translation and vibrational energy. Particular attention has been paid to the threshold region reactivity. The main conclusions are:

(a) The overall effectiveness of vibrational energy in promoting reaction is consistent with the late location of the reaction barrier, namely that vibration is more effective than translation for enhancing the reactivity of this type of reaction. It was found, however, that this global effect results from two different contributions to reactivity when the different fixed-angle results are analyzed. Thus, on one hand, for bent orientation angles, the reaction is clearly favoured by high translational energy while an increase of the initial vibrational energy is less effective. On the other hand, the reactivity for open orientation angles is enhanced by vibrational energy while an increase of initial translational energy is less effective. Such a behaviour has been put down to the different effectiveness of translation and vibration in insertion and collinear like mechanisms.

(b) The threshold energy location was found to be mainly due to tunneling. It was also found that the threshold energy for fixed γ contributions to the cross section moves to lower values as γ increases, in spite of the fact that the transition state is bent (small γ). This behaviour was rationalized in terms of fixed angle adiabatic curves. It was found that the lowering of the threshold as γ increases is caused by a gradual decrease of the width of the effective potential barrier, which ultimately leads to an increase of tunneling reactivity.

(c) It was also found that the threshold shifts to lower positions as the initial v increases from 0 to 3. This effect can be understood in terms of analytical permeabilities calculated for a model barrier. In this case, the initial translational energy is inversely proportional to the permeability, giving rise to an increase of tunneling as vibrational energy is increased (since, at the same total energy, translation correspondingly decreases).

The importance of these findings lies in the fact that the Mg + FH reaction implies a heavy atom transfer, for which quantum effects are usually believed to be negligible [22]. To evaluate these effects we have used the approximate QM RIOS method. This has the obvious disadvantage of ignoring the bending degree of freedom in computing the tunneling reactivity, which would lead to important dis-

agreements if comparisons were made with experimental or more accurate results. In this work, however, we have been mainly interested in comparing tunneling reactivities at different orientation angles, showing that, with particular PES topographies, results can substantially differ from those corresponding to TST concepts. This comparison between different orientation angles has been made on an equal theoretical footing, so as to ensure that the calculated effects are due to special features the interaction potential, the main conclusion of the present work.

Acknowledgements

References

[1] K.J. Laidler, Chemical Kinetics, Harper and Row, New York, 1987.
[2] R.D. Levine, R.B. Bernstein, Molecular Reaction Dynamics and Chemical Reactivity, Oxford University Press, New York, 1987.
[3] R.P. Bell, The Tunnel Effect in Chemistry, Chapman and Hall, London, 1980.
[4] W.H. Miller, Acc. Chem. Res. 9 (1976) 306.
[5] B.C. Garrett, D.G. Truhlar, A.F. Wagner, T.H. Dunning Jr, J. Chem. Phys. 78 (1983) 4400.
[6] V. Khare, D.J. Kouri, M. Baer, J. Chem. Phys. 71 (1979) 1188.
[7] J.M. Bowman, K.T. Lee, J. Chem. Phys. 72 (1980) 5071.
[8] D.G. Barg, D. Drohlshagen, Chem. Phys. 17 (1980) 209.
[9] A. Aguilar, M. Alberti, X. Giménez, X. Grande, A. Laganà, Chem. Phys. Lett. 233 (1995) 201.
[10] X. Giménez, J.M. Lucas, A. Aguilar, A. Laganà, J. Phys. Chem. 97 (1993) 8578.
[11] M. Gilibert, X. Giménez, M. González, R. Sayós, A. Aguilar, Chem. Phys. 191 (1995) 1.

7.1. The $Mg + FH \rightarrow MgF + H$ system.

[12] A. Aguilar, M. Gilibert, X. Giménez, M. González, R. Sayós, J. Chem. Phys. 103 (1995) 4496.

[13] A. Laganà, G. Ochoa de Aspuru, A. Aguilar, X. Giménez, J.M. Lucas, J. Phys. Chem. 99 (1995) 11696.

[14] M. González, R.M. Blasco, X. Giménez, A. Aguilar, Chem. Phys. 209 (1996) 355.

[15] A. Laganà, M. Dini, E. García, J.M. Alvariño, M. Paniagua, J. Phys. Chem. 95 (1991) 8379.

[16] J.M. Alvariño, A. Laganà, J. Chem. Phys. 95 (1991) 998.

[17] J.M. Alvariño, A. Laganà, J. Phys. Chem. 96 (1992) 3587.

[18] J.M. Alvariño, L. Cuadrado, M.L. Hernández, A. Laganà, Chem. Phys. Lett. 241 (1995) 408.

[19] J.C. Light, R.B. Walker, J. Chem. Phys. 65 (1976) 1598.

[20] J.C. Light, R.B. Walker, J. Chem. Phys. 65 (1976) 4272.

[21] A. Laganà, A. Aguilar, X. Giménez, J.M. Lucas, Chem. Phys. Lett. 189 (1992) 138.

[22] A. Kuppermann, Theoretical Chemistry, Advances and Perspectives, in: D. Henderson (Ed.), vol. 6A, Academic Press, New York, 1981, pp. 79–164.

7.1.2 The influence of initial energy on product vibrational distributions and isotopic mass effects in endoergic reactions: the $Mg + FH$ case.

In this second work, we concentrated our effort on a rather thorough study of the Products Vibrational Distribution and an extensive comparison of the R-IOS results for the reactive cross section with those obtained by quasiclassical trajectories performed by ourselves as well. For this work, besides the results we already had, additional calculations were run on their D, T isotopical variations as well as their corresponding QCTs in order to have a reliable benchmark.

Concerning the PVDs, although they are in general agreement with Polanyi's rules, the distributions show qualitatively different behaviours depending not only on the collision energy but also on the initial vibrational level. This is a field which we found worth exploring since it could give some interesting conclusions regarding the state-specificity of reactions. So, at low collision energies, PVD for initial vibrational levels below $v = 4$ are *statistical* while PVD corresponding to that level is rather adiabatic. When moving towards higher collision energies, the PVD broaden as expected but those corresponding to $v \leq 3$ tend to shift towards greater values of the final vibrational level (v') while that for $v = 4$ proceeds inversely, shifting towards lower products vibrational levels. This we have tried to justify in the article through the role played by the different values of the angular momentum by plotting the opacity functions.

Besides, isotopic mass variations on the light atom were performed (H, D, T) in order to get better knowledge of the reaction mechanism. Accordingly to the reaction's selectivity towards the vibrational energy mode, the cross section for a given energy, at a given initial vibrational level, decreased as the light atom mass was increased. In order to have a practical benchmark to test the reliability of our results, QCT calculations were run on the title system and its isotopic variations. Agreement between the two methodologies was generally good and was attributed to a low influence of relatively both quantum and orientational effects.

The influence of initial energy on product vibrational distributions and isotopic mass effects in endoergic reactions: the Mg + FH case

Fermín Huarte-Larrañaga,[a] Xavier Giménez,[a] Margarita Alberti,[a] Antonio Aguilar,[a] Antonio Laganà[b] and José M. Alariño[c]

[a] Departament de Química Física, Universitat de Barcelona, Martí i Franquès, 1, 08028 Barcelona, Spain
[b] Dipartimento di Chimica, Università di Perugia, Via Elce di Sotto, 8, 06123 Perugia, Italy
[c] Departamento de Química Física, Universidad de Salamanca, Salamanca, Spain

Extended Quasiclassical Trajectory and quantum Reactive-Infinite Order Sudden calculations were performed on a previously developed potential energy surface to investigate the dynamics of the endoergic (1.33 eV) Mg + FH → MgF + H reaction. The study focused on both the product vibrational distributions and the spectator-atom isotopic mass effect. In particular, their dependence upon varying, over a wide range, both translational and vibrational energy of reactants was investigated in detail. It was found that an increase of the translational energy shifts the maximum of the product vibrational distribution to a higher product vibrational state (v') when the reactant vibrational state (v) is low. However, the maximum of the product vibrational distribution is shifted to lower v' values when v is high. At the same time, it was found that the vibrational energy has less influence on the shape of the product distributions than does the translational energy, except when several (four in our case) vibrational quanta are added. In this case, a product vibrational distribution having a vibrational adiabatic-like shape was obtained. At high translational and vibrational energy, collisions were found to be direct enough to allow for the kinematic heavy heavy–light constrictions to largely determine the product vibrational distribution, as confirmed by the analysis of quantum state-to-state opacity functions. Isotopically substituted reactions showed a generally good agreement between quasiclassical and quantum results for all initial v values. Despite that, an unexpected shift of quasiclassical reactive thresholds towards higher translational energies was found for the D and T isotopic variants at low vibrational energies. A rationale for these and other dynamical effects is discussed.

1 Introduction

The basic mechanisms that lead to molecular energy transfer have been the subject of extended studies during the last few decades, with most of the work being focused on inelastic collisions.[1] However, energy transfer is also intimately connected to reactive processes. It is only because of the additional difficulties that arise when dealing with reactive processes that a systematic study has not yet been performed, especially for those processes for which the energy flow directly involves reactive modes. In spite of that, the key role played by reactive processes in transferring energy has been widely recognized, for instance, by the fluid dynamics and the plasma physics communities, who have shown that a proper inclusion of the reactive processes into the modelling greatly enhances the accuracy of theoretical predictions.[2]

A great deal of theoretical work has already been performed to understand the way energy is allocated into product modes, for a large number of elementary reactions, when reactants are in low vibrational states. Conversely, relatively little is known on the effect on product energy distributions of increasing either the vibrational excitation of the reactant molecule or the translational energy of the system. Some of the available results[3–7] indicate that product distributions may be drastically altered if initial conditions involve moderately or highly excited vibrational states and/or large translational energies. For these reasons, more work aimed at rationalizing these effects is needed, especially if the passive control of chemical processes, as it is currently termed, is to be reached.[8]

On the experimental side, Berg and Sloan[3] have measured the product vibrational distribution (PVD) for exoergic reactions and its evolution with translational energy. An interesting observation made in their paper was that PVDs measured for reactants in the ground vibrational state ($v = 0$) differ from those predicted for exoergic reactions by collinear calculations,[9] even when the minimum energy path of the related potential energy surface (PES) is collinear. In particular, it was found that there is not the expected shift in the PVD ($v = 0$) maximum to higher v' values when the collision energy increases. On the contrary, a shift to lower v' values was found. A reactive-infinite order sudden (R-IOS) study was also performed.[10] It showed that the discrepancy between collinear and experimental findings may be rationalized, for the above mentioned exoergic reactions, in terms of the different range of angular momentum values that contribute to the reaction at different product v' values, rather than in terms of a weakening of the collinear nature of the reactive event. More recently, Kalogerakis and Zare[4] performed a crossed-beam study of the strongly heavy heavy–light (HHL) Ba + HI → BaI + H reaction at several translational energies. The product energy distribution showed a remarkable collision energy dependence. For instance, the PVD at 5 kcal mol^{-1} is bell-shaped and peaks at $v' = 12$, while at higher energies a second maximum located at $v' = 0$ shows up. The mechanisms controlling the observed behaviour were found to be related to the angular momentum centrifugal barrier at low energy and to energy conservation at high energy. Related

arguments will be used here to rationalize some of the results obtained for the title reaction.

Our investigation was motivated by the wish to know more about the PVDs of endoergic reactions and about their change in shape when initial conditions vary over a wide range of values. The investigation focused on the $Mg + FH \rightarrow MgF + H$ reaction, since this process is strongly endoergic, has a clear HHL nature and allows an extended study of both selectivity and specificity of vibrational energy, thanks to the small vibrational spacing in the product arrangement and the existence of a reaction barrier (1.826 eV from the reactants side) in the PES. Owing to the fact that the key issue of the paper is the investigation of the relationships linking the vibrational modes and the reactive behaviour of the system, the calculations were carried out using the quantum time-independent R-IOS technique. The approach provides, in fact, the whole fixed energy vibrational state-to-state S-matrix by averaging over rotations.[11-15]

Using the same technique, the isotopic substitution of the spectator H-atom was also investigated. The interest in this is based on the fact that, in addition to allowing an evaluation of the kinetic isotope effect, the mass change allows also an additional comparison of the role played by vibrational energy. Therefore, results from isotopic variants will be used as a complement to those obtained by varying v. Furthermore, the isotopic variation of the constant of inertia of the reactant diatom also allows a qualitative evaluation of the importance of reorientation in determining reactivity. This means that results obtained for the isotopic substitutes will be used not only to gain a better knowledge of the reaction mechanism but also to gather indications about the validity of the fixed angle assumption of the R-IOS calculations.

Other theoretical investigations of the $Mg + FH$ reaction have been carried out in the past. A reliable PES[16] based on a bond order (BO) functional was developed. QCT and, more recently, some quantum R-IOS calculations[16-20] were performed on that PES to investigate the reactive properties of this system. Particular attention was paid to the rationalization of energy mode effectiveness and tunneling properties. It was found that the energy mode more suited to enhance reactivity switches from vibration (at open atom–diatom orientation angles) to translation (at bent angles) and that the threshold reactivity is largely determined by the tunneling at angles different from that of the saddle geometry, in spite of the fact that a fairly heavy atom is transferred during the process.

This paper is organized as follows: the PES used and the methodology adopted are briefly described in Section 2. Results are presented in Section 3 and their main features are discussed in Section 4. Conclusions are given in Section 5.

2 Potential energy surface and computations

As mentioned above, we used for our calculations the $Mg + FH \rightarrow MgF + H$ PES,[16] fitted to *ab initio* potential energy values using an RBO functional. The PES is 1.33 eV endoergic and has a late barrier placed well inside the product channel. The barrier is 1.826 eV higher than the reactants' asymptote. The transition state geometry is bent, with γ (the angle formed by the Jacobi vectors) being 72°. In the strong interaction region the MEP shows two minima: one for the collinear ($\gamma = 180°$) geometry, which lies 0.34 eV below the reactants' asymptote and is placed just before the reaction barrier, and one for a highly bent ($\gamma = 35°$) geometry, which lies 1.30 eV below the reactants' asymptote and is placed late in the product channel. There is also a large barrier interposed between the two minima, being *ca.* 3.0 eV for the fixed-angle energy path and gradually reduced through reorientation. Another important feature of this PES is that the fixed-angle barrier to reaction (which, as already noted, has a

minimum at $\gamma = 72°$) rises sharply on moving to smaller values of γ (more bent geometries) but rises very little (*ca.* 0.2 eV in the range $74 \leqslant \gamma \leqslant 115°$ and *ca.* zero from $\gamma = 115$ to 180°) on moving to larger γ values.

As already mentioned, a program based on the R-IOS approximation was used to obtain 3D estimates of the quantum reaction probabilities. For a detailed description of the methodology, see refs. 10–15 and 21–23. Owing to the characteristics of the system (heavy particles, highly structured PES), particular attention was paid to make the numerical procedures highly accurate. A total of 50 energy values were considered. The computational parameters[10-15] leading to converged reactive probabilities are as follows: 35 vibrational basis functions, 390 sectors (240 for the reactants channel and 150 for the products channel), up to 200 angular momentum partial waves and 16 values of the orientation angle γ (ranging from 45 to 180°). The calculation of the energy-independent part (potential profiles, vibrational eigenvalues and eigenfunctions and potential matrix elements for each sector and overlaps between sectors) took approximately 25 s, while the propagation along the reaction coordinate, by means of a standard invariant embedding R-matrix method,[24] for all relevant partial waves and all orientation angles, took an average of 15000 s per energy, on a single processor (R8000) Silicon Graphics Power Challenge L Workstation. Additional calculations were performed to estimate the isotopic mass effects at 10 energy values for each isotopic variant (D and T) of the hydrogen atom. To ensure the proper convergency, all numerical parameters were rechecked when varying the mass. Only the dimension of the vibrational basis needed to be adjusted for each isotope. In fact, because of the non-negligible shrinking of the vibrational level spacing when going from H to D and T (changes in the skewing angle and scaling factors were found to be less important) the dimension of the basis needed to be increased to 40 for D and to 45 for T.

Existing QCT results[15-18] were integrated by performing further calculations aimed at completing the range of initial v values and translational energies already considered. A total of 100000 trajectories were run for each set of initial conditions. Equivalent calculations were performed also for the D and T isotopic variants, at 10 energy values.

3 Results

Fig. 1 shows the variation of the PVD when plotted as a function of the total energy (E_{tot}) and the reactant vibrational number (v). In the figure, the energy increases on going from bottom to top panels and the reactant vibrational number increases in going from left to right panels. In general—with the exception of $v = 4$—an approximately statistical PVD, having a maximum at $v' = 0$, is obtained. Such a behaviour is consistent with Polanyi rules: the late barrier of the endoergic PES leads to a repulsive energy release, thus favouring the population of the lowest product vibrational states. However, several deviations were found, depending on both total energy and the reactant vibrational state.

When the total energy increases, the distribution always becomes wider, covering a larger interval of product vibrational states. It was also found that for $v \leqslant 3$ the PVD maximum tends to shift towards higher v' states as the energy increases. In particular, this is apparent for $v = 0$ and 2. At $v = 1$ this leads to the appearance of a local maximum that peaks at $v' = 5$. However, this is not the case of $v = 4$. Its PVD peaks at $v' = 5$ at low energy values (suggesting a tendency to vibrational adiabaticity). In this case the maximum moves towards lower v' values (it is located at $v' = 2$ at $E_{tot} = 3.00$ eV) as the energy increases.

As for the isotopic mass effect, Fig. 2 compares QCT and R-IOS cross sections of $Mg + FH$, $Mg + FD$ and $Mg + FT$
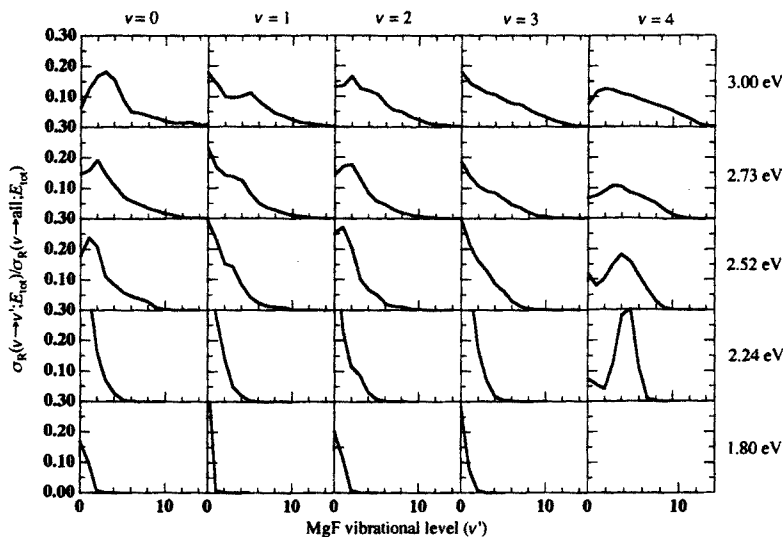
7.1. The $Mg + FH \rightarrow MgF + H$ system.

Fig. 1 Product vibrational distributions, plotted as a function of the initial vibrational state (columns) and the total energy (rows).

for the first six reactant vibrational states. The curves are plotted as a function of translational energy. From the figure the significant enhancement of the reactivity as the vibrational energy is increased is clearly apparent, as is typical of endoergic reactions with late barriers. This holds for all isotopic variants when going from low to high v. However, at a fixed initial vibrational level, the absolute value of the total cross
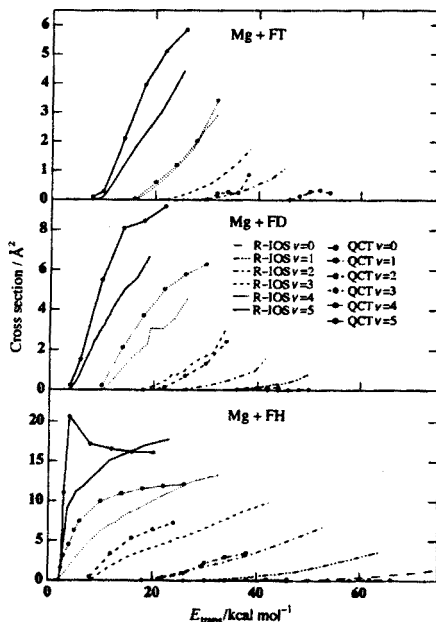

Fig. 2 Reactive cross sections plotted as a function of the translational energy for the first six initial vibrational states and for the H, D and T spectator-atom isotopic variants. Lines: R-IOS results. Lines and circles: QCT results.

section decreases, on average, as the isotopic mass is increased. Such a result is in accord with the role played by vibrational excitation in enhancing the reactivity of endoergic processes: as the isotopic mass increases, the content of vibrational energy for a given vibrational state decreases and so does the reactivity. Such a result also agrees with transition state theory (TST) predictions. The density of states of the reactants increases on going from H to T. However, the density of states at the transition state is almost unaffected by the isotopic substitution. This is, in fact, essentially that of the products since the endoergicity of the process causes the reaction barrier to be located late in the product region. Accordingly, the reactive probability, defined in TST as the ratio of the two quantities, decreases in the same sense.

According to the shrinking of the vibrational spacing, the value of translational energy at the threshold shifts gradually upwards when going from H to T, for both QCT and R-IOS calculations. On the average, the agreement between QCT and R-IOS results is good for all initial vibrational levels and isotopic variants. In previous papers[10-14] this agreement has been shown to be essentially owing to the rather weak variation of the PES with the orientation angle and to the HHL nature of the reaction. As a matter of fact (see Fig. 2), the agreement is particularly good at $v = 2$, 3 and 4 for H, D and T, respectively. These are the vibrational states which at threshold lead to an approximately equal amount of translational energy for the three isotopes. At larger v values, QCT reactivity is always higher than that of R-IOS, while the opposite is true for smaller v values. It has also to be mentioned that, for the lowest v values, the QCT and R-IOS threshold energies differ significantly. The difference increases with the mass of the isotope while it decreases with v.

4 Discussion

4.1 Product vibrational distributions

.. ra ionalizati_n _f the variati_n _f the PVD shape with b_th the total energy and the reactant vibrational energy may be obtained from a detailed analysis of the R-IOS state-to-state opacity functions, since they single out the role played by individual orbital angular momentum contributions to the reactive probability. The state-to-state opacity functions, from the

initial vibrational states $v = 0$ and 4 (each taken as a representative of the two types of PVDs found) to several product vibrational states are shown in Fig. 3 and 4, at $E_{tot} = 2.24$ and 3.00 eV (for low and high total energy, respectively).

4.1.1 Low translational energy. At low energy, the shape of the opacity function is sufficiently close to a step function. What makes the difference between $v = 0$ and $v = 4$ results is the range of allowed orbital angular momentum (ℓ) values (0–70 for $v = 0$ and 0–40 for $v = 4$) and the height of the plateau. However, the range of angular momentum values that contribute to the reaction changes negligibly as a function of the final vibrational state considered. This means that for a given v value the final shape of the PVD depends only on the height of the opacity function plateau. The reason why the allowed angular momentum range becomes larger when the initial vibrational state becomes small resides in the larger initial translational energy available. This causes larger ℓ values come into play. For these ℓ values, however, orbital angular momentum barriers are larger and generate a centrifugal repulsion sufficient to prevent collision partners from coming close enough to react.

4.1.2 Low translational energy and high vibrational content: vibrationally adiabatic PVDs. The particular behaviour found at low energy for $v = 4$ can be understood in terms of the conditions for adiabaticity discussed by Light and co-workers.[25] In a series of studies employing an adjustable potential, they found that a process is vibrationally adiabatic when some requirements on the local kinetic energy along the translational coordinate on the curvature of the reaction path and on the vibrational spacing and its variation along the translational coordinate are fulfilled. These requirements are, indeed, matched by the Mg + FH reaction at high vibrational excitation and low total energy, as is the case for $v = 4$ and $E_{tot} = 2.24$ eV. In agreement with the findings of Light and co-workers, an increase in translational energy tends to weaken the adiabaticity of the PVD.

The way vibrational adiabaticity is enforced needs, however, a comment. In the previous quantum study of the Mg + FH reaction,[20] the reaction mechanism was found to depend significantly upon the orientation angle. It was seen, for instance, that tunneling contributions to the reaction differ significantly when the collision angle varies from bent to open. Other examples of the angular dependence of reactivity are given in Fig. 5. In the figure, the fixed angle PVDs for $v = 0$ and 4 at $E_{tot} = 2.24$ and 2.73 are shown. The $v = 0$ PVD is determined by the $\gamma = 75°$ one (it well represents the situation at the transition state). This is strictly the case at low energy, while at $E_{tot} = 2.73$ eV there is a significant contribution from collisions occurring at more open angles, which causes the

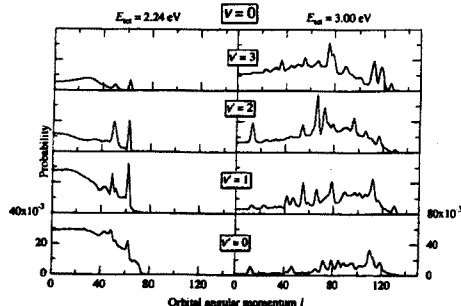broadening of the PVD in the high v' region. PVDs calculated at various values of γ do not differ significantly from that for $\gamma = 75°$, though collisions occurring at open angles show a tendency to lead to larger populations at high v' states. This means that a correlation between open angles and vibrational excitation can be established. Such a behaviour was first singled out by Blais and Truhlar[26] and then confirmed by others.[13] Its relevance, for the present case, is owing to the dominance of open angle contributions in the characterization of the integral quantity. In fact, for this reaction, an increase of the translational energy brings in contributions from PVDs calculated at all values of the orientation angle.

4.1.3 High translational energy. As already mentioned, an increase in the total energy makes the calculated PVDs change markedly. A result of increasing total energy is the widening of the range of angular momentum values (about 0–140 for both $v = 0$ and 4) that appreciably contribute to reaction. For $v = 0$ the height of the opacity function calculated at different v' values varies significantly when going from low to high translational energy. This causes a shift of the PVD maximum towards larger v' values as translational energy is increased. At $v = 4$, however, the situation is slightly more complex because of the different energy disposal associated with low and high orbital angular momentum collisions. Contrary to the $v = 0$ case, in fact, at $v = 4$ and $E_{tot} = 3.00$ eV the height of the specific opacity function at low angular momentum values little differs from that at $E_{tot} = 2.24$ eV. This means that, at least qualitatively, the probability of populating the various product vibrational states is essentially unaffected by an increase in translational energy. On the contrary, at large ℓ values the opacity function changes from a flat into a structured profile, owing to the appearance of a maximum. This maximum shifts towards higher angular momentum values and becomes higher as v' decreases. Since high angular momentum terms significantly contribute to the cross section due to the $2\ell + 1$ factor, this makes the PVD peak shift towards lower v' values as the total energy increases.

Such behaviour is typical of HHL systems exhibiting direct dynamics.[4,27,28] It can be understood in terms of the propensity of HHL systems to keep the product translational energy constant (translational energy is mainly stored in heavy atoms) and to allow a quantitative transfer of ℓ to the product rotatonal quantum number j'. For this process, the state-to-state opacity function shows a maximum for a given v' state when the conservation of total energy is satisfied by means of a complete conversion of reactant orbital into product rotational energy, i.e. a suitable condition for the above-mentioned kinematic rules to hold. Despite this, the opacity function has inequivocal HHL characteristics only when both vibrational and total energies are sufficiently large. This fact indicates that the PES structure plays a key role in determining the reactive behaviour of Mg + FH and allows a limiting kinematic behaviour to become dominant only when the energy is large and it is allocated to the appropriate reactant mode (vibration in this case).

4.2 Reaction cross sections and isotopic mass effects

The general good agreement between QCT and R-IOS cross sections for all initial vibrational levels and H-atom isotopic masses, as shown in Fig. 2, provides, in principle, a rather direct insight into the importance of initial energy in determining the accuracy of the infinite order sudden approximation (IOSA). It is well known, from its use in inelastic collisions, that the IOSA becomes more accurate as translational energy increases. However, as already mentioned, the features of the PES characterizing the reactive process make additional factors to come into play. For instance, it has been repeatedly found that the anisotropy of the PES favours reorientation of the collision partners and the coupling of angular
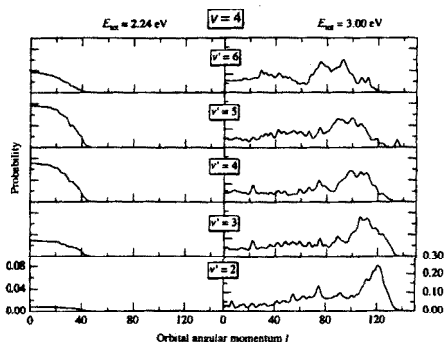

Fig. 3 R-IOS state-to-state opacity functions, at initial $v = 0$, $E_{tot} = 2.24$ eV (first column) and 3.00 eV (second column), for v' = 0, 1, 2 and 3 (from bottom to top row, respectively). Note the change of scale between the first and the second columns.

7.1. The $Mg + FH \rightarrow MgF + H$ system.

Fig. 4 State-to-state opacity functions, for initial $v = 4$, at $E_{tot} = 2.24$ eV (first column) and 3.00 eV (second column), for $v' = 2, 3, 4, 5$ and 6 (from bottom to top rows). Note the change of scale between the first and the second columns.

motions. On the other hand, when the variation of the PES with the orientation of the target molecule is small, the frozen collision angle approximation holds better. This is also the case of the Mg + FH reaction, since its PES shows little variation for a wide angular range (70–180°) and in the remaining angular range it is repulsive enough to not contribute to reactivity.

4.2.1 Low translational energy—high initial v states. At sufficiently low translational energies, QCT cross sections are larger than R-IOS ones. This is owing to the fact that, when the velocity is sufficiently low, reorientation of the target molecule from an initial unfavourable orientation to a more favourable one is easier. This leads to an enhancement of the 3D reactivity with respect to the fixed-angle collision one.

A reorienting effect—and not only a decrease in vibrational energy—plays a key role in determining the decrease of the cross section as the isotopic mass increases. However, since it is known that FD and FT molecules reorient themselves less promptly than FH, low translational energy QCT reactivity becomes smaller when the hydrogen isotope becomes heavier, as confirmed by the decreasing difference between QCT and R-IOS results as the H-mass increases (Fig. 2). In particular, the spike foun.. in the low translational energy region of the QCT excitation function of Mg + FH at $v = 5$ may be explained in terms of reorientation effects. This is confirmed by the fact that both QCT and R-IOS results do not exhibit
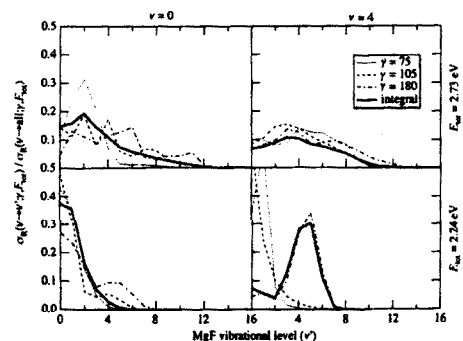
any peak for FD and FT. In other words, the sharp maximum is obtained only when the isotope is light enough and the computational approach correctly takes into account reorientation effects.

4.2.2 High translational energy—low initial v states. The observed behaviour changes markedly when low initial vibrational states are considered. First, for all isotopes high translational energies are necessary to obtain appreciable cross sections. This result is in accord with the enhancing role played by vibration in promoting reactivity and the less effective role played by translation. Second, the QCT reactivity is found to be smaller t an the R-IOS one, w t t s effect e ng enhanced by an increase of the isotopic mass. The smaller QC_ rea_tivity is ...... t_ _e _a_se_ _y an _n_xp_t_ _ _t significant upwards (along the translational energy scale) shift of the threshold energy for the isotopically substituted QCT cross sections, at low v values. The energy shift is much larger than the decrease in vibrational energy associated with the isotopic substitution of H by D and T.

To find a rationale for the observed behaviour, it was suggested that, below a certain content of vibrational energy, the reaction mechanism may become complex.[18] A later paper[19] shows, in fact, that under certain conditions the reaction may occur *via* an insertion of Mg into HF. We have investigated the rate of occurrence of complex collisions as a function of the initial vibrational level and of the isotopic mass. The results of this study are shown in Figs. 6–8. An inspection of the figures makes it clear that the anomalous shift of the QCT results takes place at the same vibrational level that (as one goes from high to low v values for each isotope) is the first to show a relevant contribution of complex collisions to the total cross section. It is important to emphasize here that for higher vibrational levels the contribution of complex collisions to the integral cross section vanishes. Then, it is perfectly legitimate to conclude that the shift in threshold energy for QCT results is due to the accessibility of insertion pathways when not enough energy is put into the enhancing mode (vibration). This causes a decrease of the reactivity because when a collision complex is formed energy redistribution may take energy away from the reaction mode and allocate it to other modes that are less effective in promoting
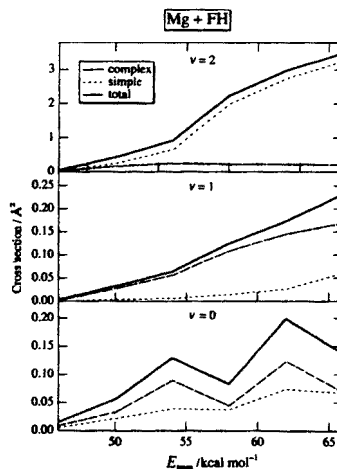

Fig. 5 Integral and γ-dependent product vibrational distributions, at γ = 75, 105 and 180°. Left column: $v = 0$. Right column: $v = 4$. Bottom row: $E_{tot} = 2.24$ eV. Upper row: $E_{tot} = 2.73$ eV. (———) Integral PVD. (·······) γ = 75°. (– – – –) γ = 105°. (—·—·) γ = 180°.
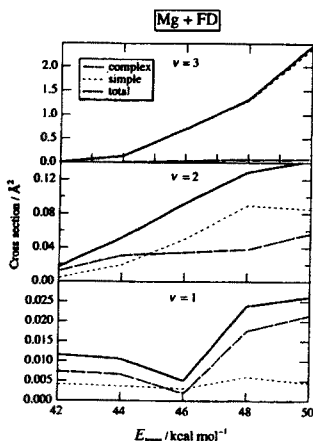

Fig. 6 Contributions of simple and complex trajectories (see text) to the total cross section, for Mg + FH and initial $v = 0$, 1 and 2. (———) Total cross section. (– – – –) Contribution of complex trajectories. (-----) Contribution of simple trajectories.

Mg + FD

Fig. 7 Contributions of simple and complex trajectories (see text) to the total cross section, for Mg + FD and initial $v = 1$, 2 and 3. (———) Total cross section. (— — — —) Contribution of complex trajectories. (-----) Contribution of simple trajectories.

reaction. However, when enough energy is put into the enhancing mode, the system reacts *via* a direct abstraction.

In summary, for this endoergic reaction, when the fixed angle constraint (typical of the R-IOS approach) is released in favour of a full 3D motion, reactivity is penalized for insertion-like mechanisms, while it is enhanced for abstraction (with reorientation) ones. The reason is that in 3D motion, during the formation of an insertion complex, energy is redistributed among all degrees of freedom and the come-back to the energetically favoured reactant channel is more likely. Obviously, the opposite is true in abstraction *via* a reorientation mechanism, for which the 3D motion allows an exit into the product channel. Conditions at which 3D-QCT and R-IOS reactive cross-sections become almost equivalent are $v = 2$, 3 and 4 for H, D and T respectively (Fig. 2). Under these conditions, the decreased contribution of insertion is counterbalanced by the increasing contribution of reorien-
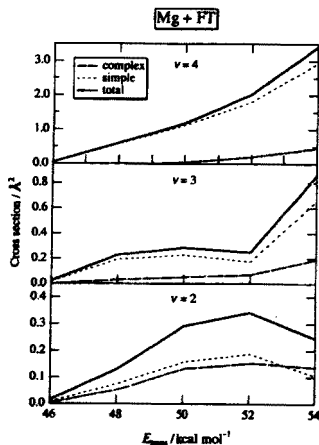
Mg + FT

Fig. 8 Contributions of simple and complex trajectories (see text) to the total cross section, for Mg + FT and initial $v = 2$, 3 and 4. (———) Total cross section. (— — — —) Contribution of complex trajectories. (-----) Contribution of simple trajectories.

tation. This compensation occurs, for all three isotopes, at a translational energy of about 0.75 eV, pointing out the critical role of translation energy in favouring a switch from insertion to abstraction mechanisms.

5 Conclusions

The influence of both initial vibrational and translational energy has been studied in detail for the Mg + FH → MgF + H reaction, including also its influence on the spectator-atom isotopic processes. In particular, in this paper we have discussed the following items.

At low translational energies, PVDs were found to peak at $v' = 0$ for all initial vibrational states (except for $v = 4$, which shows a tendency towards vibrational adiabaticity). This behaviour was rationalized in terms of the rules of Polanyi and of Light and co-workers about the vibrationally adiabatic reactive processes ($v = 4$ fulfills optimum conditions for the vibrational adiabaticity). In this respect, a decisive influence of the collision angle was also singled out. For instance, it was found that the $v = 0$ PVD is essentially determined by the behaviour of the system at the transition state angle. This is essentially true also for all other $v < 4$ values. At $v = 4$, a clear correlation between open angles and vibrational excitation was found (the PVD shape is mainly determined by the collinear (180°) contribution). The vibrationally adiabatic behaviour and the shift to a dominant, collinear-like reactive dynamics were found to be linked, with both providing to the system an amount of vibrational energy sufficient to overcome the reaction barrier and keeping the initial translational energy low.

At higher translational energy a different behaviour was observed for low and high vibrational excited reactants. For the $v = 0$ case, the PVD tends to broaden and to peak at higher v' values. This was found to be owing to a switch from $v' = 0$ to $v' = 2$ in the most effective state specific, single-ℓ reaction probability. This is caused by an increasing contribution to reaction of more open orientation angle collisions, among which are those favouring product vibrational excitation. When both vibrational and translational energy are high, as is the case of $v = 4$ and $E_{tot} = 3.00$, the PVD shape was found to be strongly dominated by the HHL nature of the mass-combination of the system, since reaction is, to a large extent, direct. As a result, the state-to-state opacity functions show a high angular momentum maximum which appears at higher ℓ values as v' decreases. This causes the PVD to peak at lower v' values as translational energy is increased. On the other hand, the PVD becomes highly isotropic as a function of the orientation angle.

As for the isotopically substituted processes, an agreement was found, as expected, between the vibrational energy content and the reactivity enhancement. A remarkably good agreement was also found, for all initial v, between QCT and R-IOS cross sections and all isotopes. Reorientation of the system during the reactive encounter was found to explain the (small) discrepancies between QCT and R-IOS results at low translational energy (the QCT cross section being larger than R-IOS ones) as well as the $v = 5$ post-threshold Mg + FH cross section maximum. However, as initial v is decreased, the QCT reactivity becomes much lower than the R-IOS one, with such a difference increasing with the isotope mass. This difference manifests itself as an unexpected large shift towards higher energy values for the low v QCT cross sections. The shift has been found to be associated with the replacement of complex (insertion) by direct (abstraction) collisions. The reactivity decrease is then caused by a redistribution of the energy from the already unfavourable translational mode. The final result is that the release of the fixed angle constraint increases QCT reactivity in abstraction-like collisions but diminishes it in insertion-like encounters. The switching from insertion to

abstraction mechanisms is found to be controlled by both translational and vibrational energy. This control is evidenced with the occurrence of transition conditions which make QCT and R-IOS essentially coincident, found at 0.75 eV (translational energy) and $v = 2$, 3 and 4 for the H, D and T isotopes, respectively.

Acknowledgements

References

1   V. N. Kondratiev and E. E. Nikitin, *Gas-Phase Reactions*, Springer-Verlag, Berlin, 1981; *Bimolecular Collisions*, ed. M. N. R. Ashfold and J. E. Bagott, The Royal Society of Chemistry, London, 1989; P. J. Dagdigian, *Annu. Rev. Phys. Chem.*, 1997, **48**, 95.
2   *Molecular Physics and Hypersonic Flows*, ed. M. Capitelli, Nato ASI Series C, vol. 482, Kluwer, Dordrecht, 1996.
3   P. A. Berg and J. J. Sloan, *J. Chem. Phys.*, 1994, **100**, 1075.
4   K. S. Kalogerakis and R. N. Zare, *J. Chem. Phys.*, 1996, **104**, 7947.
5   A. Laganà, E. García and L. Cicarelli, *J. Phys. Chem.*, 1987, **91**, 312; A. Laganà and E. García, *J. Phys. Chem.*, 1994, **98**, 502; A. Laganà, A. Riganelli, G. Ochoa de Aspuru, E. García and M. T. Martínez, in *Molecular Physics and Hypersonic Flows*, ed. M. Capitelli, Nato ASI Series C, vol. 482, Kluwer, Dordrecht, 1996, p. 35.
6   M. Gilibert, M. González, R. Sayós, A. Aguilar, X. Giménez and J. Hijazo, in *Molecular Physics and Hypersonic Flows*, ed. M. Capitelli, Nato ASI Series C, vol. 482, Kluwer, Dordrecht, 1996, p. 53; D. Bose and G. V. Candler, *J. Chem. Phys.*, 1997, **107**, 6136.
7   J. M. Lucas, A. Aguilar and A. Solé, *Chem. Phys.*, 1988, **123**, 277; X. Giménez, J. M. Lucas and A. Aguilar, *Chem. Phys.*, 1989, **136**, 115.
8   R. J. Gordon and S. A. Rice, *Annu. Rev. Phys. Chem.*, 1997, **48**, 601.
9   M. Baer, *J. Chem. Phys.*, 1974, **60**, 1057; 1975, **62**, 4545; *J. Phys. Chem.*, 1981, **85**, 3874; J. N. L. Connor, A. Laganà, J. C. Whitehead, W. Jakubetz and J. Manz, *Chem. Phys. Lett.*, 1979, **62**, 479; J. N. L. Connor, W. Jakubetz, A. Laganà, J. Manz and J. C. Whitehead, *Chem. Phys.*, 1982, **65**, 29; J. N. L. Connor, J. C. Whitehead, W. Jakubetz and A. Laganà, *Il Nuovo Cimento*, 1985, **63**, 116; A. Laganà, *J. Chem. Phys.*, 1987, **86**, 5523; A. Laganà, E. García and J. M. Alvariño, *Il Nuovo Cimento, D*, 1990, **12**, 1539; A. Laganà, M. Paniagua and J. M. Alvariño, *Chem. Phys. Lett.*, 1990, **168**, 441.
10 A. Aguilar, M. Albertí, X. Giménez, X. Grande and A. Laganà, *Chem. Phys. Lett.*, 1995, **233**, 201.
11 X. Giménez, J. M. Lucas, A. Aguilar and A. Laganà, *J. Phys. Chem.*, 1993, **97**, 8578.
12 M. Gilibert, X. Giménez, M. González, R. Sayós and A. Aguilar, *Chem. Phys.*, 1995, **191**, 1.
13 A. Aguilar, M. Gilibert, X. Giménez, M. González and R. Sayós, *J. Chem. Phys.*, 1995, **103**, 4496.
14 A. Laganà, G. Ochoa de Aspuru, A. Aguilar, X. Giménez and J. M. Lucas, *J. Phys. Chem.*, 1995, **99**, 11696.
15 M. González, R. M. Blasco, X. Giménez and A. Aguilar, *Chem. Phys.*, 1996, **209**, 355.
16 M. Dini, Tesi di Laurea, University of Perugia, 1987; A. Laganà, M. Dini, E. García, J. M. Alvariño and M. Paniagua, *J. Phys. Chem.*, 1991, **95**, 8379.
17 J. M. Alvariño and A. Laganà, *J. Chem. Phys.*, 1991, **95**, 998.
18 J. M. Alvariño and A. Laganà, *J. Phys. Chem.*, 1992, **96**, 3587.
19 J. M. Alvariño, L. Cuadrado, M. L. Hernández and A. Laganà, *Chem. Phys. Lett.*, 1995, **241**, 408.
20 F. Huarte-Larrañaga, X. Giménez, M. Albertí, A. Aguilar, A. Laganà and J. M. Alvariño, *Chem. Phys. Lett.*, 1998, **282**, 91.
21 V. Khare, D. J. Kouri and M. Baer, *J. Chem. Phys.*, 1979, **71**, 1188.
22 J. M. Bowman and K. T. Lee, *J. Chem. Phys.*, 1980, **72**, 5071.
23 D. G. Barg and D. Drohlshagen, *Chem. Phys.*, 1980, **17**, 209.
24 J. C. Light and R. B. Walker, *J. Chem. Phys.*, 1976, **65**, 1598; *J. Chem. Phys.*, 1976, **65**, 4272.
25 C. C. Rankin and J. C. Light, *J. Chem. Phys.*, 1969, **51**, 1701; G. Miller and J. C. Light, *J. Chem. Phys.*, 1971, **54**, 1635, 1643.
26 N. C. Blais and D. G. Truhlar, *Chem. Phys. Lett.*, 1985, **118**, 379.
27 P. H. Vaccaro, A. A. Tsekouras, D. Zhao, C. A. Leach and R. N. Zare, *J. Chem. Phys.*, 1972, **96**, 2786.
28 D. Zhao and R. N. Zare, *J. Chem. Phys.*, 1992, **97**, 6208.

Paper 8/07823H

7.2 The $B + OH \to BO + H$ system.

In this section we will present the work we have published concerning the R-IOS quantum mechanical study of the above combustion reaction.

7.2.1 Cross sections exhibiting quantum resonances: the $B + OH$ case.

Journal of Molecular Structure (Teochem) 463 (1999) 65-74

Resonances are one of most noticeable quantum effects that can be found in reaction dynamics. Appearing as Lorentzian peaks in the reaction probability, resonances are related to the formation of metastable compound systems and provide extremely accurate information on the structure of the strong interaction region of the PES. These phenomena are, therefore, when experimentally observable, a unique benchmark to improve the theory. However, two main difficulties arise when it comes to theoretically predicting resonances at the three dimensional cross section level. The first one is related to the relatively short lifetimes of the collision complexes, which lead to broad probability peaks, easily smoothed out when one sums over the angular momentum. This may, however, be of less importance if there exists a stable complex. The second shortcoming concerns the high computational cost of a complete rigorous reactive scattering calculation. To overcome this second problem, one may employ reduced dimensionality models, such as IOS, as a first estimation of the resonance pattern relevance of a reactive system.

In this context, we considered the approximate study of the resonance pattern presented by the title system. The interest of the system lies in the importance of the HBO and HOB stable intermediates, which may be important in the formation of resonance states. The HBO is experimentally known and theoretical studies have predicted a linear geometry for this minimum. The second HOB minimum geometry has caused some controversy and, apparently, fitting the PES to a collinear minimum gives the better description of the reactivity. Thus, a Sorbie-Murrell fit was used, considering a linear geometry for both intermediate states. On this PES, the reaction is 3.60 eV exoergic and its alternative channel can be neglected at the energies considered in the work since it is over 1.75 eV endoergic. The BOH lies around 6.4 eV below the reactants' asymptote and is located early in the entrance region. Following the minimum energy path, a barrier of 1.21 eV connects this minimum to the HBO one, lying 4.9 eV below products' asymptote.

In the present article we showed how the resonant component of the global reactivity was significant for the title system. The plots of opacity functions as well as differential cross sections confirmed this fact, giving strongly structured opacity functions and highly symmetric differential cross section. The outstanding structure surviving in the integral cross section indicates that its experimental measurement may be of great use for the refinement of the interaction potential.

Cross-sections exhibiting quantum resonances: the B + OH case

Xavier Giménez*, Fermín Huarte-Larrañaga, Xavier Grande, Yolanda Quirós, Margarita Albertí, Antonio Aguilar

Departament de Química Física, Universitat de Barcelona, Martí i Franquès 1, 08028 Barcelona, Spain

Abstract

Extensive theoretical quantum-mechanical calculations are reported for the cross-section and related dynamical quantities of the B + OH → BO + H reaction, on a previously developed potential-energy surface (PES) describing the ground electronic state. These calculations show, as an outstanding feature, the presence of marked structures in the shape of the excitation function as a consequence of the existence of a dense spectrum of rather long-lived resonance states. These are narrow enough to survive the angular momentum averaging, thanks to an important stabilization caused by an electronic minimum corresponding to a linear HOB configuration. The centrifugal barriers due to high values of the orbital angular momentum are found to lead to several orbiting shape resonances, as revealed by the opacity function plots and the dependence of the reaction probability on energy. Differential cross-sections corresponding to energies lying at either reactivity peaks or valleys in the integral cross-section show a highly symmetric dependence on scattering angle, indicating an important resonant contribution to reactivity in both cases. The possibility of directly observing resonances in experimental integral cross-section measurements is analysed in the light of the present results. © 1999 Published by Elsevier Science B.V. All rights reserved.

Keywords: Reaction dynamics; Scattering; Resonance; Potential-energy surface (PES)

1. Introduction

Resonances constitute one of the most striking phenomena in physics [1,2]. In scattering processes, they were first measured experimentally in nuclear and particle physics as a consequence of the formation of new compound particles emerging from collisions of simpler systems. They are manifested as Lorentzian-type peaks in the reaction probability, the maximum being identified as the resonance energy and the width proportional to the inverse of the compound system's lifetime. In chemical reaction dynamics, resonances were first predicted theoretically 28 years ago by Truhlar and Kuppermann [3], in collinear exact quantum calculations of the reaction probability as a function of energy for the H + H$_2$ → H$_2$ + H reaction.

From the very beginning the importance of such phenomena was realized, since they provide very accurate information on the structure of the close interaction region of the potential-energy surface (PES). However, predictions had to be made on quantities amenable for experimental detection. About six years ago, remarkable improvements in theoretical methodology allowed Miller and Zhang [4] to point out the possibility of directly observing resonances for the H + H$_2$ → H$_2$ + H reaction, by looking at ridges in the simultaneous energy and angular dependence of the state-to-state differential cross-section. More recently, Kuppermann and Wu [5] succeeded in refining the above ideas and performed the first quantitative prediction, for the H + D$_2$ → HD + H reaction, of a reactive scattering resonance. They used symmetrized hyperspherical coordinates to perform exact quantum calculations of the reaction probability,

* Corresponding author.

including the effect of the geometric phase due to conical intersections between electronic surfaces. These predictions concerned highly energy- and scattering-angle-resolved state-to-state differential cross-sections, quantities which are rather difficult to measure experimentally, although remarkable successful experiments along this line have been reported quite recently [6].

Other recent and detailed studies where resonances have been measured in molecular (heavy particle) processes concern van der Waals' complexes, for which resonances are analysed in highly resolved electronic spectra as predissociation phenomena [2,7,8]. Photoelectron detachment spectra (PhES) have also been a source of detailed information about transition state (TS) resonances. This has been shown in experiments where an electron is photoejected from a stable anion, leading to an unstable neutral, which is usually found to be formed in the TS region [9,10]. A paradigmatic result illustrating this series of experiments can be given by the excellent agreement between the experimental PhES spectrum and its rigorous theoretical simulation found in the study of the $F + H_2$ system, which allowed the authors to conclude that "the nature of the FH_2 transition state has been essentially solved" [11]. Also, from experimental measurements on the photodissociation and photoisomerization of ketene, Lovejoy and Moore [12] deduced the direct isomerization rate of the same molecule. They obtained a strongly structured shape of the isomerization rate versus energy relationship, which they attributed to resonance states of oxirene, the intermediate species found in the route to isomerization. Gezelter and Miller [13] calculated theoretically the corresponding microcanonical rate of isomerization and found reasonable qualitative agreement with the experimental results, confirming the resonance features present in the microcanonical (i.e. energy-selected) rate constant.

The above examples suggest that it is becoming increasingly possible to make a direct comparison between calculated and measured resonance phenomena. Thus it appears necessary to accumulate additional studies on different molecular processes and other experimentally measurable quantities. In particular, it is highly interesting, on one hand, to have such information for elementary chemical processes

other than the "canonical" $H + H_2 \rightarrow H_2 + H$, since metastable states play a decisive role in controlling the reaction outcome and much richer and varied energy dependences are found in non-academic reactions. On the other hand, it is also desirable to explore the possibility of directly observing resonances in integral cross-section measurements, since highly resolved related experiments are becoming available. For instance, recent improvements are making the proper energy resolution at hand to characterize resonance peaks adequately [14].

In the present work we are concerned with resonances that are manifested in the integral cross-sections of elementary chemical reactions; i.e. the sum for all relevant total angular momentum values of the reaction probability. However, two main problems arise in this case. The first one is related to the relatively short lifetimes of the collision complexes that are frequently found in chemical reactions. Short lifetimes lead to broad Lorentzian peaks, being easily smoothed out in the sum over the angular momentum. Thus, in these cases, resonances become undetectable at the cross-section level. The second problem is related to the computational cost of a complete reactive scattering calculation. At present, calculations involving non-academic systems demand such a computational effort that the computation of most exact quantum reactive cross-sections is rendered extremely expensive. Thus, even in the case that the resonance structure survives the angular momentum sum, its exact computation is a formidable task.

The first shortcoming may be of less importance if strongly stable complexes can exist during the reaction. Previous experience with reduced-dimensionality and one-partial-wave exact quantum calculations indicate that if the PES supports stable electronic complexes, the resonance pattern of the reaction probability is much richer and intense [15–20]. In these cases several resonances are much sharper (or lifetimes much longer), thus increasing the probability of survival after the angular momentum averaging. The second shortcoming can be partially overcome with the use of reduced-dimensionality quantum-mechanical (QM) scattering methods. Although approximate, they provide a first estimation of how relevant the resonance reactivity is. For instance, they may serve as an initial guess to more accurate

methods for the characterizing properties of the resonances (i.e. width, intensity and density of the resonance peaks), how they are manifested in averaged quantities, etc. In addition, they could provide rather accurate information on those resonance states that are due to the degrees of freedom included exactly in the approximate scattering method.

The present study deals with a QM study of the combustion-related B + OH → BO + H reaction, performed by means of the Reactive-Infinite Order Sudden (R-IOS) technique [21–27]. The interest in the B + OH system lies in the importance of the HBO and HOB stable intermediates, which are supposed to have a determining role in the formation of resonance states. In particular, HBO has been known experimentally since 1971 [28]. Theoretical studies at ab initio level [29–32] indicate the existence of the HBO structure as a minimum on the doublet ground-state surface of the HBO system. A second HOB minimum is also predicted, less stable than the former. All theoretical works predict a linear configuration for the HBO intermediate, but certain controversy exists on the nature of the HOB minimum geometry, since both linear and angular geometries have been reported in the literature.

2. Potential-energy surface and method numerical parameters

As part of a systematic study of some boron atom reactions, the problem of determining the best geometry for the second minimum was undertaken [31–35]. These studies used a reasonable PES that was tested previously [31,32], showing a linear geometry for HBO but angular geometry for the HOB minimum. The influence of the HOB minimum geometry was then checked by comparing the previous results with those obtained on a new PES fit with linear HOB geometry [35]. It was found that the last surface described the experimental evidence better, since it predicted a strong product vibrational population inversion, in accordance to related reactions where the BO molecule is also produced [36–39]. In addition, comparison between quasiclassical trajectory (QCT) and long-range behaviour [40,41] showed that the long-range interaction, which is the dominant

one in this kind of surface, was better described with the second surface.

A Sorbie–Murrell fit, the main features of which have been discussed elsewhere [35], was used, corresponding to the surface with both linear HBO and HOB minima. On this PES, when B approaches OH (4.147 eV below the B + O + H dissociation plateau), strongly bound BOH (10.601 eV) stabilized by a ca. 6.4 eV well located early in the entrance channel can be formed, from which the minimum-energy path goes through a barrier of 1.21 eV connecting with the HBO (12.671 eV) well before reaching the product asymptote (7.747 eV). The B + OH → BO + H reaction is thus exoergic by 3.60 eV, and the ground reactant vibrational level lies 0.24788 eV above the reactant minimum. The alternative BH-forming channel is endoergic by 1.7531 eV, so it is not considered at the energies of the present study.

Calculations have been performed by means of the same R-IOSA procedure used in previous works [42–51]. The calculation procedure can be divided into two parts. In the first part, potential cuts, vibrational eigenvalues and eigenfunctions and overlaps are computed for each sector into which the configuration space is divided. In the second part, the solution is propagated through the sectors, by means of the invariant embedding R-matrix method [52,53], to get the fixed-angle S-matrix elements for all relevant (i.e. non-negligibly contributing to reactivity) values of the orbital angular momentum and each collision energy. The global procedure is repeated at each relevant collision angle (the Jacobi atom–diatom orientation angle).

Configuration space was divided into 450 sectors, 225 for each reaction channel. For the energy range of interest, convergence was obtained by using 40 vibrational basis functions. The scanned collision energy range was from 0.01 eV to 0.41 eV, with a total of 55 points for the integral cross-section. For each energy value a total of 20 collision angles was included, ranging from 80 to 180° in steps of 5°. For each collision angle and energy, the number of angular momentum partial waves leading to convergency varied from $l_{max} = 34$ at $E_{tr} = 0.01$ eV and $\gamma = 100°$, to $l_{max} = 124$ at $E_{tr} = 0.41$ eV and $\gamma = 140°$. The first part of the calculation lasted an average of 60 s on an IBM 3AT Workstation, while each vibrational state-to-state $(v \rightarrow v')$ S-matrix element $(S^j_{vv'}(\gamma))$ took 2 s on average
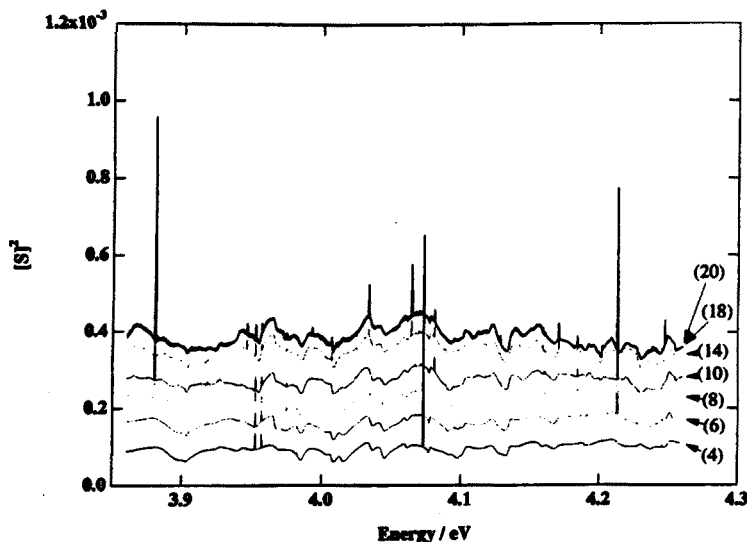
Fig. 1. Partial cumulative R-IOS 3D reaction probabilities as a function of total energy (zero placed at the bottom of the products arrangement), for OH in the ground vibrational state, summed over all open vibrational product states and for the orbital angular momentum quantum number $l = 0$. Numbers in parenthesis indicate the number of angles included in the partial integration (the integration range is 80–180° in steps of 5°). The curve labelled with (20) is the complete R-IOS 3D reaction probability.

to be obtained, for each energy, collision angle (γ) and partial wave (l), on the same computer. Additional calculations were performed to obtain the single-l reaction probability. In this case, a total of 1000 energy points was computed, in the same energy range, for the same number of collision angles. Finally, differential cross-sections were computed for a total of 721 scattering angle values, this large number being necessary to characterize the strongly oscillatory structure properly (see below).

3. Results and discussion

An extensive study of the reaction dynamics of the title system has been performed. The main goal was to compute both averaged quantities (i.e. easier to measure experimentally), such as differential and integral cross-sections, as well as more detailed ones, such as state-to-all opacity functions and reaction probabilities, to see how resonance features are manifested, and also how they evolve from detailed to averaged quantities. The calculation obviously starts

by solving the R-IOS Schrödinger equation, which provides the corresponding S-matrix elements. Its squared modulus, integrated over the collision angle, is the state-to-state single-energy, single-angular momentum reaction probability

$$P_{vv'}^l = \frac{1}{2} \int_{-1}^{1} \left| S_{vv'}^l(\gamma) \right|^2 d \cos \gamma \qquad (1)$$

which, when summed over all product vibrational states v' and plotted as a function of energy, leads to the results shown in Fig. 1. This graph shows the reaction probability for zero orbital angular momentum. The global shape is described by an overall almost constant dependence upon energy, with several broad peaks and valleys. Superimposed on this background behaviour intense and sharp peaks are found, due to strongly bound metastable states. In addition, partial cumulative angular integrations are also shown, with the purpose of visualizing how the global three-dimesional (3D) probability profile is gradually built up (although in an approximate way). Remarkable is the homogeneity of the reaction probability profile as the fixed-angle probabilities are
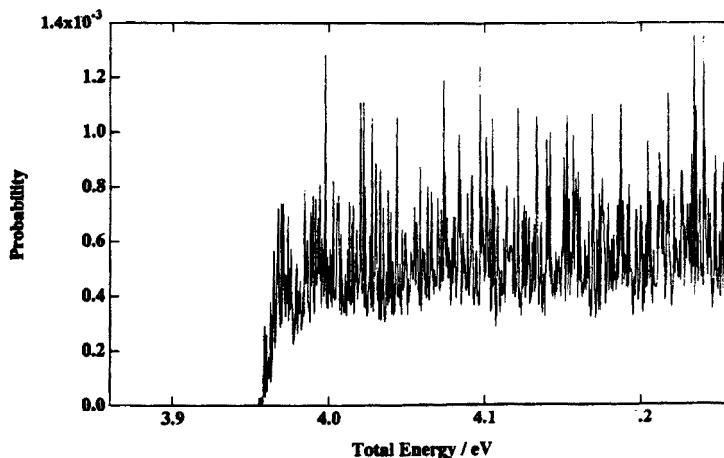
7.2. The $B + OH \rightarrow BO + H$ system.

Fig. 2. R-IOS 3D reaction probabilities as a function of total energy (zero placed at the bottom of the products arrangement), for OH in the ground vibrational state, summed over all open vibrational product states and for the orbital angular momentum quantum number $l = 70$.

being added. Most of the broad peaks and valleys present in those graphs containing less angles are kept during the rest of the integration, with minor changes causing only slight variations in their intensity. This is a clear consequence of the important degree of isotropy of the potential. The only major difference is the appearance of the sharp and intense peaks, which is strongly dependent on the collision angle. This fact clearly shows the dramatic dependence of the resonance features on small changes in the PES topography, thus stressing the importance of putting effort towards characterizing resonances in chemical reactions.

Fig. 2 shows the state-to-all reaction probability, as a function of energy, for the orbital angular momentum $l = 70$. Two main differences arise upon comparison with the $l = 0$ case. The first is that the centrifugal barrier, for the $l = 70$ case, shifts the reactivity threshold by about 0.1 eV towards higher energies. The second and major difference is that the $l = 70$ reaction probability is dominated by an extremely dense resonance spectrum. To give more details on it, Fig. 3 shows several state-to-state reaction probabilities, again for $l = 70$. It is clearly seen that resonances manifest themselves in an essentially similar way in all state-to-state transitions. In addition, several peaks appear at the same energy position, independently of the final v' state, as is well known for resonances in

chemical reactions. When the total energy coincides with the energy of the metastable state — the resonance, the reaction outcome is dominated by the resonance formation, independently of the state from which the collision occurs. Then, the longer transit time in the strong-interaction region allows for energy redistribution and a higher probability for reaction. The transitions to different v' states differ only in the amount of background or direct reactivity. While being roughly constant as a function of energy, it is increasingly higher as v' is increased, indicating a propensity towards translational energy conservation from reactants to products.

A main conclusion to be extracted from Figs. 1–3 is that resonances appear mainly as a consequence of orbital angular momentum barriers, which allow the formation of shape resonances on the electronic–vibration–orbital effective potentials. It is the intervention of all these components of motion that causes the dense resonance spectrum to appear. On the contrary, the absence of an effective barrier is the key feature preventing the resonance mediation to reaction, the direct reaction mechanism then being dominant. This fact implies that compound (Feshbach) resonances are rarely formed during the collision, as a consequence of a weak vibrational non-adiabatic coupling.

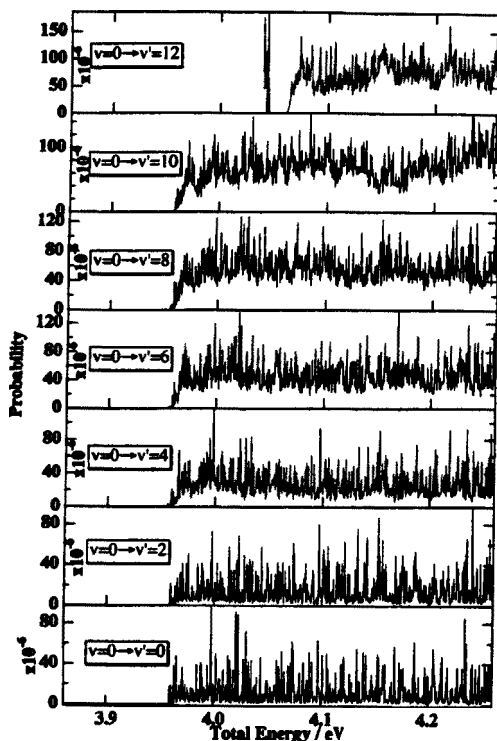However, vibrational non-adiabatic transitions

Fig. 3. R-IOS 3D state-to-state reaction probabilities as a function of total energy (zero placed at the bottom of the products arrangement), for OH in the ground vibrational state. Orbital angular momentum quantum number $l = 70$.

must exist, since the product's vibrational distribution is clearly different from that coming from a vibrationally adiabatic mechanism. These couplings occur in the direct scattering since the background reactivity, not the resonant one, is the component that increases gradually as v' is increased in Fig. 3.

When Eq. (1) is summed again over the product vibrational states and plotted against the orbital angular momentum, at fixed energy values, the opacity functions represented in Fig. 4 are obtained. The most interesting feature is the presence of resonance structure, except for the first 10 to 15 values of the orbital angular momentum, whose density increases gradually with l. The background behaviour (disregarding the resonant peaks) of the opacity function is close to a step function.

The results of Fig. 4 confirm the analysis performed from Figs. 1–3; i.e. shape resonances can be formed as the centrifugal term interposes a barrier just before the strong stabilization due to the HOB well. The three plots shown in Fig. 4 correspond to energies lying on a reactivity peak and on the valleys immediately before and after the peak, respectively. No major differences are found between them so that, in principle, we cannot attribute a pure resonant behaviour to the cross-section peaks nor a purely direct reactivity mechanism to the cross-section valleys. This seems fairly reasonable, in view of the fact that each energy point represents a sum over all angular momentum values (up to 200 at the highest energies) and all vibrational product states (up to 18).

The above statements have been confirmed by studying the behaviour of the differential cross-section. It is calculated by means of products of S-matrix elements times Legendre polynomials $P_l(\cos\theta)$ in the form:

$$\frac{\partial\sigma_{vv'}}{\partial\Omega} =$$

$$\frac{1}{4\bar{k}_{vj}^2}\sum_{l=0}^{\infty}\sum_{l'=0}^{\infty}(2l+1)(2l'+1)P_l(\cos\theta)P_{l'}(\cos\theta)$$

$$\times\frac{1}{2}\int_{-1}^{1}S_{vv'}^{l*}(\gamma)S_{vv'}^{l'}\,d\cos\gamma$$

(2)

θ being the centre-of-mass scattering angle. Fig. 5 shows the differential cross-sections for the same three conditions as the opacity function, always for OH in the ground vibrational state. In all cases, the differential cross-section shows a high forward/backward symmetry, typical of the formation of a long-lived complex. Although the R-IOS method describes the angular variables crudely, these results are in agreement with the dominating resonance mechanism found for this reaction. In addition, previous QCT studies [35] also predicted a highly symmetric shape for this quantity.

The final quantity to be analysed in the present work is the R-IOS integral cross-section, which is given by:

$$\sigma_{vv'} = \frac{\pi}{\bar{k}_{vj}^2}\sum_{l=0}^{\infty}(2l+1)\frac{1}{2}\int_{-1}^{1}\left|S_{vv'}^{l}(\gamma)\right|^2\,d\cos\gamma \quad (3)$$
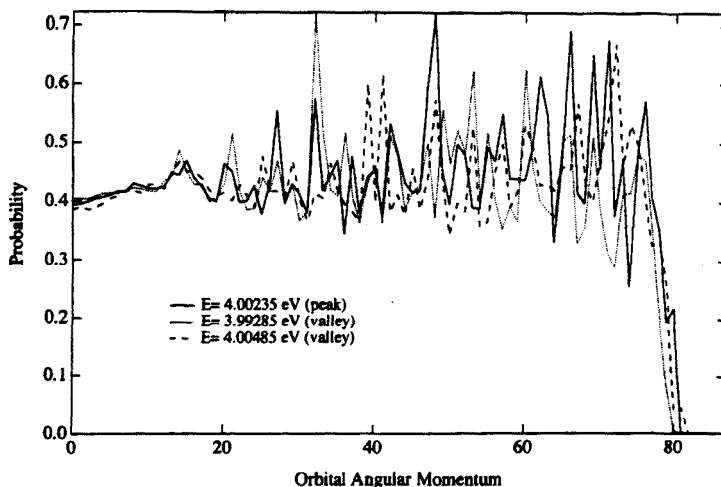
Fig. 4. R-IOS 3D summed over all product vibrational states' opacity functions, at three selected energies, corresponding to a reactivity peak found in the integral cross-section ($E = 4.00235$ eV) and the valleys before and after ($E = 3.99825$ eV and 4.00485 eV, respectively).

In the present case, it has been calculated by summing over all product states. Its dependence on energy is shown in Fig. 6, again for OH in the ground vibrational state. The general shape follows an exponentially (or potentially) decreasing trend as a function of collision energy, in agreement with the general behaviour expected for systems with zero or negative activation energies [54–56]. The background profile is superimposed on a relevant structure reflecting, at the cross-section level, the fingerprint of reactive scattering resonances.

As seen from the preceding analysis, the dependence of the integral cross-section on energy, while resulting from the sum for all angular momentum partial waves, is characterized by the fact that low l values do not lead to a strong resonant behaviour; but as l is increased, shape resonances become completely dominant over the whole energy range. Resonance
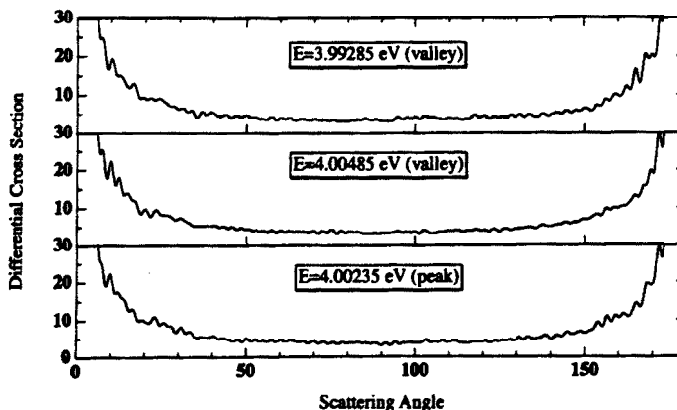

Fig. 5. R-IOS summed over all product vibrational states' differential cross-sections, at three selected energies, corresponding to a reactivity peak found in the integral cross-section ($E = 4.00235$ eV) and the valleys before and after ($E = 3.99825$ eV and 4.00485 eV, respectively).
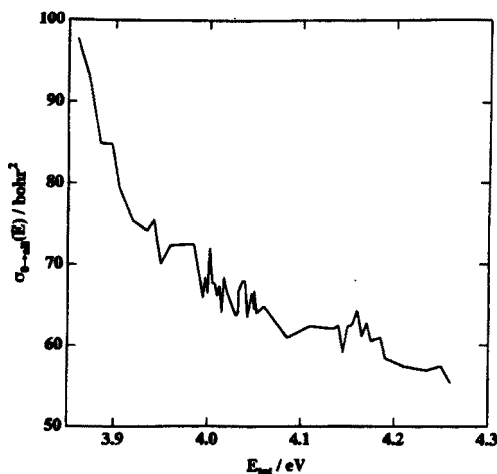
Fig. 6. R-IOS summed over all product vibrational states' integral cross-sections as a function of total energy, for OH in the ground vibrational state. In total 55 points have been calculated, using a finer mesh around the 4.0 eV region.

peaks are very narrow, indicating rather long life-times. As seen from the opacity function plots, changing the total energy slightly makes the resonance peaks change their position and intensity slightly. These are the conditions, as has been previously discussed in the literature [2], for the peaks to disappear with the partial wave summation. However, in the present case, peak superposition due to partial wave summation resembles what is obtained in a random signal accumulation, given the high value of partial waves to be included and the sharpness and high number of resonant peaks. As a consequence, the structure surviving in the integral cross-section is similar to a "noise" variation, as far as the shape of the integral cross-section curve is concerned, but, of course, the structure is by no means aleatory. In spite of this, we think that a back-and-forth interaction between theory and experiment is still possible in such cases. Although peaks in the excitation function are not attributable to particular resonance states, the structure is still reflecting a lot of information and, as is well known [15–20], it is strongly dependent on the interaction potential. Thus it can be used to refine the PES until theory and experiment become coincident enough. However, this process would avoid the need for an accurate dynamical method to compute the

cross-section. The u"ty o" an approx mate stu y like the present one is that, in addition to the dynami-cal trends established here, it points us in the right direction to look. Thus when looking for relevant resonance structures, we avoid the highly time-consuming task of directly determining the exact cross-section.

4. Summary and conclusions

In this work a detailed approximate QM study of the B + OH → BO + H reaction has been performed, with the aim of determining how resonance features manifest themselves in the integral cross-section. For this purpose, the 3D reaction probability for a single angular moment_m w_s comp_t_d _si_g a v_ry fi_ energy grid. It has been found that resonances become dominant as the centrifugal barriers interposed by the orbital angular momentum gradually increase. Thus, shape resonances due to orbiting processes are the kind of metastable state responsible for the observed behaviour.

The resonant reactivity contributes an appreciable fraction to the total reactivity. This has been confirmed by computing both the opacity function and the differential cross-section, for energies lying on a reactivity peak (in the integral cross-section) and on a reactivity valley. In all cases results are essentially equivalent, giving a marked structured behaviour for the opacity function and a highly forward/backward symmetric differential cross-section.

The predominantly non-resonant reactivity found for low values of the orbital angular momentum indicates that Feshbach-type resonances rarely occur, so that non-adiabatic vibrational coupling is weak in the configuration space region where resonances are formed. However, this coupling must exist in neigh-boring configuration space regions, since strongly non-adiabatic product vibrational distributions are obtained for this surface, owing to direct, non-resonant reactivity.

Finally, the structure surviving in the integral cross-section results largely from what could be described as the noise of a random summation process, as far as resonance peaks are concerned. As a consequence, experimental measurement of its fine energy grid

7.2. The $B + OH \rightarrow BO + H$ system.

may be of great use for refinement of the interaction potential, but no identification of the quantum states of the metastable complex is possible.

Acknowledgements

References

[1] R.P. Feynman, R.B. Leighton, M. Sands, The Feynman Lectures on Physics, vol. 1, Addison Wesley, Reading, MA, 1963, Ch. 23.

[2] D.G. Truhlar (Ed.), Resonances in Electron–Molecule Scattering, van der Waals Complexes and Reactive Chemical Dynamics, ACS Symp. Ser. vol. 263, American Chemical Society, Washington, DC, 1984.

[3] D.G. Truhlar, A. Kuppermann, J. Chem. Phys. 52 (1970) 3841.

[4] W.H. Miller, J.Z.H. Zhang, J. Phys. Chem. 95 (1991) 12.

[5] A. Kuppermann, Y.-S.M. Wu, Chem. Phys. Lett. 241 (1995) 229.

[6] G. Dharmasena, T.R. Phillips, K.N. Shokirev, G.A. Parker, M. Keil, J. Chem. Phys. 106 (1997) 9950.

[7] O. Atabek, Resonances in molecular dynamics: concepts and applications, in: E. Yurtserver (Ed.), Frontiers of Chemical Dynamics, Kluwer, Dordrecht, 1995.

[8] T. González-Lezana, M.I. Hernández, G. Delgado-Barrio, P. Villareal, J. Chem. Phys. 106 (1997) 3216.

[9] D.M. Neumark, Annu. Rev. Phys. Chem. 43 (1992) 153.

[10] D.M. Neumark, Acc. Chem. Res. 26 (1993) 33.

[11] D.E. Manolopoulos, K. Stark, H.-J. Werner, D.W. Arnold, S.E. Bradforth, D.M. Neumark, Science 262 (1993) 1852.

[12] E.R. Lovejoy, C.B. Moore, J. Chem. Phys. 98 (1993) 7846.

[13] J.D. Gezelter, W.H. Miller, J. Chem. Phys. 103 (1995) 7868.

[14] A. González Ureña, Personal communication.

[15] B. Kendrick, R.T. Pack, J. Chem. Phys. 104 (1996) 7502.

[16] B. Kendrick, R.T. Pack, J. Chem. Phys. 106 (1997) 3519.

[17] G.A. Parker, R.T. Pack, A. Laganà, Chem. Phys. Lett. 202 (1993) 75.

[18] X. Giménez, J.M. Lucas, A. Aguilar, Chem. Phys. 136 (1989) 115.

[19] N. Balakrishnan, N. Sathyamurthy, Chem. Phys. Lett. 201 (1993) 294.

[20] J.D. Kress, R.B. Walker, E.F. Hayes, P. Pendergast, J. Chem. Phys. 100 (1994) 2728.

[21] V. Khare, D.J. Kouri, M. Baer, J. Chem. Phys. 71 (1979) 1188.

[22] J.M. Bowman, K.T. Lee, J. Chem. Phys. 72 (1980) 5071.

[23] D.G. Barg, D. Drohlshagen, Chem. Phys. 17 (1980) 209.

[24] H. Nakamura, A. Ohsaki, M. Baer, J. Phys. Chem. 90 (1986) 6176.

[25] A. Laganà, X. Giménez, E. García, O. Gervasi, Chem. Phys. Lett. 176 (1991) 280.

[26] A. Laganà, A. Aguilar, X. Giménez, J.M. Lucas, Chem. Phys. Lett. 189 (1992) 138.

[27] A. Aguilar, X. Giménez, J.M. Lucas, O. Gervasi, A. Laganà, Theor. Chim. Acta 79 (1991) 191.

[28] E.R. Lory, R.F. Porter, J. Am. Chem. Soc. 93 (1971) 6301.

[29] J. Tyrrell, J. Phys. Chem. 83 (1979) 2906.

[30] S. Sakai, K.D. Jordan, J. Phys. Chem. 87 (1983) 2293.

[31] A. Solé, R. Sayós, J.M. Lucas, M. González, X. Giménez, M. Albertí, A. Aguilar, in: R. Carbó (Ed.), Studies in Physical and Theoretical Chemistry, vol. 62, Elsevier, Amsterdam, 1989, p. 535.

[32] M. Albertí, Ph.D. thesis, Universitat de Barcelona, 1990.

[33] M. Albertí, A. Solé, A. Aguilar, J. Chem. Soc., Faraday Trans. 87 (1991) 37.

[34] M. Albertí, M. Prieto, A. Aguilar, J. Chem. Soc., Faraday Trans. 88 (1992) 1615.

[35] X. Grande, M. Albertí, X. Giménez, J.M. Lucas, A. Aguilar, J. Chem. Soc., Faraday Trans. 89 (1993) 1587.

[36] W.R. Graham, W. Weitner Jr., J. Chem. Phys. 65 (1976) 1516.

[37] U.C. Sridharan, T.G. DiGiuseppe, D.L. McFadden, P. Davidovits, J. Chem. Phys. 70 (1979) 5423.

[38] G.J. Green, J.L. Gole, Chem. Phys. Lett. 69 (1980) 45.

[39] T.G. DiGiuseppe, P. Davidovits, J. Chem. Phys. 74 (1981) 3287.

[40] R.D. Levine, R.B. Bernstein, Molecular Reaction Dynamics and Chemical Reactivity, Oxford University Press, Oxford, 1987.

[41] G.C. Maitland, M. Rigby, E. Brian Smith, W.A. Wakeham, Intermolecular Forces. Their Origin and Determination, International Series of Monographics on Chemistry, Clarendon Press, Oxford, 1981.

[42] A. Laganà, A. Aguilar, X. Giménez, J.M. Lucas, J. Chem. Phys. 95 (1991) 2218.

[43] A. Laganà, A. Aguilar, X. Giménez, J.M. Lucas, Faraday Discuss. Chem. Soc. 91 (1991) 121.

[44] A. Laganà, A. Aguilar, X. Giménez and J.M. Lucas, in: J.M. Bowman (Ed.), Advances in Molecular Vibrations and Collision Dynamics: Quantum Reactive Scattering, vol. IIA, JAI Press, Greenwich, 1994.

[45] X. Giménez, J.M. Lucas, A. Aguilar, A. Laganà, J. Phys. Chem. 97 (1993) 8578.

[46] M. Gilibert, X. Giménez, M. González, R. Sayós, A. Aguilar, Chem. Phys. 191 (1995) 1.

[47] A. Aguilar, M. Albertí, X. Giménez, X. Grande, A. Laganà, Chem. Phys. Lett. 233 (1995) 201.

[48] A. Aguilar, M. Gilibert, X. Giménez, M. González, R. Sayós, J. Chem. Phys. 103 (1995) 4496.

[49] A. Laganà, G. Ochoa de Aspuru, A. Aguilar, X. Giménez, J.M. Lucas, J. Phys. Chem. 99 (1995) 11696.

[50] M. González, R.M. Blasco, X. Giménez, A. Aguilar, Chem. Phys. 209 (1996) 355.

[51] F. Huarte-Larrañaga, X. Giménez, M. Albertí, A. Aguilar, A. Laganà, J.M. Alvariño, Chem. Phys. Lett. 282 (1998) 191.

[52] J.C. Light, R.B. Walker, J. Chem. Phys. 65 (1976) 1598.

[53] J.C. Light, R.B. Walker, J. Chem. Phys. 65 (1976) 4272.

[54] D.C. Clary, Annu. Rev. Phys. Chem. 41 (1990) 61.

[55] D.C. Clary, Mol. Phys. 53 (1984) 3.

[56] D.C. Clary, Mol. Phys. 54 (1985) 605.

Chapter 8

NIP implementation and application.

Contents

In the following sections we will present the articles concerning our work on the implementation of the Negative Imaginary Potentials (NIPs) technique on an invariant embedding propagation scheme, in particular the R-matrix method, as well as its application to a family of reactive systems, covering a wide range of possible cases. The work we have done has yielded until now three regular articles and a communication, each of them covering different aspects of the development and application of the method. In a first article, we showed the accuracy and reliability of the approach by reproducing the extremely sharp resonances of the collinear $Cl+HCl$ symmetric exchange reaction. Then followed a communication in which we explicitly showed the applicability of the method to easily obtain the cross section for a large number of energy values. In a latter publication, the theory was developed in full detail trying to explain carefully the modifications on the R-matrix propagation scheme that the introduction of a complex potential implied. A fourth paper focused on the application of the developed methodology,

employing an IOS Hamiltonian, to study different reactive systems and trying to cover various ergicities and mass combinations.

8.1   On the accuracy of reactive scattering calculations with absorbing potentials: a new implementation based on a generalized R-matrix propagation.

In this work, we intended to give a short communication on the successful implementation of absorbing potentials in an invariant embedding propagation method, focusing on its feasibility and the good performance of the numerical code developed.

The idea, as explained in section 2.7, is basically to reduce a reactive scattering problem into an inelastic one introducing a properly located complex potential. As we have already explained, knowing the ability of NIPs to absorb the flux associated to the wavefunction, if one places such an absorbing potential beyond the transition state region, where reactive transitions are assumed to already have taken place, one may then assign the flux lost to the reactive component. Thus, by properly introducing a NIP and carrying out a straightforward inelastic R-matrix propagation, one may obtain reactive global probabilities. Of course, the propagation scheme has to be accordingly modified to take complex valued interaction matrices into account. However, the goal in this article was to inform briefly and as clearly as possible on the feasibility and reliability of the method and therefore further theoretical explanations were left for the next publication.

Rather than testing our methodology with prototypic reactions, we found more challenging to study the collinear $Cl + HCl$ reaction, for which already exact results had been published. Numerical results were found to fully coincide with the published ones even when comparing the sharp resonances shown by the system. Moreover, the present implementation proved to be more efficient than previous calculations which used a standard R-matrix propagation, since the number of sectors and basis functions used could be more than halved, resulting in great savings of calculation time.

**CHEMICAL
PHYSICS
LETTER**

ELSEVIER

On the accuracy of reactive scattering calculations with absorbing potentials: a new implementation based on a generalized R-matrix propagation

Fermín Huarte-Larrañaga [a], Xavier Giménez [a], Antonio Aguilar [a,*], Michael Baer [b]

[a] Departament de Química Física, Universitat de Barcelona, Martí i Franquès, 1, 08028 Barcelona, Spain
[b] Department of Physics and Applied Mathematics, Soreq NRC, Rehovot, Israel

Abstract

A quantum scattering method based on combining a generalization of the propagative R-matrix technique with negative imaginary potentials is presented. Reactive probabilities are then obtained considering only the reactants arrangement channel and Jacobi coordinates. Collinear and infinite order sudden results are shown for the Cl + HCl symmetric reaction, showing excellent agreement with previous results, including the reproduction of sharp reactive scattering resonances, at a fraction of the computer time and memory requirements. © 1998 Elsevier Science B.V. All rights reserved.

1. Introduction

Among the algebraic, numerical and computational developments in molecular reactive scattering theory, special impetus has been taken recently in the use of complex absorbing potentials to decouple a subset of the close-coupling equations [1,2]. This began when Neuhauser and Baer realized that decoupling the rearrangement channels could be achieved by simply adding a purely negative imaginary linear potential (NIP) ramp at the entrance of the products arrangement [3–5]. This idea exploited the fact that, for reactive collisions, the probability flux loss towards rearrangement states takes place in a rather

well-delimited region of configuration space, which is different from that where the inelastic flow transfer processes take place, between states of the same rearrangement channel. Therefore, a suitably defined function, depending on physical coordinates, is found to be able to discriminate the reactive component of the wavefunction and absorb it. This results in a local, smooth and weakly energy-dependent NIP.

On such basis, powerful state-to-all time-dependent (TD) and time-independent (TI) methods for reactive scattering were developed, which avoided the well-known problem of artificial back-reflection of the wavepacket at the grid limits (in TD methods) and the coordinate transformation between rearrangement channels. The combination of the TI approach with a variational technique, applied to solving the scattering problem by a splitting of the

---

* Corresponding author.

hamiltonian between a reference problem and the remainder perturbation, allowed extracting state-to-state reactive probabilities. This methodology has been successfully applied to several triatomic and tetraatomic systems, within coupled-states and infinite order sudden (IOS) approaches, respectively, as well as to electronic non-adiabatic reactions [6,7]. Other TI methods, using one form or another of absorbing potentials, have been proposed since then. For instance, Miller's group [8] have successfully used NIPs to force outgoing boundary conditions in the calculation of the cumulative reaction probability, as a means for the direct rate constant calculation without solving the whole state-to-state problem. Another promising class of methods which make use of NIPs are those classified as 'artificial boundary inhomogeneity' [9–11].

The alternative approach to treating reactive scattering by means of TI methods, namely the use of propagation techniques on a suitably expressed hamiltonian — concerning coordinate systems and/or reduced dimensionality approximations — has been less explored in terms of incorporating the NIPs. Neuhauser et al. [12] added to a propagative inelastic method a NIP, using an adiabatic basis set and the Numerov method for propagation. It led to the calculation of state-to-all reactive probabilities for the collinear $H + H_2$ reaction. Shortly afterwards, Baer et al. [13] extended the previous method to the reactive infinite-order sudden approximation and applied it to the $Ar + H_2^+$ system. Results appeared to be closer to experiments than those obtained with a 'traditional' (i.e. without NIP) R–IOS method.

A new implementation of a propagation method, which is intended to improve the efficiency of the previous techniques, is presented here, focusing in this work on its feasibility and the good performance of the numerical code. Results for the present test appear to be easily and well converged, as well as coincident with those obtained with a completely different numerical technique. Remarkably, it has been found that strongly sharp reactive scattering resonances have been well reproduced. Computer times and RAM memory requirements keep into reasonably low values, thus improving the already well-known performances of propagation-based methods.

2. Outline of the method and numerical results

The method is based on the inelastic R-matrix propagation [14] of a Hamiltonian expressed in reactants Jacobi coordinates, generalized to deal with the complex interaction matrix which results with the inclusion of a NIP at the entrance of the products arrangement channel. The collision is then treated as being inelastic and reactivity is calculated from the flux loss, i.e. the difference between unity and each state-to-all inelastic probability sum.

In opposition to the variational methods, for which an eigen problem must be solved for a large matrix for each partial wave and energy, the propagation methods use a larger number of smaller dimensionality matrices to propagate the solution along the scattering coordinate. This latter method leads to much smaller memory requirements than the variational, but to a larger amount of input–output to secondary memory. The use of an absorbing potential appears then well suited to this problem, since it greatly reduces the number of translational sectors to propagate along. It thus leads to a diminution in those input–output operations which are the slowest. Moreover, within the large class of propagation methods available in the literature, the invariant embedding methods [15] have shown to be not only the fastest but especially adapted to deal with the closed-channel explosion problem [16]. Therefore, it appears that the use of an invariant imbedding propagator, adapted to include complex interaction matrices, is one of the key factors leading to a good numerical performance. Here just the novel features of the present approach will be outlined and full details of the theoretical methodology, as well as an extended 3-dimensional application to several triatomic systems, will be given elsewhere [17].

The method essentially consists of the reduction of a reactive scattering problem to an inelastic problem through the introduction of a proper complex potential and then applying the inelastic scattering R-matrix propagation scheme [14]. This propagation technique had to be properly generalized to take into account the complex-valued algebra arising from the use of an absorbing potential. In particular, a suitable reference problem [14,18] had then to be formulated consistently with the resulting complex eigenvalues of the interaction matrix. This led to a modified

expression of the sector propagators [14,18] and
furth~r t~ t~~ ~~ll~wing recursion rel~ti~~ ~f th
R-matrix,

$$\mathbf{R}^{(k)} = \mathbf{r}_1^{(k)} - \mathbf{r}_3^{(k)}\mathbf{Z}^{(k)}\mathbf{r}_2^{(k)}$$

$$\mathbf{Z}^{(k)} = \left[\mathbf{r}_1^{(k)} - \mathbf{Q}^{-1}(k-1,k)\mathbf{R}^{(k-1)}\mathbf{Q}(k-1,k)\right]^{-1}$$

Here, $\mathbf{R}^{(k)}$ is the global R-matrix up to the kth
sector, $\mathbf{r}_i^{(k)}$ ($i = 1, 2, 3, 4$) are the kth sector R-
matrices and $\mathbf{Q}(k = 1, k)$ is a transformation matrix
which relates the solutions across the sectors. The
present expressions differ from those given in Ref.
[19] basically in the complex valued nature of the
matrices involved and in the explicit inversion of the
Q matrix instead of having taken its complex trans-
pose. State-to-all reactive S-matrix elements are then
obtained subtracting from one, the state-to-all inelas-
tic counterpart, which is obtained directly from in-
elastic boundary conditions [14], instead of the reac-
tive boundary conditions emerging from the standard
reactive R-matrix technique [19].

Rather than testing the method with the prototypic
$H + H_2$ reaction, we thou ht more challen in to
look at its applicability to the collinear Cl + HCl
symmetric reaction. As is well known, the acute
skew-angle characterizing the system poses special
difficulties when treating it with hamiltonians ex-
pressed in other than hyperspherical coordinates.
However, since propagation is performed in a single
arrangement channel, those problems arising as a
consequence of the strong reaction-path curvature at
the transition state region are directly avoided.

The inclusion of a NIP required an independent
tunning of its adjustable parameters before undertak-
ing the scattering calculations. The final set of pa-
rameters was easily found, once the proper location
of the linear ramp after the transition state zone was
stablished, since a wide range of both the width and
height of the linear ramp led to essentially stable
results, in agreement with previous experience [3–6].
In particular, ramp heights (U) between 0.3 and 1.0
eV and ramp widths (D) between 0.5 and 1.5 Å
determined the region for which probabilities were
stable. Then, the reactive probabilities obtained with
the final set, chosen to be 0.5 eV (U) and 1.0 Å (D),
were compared and found to coincide with the R-ma-
trix results of the detailed hyperspherical propagation
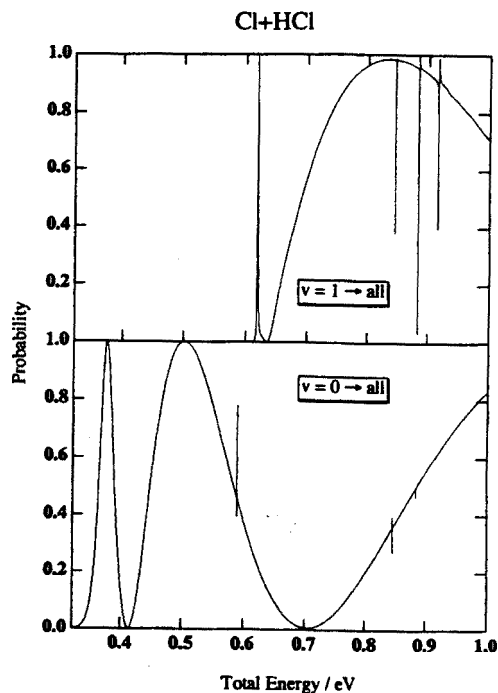calculations of Bondi et al. (BCMR), performed on

Fig. 1. State-to-all collinear reaction probabilities for the Cl + HCl
symmetric exchange reaction, as a function of total energy, for the
$v = 0$ and $v = 1$ initial vibrational states, on the BCMRSsLEPS
surface.

the same LEPS [20]. It is important to emphasize that
a unique set of NIP parameters was used for the
whole energy range. Fig. 1 shows the dependence of
the state-to-all reactive probabilities with total en-
ergy, in the range of 0.32–1.00 eV, for the $v = 0$ and
$v = 1$ initial vibrational states. A total of 2156 en-
ergy points have been calculated, using a finer grid,
as explained below, around the sharp resonance re-
gions. Convergence was reached with the inclusion
of 10 vibrational states, although the final number
used was 15 in order to allow for a high degree of
accuracy testing. Propagation ran from 2 to 8 Å.
Numerical results are found to coincide well, within
the whole energy range and for all initial vibrational
states, with those of BCMR.

As a further fine-tuned test of scattering methods
incorporating NIPs, the extremely sharp reactive

Table 1
Comparison between BCMR and the present work resonance positions (in eV) for the collinear Cl + HCl symmetric exchange reaction

BCMR	Present work
0.58848	0.58886
0.61960	0.62000
0.84492	0.84529
0.88359	0.88397
0.91609	0.91645

scattering resonances shown in the BCMR results were also searched in the present case. As seen in Fig. 1, they have been properly characterized by including a sufficiently fine grid of energy points (the energy step size being up to 0.00001 eV). Their positions and widths are found to be close to BCMRs, as shown in Table 1. In particular, the position agrees within approximately four-tenths of meV, for all resonances considered. After checking accurately the origin for the discrepancies found (masses, potential parameters, ...) and given the fact that the differences between BCMR and the present work results are essentially constant, their origin may be due to an energy shifting caused by small differences in the units conversion factors used. Nevertheless, given the remarkable differences between the numerical approaches used in both calculations, the present results constitute a good benchmark for stablishing the ability of absorbing potential-based methods to reproduce exact quantum scattering calculations.

As for computer performances, it is found that the simplicity introduced by avoiding the reagent-to-product channel transformation makes the calculation of each reaction probability quite fast. Therefore, the calculation becomes shorter because the number of sectors is approximately halved and, in most cases, fewer basis functions are necessary than in the traditional propagation calculations. The complications introduced by the absorbing potential, namely the major width and reduced simplicity of the potential profiles along the vibrational coordinate, as well as the slightly more involved algorithm for propagation [17], clearly do not reverse the savings introduced by the above simplifications. Explicit figures on CPU time consumption and relative accu-

racy are given in Table 2, for different sets of total sector number and dimension of the vibrational basis. An infinite order sudden hamiltonian was considered for this case (resulting the hereafter named NIP–IOS method). In the table it can be seen that NIP–IOS execution times are four times smaller than R–IOS (i.e. the traditional reactive–IOS method [21]), at the same accuracy. This elapsed time can even be reduced by a factor of six and the error still would remain acceptable. It therefore shows that accurate results can be obtained with a fraction of the computer time necessary when the standard R–IOS technique is used. In the present Cl + HCl case, results from Table 2 clearly indicate that the major gain in CPU time and memory consumption come from the much smaller basis set dimension necessary, due to the use of reactants arrangement Jacobi coordinates instead of circular collision coordinates and the smaller number of sectors necessary for propagation.

In conclusion, further evidence has been provided, in the present work, for the ability of NIP-based methods to reproduce accurately exact results obtained by means of other well-stablished techniques. A most remarkable fact is that even those dynamical features dramatically depending on colli-

Table 2
Comparison of accuracy and CPU time consumption between converged R–IOS fixed-angle ($\gamma = 180°$) cross-section calculations (last row and bold) for the Cl + HCl system, for a total energy of 0.6 eV, and equivalent NIP–IOS results for different values of the main numerical parameters (from first to last but one row)

NS	NV	% ERR	Time (s)
300	30	0.00	3508
300	10	0.00	389
300	7	0.03	258
200	15	0.13	503
200	10	0.13	261
150	15	0.30	378
150	10	0.30	194
400	**27**	**–**	**1174**

NS, number of translational sectors; NV, vibrational basis set dimension; % ERR, percentage error with respect to the first row calculations; time: elapsed time on a RISC 6000 IBM Workstation.

sion energy, i.e. the sharp resonances which characterize the collinear $Cl + HCl$ reaction, have been reproduced in the present calculations. Furthermore, the present calculations constitute a most demanding test concerning the accuracy of NIP-based methods, when compared against well-stablished exact techniques. Moreover, our new implementation of the invariant imbedding R-matrix propagation technique has shown to be computationally competitive when compared to methods which need to propagate along both reactant and product arrangements. It is worth mentioning that a unique, easily found linear absorbing potential ramp has been used for the whole calculation.

Finally, it is interesting to point out that the present method is close in spirit to the detailed quantum transition state theory of Light and Altenberger-Siczek [22,23]. However, the use of complex absorbing potentials removes the approximations resulting from the imposition of the boundary conditions at the transition-state surface. Work is in progress for extending the present code to 3D (both exact and approximate) calculations for triatomic systems and to approximate calculations of polyatomic systems.

Acknowledgements

References

[1] I. Last, M. Baer, Variational treatments of reactive scattering: application of negative imaginary absorbing potentials and contracted L^2 basis sets to calculate S-matrix elements. in: J.M. Bowman (Ed.), Advances in Molecular Vibrations and Collision Dynamics, Vol. IIA (JAI Press, Greenwich, CT, 1994) p. 85.

[2] J.M. Bowman (Ed.), Advances in Molecular Vibrations and Collision Dynamics, Vols. IIA and IIB (JAI Press, Greenwich, CT, 1994).

[3] D. Neuhauser, M. Baer, J. Chem. Phys. 90 (1989) 4351.

[4] D. Neuhauser, M. Baer, J. Phys. Chem. 93 (1989) 2862.

[5] D. Neuhauser, M. Baer, J. Chem. Phys. 91 (1989) 4651.

[6] M. Gilibert, R.M. Blasco, M. González, X. Giménez, A. Aguilar, I. Last, M. Baer, J. Phys. Chem. 101 (1997) 6821, and references therein.

[7] I. Last, M. Gilibert, M. Baer, J. Chem. Phys. 107 (1997) 1451, and references therein.

[8] U. Manthe, T. Seideman, W.H. Miller, J. Chem. Phys. 101 (1994) 4759, and references therein.

[9] D.K. Hoffman, Y. Huang, W. Zhu, D.J. Kouri, J. Chem. Phys. 101 (1994) 1242.

[10] V.A. Mandelstham, T.R. Ravuri, H.S. Taylor, J. Chem. Phys. 101 (1994) 8792.

[11] H.W. Jang, J.C. Light, J. Chem. Phys. 102 (1995) 3262.

[12] D. Neuhauser, M. Baer, D.J. Kouri, J. Chem. Phys. 93 (1990) 2499.

[13] M. Baer, C.Y. Ng, D. Neuhauser, Chem. Phys. Lett. 169 (1990) 534.

[14] E.B. Stechel, R.B. Walker, J.C. Light, J. Chem. Phys. 69 (1978) 3518.

[15] B.R. Johnson, J. Comput. Phys. 13 (1973) 445.

[16] D.E. Manolopoulos, J. Chem. Phys. 85 (1986) 6425.

[17] F. Huarte-Larrañaga, X. Giménez, A. Aguilar, manuscript to be published.

[18] F. Mrugala, D. Secrest, J. Chem. Phys. 78 (1983) 5954.

[19] J.C. Light, R.B. Walker, J. Chem. Phys. 65 (1976) 4272.

[20] D.K. Bondi, J.N.L. Connor, J. Manz, J. Römelt, Mol. Phys. 50 (1983) 467.

[21] H. Nakamura, A. Ohsaki, M. Baer, J. Phys. Chem. 90 (1986) 6176.

[22] J.C. Light, A. Altenberger-Siczek, Chem. Phys. Lett. 30 (1975) 195.

[23] J.C. Light, A. Altenberger-Siczek, J. Chem. Phys. 64 (1976) 1907.

8.2 Comment in the 110 Faraday Discussion on Chemical Reaction Theory. General Discussion.

Faraday Discussion 110 (1998) 236-238

Here we present the comment with which we contributed to the General Discussion in the 110 Faraday Discussion on Chemical Reaction Theory. Our comment concerned an article by Peng *et al.*[69] in which they decoupled reactants and products. We thought it would be interesting to present in this context our recent implementation of the NIP to the R-matrix propagation scheme. In particular we showed the results obtained for the application of the new method to the $Ne + H_2^+ \rightarrow NeH^+ + H$ reaction. Cross-sections for about 200 energy values, ranging from 0.7 eV to 1.1 eV, were computed and evidenced a markedly structured reactivity.

236   *General Discussion*

use of a ground-state transmission coefficient for including dynamical tunneling and nonclassical reflection contributions.[4]

1 S. L. Mielke, G. C. Lynch, D. G. Truhlar and D. W. Schwenke, *Chem. Phys. Lett.*, 1993, **216**, 441; S. L. Mielke, G. C. Lynch, D. G. Truhlar and D. W. Schwenke, *J. Phys. Chem.*, 1994, **98**, 8396; S. L. Mielke, T. C. Allison, D. G. Truhlar and D. W. Schwenke, *J. Phys. Chem.*, 1996, **100**, 13588.
2 H. Eyring, *J. Chem. Phys.*, 1935, **3**, 107.
3 K. S. Pitzer, *Quantum Chemistry*, Prentice-Hall, Englewood Cliffs, NJ, 1953.
4 B. C. Garrett and D. G. Truhlar, *Proc. Natl. Acad. Sci. USA*, 1979, **76**, 4755; B. C. Garrett and D. G. Truhlar, *J. Chem. Phys.*, 1980, **72**, 3460; B. C. Garrett, D. G. Truhlar, R. S. Grev and A. W. Magnuson, *J. Phys. Chem.*, 1980, **84**, 1730; D. G. Truhlar and B. C. Garrett, *Acc. Chem. Res.*, 1980, **13**, 440.

Dr Nyman commented: From calculations on reactions where a light atom is transferred through a potential barrier, it is my experience that the J-shifting approximation works well in the tunnelling regime and less well as the energy is increased (see, for example, ref. 1). It has already been mentioned that the J-shifting approximation is expected to work best for reactions with a potential barrier so that there is a localized transition state, where the rotational constants used in the J-shifting approximation are evaluated. My observation is in agreement with this and indicates that, as the energy is increased, the potential barrier is less efficient in localizing the transition state.

1 G. Nyman, *J. Chem. Phys.*, 1996, **104**, 6154.

Prof. Truhlar commented: I would like to draw attention to one aspect of the spin–orbit coupling in halogen reactions that has very general implications, as we have noted elsewhere.[1] This is the effect of the spin–orbit splitting on barrier heights. For most halogen atom reactions with tight transition states (*e.g.*, Cl + CH_4 but not necessarily downhill association reactions), the spin–orbit splitting ΔE_{SO} is effectively quenched at the transition state. This rather general conclusion arises not from detailed calculations of spin–orbit matrix elements but rather from the large energy gap between the ground and first excited electronic state at the transition state geometry; hence the second order perturbation theory expression for ΔE_{SO} is small. This quenching of the spin–orbit splitting means that any calculation of the barrier height that neglects this effect will underestimate the barrier height by one third of the spin–orbit splitting, *i.e.*, by 0.4, 0.8, 3.5 and 7.2 kcal mol^{-1} for reactions of F, Cl, Br and I, respectively. Electronic structure theorists may be loath to include this effect because their calculated barrier heights are usually too large (due to the incomplete treatment of electron correlation), and raising the barrier by including spin–orbit lowering of the reactant energy will only make the situation worse. Nevertheless, the effect is real, and it will have to be included as the accuracy of the electronic structure calculations improves.

1 O. Roberto-Neto, E. L. Coitiño and D. G. Truhlar, *J. Phys. Chem. A*, 1998, **102**, 4568.

Mr Huarte-Larrañaga and **Dr Gimenez**¶¶ communicated regarding the paper by Peng *et al.*: Peng *et al.* suggest in their article that, in their attempt to get state-to-state information by means of the reactant–product decoupling method, the product scattering wavefunction can be calculated solving either (i) the time-independent Schrödinger equation with an energy-dependent source term or (ii) the time-independent homogeneous equation for the full vector wavefunction, through the use of an adequate propagation scheme.

We have recently implemented a procedure which is rather close in spirit to the second case, although it is devised to obtain state-to-all information. It is based on combining a generalization of the propagative R-matrix technique with negative imagin-

¶¶ Also Prof. Aguilar, Universitat de Barcelona, Spain.

ary potentials (NIP). State-to-all reactive probabilities are then obtained considering only the reactants arrangement channel and Jacobi coordinates. In particular, the method is based on the inelastic R-matrix propagation, generalized to deal with the complex interaction matrices resulting from the inclusion of an NIP at the entrance of the products arrangement channel. The collision is then treated as being inelastic and reactivity is calculated, as usual, from the flux loss, *i.e.* by subtracting from unity each state-to-all inelastic probability sum.

The modification of the R-matrix propagation scheme starts with the formulation of the reference problem consistent with the resulting complex eigenvalues of the interaction matrix. This leads to a modified expression of the sector propagators and further to the following recursion relation for the R-matrix,

$$R^{(k)} = r^{(k)} - r^{(k)}Z^{(k)}r_2^{(k)}$$

$$Z^{(k)} = [r^{(k)} - Q^{-1}(k-1,k)R^{(k-1)}Q(k-1,k)]^{-1}$$

where $R(k)$ is the global R-matrix up to the kth sector, $r_i^{(k)}$ ($i = 1, 2, 3, 4$) are the kth sector R-matrices and $Q(k-1, k)$ is the transformation matrix which relates solutions across the sectors. The present expressions differ from those given in the original formulation of the inelastic R-matrix method[1] basically in the complex-valued nature of the matrices involved and in the explicit inversion of the Q matrix instead of taking its complex transpose. State-to-all reactive S-matrix elements are obtained by substracting from one the state-to-all inelastic counterpart. It is in turn obtained directly from inelastic boundary conditions, instead of the reactive boundary conditions applied in the standard reactive R-matrix technique.[2]

The method was first tested with the collinear Cl + HCl symmetric reaction. A unique set of NIP parameters was found to be able to reproduce the previously available collinear reaction probabilities, including the extremely sharp reactive scattering resonances.[3] Reactive state-to-all infinite order sudden (IOS) cross-sections were obtained, with the same accuracy, using *ca.* one third of the vibrational basis dimension and one fifth of computer time than the standard Reactive IOS method. This reduction in computational needs is found to be due essentially to two factors: first, only one half of the sectors are necessary for propagation and, second, fewer basis functions are required since the complications introduced by the transition from reactants to products are directly avoided.[4] As a consequence, the present approach seems to be well suited to propagative techniques, since these are based on the use of a large number of relatively small matrices to propagate the solution along the scattering coordinate, so that much smaller memory requirements are necessary than, for instance, variational methods. However, a larger amount of input–output to secondary memory exists. Therefore, decreasing the number of translational sectors to propagate along leads to a diminution of those input–output operations which are the slowest.

The application to other involved triatomic systems (Li + FH, Mg + FH, ...) will be given in a future article.[5] Here we outline the ability of the present approach for resolving structured reaction probability profiles. Fig. 12 shows the fixed-angle IOS cross-section, for the collinear geometry of the $Ne + H_2^+ \rightarrow NeH^+ + H$ reaction. This is a collinearly dominated endoergic process with an electronic minimum found just before the transition state configuration. The energy dependence of the fixed-angle cross-section is found to be dominated by a pattern of resonance peaks, which survive the angular momentum summation. This result is in accord with the complex-forming nature of the collision process, as established in previous studies.[6] The results in Fig. 12 have been obtained, after careful checking for convergence, with one set of NIP parameters, 15 vibrational basis functions and 200 total energy values in the 0.7–1.1 eV range.

1 E. B. Stechel, R. B. Walker and J. C. Light, *J. Chem. Phys.*, 1978, 69 3518.
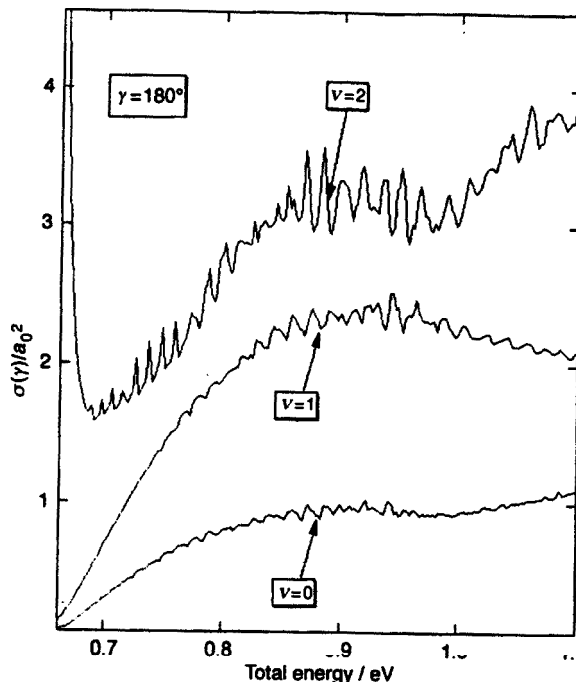2 J. C. Light and R. B. Walker, *J. Chem. Phys.*, 1976, 65 4272.

Fig. 12 Fixed-angle IOS cross-sections $[\sigma(\gamma)]$, for the collinear geometry of the Ne + H_2^+ → NeH^+ + H process, within the 0.7–1.1 eV total energy range. Results are shown for the reactants vibrational state $v = 0$, 1 and 2.

3 F. Huarte-Larrañaga, X. Gimenez, A. Aguilar and M. Baer, *Chem. Phys. Lett.*, 1998, **291**, 346.
4 F. Huarte-Larrañaga, X. Gimenez and A. Aguilar, *J. Chem. Phys.*, in press.
5 F. Huarte-Larrañaga, X. Gimenez, J. M. Lucas and A. Aguilar, in preparation.
6 M. Gilibert, R. M. Blasco, M. Gonzàlez, X. Gimenez, A. Aguilar, I. Last and M. Baer, *J. Phys. Chem.*, 1997, **101**, 6821.

Prof. J. Z. H. Zhang opened the discussion of Prof. Balint-Kurti's paper: When state-to-state scattering results are needed. It is not desirable to use a single set of Jacobi coordinates to carry out the wavepacket propagation since this will drastically increase the number of basis functions and numerical grids as a penalty for not choosing the correct coordinates. In such case, it is advisable to use more suitable methods to do state-to-state calculations. The RPD (reactant–product decoupling) method is a general and attractive method for such applications.

Dr Althorpe addressed Prof. Balint-Kaurti: Might I suggest that your wavepacket calculations on O + H_2 and O + HD would benefit from an application of the reactant–product decoupling (RPD) approach of Zhang and co-workers?[1] This would reduce the size of the Hamiltonian matrices (used to propagate the wavepacket) and would enable you to switch from reactant to product coordinates. I would like to propose a modification to Zhang's original RPD approach, which is applicable whenever one wants to calculate the state-to-state reaction probabilities into one product channel.

The original RPD scheme[1] partitions a reaction as shown by arrow I in Fig. 13, for the simplest example of the two-dimensional A + BC → AC + B reaction. The coordi-

8.3 The application of complex absorbing potentials to an invariant embedding scattering method: I. Theory and computational details.

In this article, the theory of our extension of quantum scattering methods, based on the propagative R-matrix method, to deal with complex absorbing potentials was developed in detail. Assuming we had not been by no means pioneers in the use of optical potentials, nevertheless we have just implemented them in a propagative scheme, the article intended to give first a careful review on the historical use and development of such optical potential techniques. Some brief outlines on this have already been given in section 2.7. The main aim of the published work was to describe in full detail the key aspects that had to be modified on the R-matrix propagation scheme, so that it could take into account the complex valued nature of the interaction matrix. As we have already stated in sections 2.7 and 8.1, through the proper introduction of a negative imaginary potential (NIP) one can reduce the reactive problem into what we have called a *pseudo-inelastic* one. Then, one can carry out a calculation as if there would be only inelastic scattering which is much more simple to treat and then assign the flux lost to the reactive probability flux. This absorbing potential is in our case a negative imaginary linear ramp which depends on the physical coordinates of the system. The introduction of such imaginary potential causes the interaction matrix in the close coupling equations to become complex-valued. The R-matrix propagation method, as originally formulated, assumes the interaction matrix is real and symmetric and this was no longer our case. Therefore, the propagation scheme had to be revised in order to generalize it to complex-valued interaction matrices. Essentially, modifications imply basically a generalization of the sector constant potential solutions to quotients of exponential functions, instead of the usual trigonometric and hyperbolic functions, as well as the explicit inversion of some transformation matrices which are no longer real and symmetric and therefore its transpose does not correspond to its inverse. The asymptotic matching was carried out as in the standard inelastic R-matrix propagation and then state-to-state inelastic probabilities were obtained.

Once the R-matrix propagation had been generalized, we employed a infinite order sudden (IOS, see section 6.1) Hamiltonian for obtaining an explicit expression for the interaction matrix. Moreover, since we had already several results at hand using the traditional R-IOS methodology, in which the solution was propagated in both reactants and products region, we thought it could be a good test of the new approach's performance. Thus, different runs of the developed computer code were undertaken for the calculation of the $Cl + HCl \rightarrow ClH + Cl$

exchange reaction. Reliability of our collinear results had already been proven in the previous communication when compared to exact results from the literature (see 8.1). In this paper we showed the method stability, not only concerning the NIP parameters but also propagation parameters which turn into a better performance of the NIP-IOS code, as compared to that of the R-IOS.

The application of complex absorbing potentials to an invariant embedding scattering method: I. Theory and computational details

Fermín Huarte-Larrañaga, Xavier Giménez, and Antonio Aguilar[a]

Departament de Química Física, Universitat de Barcelona, Martí i Franqués, 1, 08028, Barcelona, Spain

In this article, an extension of quantum scattering methods based on propagative R-matrix techniques to deal with negative imaginary potentials is presented. Reactive probabilities can be then obtained, considering only the reactants arrangement channel and Jacobi coordinates. It has been necessary to generalize the R-matrix propagation method, in order to consider the complex-valued nature of the interaction matrix. The new formulation has been particularized, in the present case, to the Infinite-Order Sudden Approximation, for which several results, focusing on the reliability and numerical performances of the method, will be shown. © *1998 American Institute of Physics.* [S0021-9606(98)02338-1]

I. INTRODUCTION

The use of Negative Imaginary Potentials (hereafter referred as NIP) as a tool for simplifying the complexity of close-coupling scattering calculations has been considered for a long time.[1] Several applications to molecular systems, based on rather different formal approaches, have been proposed in the literature during the last years. For this reason, in order to put in the adequate context the contributions developed here, it is worth beginning with a short revision of what has been performed up to the date on this subject.

Based on the well-known Feshbach decomposition,[2] the absorbing potentials were first used in the field of nuclear physics.[3] Typical applications considered both formal and phenomenological approaches for dealing with elastic processes. For instance, complex phase shifts determined from more or less approximated estimations of optical potentials, were used to account for processes such as the absorption of particles by atomic nuclei.

As for its application to molecular collisions, two rather well-differentiated stages ought to be considered. The first focused essentially on elastic events when both inelastic and reactive processes take place at the same time, that is, solving the close-coupling equations retaining only one term.[4] On one hand, formal developments dealt with well-known problems associated with the use of NIPs as, for instance, the nonlocality of the potential.[5] Adiabatic and decoupling approximations were also taken into account to simplify the dimensionality of the problem.[6] Among other relevant works, that of Wolken[7] can be pointed out, who devised a procedure for, given a numerically solved problem, extracting that optical potential which allowed reproducing a desired S-matrix subset. This method was subsequently used by Truhlar and co-workers[8] to study electron–atom collisions. The main results found were that the sharp variations of the optical potential, found when the radial wave function has a node, could be smoothed without significantly altering the results. On the other hand, phenomenological approaches

were also adopted for the form of the NIP. Different *ad hoc* functional forms with adjustable parameters were used by Marriot and Micha,[9] Micha and Rotenberg[10] and Ross and colleagues,[11] to succesfully reproduce experimental information on elastic data by means of parametrizing the absorption as a function of the orbital angular momentum. Although some insights on the elastic behavior of collisions in the presence of inelastic and reactive phenomena were obtained, no systematic procedure became available and the use of adjustable parameters limited its predictive capability.

The second stage that we distinguish in the development of the optical potentials application to molecular systems begins in 1986, when Kosloff and co-workers[12] considered the problem of artificial back-reflection of wave packets. It usually takes place at the boundaries of the point grid defined on the configuration space for time-dependent wave packet propagations. Initially, this problem was avoided extending the grid size, but this required very large computational resources and limited its applicability. As an alternative solution, they proposed the use of empirical forms of NIPs, based on similar treatments proposed for the stabilization of resonance calculations[13] and the photodissociation of molecules,[14] so that the wave packet is absorbed before the grid edges have been reached, without being altered in the inner regions. This inspiring idea was further considered in detail by Neuhauser and Baer,[15] who analyzed the conditions for which a linear ramp, is an optimal functional that allows effective wave packet absorption conditions.

Shortly after, the same authors[16] proposed a completely different use of the absorbing linear ramp. Instead of placing it in the far asymptotic region, it was situated right after the transition state, at the entrance of the products channel. With this location, it is possible to consider that the absorbed flux corresponds to that fraction of the total flux that flows toward the products channel. Moreover, the optimal absorption conditions were found to be basically the same than those determined in their first study, i.e., in the asymptotic region. Therefore, it results in a local, soft, little system- and energy-dependent and easy to implement optical potential, which

[a] Electronic mail: antonio@vystup.qf.ub.es

Chapter 8. NIP implementation and application.

can be used to obtain quantitative information on the total reactive flux. This phenomenological use of NIPs differs from the one previously discussed for the elastic scattering in that the actual flux absorption takes place in a completely differentiated region of configuration space, i.e., the reactive part of the flux does not overlap in this region with the elastic and inelastic parts. Therefore, a suitably placed NIP depending on physical coordinates should be, in principle, able to discriminate the reactive component of the flux and absorb it selectively, since it is the only fraction of the flux reaching the region of configuration space where the NIP is placed.

The main well-known advantage of this approach stems on the fact that the close coupling calculations simplify basically to an inelastic scattering calculation. Since reactive flux is absorbed fairly near to the strong interaction region, one solves the problem considering only one (although somewhat perturbed) rearrangement channel. Therefore, the calculation is simplified since Hamiltonians defined on a single arrangement channel can be used and basis set expansions may also be accordingly devised. On the other hand, the method, as originally formulated, is only capable of providing total reaction S-matrix elements and the calculation becomes more complicated since complex algebra must be then considered.

The first implementation of the NIP method to reactive scattering was based on the time-dependent (TD) methodology.[16] However, nothing prevented to implement the above idea, as originally formulated, to time-independent (TI) approaches. This idea led Neuhauser and Baer[17] to develop a TI-NIP method. In particular, it was based on the partition of the Hamiltonian into a reference and a perturbation problem. They also added another NIP in the far reactants asymptotic region, so that the scattering problem was converted to a boundlike problem. Probabilities were initially calculated by means of flux formulas.

The calculation of state-to-state probabilities and differential cross sections was made possible with the incorporation of a variational principle to the above formulation.[18] Efficiency was further improved with the use of localized Gaussian functions as the translational basis set. This basis set is defined using only reactants-arrangement channel Jacobi coordinates,[19] and not a simultaneous expansion in all arrangement channels, as it is common to traditional variational methods (which leads to nonlocal, exchange-type integrals and overcompleteness with the basis set may also occur).[20]

The application of the above TD and TI methodologies has led to accurate studies of triatomic (using exact[21] and coupled-states[22] Hamiltonians) and tetratomic (using IOS Hamiltonians[23]) reactions at the cross section level. Four-mathematical dimension treatments[24] and exact probabilities have been produced for the prototypic tetratomic reactions H_2+OH[25] and H_2+CN.[26] The most refined version of the TI-NIP method has also been the basis for the formulation of a new approach to treating electronically nonadiabatic processes.[27]

Other TI approaches have been proposed in the literature that use one form or another of absorbing potentials. Among them, it is interesting to mention those by Seideman, Manthe

and Miller,[28] who use absorbing boundary conditions by means of a Wood–Saxon potential to ensure outgoing boundary conditions for the direct calculation of rate constants via a flux–flux autocorrelation operator. The method has been recently applied to the calculation of the rate constant for several reactions: H_2+OH,[29] $Cl+H_2$,[30] $O+HCl$,[31] $H+O_2$[33] and the ketene isomerization.[34] Other promising methods, although not yet so extensively tested, which can make use of NIPs, are those classified as "*artificial boundary inhomogeinity*":[35] the time-independent wave packet method of Kouri et al.,[36] the spectral projection approach of Mandelshtam and Taylor[37] and the generalized boundary inhomogeneity method of Jang and Light.[35] This latter method actually demonstrates that it is possible to handle the correct reaction probabilities with the use of real, short-ranged terms.

The well-known alternative approach to treating reactive scattering by means of TI methods, namely the use of propagation techniques on a suitably expressed Hamiltonian—concerning coordinate systems and/or reduced dimensionality approximations—has been less explored in terms of incorporating the NIPs. Neuhauser, Baer, and Kouri[38] added to a propagative inelastic method a NIP, using an adiabatic basis set and the Numerov method for propagation. It led to the calculation of state-to-all reactive probabilities for the collinear $H+H_2$ reaction. Shortly after, Baer, Ng, and Neuhauser[39] extended the previous method to the reactive infinite-order sudden approximation and applied it to the $Ar+H_2^+$ system. Results appeared to be closer to experiments than those obtained with a *traditional* (i.e., without NIPs) R-IOS method.

The introduction of a propagation scheme into a NIP-based scheme scattering method may be understood in terms of the seek for higher efficiency while keeping the accuracy. In opposition to the variational methods, for which an eigenproblem must be solved for a very large matrix for each partial wave and each energy, the propagation methods use a larger number of smaller dimensionality matrices to propagate the solution along the scattering coordinate. This latter method has much smaller memory requirements, but needs a larger amount of input–output to secondary memory. The use of an absorbing potential appears then well suited to this problem, since it greatly reduces the number of translational sectors to propagate along. It thus leads to a diminution in those input–output operations which are, by far, the slowest. Moreover, within the large class of propagation methods available in the literature, the invariant embedding methods[40] have shown to be not only the fastest but especially adapted to deal with the closed-channel explosion problem.[41] In addition, while invariant embedding methods display the so-called symplectic symmetries,[42] which ensure the unitarity and symmetry of the S-matrix in standard applications, the Numerov and related propagation schemes do not show them, so that unitarity and symmetry is not always guaranteed.

At this point, an additional reason for exploring the combination between invariant embedding propagation and absorbing potential emerges, since the present application makes an explicit use of nonunitarity. This leads to the ques-

ti--- -f h--- ---ll- ----rate NIP-base ' me ' o 's are, since t e simplectic properties have not been checked with non-unitary operators.[43] Although remarkable studies have been performed, in general, on the comparison between well-established traditional methods and NIP ones, which show that results are basically identical or, at least, that differences are reasonably small, the above discussion stresses that there is still missing a detailed test on the accuracy limits of the NIP methods. Moreover, such a study would connect the rather numerous studies on the relative efficiencies of several functional forms of NIPs[44] with its actual use in scattering methods. For all these reasons, a rather demanding test has been already p   [45]   . . --------- --- --- --e--o- presented here. It showed, in particular, its ability to reproduce the extremely sharp resonances that are characteristic of the Cl+HCl collinear reactive scattering. An interesting result is that symmetry has been found to be highly preserved in all applications. In addition, since an explicit use is made of the *amount of unitarity* lost when the absorbing potential actually modifies the radial solution, the present application shows to be consistent with the formal requirements, as it will be discussed below.

The remainder of this paper is structured as follows: In Sec. II an outline of the theoretical methodology, stressing on the modifications that have arisen with the introduction of the NIP, is presented. In Sec. III we deal with the practical implementation and numerical performances, while in Sec. IV we conclude.

II. THEORETICAL FUNDAMENTALS

A. Treatment of the reactive system as a pseudoinelastic process

It is well known that the Close-Coupling treatment of a multiarrangement reactive system requires the solution of a $N_1 + \cdots + N_M$ equation set, where $N_1, \ldots, N_M$ are the different arrangement open channels. Moreover, a transformation from the reactants coordinates to those of the products is required or, alternatively, more involved coordinate systems have to be used. Therefore, the treatment of a reactive system is commonly much more complicated than inelastic scattering.

As outlined in the Introduction, the complex absorbing potentials can be used for the study of a reactive system without having to propagate the solution into the products arrangement. The consequence is that we will not only save the product arrangement channels (Fig. 1) but, even in the case of simpler coordinate systems, the transformation between coordinates as well. As already noted, the basic idea is to insert a NIP, $V_i(R,r)$, at the products channel entrance. According to Ref. 38 we have chosen a linear function of the vibrational coordinate (r) as a convenient form of the NIP such that

$$V_{NIP}(R,r) = \begin{cases} -iV_{i0}[(r-r_1)/(r_2-r_1)], \\ \quad r_1 < r < r_2, \quad R_1 < R < R_2, \\ 0, \quad \text{outside.} \end{cases} \quad (1)$$

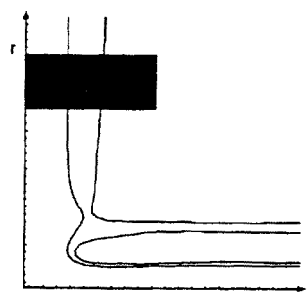Therefore, a phenomenological (rather than formal) ap-

FIG. 1. Schematic representation of a reactive fixed angle PES where a NIP has been placed on the entrance to the products arrangement

proach has been assumed to incorporate the optical potential into the scattering equations. The complex potential is directly added to the Hamiltonian,

$$\hat{H}' = \hat{H} + V_{NIP}. \quad (2)$$

Since this potential is a function of the physical coordinates it can be placed so that only the reactive flux is absorbed. The reactive system can then be considered from the computational perspective as an inelastic calculation and therefore be solved by an inelastic scattering algorithm, but taking into account that the interaction matrix will now contain complex factors. The calculation then yields all the state-to-state inelastic probabilities that result when the reactive process is present, and one can easily obtain global reactive probabilities, for a given reactants state, by subtracting from unity the sum of all state-to-state inelastic probabilities corresponding to a given initial state.

B. Treatment of the inelasticlike system. Generalization of the R-matrix propagation method

The set of coupled equations that describes the scattering processes can be written in matrix notation, independently of which specific Hamiltonian is used, as

$$\frac{d^2}{dR^2} \psi = W(R)\psi, \quad (3)$$

where ψ are the translational scattering functions and W is the so-called interaction or coupling matrix. These equations are obtained, for instance, through the expansion of the total wave function in an orthonormal target basis set $\{\phi\}$,[1] or in an adiabatic basis set,

$$\Psi(R,x) = \sum_{n=1}^{N} \phi_n(x)\psi_n(R), \quad (4)$$

where R is the translational scattering coordinate, orthogonal to all internal coordinates, x. This equation can be efficiently solved by propagation jointly with an adiabatic basis set. In particular, we will use in the present case the R-matrix propagation method, which propagates the inverse logarith-
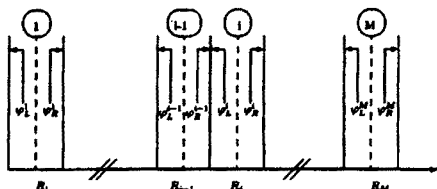
Huarte-Larrañaga, Giménez, and Aguilar

FIG. 2. Schematic representation of the propagation sectorization. L stands for the left side of the sector limit and R stands for the right side of the sector limit.

mic derivative of the solution rather than the function itself. For inelastic problems, the global R matrix is defined so as to always relate functions and derivatives,

$$\psi = \mathscr{R}\psi'. \tag{5}$$

1. The R-matrix propagation

In this section, the R-matrix propagation technique will be briefly summarized. For a detailed presentation, see Refs. 46, 47. Essentially, solving the close-coupling radial equations by propagation methods consists in dividing the entire range of the radial (scattering) coordinate into small sectors. Inside each sector, the solution of a reference problem is built by means of a local sector propagator and imposing the invariant embedding boundary conditions, yielding a local R matrix. Then a global R matrix is constructed by assembling the local R matrices. In Fig. 2 a schematic representation of the sector partitioning is presented. The translational coordinate is divided into M sectors, the first of which (1) is nearest to the origin and the last sector (M) is in the asymptotic range. Each sector is characterized by its translational coordinate value at the center, $R=R_k$, and its width, $h=h_i$.

The explicit derivation of the propagation algorithm starts expanding the total wave function at each sector in terms of the actual truncated set of internal motion adiabatic eigenfunctions,

$$\Psi(R,x) = \sum_{n=1}^{N_k} \phi_n^k(x)\psi_n^k(R). \tag{6}$$

Then a local translational Schrödinger equation is obtained for each sector as

$$\frac{d^2}{dR^2}\psi^{(k)} = \mathbf{W}(R)\psi^{(k)}. \tag{7}$$

A transformation to a new basis of local translational functions, in which all the couplings are eliminated, is carried away through the diagonalization of the interaction matrix:

$$(\mathbf{T}^{(k)})^{-1}\mathbf{W}(R_k)\mathbf{T}^{(k)} = \lambda^2(k), \tag{8}$$

$$\varphi^{(k)} = \psi^{(k)}\mathbf{T}^{(k)}. \tag{9}$$

At this point, in the usual description of the R-matrix propagation for inelastic scattering, the eigenvalues of this interaction matrix were identified with the negative of the local kinetic energy available for translation.[46] Now, this is no longer so since we have artificially introduced a complex

potential in the interaction matrix and its eigenvalues will be, in principle, complex. This statement can, however, still be made for those regions where no NIP is set, such as the reactants' asymptotic region. Note also that $(\mathbf{T}^{(k)})\dagger$ has been substituted by $(\mathbf{T}^{(k)})^{-1}$, since $\mathbf{W}(R_k)$ is no longer real symmetric.

Thus, the sector translational Schrödinger matrix equation in this locally uncoupled representation takes the form

$$\frac{d}{dR}\begin{bmatrix}\varphi\\\varphi'\end{bmatrix} = \begin{bmatrix}0 & \mathbf{I}\\\lambda^2 & 0\end{bmatrix}\begin{bmatrix}\varphi\\\varphi'\end{bmatrix}; \tag{10}$$

this equation can be solved for each sector together within invariant embedding boundary conditions,[48]

$$\frac{d^2}{dR^2}\varphi = \lambda^2\varphi \Rightarrow 2 \text{ solutions} \begin{cases}\varphi^+,\\\varphi^-,\end{cases} \tag{11}$$

$$\varphi_R^+ = \varphi^+(R'')=1, \quad \varphi_L^+ = \varphi^+(R')=0,$$

$$\varphi_R^- = \varphi^-(R'')=0, \quad \varphi_L^- = \varphi^-(R')=1;$$

here, $\varphi_R^\pm$ and $\varphi^\pm(R'')$ both label the value of the function at the right coordinate boundary $(R=R'')$. Equivalently, $\varphi_L^\pm$ and $\varphi^\pm(R')$ stand for its value at the left boundary $(R=R')$. Solutions then are

$$\varphi^+(R) = \frac{e^{-\lambda R}-e^{\lambda R}e^{-2\lambda R''}}{e^{-\lambda R'}-e^{\lambda R'}e^{-2\lambda R''}},$$

$$\varphi^-(R) = \frac{e^{-\lambda R}-e^{\lambda R}e^{-2\lambda R'}}{e^{-\lambda R''}-e^{\lambda R''}e^{-2\lambda R'}},$$

where the φ^+ and φ^- functions are the generalization of the local sector solutions to complex eigenvalues. Since the inverse of the logaritmic derivative is the magnitude that is actually propagated and this relates the function and its derivative, the expressions for the propagator are

$$\varphi_L = a\varphi_L' + b\varphi_R',$$

$$\varphi_R = c\varphi_L' + d\varphi_R', \tag{12}$$

which is usually expressed in a convenient matrix notation as

$$\begin{bmatrix}\varphi_L^{(k)}\\\varphi_R^{(k)}\end{bmatrix} = \begin{bmatrix}\mathbf{r}_1^{(k)} & \mathbf{r}_2^{(k)}\\\mathbf{r}_3^{(k)} & \mathbf{r}_4^{(k)}\end{bmatrix}\begin{bmatrix}-\varphi_L'^{(k)}\\\varphi_R'^{(k)}\end{bmatrix}, \tag{13}$$

the r-matrix being called the (k)th sector R matrix; its block elements are

$$(\mathbf{r}_1^{(k)})_{ij} = (\mathbf{r}_4^{(k)})_{ij} = \delta_{ij}\frac{1}{|\lambda|_j}\frac{e^{\lambda_j\Delta h}+e^{-\lambda_j\Delta h}}{e^{\lambda_j\Delta h}-e^{-\lambda_j\Delta h}},$$

$$(\mathbf{r}_2^{(k)})_{ij} = (\mathbf{r}_3^{(k)})_{ij} = \delta_{ij}\frac{1}{|\lambda|_j}\frac{2}{e^{\lambda_j\Delta h}-e^{-\lambda_j\Delta h}}, \tag{14}$$

where λ_j is the corresponding jth sector solution eigenvalue and Δh is the sector width.

Once the function has been propagated from the inner to the outer boundary of the sector, constraints have to be applied to ensure the function's continuity between sectors. Thus, the $\varphi^{(k-1)}$ locally uncoupled sector basis set is transformed to the ψ representation and back to the $\varphi^{(k)}$ representation corresponding to the next sector,

$$\varphi_R^{(k-1)} = Q(k-1,k)\varphi_L^{(k)},$$

$$\varphi_R'^{(k-1)} = Q(k-1,k)\varphi_L'^{(k)}, \qquad (15)$$

where

$$Q(k-1,k) = (T^{(k-1)})^{-1}\Theta(k-1,k)T^{(k)}$$

$$= (T^{(k-1)})^{-1}\phi'^{(k-1)}\phi^{(k)}T^{(k)}. \qquad (16)$$

Note that the basis change is now performed using the inverse of the transformation matrix instead of the transposed used in the original formulation.[46]

The R-matrix propagation scheme consists in assembling recursively the sector R matrices, starting from the sector nearest to the origin and continuing toward the asymptotic configuration. The algorithm that assembles a new sector R matrix $r^{(k)}$ to an old global R-matrix $R^{(k-1)}$ and builds up a new global $R^{(k)}$ is the following:[46,47,48]

$$R^{(k)} = r_1^{(k)} - r_3^{(k)} Z^{(k)} r_2^{(k)},$$

$$Z^{(k)} = [r_1^{(k)} - Q^{-1}(k-1,k)R^{(k-1)}Q(k-1,k)]^{-1}, \qquad (17)$$

where again Q^{-1} appears instead of $Q\dagger$. These arise from the basic properties of the Cauchy standard propagators[48] and they can be derived by relating these standard propagators to the invariant embedding ones.

As in every recursion, one needs a point at which to start. We therefore define an initial R matrix $R^{(1)}$ by

$$(R^{(1)})_{ij} = \delta_{ij}\frac{1}{\lambda_j}, \qquad (18)$$

which is the appropiate expression for regular boundary conditions given a large repulsive constant potential.[46]

Thus, the final global R matrix is obtained, beginning with the initial matrix (18) and assembling recursively the sector R matrices, under the continuity requirement, until the range of the global R matrix reaches the asymptotic region of the potential where the asymptotic boundary conditions are to be applied:

$$\varphi_R^{(M)} = R^M \varphi_R'^{(M)}, \qquad (19)$$

Once the propagation scheme reaches the asymptotic final sector, it is useful to transform the translational solution from the uncoupled representation, $\varphi^{(M)}$, to the representation to be used for applying scattering boundary conditions, which could be a return to the primitive basis. Under this transformation we have, for the R matrix,

$$\psi_R^{(M)} = \mathscr{R}^{\text{final}}\psi_R'^{(M)}, \qquad (20)$$

where $\mathscr{R}^{\text{final}} = T^{(M)}R^{(M)}(T^{(M)})^{-1}$ and $(T^{(M)})^{-1}$ is used in place of $(T^{(M)})^\dagger$.

2. Asymptotic matching

The scattering information is extracted, as usually, by means of the scattering S matrix, which relates our translational asymptotic functions with the incoming and outgoing asymptotic solutions, so that

$$\psi = I - OS^0,$$

$$\psi' = I' - O'S^0. \qquad (21)$$

An expression for the S matrix is obtained in terms of the quantities actually computed, by combining (20) and (21), which leads to

$$S^0 = (O - \mathscr{R}^{\text{final}}O')^{-1}(I - \mathscr{R}^{\text{final}}I'), \qquad (22)$$

which needs only a further scaling to satisfy the flux conservation condition,

$$k^{1/2}Sk^{-1/2} = (O - \mathscr{R}^{\text{final}}O')^{-1}(I - \mathscr{R}^{\text{final}}I'), \qquad (23)$$

to get the desired result. Here $k^{1/2} = 2\mu(E - \epsilon_{v_j})^{1/2}$ is the wave vector matrix. According to Refs. 47 and 49, O and I are

$$O_{nm} = \delta_{nm} i k_n^{-1} h_l^{(1)}(k_n R^\infty),$$

$$O_{nm}' = \delta_{nm} i \frac{d}{d(k_n R^\infty)} h_l^{(1)}(k_n R^\infty),$$

$$\qquad (24)$$

$$I_{nm} = \delta_{nm} i k_n^{-1} h_l^{(2)}(k_n R^\infty),$$

$$I_{nm}' = \delta_{nm} i \frac{d}{d(k_n R^\infty)} h_l^{(2)}(k_n R^\infty),$$

where n,m label v, j and v', j', respectively, and $h^{(1)}$, $h^{(2)}$ are the first and second kind Hankel spherical functions and, in the present context, l labels the orbital angular momentum quantum numbers.

This treatment yields, finally, all state-to-state single angular momentum inelastic probabilities that will be treated later on.

C. Implementation of the absorbing potential in an IOS method

Once the R-matrix method has been generalized to deal with complex potentials, constructing the relevant scattering quantities needs the specification of the means for obtaining an explicit interaction matrix W. In the present work, a simple infinite-order sudden (IOS) Hamiltonian[49,50] has been used for that purpose, with the aim of using a simple method to test the present implementation but at the same time testing it extensively. For the latter purpose, we have on hand, several results using the traditional R-IOS method,[51–56] including systems with involved PES', so that a direct comparison is actually possible. The Schrödinger equation, under the IOS approximation for an inelastic scattering problem, in Jacobi coordinates, is:[50]

$$\left(\frac{\partial^2}{\partial r^2} + \frac{\partial^2}{\partial R^2} - \frac{\bar{l}(\bar{l}+1)}{R^2} - \frac{\bar{j}(\bar{j}+1)}{r^2}\right)\psi_{J\bar{j}\bar{l}}(r,R,\gamma)$$

$$= \frac{2\mu}{\hbar^2}[V(r,R,\gamma) - E]\psi_{J\bar{j}\bar{l}}(r,R,\gamma), \qquad (25)$$

where J, $\bar{j}$ and $\bar{l}$ label the total, rotational and orbital angular momentum quantum numbers, respectively. Global reaction probabilities will be obtained letting $V = \bar{V} - V_{\text{NIP}}$, where $\bar{V}$ stands for the actual potential for the reactive process.

After the corresponding sectorization of the propagation region and expansion of the total IOS wave function in a

Huarte-Larrañaga, Giménez, and Aguilar

TABLE I. CPU execution times (in milliseconds) for both Cooley and DVR methods on a single minimum potential profile. By resolution it is meant the number of points used to describe the potential cut. Calculations were run on an R-6000 3AT IBM Workstation. *"Not converged"* stands for calculations that exceeded a given maximum number of iterations without accomplishing the convergency criterion.

| Resolution	Cooley/ms	DVR/ms
287	60	710
148	40	120
79	Not converged	20
56	Not converged	10

FIG. 3. Variation of colinear and $\gamma=150°$, $l=0$ reactive probabilities for Cl+HCl ($v=0$) with the potential ramp height.

locally vibrationally adiabatic basis for each sector (as explained in Sec. II B 2), the interaction matrix for a given sector, k, has the form

$$(W)_{ij} = \delta_{ij}\left(\frac{2\mu}{\hbar^2}(\epsilon_i - E) + \frac{\bar{l}(\bar{l}+1)}{R^2}\right) + \left\langle\phi_i\left|\frac{\bar{j}(\bar{j}+1)}{r^2}\right|\phi_j\right\rangle$$

$$- \frac{2\mu}{\hbar^2}\langle\phi_i|V_{NIP}|\phi_j\rangle, \tag{26}$$

and once the coupling matrix is calculated, one can proceed with the propagation as described in Sec. II B.

III. APPLICATION

A computer code has been developed in order to solve the close-coupling equations of reactive scattering that combines the use of a NIP with the R-matrix propagation algorithm. The current version uses Jacobi coordinates and divides the integration range in Cartesian sectors of constant width. Using Jacobi coordinates leads to a shape of the potential cuts, in the strong interaction region, which is rather different from the shape resulting when, for example, circular collision coordinates are used. In particular, one has to deal with double minimum potential profiles, instead of simpler single minimum profiles. Because of that, a DVR using a primitive Fourier basis[57] was found to be a convenient method for reliably solving the internal problem, rather than standard shooting algorithms, like the Numerov method as implemented by Cooley.[58] Although the present method involves explicitly a matrix inversion, which could considerably slow down the performance of the code, the significantly faster convergence of this DVR technique enables us to describe the potential profiles with few enough points (up to 38 points compared with 130 for Cooley, in the specific example reported in Table I), so as to overcome the Cooley performance, even in the simpler case of single minimum profiles (those encountered in the asymptotic region).

A previous step in every scattering calculation when dealing with NIP-based methods, is the definition of the proper NIP. This complex potential has to be placed conveniently so that it only absorbs the reactive flux. To do so, one needs to have a rather good knowledge of the potential energy surface topography. Then one can set the NIP beyond the transition state but not too deep into the products arrangement, so that one can save as much as possible propagation time. Within the IOS context, a first scan through the
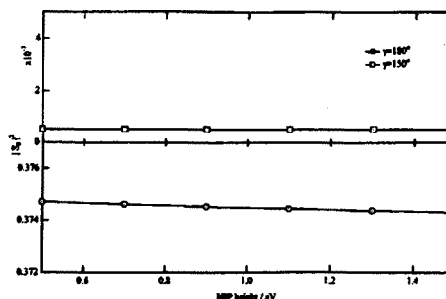
different fixed angle PES contours has to be performed. Then the optimal NIP parameters are set so as to lead to a maximum in the reactivity without infringing the transition state region. Once the optimal NIP parameters are found, calculations of reaction probabilities can be performed.

The program has been tested on a variety of reactive scattering problems.[45,59] We have concentrated in this paper on the Cl+HCl system[60] with the purpose of completing the good results already given in Ref. 59 and giving a detailed illustration of the theory here presented. In that article we compared colinear (i.e., $l=0$ and $j=0$ with $\gamma=180°$) reactive probabilities obtained by the present method, hereafter named NIP-IOS, to the same probabilities obtained by Bondi et al.[60] Results came out to be outstandingly satisfactory, since even the very sharp resonances which characterize the Cl+HCl were well predicted by the NIP-IOS. Therefore, as a numerical example of the method we have chosen to present further calculations on the Cl+HCl and leave an extensive application to other systems for a coming article.[59]

We then focus on the symmetric exchange Cl+HCl (v) reaction on the LEPS potential energy surface given by Bondi et al.[60] The reaction has been studied, under the NIP-IOS approximation, for a total energy range going from 0.2 to 1.0 eV, and considering a reactants atom–diatom orientation angle (γ) range between $125°-180°$. In this energy range, for both reactants and products, mainly two open vibrational channels can be found and a third at the end of the energy range, which, for practical reasons, we will not consider hereinafter.

First of all, we will present a series of results stressing on the stability and performance of the method. To what the stability of the results against variations in the NIP parameters concerns, in Fig. 3 the collinear and the $\gamma=150°$ $l=0$ reactive probabilities, for Cl+HCl ($v=0$, $j=0$) at a total energy of 0.6 eV, are shown as a function of the NIP height (W_0). It can be seen how, for a wide range of W_0, both do not vary noticeably. Essentially similar results have been obtained for the ramp width, being the stability region given by the 0.5–1.5 Å range. Therefore, we can state that the calculation is essentially stable under a wide variation of the NIP parameters.

Concerning the reliability of the present application, we

TABLE II. $j=0,l$ inelastic probabilities for the Cl+HCl ($\gamma=180°$) system at a total energy of 1 eV. i (j) stands for intial (final) reactants arrangement vibrational states.

l	$|(S)_{ij}|^2$			$\Sigma_j|(S)_{ij}|^2$	$1-\Sigma_j|(S)_{ij}|^2$
	0.16749E+00	0.37234E−03	0.22695E−05	0.16786E+00	0.83214E+00
0	0.37234E−03	0.27740E+00	0.15648E−01	0.29342E+00	0.70658E+00
	0.22695E−05	0.15648E−01	0.61432E+00	0.62997E+00	0.37003E+00
	0.54466E+00	0.17607E−01	0.11157E−03	0.56238E+00	0.43762E+00
80	0.17607E−01	0.13501E−01	0.16541E−02	0.32762E-01	0.96724E+00
	0.11157E−03	0.16541E−02	0.33018E+00	0.33195E+00	0.66805E+00
	0.27156E+00	0.38269E−02	0.25034E−15	0.27539E+00	0.72461E+00
160	0.38269E−02	0.88630E+00	0.22257E−12	0.89013E+00	0.10987E+00
	0.25034E−15	0.22257E−12	0.10000E+01	0.10000E+01	0.74385E-14

present in Table II the inelastic block of the S matrix (which is the whole S-matrix since we are actually running an inelastic calculation) for selected values of the orbital angular momentum, where it can be easily seen how symmetry of the S matrix is highly preserved, even at the highest energy considered in the present work. The fourth column of the table corresponds to the global inelastic probabilities (that is, the sum for a given starting vibrational level of the elastic and all inelastic transition probabilities) and the fifth column contains simply the substraction of the latter probability from unity, thus illustrating how the global reaction probabilities are extracted. In order to check the unitarity, it must be said that, previous to the current calculation, a first run was performed where no NIP was placed but only an infinite potential wall in the products arrangement. All the state-to-all inelastic probabilities summed unity. Then reactive probabilities, obtained with the optimal set of NIP parameters, were compared with those given by BCMR[60] and found to be extremely coincident, as shown in Ref. 45. Therefore, it can be stated that the combination of the generalized R-matrix-invariant embedding with absorbing potentials adequately accounts for the flux loss due to absorption and "global" unitarity is preserved.

The present application shows a faster convergence than the *traditional* two-arrangement method. The key parameters for the calculations have been minimized up to their limit convergence values (for $\gamma=180°$) and then compared to previously available R-IOS results obtained with a traditional technique.[52] While a fully converged R-IOS calculation for the Cl+HCl system, at the atom–diatom orientation angle $\gamma=180°$, for a total energy of 0.6 eV, used 400 (200 for each arrangement channel) translational sectors (NTS in Table III) and 27 basis functions (NV in Table III) for the propagation and lasted 1174 s to yield the final cross section, in Table III it is shown how for the same calculation, the present program leads to accurate results with a significantly lower number of vibrational basis functions for the propagation and also less translational sectors. Lower sector resolution is needed (see Table I) in the NIP-IOS because of the better convergence of the DVR method, which solves the internal problem instead of the modified Numerov[58] method used in the IOS program. It should be taken into account that the difference in the number of sectors relies mainly on the

fact that we are studying basically *half* of the surface. Moreover, this number of sectors may still be lowered with the use of sectors of variable width.

Next, some results obtained for the BCMR potential energy surface of the Cl+HCl (v) with the NIP-IOS method are presented and compared to those previously obtained with our previous R-IOS method.[51] In particular, in Fig. 4 (lower panel), both NIP-IOS and R-IOS $\gamma=180°$ state-to-all reactive cross sections are drawn as a function of the total energy. Both methods show a noticeable oscillation in the cross section curve, reminiscent of the strongly oscillatory behavior of the reaction probability characteristic of light-atom symmetric exchange reactions. For this case, both methods yield almost exactly the same result. However, when we consider the upper pannel in Fig. 4, where the same functions are represented at $\gamma=160°$, we can see that this agreement is not so good, although the qualitative behavior is still the same. Differences are attributable to the different PES probed by the NIP-IOS and the R-IOS method. While NIP-IOS method considers the $\gamma=160°$ cut of the PES, the traditional R-IOS technique is based on a matching between the reactant's and product's constant-γ potential energy cuts. When moving from the reactants toward the products surface, across the B-matching line,[61] a reactants-to-products

TABLE III. Convergence table for Cl+HCl ($\gamma=180°, E=0.6$ eV). Relative errors are given, considering the result for NTS=300 and NV=30 as the exact value. Bold-faced figures correspond to results obtained by means of the traditional R-IOS technique.

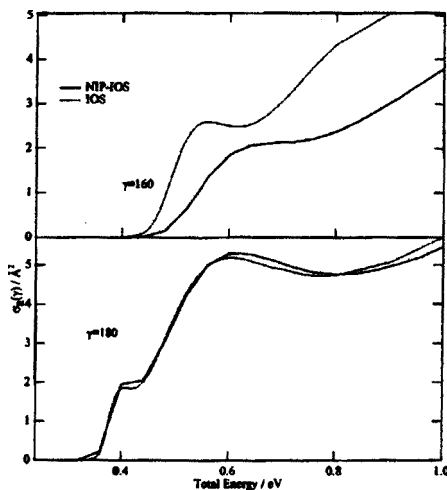| NTS	NV	ERR %	time / s
300	30	···	3508
300	15	0.00	756
300	10	0.00	389
300	7	0.03	258
200	15	0.13	503
200	10	0.13	261
200	7	31.00	152
150	15	0.30	378
150	10	0.30	194
150	7	32.01	113
400	**27**	···	**1174**

Huarte-Larrañaga, Giménez, and Aguilar

FIG. 4. Fixed Jacobi angle excitation functions for Cl+HCl ($v=0$). A comparison between R-IOS and NIP-IOS.

coordinate change is performed, thus modifying the numerical value of the interaction matrix elements. This would have no effect if boundary conditions were applied in both reactants and products channel. But the use of the reactants asymptote only in the NIP-IOS method makes that those terms entering in the interaction matrix, such as the centrifugal term, contribute differently than when the coordinate change is performed.

To conclude this section, in Fig. 5 we show the tridimensional global reactive cross sections again as a function of the total energy. This magnitude is obtained by integration,
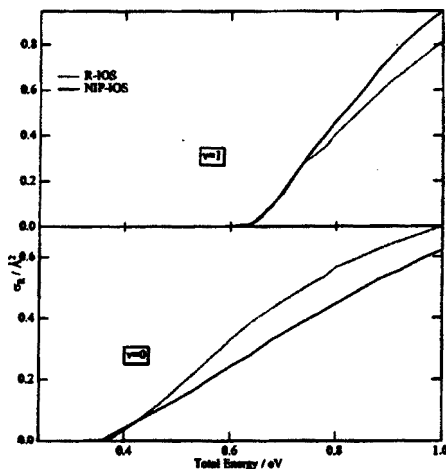
over all contributing angles, of the fixed angle reaction cross sections.[51] Again, a good agreement between both methods is met. This should not be surprising since the most contributive angles are those close to colinearity.

IV. CONCLUSIONS

A method has been developed that introduces the absorbing potential technique into a IOS reactive scattering problem reducing it into an IOS inelastic scattering problem. This has led to a generalization of the R-matrix propagation method in order to take into account the fact that the coupling matrix might be complex.

The method has shown up to be a powerful approach for computer consuming reactive calculations. In particular, the implementation of the imaginary potential linear ramp showed a better performance than a traditional R-matrix propagation R-IOS, mainly due to a faster convergence in the number of basis functions and also in the number of translational sectors. The S-matrix symmetry and unitarity tests presented here as well as the stability of the results with the variation of the linear ramp parameters (mainly its height) state the method's good reliability.

As an example, the method has been applied to the Cl+HCl system and then its results have been compared to those obtained by a traditional R-matrix propagation IOS treatment. The results agree for both the fixed-angle cross section and the all-angle integrated cross section, although for those angles far from colinearity there is a noticeable discrepancy in the curves, probably due to the different potential energy profiles scanned by the two approaches.

Finally, to conclude this section we would like to stress some singularities of the present application, which make it different from other already successfully applied methods, similar in   rit, that were mentioned in the Introduction. In comparison with Seideman, Manthe and Miller's approach,[28] one could say that the present application goes *halfway* in the application of NIPs, since we have placed the absorbing potential only in the products region while the cited authors placed a complex potential in both products and reactants arrangements. This can be understood since Seideman, Manthe, and Miller approach focused solely on the thermal rate constant $k(T)$, or, to be more precise, the cumulative reaction probability. On the other hand, our approach enables us to obtain initial state-to-all properties of the system. Light and Altenberger's approach[32] is also very close in spirit, although no absorbing potentials are used, to the implementation presented here, since it also seeks to solve the Schrödinger equation in a smaller physical region. This is performed by the application of approximate boundary conditions at a transition state hypersurface. Naturally, this results in an approximate set of S-matrix elements. In this sense, it could be stated that the present approach eliminates t e approx mate oun ary match ng, s nce asymptotic boundary conditions are only applied in the reactants asymptotic region and no matching is performed at the TS hypersurface but an absorption of the reactive flux beyond it.

FIG. 5. Tridimensional excitation function for Cl+HCl ($v=0,1$). A comparison between R-IOS and NIP-IOS.

ACKNOWLEDGMENTS

[1] J. R. Taylor, *Scattering Theory* (Wiley, New York, 1972).

[2] H. Feshbach, Ann. Phys. (N.Y.) **5**, 357 (1958); **19**, 287 (1962).

[3] N. F. Mott and M. S. W. Massey, *The Theory of Atomic Collisions* (Oxford University Press, London, 1965).

[4] T. F. George and J. Ross, Annu. Rev. Phys. Chem. **24**, 263 (1974); D. A. Micha, "Optical models in molecular collision theory," in *Dynamics of Molecular Collisions. Part A*, edited by W. H. Miller (Plenum, New York, 1976), pp. 81–129.

[5] D. A. Micha, J. Chem. Phys. **50**, 722 (1969).

[6] R. D. Levine, J. Chem. Phys. **49**, 51 (1968); **50**, 1 (1969).

[7] G. Wolken, Jr., J. Chem. Phys. **56**, 2592 (1972).

[8] D. W. Schwenke, D. Thirumalai, and D. G. Truhlar, Phys. Rev. A **28**, 3258 (1983).

[9] R. Marriot and D. A. Micha, Phys. Rev. **180**, 120 (1969).

[10] D. A. Micha and M. Rotenberg, Chem. Phys. Lett. **6**, 79 (1970); **11**, 626 (1971).

[11] J. L. J. Rosenfeld and J. Ross, J. Chem. Phys. **44**, 188 (1966); H. Y. Sun and J. Ross *ibid.* **46**, 3306 (1967); C. Nyeland and J. Ross, *ibid.* **49**, 843 (1968); R. E. Roberts and J. Ross, *ibid.* **52**, 1464 (1970).

[12] R. Kosloff and D. Kosloff, J. Comput. Phys. **63**, 363 (1986).

[13] G. Jolicard and E. J. Austin, Chem. Phys. Lett. **121**, 106 (1985).

[14] A. Goldberg and B. W. Shore, J. Phys. B **11**, 3339 (1978); C. Leforestier and R. B. Wyatt, J. Chem. Phys. **78**, 2334 (1983).

[15] D. Neuhauser and M. Baer, J. Chem. Phys. **90**, 4351 (1989); J. Phys. Chem. **93**, 2862 (1989).

[16] D. Neuhauser and M. Baer, J. Chem. Phys. **91**, 4651 (1989).

[17] D. Neuhauser and M. Baer, J. Chem. Phys. **92**, 3419 (1990); M. Baer, D. Neuhauser, and Y. Oreg, J. Chem. Soc. Faraday Trans. **86**, 1721 (1990).

[18] H. Nakamura and M. Baer J. Chem. Phys. **96**, 6565 (1992).

[19] I. Last and M. Baer, "Variational treatments of reactive scattering: application of negative imaginary absorbing potentials and contracted L^2 basis sets to calculate S-matrix elements", in *Advances in Molecular Vibrations and Collision Dynamics*, edited by J. M. Bowman (JAI Press, Greenwich, CT, 1994), Vol. IIA, p. 85.

[20] W. H. Miller, "S-matrix version of the Kohn variational principle for quantum scattering theory of chemical reactions," in Ref. 19.

[21] D. Neuhauser, M. Baer, R. S. Judson, D. J. Kouri, D. E. Adelman, N. E. Shafer, D. A. Kliner, and R. N. Zhare, Science **257**, 519 (1992).

[22] M. Baer, I. Last, and H.-J. Loesch, J. Chem. Phys. **101**, 9648 (1994); M. Gilibert, R. M. Blasco, M. González, X. Giménez, A. Aguilar, I. Last, and M. Baer, J. Phys. Chem. **101**, 6821 (1997).

[23] H. Szichman and M. Baer, J. Chem. Phys. **101**, 2081 (1994); H. Szichman, A. J. C. Varandas, and M. Baer, *ibid.* **102**, 3474 (1995); H. Szichman and M. Baer, *ibid.* **105**, 10 380 (1996).

[24] H. Szichman, H. Nakamura, and M. Baer, J. Chem. Phys. **107**, 3521 (1997).

[25] D. Neuhauser, J. Chem. Phys. **100**, 9272 (1994); D. H. Zhang and J. Z. H. Zhang, *ibid.* **101**, 1146 (1994).

[26] W. Zhy, J. Z. H. Zhang, Y. C. Zhang, Y. B. Zhang, L. X. Zhang, S. L. Zhang, and D. H. Zhang, J. Chem. Phys. **108**, 3509 (1998).

[27] M. Gilibert and M. Baer, J. Phys. Chem. **99**, 15 748 (1995).

[28] T. Seideman and W. H. Miller, J. Chem. Phys. **96**, 4412 (1992); **97**, 2499 (1992); W. H. Miller, Acc. Chem. Res. **26**, 174 (1993); U Manthe and W. H. Miller, J. Chem. Phys. **99**, 3411 (1993).

[29] T. Seideman and W. H. Miller, J. Chem. Phys. **99**, 10 078 (1993).

[30] H. Wang, W. H. Thompson, and W. H. Miller, J. Chem. Phys. **107**, 7194 (1997).

[31] W. H. Thompson and W. H. Miller, J. Chem. Phys. **106**, 142 (1997).

[32] J. C. Light and A. Altenberger-Siczek, Chem. Phys. Lett. **30**, 195 (1975); J. Chem. Phys. **64**, 1907 (1976).

[33] A. Viel, C. Leforestier, and W. H. Miller, J. Chem. Phys. **108**, 3489 (1998).

[34] J. D. Gezelter and W. H. Miller, J. Chem. Phys. **103**, 7868 (1995).

[35] H. W. Jang and J. C. Light, J. Chem. Phys. **102**, 3262 (1995); G. S. Whittier and J. C. Light, *ibid.* **107**, 1816 (1997).

[36] D. K. Hoffman, Y. Huang, W. Zhu, and D. J. Kouri, J. Chem. Phys. **101**, 1242 (1994).

[37] V. A. Mandelshtam and H. S. Taylor, J. Chem. Phys. **102**, 7390 (1995).

[38] D. Neuhauser, M. Baer, and D. J. Kouri, J. Chem. Phys. **93**, 2499 (1990).

[39] M. Baer, C. Y. Ng, and D. Neuhauser, Chem. Phys. Lett. **169**, 534 (1990).

[40] B. R. Johnson, J. Comput. Phys. **13**, 445 (1973).

[41] D. E. Manolopoulos, J. Chem. Phys. **85**, 6425 (1986).

[42] D. E. Manolopoulos and S. K. Gray, J. Chem. Phys. **101**, 4062 (1994).

[43] S. K. Gray and J. M. Verosky, J. Chem. Phys. **100**, 5011 (1994).

[44] M. S. Child, Mol. Phys. **72**, 89 (1991); A. Vibók and G. G. Balint-Kurti, J. Chem. Phys. **96**, 7615 (1992); Á. Vibók and G. G. Balint-Kurti, J. Phys. Chem. **96**, 8712 (1992); D. Macías, S. Brouard, and J. G. Muga, Chem. Phys. Lett. **228**, 672 (1994); U. V. Riss and H.-D. Meyer, J. Chem. Phys. **105**, 1409 (1996); U. V. Riss and H.-D. Meyer, J. Phys. B **26**, 4503 (1993); J.-Y. Ge and J. Z. H. Zhang, J. Chem. Phys. **108**, 1429 (1998).

[45] F. Huarte-Larrañaga, X. Giménez, A. Aguilar, and M. Baer, Chem. Phys. Lett. (submitted).

[46] E. B. Stechel, R. B. Walker, and J. C. Light, J. Chem. Phys. **69**, 3518 (1978).

[47] J. C. Light and R. B. Walker, J. Chem. Phys. **65**, 4272 (1976).

[48] F. Mrugala and D. Secrest, J. Chem. Phys. **78**, 5954 (1983).

[49] D. C. Clary, Mol. Phys. **44**, 1067 (1981).

[50] V. Khare, D. J. Kouri, and M. Baer, J. Chem. Phys. **71**, 1188 (1979); J. M. Bowman and K. T. Lee, *ibid.* **72**, 5071 (1980).

[51] A. Laganá, A. Aguilar, X. Giménez, and J. M. Lucas, in Ref. 19; J. Chem. Phys. **95**, 2218 (1991).

[52] X. Giménez, J. M. Lucas, A. Aguilar, and A. Laganà, J. Phys. Chem. **97**, 8578 (1993).

[53] M. Gilibert, X. Giménez, M. González, R. Sayós, and A. Aguilar, Chem. Phys. **191**, 1 (1995).

[54] A. Laganà, G. Ochoa de Aspuru, A. Aguilar, X. Giménez, and J. M. Lucas, J. Phys. Chem. **99**, 11 696 (1995).

[55] A. Aguilar, M. Gilibert, X. Giménez, M. González, and R. Sayós, J. Chem. Phys. **103**, 4496 (1995).

[56] F. Huarte-Larrañaga, X. Giménez, M. Albertí, A. Aguilar, A. Laganà, and J. M. Alvariño, Chem. Phys. Lett. **282**, 91 (1998).

[57] D. T. Colert and W. H. Miller, J. Chem. Phys. **96**, 1982 (1992).

[58] J. W. Cooley, Math. Comput. **15**, 363 (1962).

[59] F. Huarte-Larrañaga, X. Giménez, J. M. Lucas, and A. Aguilar (in preparation).

[60] D. K. Bondi, J. N. L. Connor, J. Manz, and J. Römelt, Mol. Phys. **50**, 467 (1983).

[61] H. Nakamura, A. Ohsaki, and M. Baer, J. Phys. Chem. **90**, 6176 (1986); A. Laganà, X. Giménez, E. Garcia, and O. Gervasi, Chem. Phys. Lett. **176**, 280 (1991); A. Laganà, X. Giménez, and J. M. Lucas, *ibid.* **189**, 138 (1992).

8.4 The application of complex absorbing potentials to an invariant embedding scattering method: II. Applications.

Following to the previous publication, another work has been recently accepted for publication, in which the novel implementation is applied to $Li + FH$, $Mg + FH$ and $H + F_2$ systems. Studying such reactions we cover different ergicities (moderately endoergic, largely endoergic and exoergic,respectively), different levels of PES complexity and different mass combinations as well.

Although the first applications of the method seemed to point out a clear improvement in the calculation of state-to-all quantities, with respect to the previous R-IOS technique, we thought it would be challenging to have available a more comprehensive test so that we could establish more confidently the method's level of performance. Besides testing the use of NIPs for varied conditions, we also intended to benefit from such a cheap method to get some deeper insights into the dynamics of some of the reactions here explored.

Although one would need in principle different NIP parameters for each different orientation angle in the IOS treatment, in practice this is not usually the case and we have been able to employ a single set of NIP parameters for all orientations except for highly anisotropic PES ($H + F_2$) where we used two sets of parameters. This, in addition to the fact that these parameters are quite easily found, shows that the time spent in obtaining an optimal NIP is small.

Comparison between R-IOS and NIP-IOS performances on these systems showed clearly the smaller computational effort for the second. Generally, the number of translational sectors is halved and the dimension of the vibrational basis is significantly reduced. Both turn into CPU time savings, reduction of the number of sectors decreases linearly CPU time while diminishing the basis scales as N^3 since an explicit matrix inversion is included in the propagation code. Through the introduction of the absorbing potential we were able to formulate the reactive scattering problem using a single arrangement coordinate system and this simplificated significantly the numerical parameters convergence, since the reactants-products matching (characteristic for R-IOS approach) can be avoided.

Although in the published work NIP-IOS and R-IOS are in good agreement, one should not expect, in principle, an exact agreement since they are not exactly equivalent approaches. We would like to emphasize that NIP-IOS strictly constrains the motion to that governed by the reactants fixed-angle approximation. No additional constrains are introduced beyond the TS in the products region where the flux is absorbed. This does not stand for R-IOS, where the solution has to be propagated as well on the products region and therefore the motion in this region is constrained and related to the reactants by the *B-matching* rule.

The relatively good efficiency and reliability of the code developed encouraged

us to perform some additional calculations in which we successfully calculated cumulative reaction probabilities (CRP) with significant saving of time. The idea underlying was, in a regular NIP-IOS run, to carry out the asymptotic matching shortly after the strong interaction region where, even if the inelastic interactions are still relevant, the reactive ones can already be neglected. This would lead to obviously wrong state-to-all reactive probabilities, but if the point is to calculate global all-to-all quantities, such as the rate constant, then all that one needs is the CRP.

The application of complex absorbing potentials to an invariant embedding scattering method: II. Applications

Fermín Huarte-Larrañaga, Xavier Giménez, Josep M. Lucas and Antonio Aguilar
Departament de Química Física, Universitat de Barcelona
and Centre de Recerca en Química Teòrica, Universitat de Barcelona.
Martí i Franqués, 1. 08028 Barcelona, Spain

Abstract

The application to several triatomic reactions of a novel implementation of absorbing potentials on a generalized R-matrix propagation method (Chem. Phys. Lett. 291 (1998) 346-350 and J. Chem. Phys. 109 (1998) 5761-5769) is presented. Specific systems chosen have been $Li + FH$, $Mg + FH$, and $H + F_2$, so that an extensive application covering a wide range of PESs has been performed: it includes moderately and largely exoergic and endoergic processes, simple and involved PES, moderate to large skew angles and direct and complex-forming collisions. In all cases it is shown that the use of the absorbing potential is simple and robust, yielding correct values at a fraction of the computer's resources consumption. The best effectiveness is obtained for exothermic, direct reactions, for which up to one order of magnitude in CPU time saving is obtained. This efficiency opened the possibility for a very detailed exploration of the reactive process, in particular on those quantities strongly dependent on the collision energy. In addition, it is shown that, as previously known from a totally different numerical approach, the cumulative reaction probability can be efficiently and accurately calculated propagating the scattering solution along a very short range of the scattering coordinate.

I. Introduction

In previous publications[1, 2, 3], a novel approach for doing reactive scattering calculations has been developed in our group, based on the application of negative imaginary potentials (NIP) on a generalization of the invariant embedding R-matrix propagation method. This use of NIPs, as a tool for reducing the computational effort in scattering calculations, is complementary to previous time-dependent and time-independent quantum molecular scattering formulations[4]to[24]. This subject has been reviewed in the literature several times and, in particular, its use throughout the years has been briefly summarized by us very recently[2]. Since then, the subject has still focused an important activity by many groups. Among the recent advances, it is interesting to notice those which introduce the use of absorbing potentials having both real and imaginary components -the Complex Absorbing Potentials (CAP)-, which allow for an important decrease in the absorption width, if compared with the typical absorption widths of the purely imaginary absorbing potentials[25].

Our new implementation consists essentially in placing, as common to some other methods, a NIP at the entrance of the products channel, so that propagation towards

the products channel is saved without losing accuracy, as far as total reaction probabilities (i.e. summed over product states) are concerned. The main advantages are: a) it avoids an important part of the slow input-output operations towards computer's secondary memory, and b) fewer basis functions are necessary, in general, in the close-coupling expansion of the total wavefunction, since only one -although slightly perturbed-, simple reaction channel has to be considered and no change to product arrangement coordinates has to be performed. The propagation algorithm which results is somewhat more involved, as a consequence of the complex-valued nature of the interaction matrix, although it has been shown that the increase in computational effort is smaller than the savings explained above.

In the previous preliminary applications, it was shown that the method is capable of reproducing very accurately extremely sharp resonances seen in the collinear $Cl + HCl$ symmetric exchange reaction[21]. Moreover, the computation of a fixed-angle IOS cross section for the $Cl + HCl$[23] and the $Ne + H_2^+$[24] systems yielded accurate values while resulting in a CPU time saving by a factor of five and memory requirements reduced by a factor of four.

Although the first applications seem to point out a clear step forward with respect to the previous R-IOS technique[26, 27, 28, 29] (i.e. no NIP is used and therefore state-to-state information is available) when state-to-all probabilities are the only information needed, it is interesting to have available a more comprehensive test, mainly in order to establish the real performance of the method under sufficiently varied conditions. The present work deals with this comprehensive test, whose main purpose is twofold: first, to show that the use of NIPs for sufficiently varied conditions is (almost) straightforward while accurate and, second, to exploit the feasibility of the calculations to cheaply get some deeper insights into the dynamics of the reactions here explored. The applications focus again on the IOS technique, for various reasons. First, several data is available[30]to[37] which can be directly used for the present tests. Second, it has long been our primary interest, to deal with "involved" systems, meaning those having large endo or exothermicities, heavy masses, non-collinear transition states and described by complicated potential energy surfaces (PES), i.e. those with barriers, minima, etc... It is well-known that these systems are very difficult to treat with more accurate scattering methods. It is also worth noticing that, for the purpose of showing the present method's usefulness, the particular Hamiltonian implemented is of less relevance, since the main changes are those involving the propagation step, which is essentially independent of the approximations built into the internal-problem Hamiltonian.

The propagation-based nature of the present method is well suited for another, interesting application, namely the calculation of cumulative reaction probabilities (CRP) using a very short range of the scattering coordinate. In a very clarifying work, Seideman and Miller[9] showed the *hoped for* advantage of the calculation of rate constants via the direct estimation of the CRP: the use of a short-ranged grid for discrete variable representation (DVR) calculations, defined around the transition state region of the potential energy surface, leads to accurate values of the CRP. This was calculated not through the standard procedure, involving the calculation of each state-to- state S-matrix element, but directly by means of an expression related to the outgoing Green's

operator. Addition of NIPs at the grid edges ensured outgoing boundary conditions and eliminated the necessity of including basis functions carrying the proper asymptotic behaviour. Here it will be shown that performing the present pseudo- inelastic propagation with a NIP allows an easy extraction of cumulative reaction probabilities. It results from the application of standard boundary conditions at similar small values of the scattering coordinate, such as those used by Seideman and Miller. This provides an alternative route for the CRP direct calculation, which explicitly shows how one can save computational effort using the same initial approach as for the state-to-state calculation. This procedure leads, as physically expected, to incorrect state-to-state inelastic probabilities but to correct estimations of the total reactive flux. It thus gives a clear indication of the role played by the different portions of the reactants channel region of the PES in inducing transitions between states.

The remainder of the paper is organized as follows. Section II describes the computational details of the several applications shown here. Section III shows the main results for the $Li + FH$, $Mg + FH$, and $H + F_2$ systems, a further general analysis, and some new features singled out thanks to the easy availability of a dense mesh of energy points in cross section calculations. Section IV presents the results of the CRP calculation for some of the above systems and, finally, section V concludes.

II. Calculations

Calculations have been performed with the same NIP-IOS Hamiltonian as used in the first tests[21, 23, 24]. The main numerical parameters which have to be controlled for numerical convergence may be divided into two groups: a) the group including the dimension of the vibrational basis (in the present case, a contraction of the initial basis whose dimension is given by the number of Fourier-basis DVR[38] points), the width of the translational sectors and the final asymptotic distance at which boundary conditions are applied and, b) the parameters of the linear potential ramp (position, height and *translational* -i.e. along the atom-center of mass of the diatom Jacobi distance, hereafter denoted by R- and "vibrational" -the internuclear diatom Jacobi distance, denoted by r- widths). This division is made in order to stress that convergence has to be, and really is, achieved independently between the two groups of parameters. The "a" group parameters are optimized in order to get stable reaction probabilities upon an increase in their values and are among the typical numerical parameters in time- independent reactive scattering methods (however, note that very few of them are necessary in the present method, as a consequence of the simplifications resulting from the fact that the reactants to products transformation is avoided). On the other hand, the search for NIP convergence means finding the parameters range leading to conditions of total absorption and minimal reflection. This interval is identified again as a stability region of the reaction probabilities.

The general procedure followed for obtaining the final set of NIP parameters has been the following: first, plots of fixed-angle cuts of each PES have been used in order to roughly localize the transition-state (TS) region and get a correct knowledge of the PES topography, mainly that corresponding to the entrance of the products channel. Then, according to previous experience, a first trial position for the NIP has been

taken, being as close as possible to the TS but not too close to allow the inelastic flux being absorbed. This latter feature has been controlled looking for the probabilities stabilization distance (along the reactants vibrational coordinate) at constant values of the remaining NIP parameters.

Afterwards, its proper height and translational and vibrational widths are searched in a global iterative process. This procedure leads, in principle, to different NIPs for different orientation angles. In practice, however, only highly enough anisotropic PES for particular mass combinations of the triatom have been found to need the use of different parameter sets for different angles. This was so since a subtle difficulty was found for systems clearly departing from the light-heavy-light (LHL) or heavy-heavy- light (HHL) mass combinations, specifically for the case when acute orientation angles non-negligibly contribute to reactivity, i.e. the $Cl + HCl$ and the $H + F_2$ system. It is due to the PES distortion found when plotting its fixed-angle cuts using Jacobi coordinates. For angles close to $90°$, variation of R describes the approach of the attacking atom towards insertion between the atoms of the diatomic molecule. However, variation of the r coordinate does not describe the departure of the ejected atom as a result of the reaction, since the center of mass, which still determines the coordinate origin, also *travels* somewhat attached to the ejected atom and so does the attacking atom (for fixed R). As a result, the product arrangement is poorly described in these cases since the attacking atom cannot be held close to the exchanged one when varying r. This is, in fact, one of the reasons why one should change from reactant to product coordinate systems when trying to efficiently describe a reactive process. As for the consequences to the present method, since only the TS portion of the products arrangement needs to be described, it just means that special care has to be taken in adequately placing the NIP. Consequently, the procedure becomes less straightforward when dealing with these problematic systems.

Table 8.1 shows the values of each numerical parameter as optimized for each of the three ($Li + FH$, $Mg + FH$ and $H + F_2$) reactive systems included in the present work, while figure 8.1 illustrates the variation of some reaction probabilities as a function of the height of the NIP. It shows that stability is clearly achieved within a sufficiently wide range of the corresponding NIP parameter. Table 8.2 shows the distance at which the NIP has been placed, along the reactants vibrational coordinate, as a function of the orientation angle, for the $H + F_2$ system, since the particular difficulties encountered for this reaction, due to an important variation of the PES topography with the orientation angle, required a much more precise tuning. We note here that only a limited number of production runs have been necessary in order to determine the optimal NIP parameters set. It is due to the fact that a unique set is used for the whole energy range. In addition, since the optimal set little varies with the specific reaction being considered, the first trial values are found to be usually within the stability range, further accelerating the optimization process.
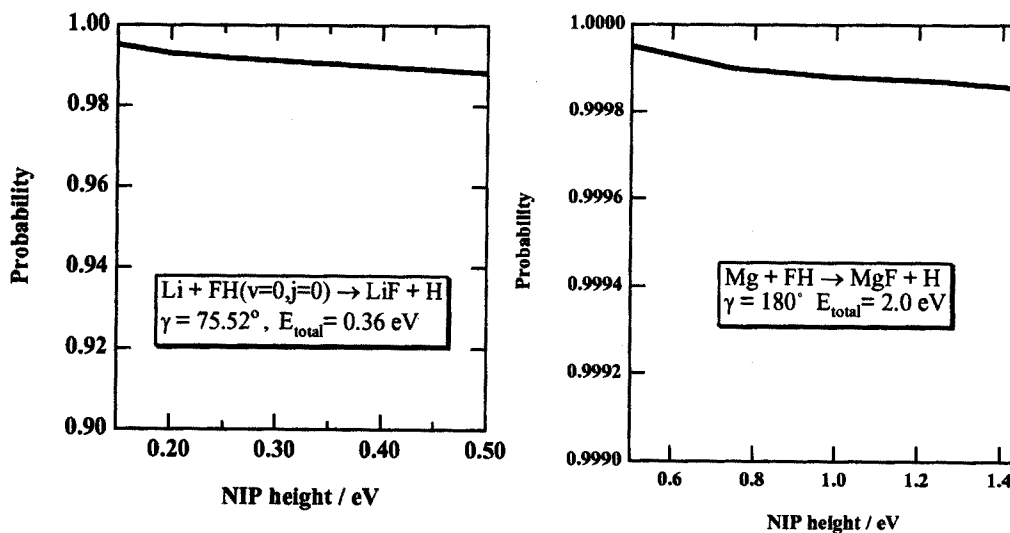
Figure 8.1: Dependence of the inelastic probabilities as a function of the NIP ramp height. (a) $Li + FH$ system. (b) $Mg + FH$ system.

System	D	W	A
$Li + FH$	2.5	0.2	1.0
$Mg + FH$	3.0	0.56	1.0
$H + F_2$	*	0.75	0.5

Table 8.1: Best NIP parameters for the $Li + FH$, $Mg + FH$ and $H + F_2$ systems. D: upper limit of the NIP along the vibrational coordinate r; W: height of the NIP linear ramp; A: width of the linear ramp along the vibrational coordinate. * See Table 8.2.

Orientation angle	D
180	1.8
170	1.8
160	1.8
150	1.8
140	1.8
130	1.8
120	2.1
110	2.1
100	2.1
90	2.1

Table 8.2: Upper limit along the vibrational coordinate r (D), as a function of the atom-diatom orientation angle, for the $H + F_2$ system.

III. Results for the $Li + FH$, $Mg + FH$, and $H + F_2$ systems and analysis

This section shows the results of the application of the NIP-IOS method to several triatomic systems. As introduced before, our aim has been to cover a sufficiently wide class of reactions so as to allow us to characterize the accuracy and applicability of the method. Results will be presented separately for each system, while the corresponding analysis will be performed afterwards in general terms. Only few specific details will be given about the general features of each reaction. The interested reader should consult the quoted references.

The $Li + FH$ system

As the starting point in the applications, the $Li + FH$ system has been chosen. This is a moderately endoergic (0.157 eV) system showing a weakly bound stable reactant complex (-0.302 eV) whose minimum energy path exhibits a barrier of 0.182 eV. Several theoretical calculations have been performed in the past on its reaction dynamics[27, 28, 34, 39, 40]. Among them, those obtained by means of a Reactive Infinite Order Sudden (R-IOS) technique[27, 28] on a Bond Order (BO) surface[34] will be explicitly used here for comparison purposes. For more details on the R-IOS calculations, see refs [27, 28] and [34]. Figure 8.2 shows 600 closely spaced energy points for the integral cross section, which were calculated with the proper NIP parameters given in table 8.1. An additional purpose of the fine energy scanning has been to resolve the structure previously anticipated in standard R-IOS cross section calculations41. Remarkably, the basis dimension could be reduced from 16 (R-IOS) to 10 (NIP-IOS), in spite of the fact that, in this case, the arrangement channel whose description is (almost) completely avoided (the products $LiF + H$) is the one lying higher in energy.

Figure 8.2 shows the integral cross section as a function of total energy, for both the NIP-IOS and the R-IOS techniques. Both methodologies lead to rather similar results, showing an initial decrease of the integral cross section, then reaching a minimum and finally leading to an uniform moderate increase. Differences are then more quantitative than qualitative, being larger at the transition region between the decreasing and the smooth increasing behaviours. The initial decrease is known[34, 39] to be a consequence of the zero point vibrational energy (ZPE), since, although the reaction is electronically endoergic, after consideration of both the reactant and product ZPE, the reaction becomes slightly exoergic. In addition, the reactant ZPE lies above the minimum energy path electronic barrier. The minimum occurrence and the subsequent increase in the integral cross section are interpreted as the result of the increasing contribution, to the integral cross section, of reaction events at angles away from the TS orientation angle at higher total energy.

The differences between both calculations can be attributed to the different PES probed by each techniques in the product arrangement region, as it will be discussed in more detail below. As total energy is increased, the diminishing influence of the PES on the dynamics makes both methods to approach one each other, as previously expected.
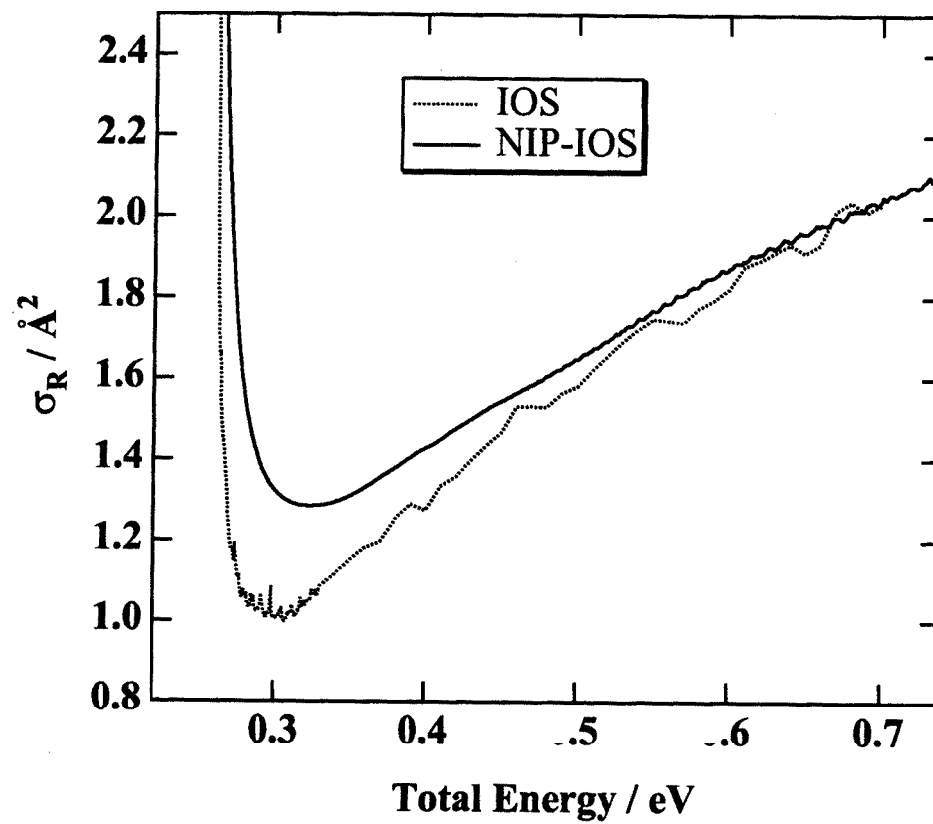
Figure 8.2: Integral cross section as a function of total energy, for the $Li + FH$ system. Continuous line: NIP-IOS results. Dotted line: R-IOS results.

The $Mg + FH$ system

The $Mg + FH \rightarrow MgF + H$ reaction is a strongly endoergic (1.33 eV) HHL reaction with a late barrier located well inside the product channel. This barrier is 1.826 eV higher than the reactants asymptote at a bent (72°) transition state geometry. The strong interaction region of the PES displays two minima: one, collinear (-0.34 eV), is located just before the reaction barrier, and the other (-1.30 eV), is located late in the products channel. The second minimum corresponds to a highly bent configuration, which is not probed in collisions approximately following the minimum energy path. Another important feature of the PES[42] is that the fixed angle barrier to reaction (that, as already noted, has a minimum at $\Theta = 72°$) rises sharply moving to smaller values of γ (more bent geometries) while it rises slightly (about 0.2 eV in the range $74° \leq \gamma \leq 115°$ and about zero from $\gamma = 115°$ to $\gamma = 180°$) moving to larger values of the collision angle.

This reaction has been recently studied by means of the standard R-IOS technique[36, 37] and, previously, by means of quasiclassical trajectory (QCT) calculations[42]. Integral cross sections are available for the ground and up to fifth excited reactants vibrational level. The peculiarities of the dynamics shown by this reaction makes this system a rather complete benchmark: reaction is enhanced by reactant vibrational energy, but its effectiveness clearly changes from open to closed orientation angles. Tunneling is rather important (although a fairly heavy atom is transferred) in establishing the position of the reactivity threshold along the energy scale. Excited reactant vibrational levels are readily available in a single calculation, which leads to relevant data on the influence of both vibrational and translational energy upon the reactivity.

Since the reaction is considerably endoergic, the discarded channel, as a consequence of including the NIP is, in principle, the less demanding. However, the closer vibrational spacing of the MgF molecule makes available, for a given total energy, more vibrational states than the reactant arrangement. For instance, at a total energy of 3.00 eV, 6 vibrational levels are open in the reactants side but these are 15 in the products side. For this reason, a reduction in the basis dimension from 35 to 25 has been possible, in addition to an approximate halving in the number of translational sectors.

Figure 8.3 shows the integral cross section, for the NIP-IOS, the R-IOS and the QCT techniques, for the $v = 2, 3, 4$ and 5 reactant vibrational levels. The semiquantitative agreement is seen to be remarkable and, most importantly, a unique set of NIP parameters sufficed to obtain correct integral cross sections for the whole set of initial vibrational levels. Given the particular features associated with the orientation angle for this reaction, and with the purpose of checking that the NIP-IOS - R-IOS coincidence is not attributable to error compensation between the different angles, Figure 8.4 (lower panel) and 8.4 (upper panel) show the corresponding fixed angle cross sections for $\gamma = 75°$ and $180°$. It can be easily seen that a rather satisfactory agreement is obtained as well. It should be noted that the two angles chosen are those most representative of the two kinds of energy effectiveness mechanisms, which are found to describe the overall reaction dynamics[36, 37].
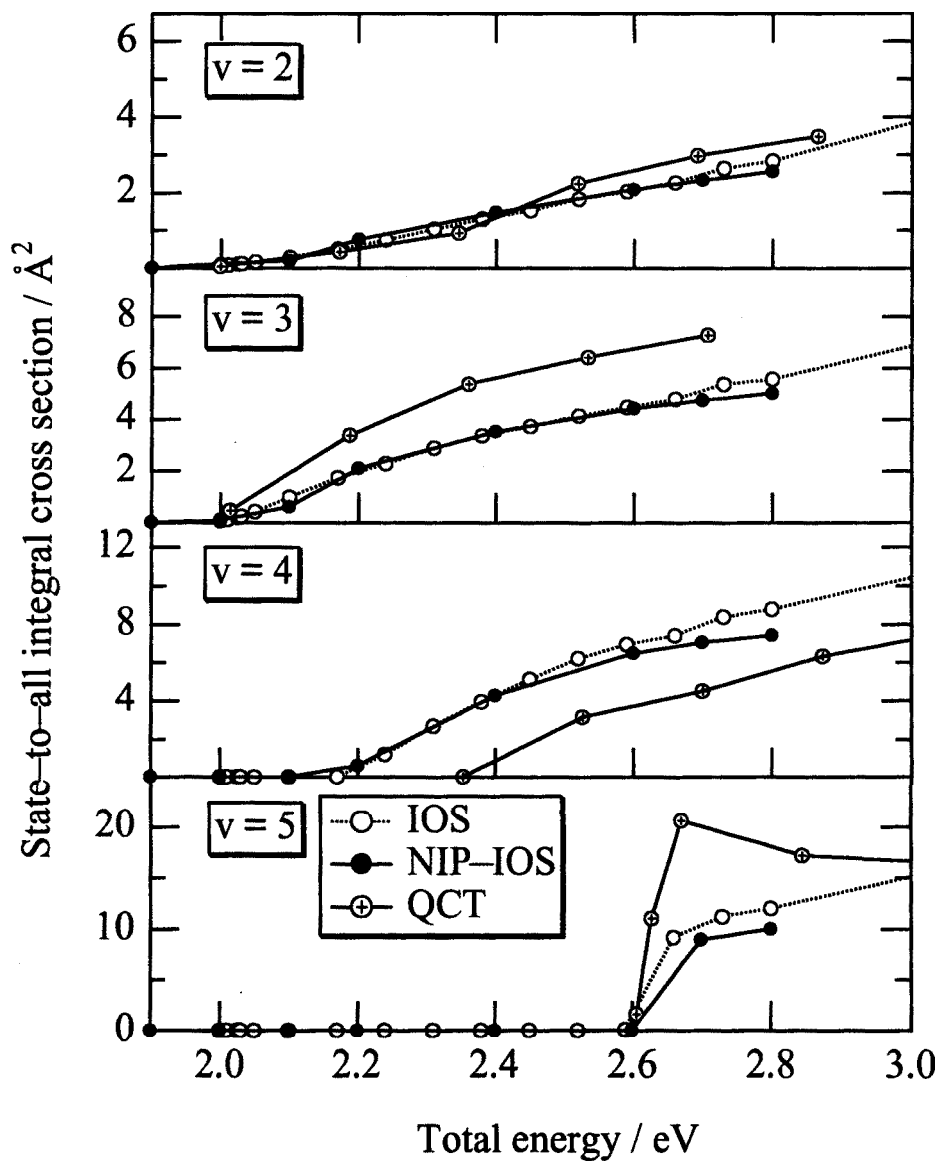
Figure 8.3: Integral cross section as a function of total energy, for the $Mg + FH$ system, for several values of the initial vibrational state. Continuous line and full circles: NIP-IOS results. Dotted line and open circles: R-IOS results. Continuous line and open circles filled with crosses: QCT results.
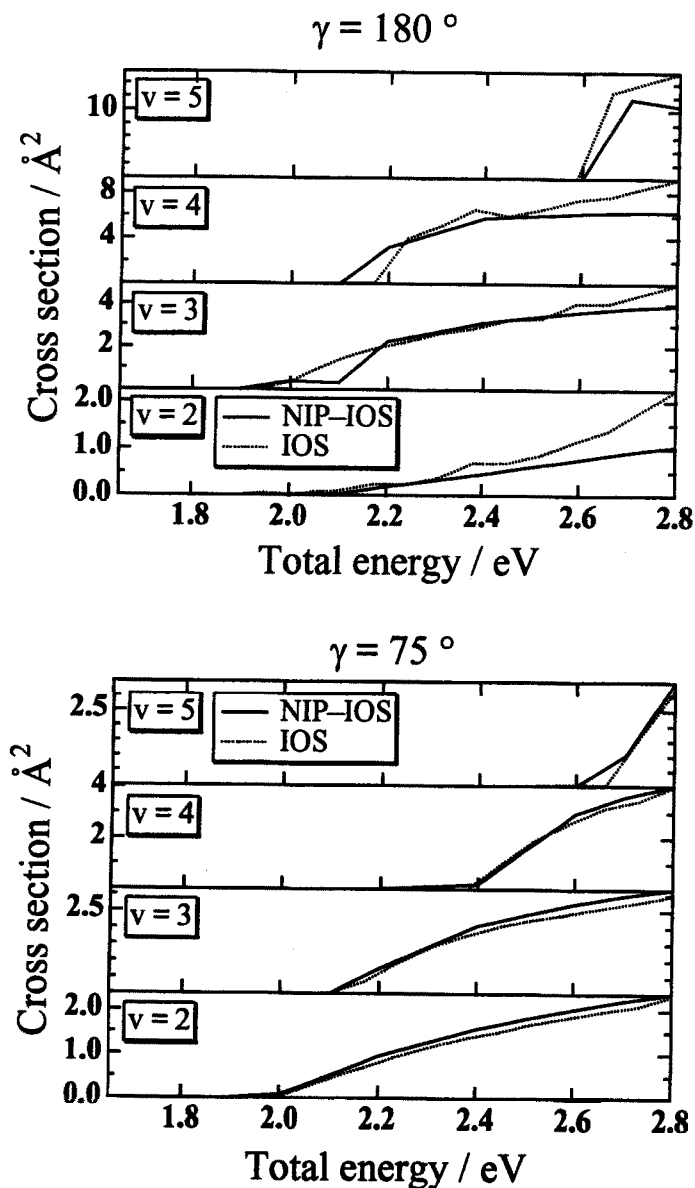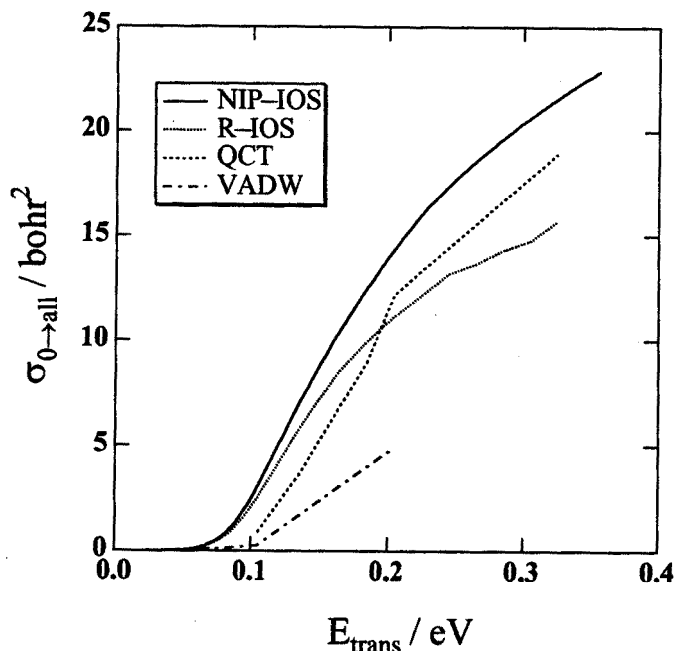
Figure 8.4: Fixed-angle cross section as a function of total energy, for the Mg + FH system, for several values of the initial vibrational state. Continuous line: NIP-IOS results. Dotted line: R-IOS results. (a) orientation angle $\gamma = 75°$ (b) $\gamma = 180°$.

Figure 8.5: Integral cross section as a function of total energy, for the H + F2 system. Continuous line: NIP-IOS results. Dotted line: R-IOS results. Dashed line: QCT results. Dashed-dotted line: VADW results.

The $H + F_2$ system

The $H + F_2$ has been long considered the prototype of a highly exothermic elementary reaction. In fact, the exothermicity is 4.5 eV, which causes a sudden change in the nature of the PES at the TS. R-IOS calculations have been performed[30] on a London-Eyring-Polanyi-Sato (LEPS) PES as developed by Jonathan et al.,[43] and so the same PES will be used here. A total of 200 energy points were calculated, within the scanned energy range, for the present work.

This system appears most suited to a treatment which avoids the description of the product arrangement, since it is the source of the main difficulties as the strong exother-micity may lead to the necessity of describing a highly excited vibrational dynamics. In this sense, a revealing fact is that the R-IOS study of ref. [30] required doubling the number of translational sectors for describing the product arrangement, as compared to the reactant arrangement (making a total of 300 sectors), while the vibrational basis set dimension had to be set at a value of 30 (although only 4 vibrational states are open, asymptotically, in the reactant arrangement at the highest energy considered). A major advantage of dealing with the reactant arrangement only is that the number of sectors could be fixed at a value only slightly higher than that used for the reactant arrangement in the R-IOS study (150 -NIP-IOS- in front of 100 -R-IOS-), while the vi-

brational basis could be reduced until 13 functions while keeping results well converged. Figure shows the integral cross section, which is not only compared with the R-IOS results but also with results of a quasiclassical trajectory (QCT) calculation[44] and, for comprehensive purposes, a vibrational-adiabatic distorted wave (VADW) approach[45]. Although some differences arise in the high-energy behaviour of the $v = 0$ case, one again observes a general good agreement between NIP-IOS and R-IOS, as well as with the QCT technique. This latter is expectable given the marked isotropy of the PES (weak reorientation) and the absence in it of particular features (no strong quantum effects and/or complex dynamics). Remarkably, the threshold behaviour is strongly coincident, in position and shape, between NIP-IOS and R-IOS, lying somewhat before the QCT threshold to reactivity. VADW results show its inherent limitations, especially at higher energies.

Analysis of the results

The comparison between the numerical scattering R-IOS and NIP-IOS parameters clearly evidences the smaller computational effort for the latter, which is due to the inclusion of the NIP just after the TS in the way, as the collision proceeds, to the product arrangement. In all cases, the number of translational sectors is roughly halved, and the number of vibrational functions may be also correspondingly decreased. The reduction in translational sectors contributes approximately linearly to the CPU time saving, but any reduction in basis dimension diminishes approximately as N^3 the CPU time (being N the number of basis functions reduced), since the most expensive part of the propagation time is spent in matrix inversion and a direct diagonalization routine has been used. This latter fact is a consequence, as previously shown[23], of the complex-valued nature of the interaction matrix due to the incorporation of the absorbing potential. Because of that, the most favourable cases correspond to exothermic reactions and, particularly, those forming a product molecule with a smaller vibrational spacing than the reactant one, as it is seen in the $H + F_2$ case. In such cases a gain in CPU time of about one order of magnitude is obtained (200 energy points for the integral cross section needed, for the $H + F_2$ system, 6 CPU hours on an IBM 3AT Work Station).

The practical implementation of the NIP-IOS method to several, sufficiently varied reactive systems demonstrates another important advantage: calculations are more straightforward than with the R-IOS technique, since the parameter optimization process, to allow for production runs, is much simpler. This is clearly a consequence of the fact that a simpler coordinate system can be used since the reactant to product transformation is avoided. One may argue that additional parameters are necessary to optimize the NIP. Notwithstanding, they have been determined with a minimum effort in all but one case and, most important, its determination is completely independent of the true reactive scattering numerical parameters optimization.

The present work shows that NIP-IOS results are found to be in general agreement with the previous R-IOS. However, one should not expect, in principle, an exact agreement since the above methods are not equivalent. NIP-IOS dynamics is based in constraining the motion to that governed by the reactants fixed-angle approxima-

tion. Since the reactive flux is absorbed just after the TS, no additional constraints are introduced concerning the product arrangement. Instead, the present R-IOS approach uses the B-matching rule[27] to relate one fixed-angle reactants arrangement with one fixed-angle products arrangement, with the constriction that the potential be continuous and that reactant to product transformation is performed along a line situated roughly around the TS (specifically, along the potential ridge). As a consequence, the reactants channel in both methods is the same but the products channel and part of the TS region may be substantially different. This difference is expected to lead to clearly different reaction probabilities in certain cases. The discrepancies between NIP-IOS and R-IOS found for the $Li + FH$ case are a clear illustration of the above statements. Figure 8.2 shows, for instance, that the structure surviving at the cross section level is entirely different, and even appears at low energies for the R-IOS case but at high energies for the NIP-IOS case. Another source of discrepancy may also arise in the fixed-angle cross section calculation, since the orbital angular momentum is included in a different manner. The NIP-IOS approach uses the same constant orbital angular momentum value through the entire propagation range, while the present implementation of the R-IOS method[46] changes the orbital angular momentum term, when performing the reactant to product transformation, according to two limiting behaviours. The orbital quantum number is kept (although the orbital angular momentum term changes as a consequence of the reactant to product coordinate transformation) for HLH mass- combination reactions, while it is exchanged with the rotational quantum number for HHL or LHL processes. According to the above discussion, we consider the NIP-IOS approach to be somewhat more general than the R-IOS, since less constraints are included into the theory.

A practical consequence of the present comparison is that a test on the limitations introduced by the B-matching rule can be performed. The general global agreement between NIP-IOS and R-IOS results indicates that using that version of the R-IOS method, to calculate state-to-all integral cross sections, does not introduce severe limitations to the reaction dynamics, when compared with the non-restricted fixed-angle dynamics built into the NIP-IOS method.

As for the general agreement between NIP-IOS calculations and less approximated or experimental results, the conclusions must be essentially the same than for the R-IOS, i.e. the technique works well for high energies, anisotropic potentials and HHL or LHL mass combinations, finding its utility in the previously termed involved reactive systems. It has the added advantage of a smaller demand on computational resources, and, as stated above, leads to a savings of up to an order of magnitude in CPU time for the most favourable case explored in the present work.

Some insights into the reaction dynamics of the Li + FH system

As pointed out above, the simplicity of the NIP-IOS method makes possible a more thorough study of the reaction dynamics of reactive systems, by more accurately exploring the range of initial conditions. Here we present some results of a detailed exploration of the energy dependence of the reactive cross section for the $Li + FH$ sys-

tem, with the aim of illustrating how new information arises when this kind of study becomes available. No attempt is made to fully explain the new results presented here, which we leave for future work.

Some structure is present in the cross section dependence versus energy, for the $Li + FH$ system, as it is shown in figure 8.2. This structure in the cross section is rather remarkable, since it may correspond to the fingerprint of reactive scattering resonances. The possibility of gaining additional knowledge on how it arises, led us to ask ourselves for a more detailed study. The resulting low cost of the NIP-IOS calculations then made possible the cheap calculation of a fine mesh of energy values. As stated before, the cross section was calculated for a total of 600 energy values.

A first analysis can be performed, thanks to the angular motion decoupling of the IOS approach, by plotting fixed-angle cross sections as a function of energy. They are shown in figures 8.6 and 8.7. Inspection of both figures clearly shows that the structure is found exclusively at orientation angles larger than the TS angle (75.52°). As a function of the orientation angle, two kinds of structures are distinguished: a) that found between 74 and 85° at high total energies, and b) that for angles larger than 85° for the whole scanned energy range. To investigate its origin, we show in figures 8.8 and 8.9. partial sums of the reaction probability, multiplied by the $(2\ell + 1)$ term, for the fixed angle cross section corresponding to 95°. These plots make explicit the way the structure appears and how it contributes to the orbital angular momentum summation. Plots of figures 8.6 and 8.7, for the 95° case, evidence a double-pattern structure. First, a long wavelength, smooth oscillation of about 0.05 eV is seen. Superimposed on it, at moderate to high energies, a short wavelength, spiked structure of about 0.006 eV is then identified. The partial sum plots reveal that the long oscillation arises from low to moderate values of the angular momentum, while the short oscillation emerges from the contribution of moderate to high values of the orbital angular momentum. Then, the structure in the 95° case originates from the whole angular momentum range, although each contribution manifests in different angular momentum regimes, so that its origin can be separately identified in the fixed-angle cross section.

Noteworthy as well is the dependence upon the orientation angle of the cross section dependence versus energy, since inspection of figures 8.6 and 8.7 evidences a dramatic qualitative change. In particular, a change in 15° is sufficient to evolve from a barrier-to-reaction to a barrierless behaviour (around 70°) and then back from barrierless to barrier-to-reaction (around 85°). This behaviour stresses the fact that, in general, the ability to perform lots of calculations at many energies opens up the possibility of investigating reaction dynamics in much greater detail than before. This is especially useful when a strongly structured energy dependence is to be singled out.

IV. Calculation of Cumulative Reaction Probabilities (CRP)

As introduced above, Seideman and Miller used a DVR and absorbing boundary conditions to efficiently calculate the outgoing wave Green's function. The DVR grid was defined using very few points around the transition state region, leading to stable
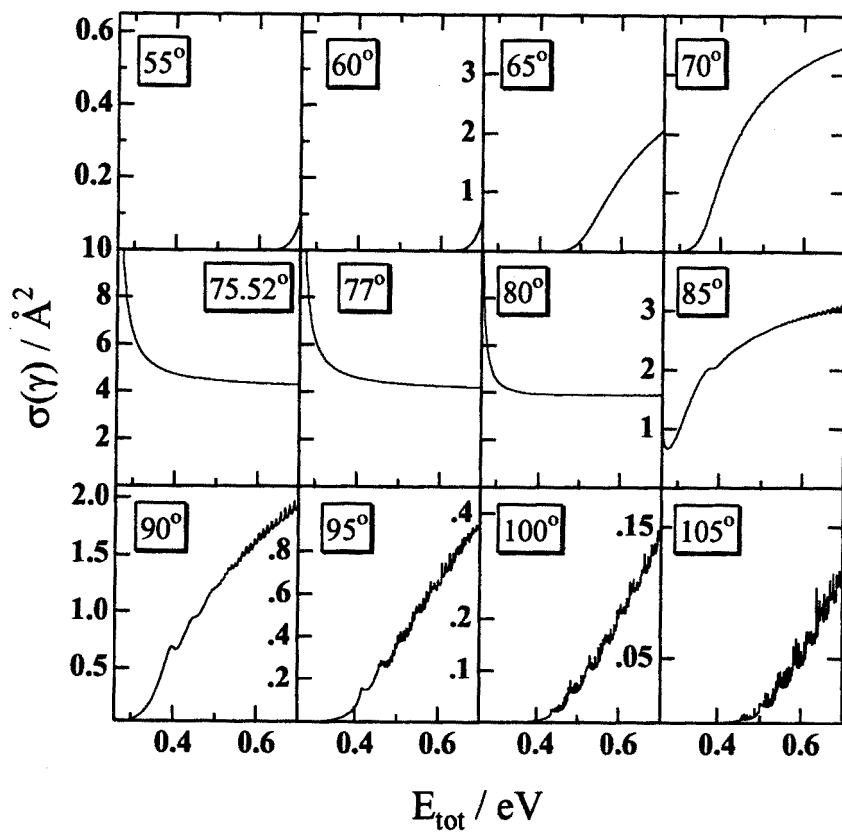
Figure 8.6: Fixed-angle cross sections as a function of total energy, for the $Li + FH$ system, at several values of the orientation angle γ. Range $55° - 105°$ in steps of 5.
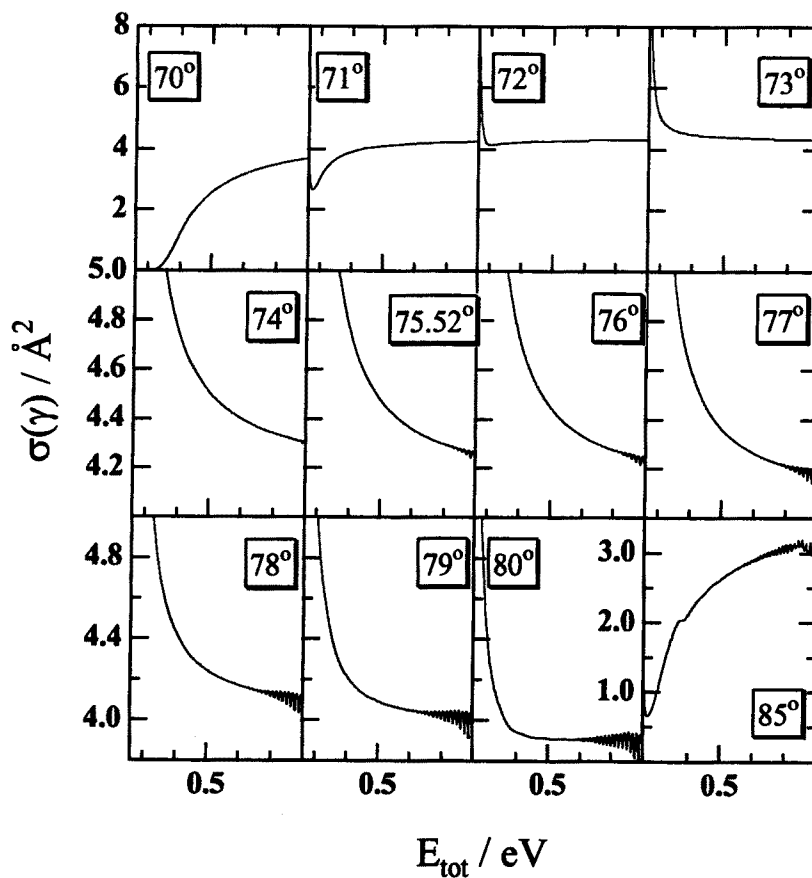
Figure 8.7: Fixed-angle cross sections as a function of total energy, for the $Li + FH$ system, at several values of the orientation angle γ. Zoom over the $70° - 85°$ range, in steps of $1°$ (except the $80° - 85°$ range, step of $5°$), which is included to emphasize the sudden change from barrierless to barrier-to-reaction and back to barrierless shape of the cross section dependence versus energy.
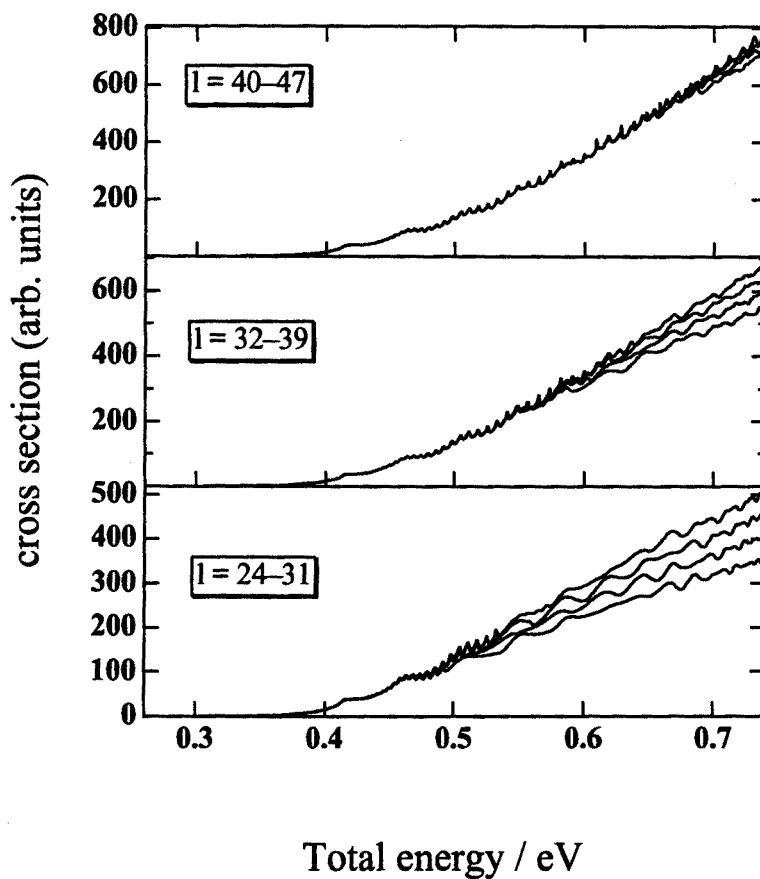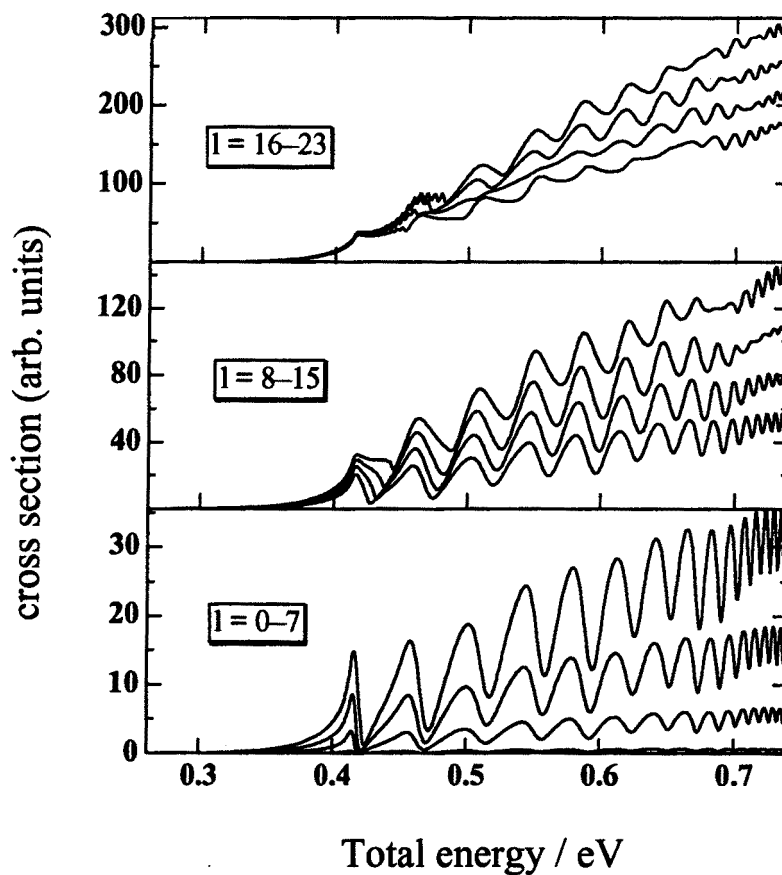
Figure 8.8: Partial cumulative sums of the probability term multiplied by $(2\ell + 1)$, as a function of total energy, for the $Li + FH$ system and $\gamma = 95°$. Each trace contains the sum up to the ℓth partial wave. Traces from $\ell = 0$ to $\ell = 23$. Only traces belonging to odd values of ℓ are shown for the sake of clarity.

Figure 8.9: Partial cumulative sums of the probability term multiplied by $(2\ell + 1)$, as a function of total energy, for the $Li + FH$ system and $\gamma = 95°$. Each trace contains the sum up to the ℓth partial wave. Traces from $\ell = 24$ to $\ell = 47$, which is the highest orbital angular momentum non-negligibly contributing to the cross section, within the scanned energy range. Only traces belonging to odd values of ℓ are shown here as well.

CRPs. This work showed explicitly that when no state-to-state information is necessary, the direct calculation of the rate constant (the global quantity) is possible and it is much cheaper than following the complete route, which starts from the state-to-state S-matrix and performs the sum over product and reactant states to get the rate constant. The same work provides also the closed expressions for both the CRP and the S-matrix in terms of the outgoing wave Green's operator, which are substantially different.

Here we intend to show, from the propagation-based perspective, the same fact, i.e. that CRPs can be efficiently calculated using a very short value of the asymptotic matching distance, at which standard boundary conditions are applied. This assumption obviously leads to incorrect state-to-state inelastic probabilities, but the reactive flux, which is captured by the NIP at the entrance of the products channel, is nevertheless correct. An advantage of this approach is that the savings introduced by this procedure are very easily accounted for, since the same expression for the CRP is used in both the long -standard- and short -only valid for CRP's- propagation cases.

Figures 8.10 show the variation of the state-to-state inelastic and cumulative reaction probabilities as a function of the final "asymptotic" matching distance, as calculated for the $H + F_2$ and $Ne + H_2^+$ systems (this latter system having been used as a preliminary test in ref. [3]). It is clearly evidenced that going from large to short scattering coordinate matching values causes the inelastic probabilities to appreciably change, while the CRP remains constant within the desired precision. Most remarkable are the results corresponding to the $H + F_2$ system, since an important variation in the inelastic probabilities is already observed at rather large values of the matching distance, without altering the CRP.

The above results (and those of ref. [9]) stress the role played by the potential ridge[47, 48, 49] in the very detailed reaction dynamics. The reduction in coordinate space sampling for the CRP calculation leads to the fact that only the region around the TS, and then around the potential ridge, is kept in the calculation. It is known that it is in this region where most of the non-adiabatic coupling between rovibrational states takes place and, in particular, those couplings affecting transitions between reactant and product states. In the present case, and mainly in the $H + F_2$ system, it is explicitly shown that important changes in the inelastic state-to-state probabilities are due to simple inelastic energy transfer processes (i.e. local to the reactant channel), since CRPs keep essentially constant until matching reaches the strong interaction region. This result clearly and remarkably indicates that it is only in the vicinity of the ridge region where non-adiabatic coupling take place between reactant and product states.

V.Summary and conclusions

In this work, an extensive application of a previously developed new method for doing reactive scattering calculations, based on assembling the use of NIPs with a generalization of the R-matrix propagation approach, has been performed. The $Li + FH$, $Mg + FH$, and $H + F_2$ systems have been studied, with the aim of testing the applicability of the method with reactions which display a rich variety of scattering dynamics.

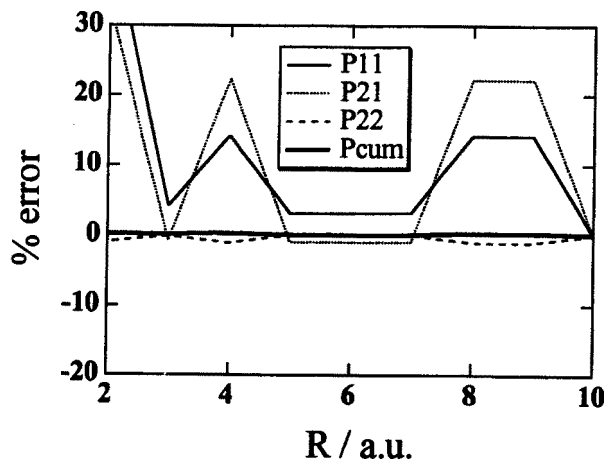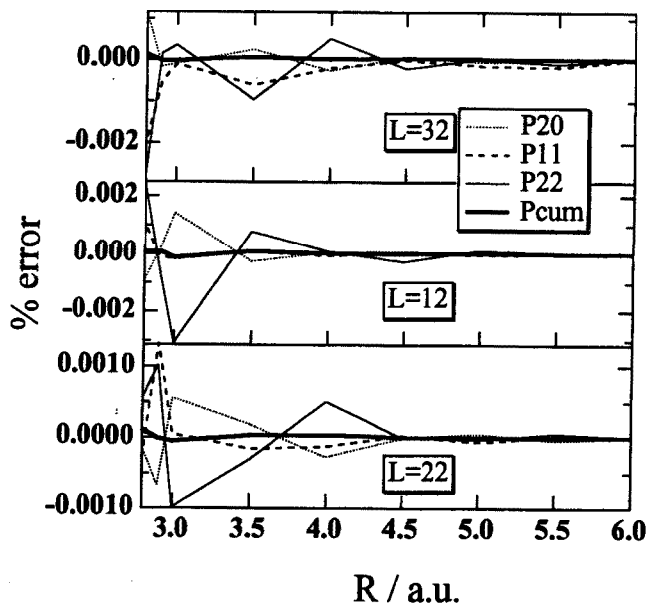It has been shown that correct results are easily obtained, and that it is possible to

Figure 8.10: Percent error of the inelastic (P_{ij}) and cumulative reaction (P_{cum}) probabilities, where i and j label initial and final vibrational quantum numbers , as a function of the asymptotic matching distance, where the standard boundary conditions are applied. (a) $H + F_2$ system, for the orbital angular momentum quantum number $L = 12$. (b) $Ne + H_2^+$ system, for $L = 22$ (bottom), $L = 12$ (middle) and $L = 32$ (top) panels, respectively.

determine the almost universal optimal numerical parameters, within a given system. CPU time consumption and RAM memory requirements are also moderately to drastically reduced, when compared to the requirements of the R-IOS technique. Special care in the NIP-IOS application must be taken for HLL systems and strongly non-collinear configurations, since distortion of the PES, when using reactant Jacobi coordinates, prevents a straightforward application of the method. Specifically, the reactant vibrational distance at which the NIP is placed requires a finer tuning, in the present case as a function of the orientation angle. Work is in progress towards considering better adapted coordinate systems (hyperspherical coordinates, etc...), so as to avoid the distortion problem while keeping into reasonable values the computational effort. The mutual agreement between NIP-IOS and R-IOS integral cross sections points towards a minor global relevance of the B-matching restriction in the R-IOS method.

The feasibility of reactive scattering calculations with the NIP-IOS method allows a more detailed investigation of the reaction dynamics of triatomic systems. As an example, we have calculated the integral cross section of the $Li + FH$ system at a very fine mesh of energy points (600 values between 0.26 and 0.8 eV) and have explored several fixed-angle collisions. This study allowed us to identify a remarkable structure present in the integral cross section, most probably revealing the survival of resonances at the cross section level. Looking for its origin, the fixed-angle orbital angular momentum partial sums of the cross section evidenced that: a) for angles smaller than 80°, only a high-energy structure is present which is attributable to oscillations in the reaction probability at very high values of the orbital angular momentum, and b) for angles higher than 80° a much richer structure is present in the whole energy range. It is formed by a double pattern, consisting of a smooth, long wavelength oscillation due to low angular momentum contributions and superposed on it, a spiked, short wavelength structure appearing at moderate to high values of the angular momentum. This high angular momentum behaviour is most remarkable, since it emphasizes the role of angular momentum in reactive collisions and makes explicit the importance of the $(2\ell + 1)$ degeneracy term.

As a final application, we have shown that the calculation of CRPs with a very short-ranged propagation, using standard boundary conditions, leads to the same values than the standard calculations. This offers an alternative way of showing the "hoped for" advantage of the direct rate constant calculation as pointed out by Seideman and Miller. In so doing, the role of the potential ridge in inducing reactant to product transitions has been also illustrated.

Acknowledgements

Bibliography

[1] F. Huarte-Larrañaga, X. Giménez, A. Aguilar and M. Baer, Chem. Phys. Lett. 291 (1998) 346.

[2] F. Huarte-Larrañaga, X. Giménez and A. Aguilar, J. Chem. Phys. 109 (1998) 5761.

[3] F. Huarte-Larrañaga, X. Giménez and A. Aguilar, Faraday Discuss. Chem. Soc. 110 (1998) 236-238.

[4] C. Leforestier and R.E. Wyatt, J. Chem. Phys. 78 (1983) 2334.

[5] R. Kosloff and D. Kosloff, J. Comput. Phys. 63 (1986) 363.

[6] D. Neuhauser and M. Baer, J. Chem. Phys. 90 (1989) 4351.

[7] D. Neuhauser and M. Baer, J. Chem. Phys. 92 (1990) 3419.

[8] M.S. Child, Mol. Phys. 72 (1991) 89.

[9] T. Seideman and W.H. Miller, J. Chem. Phys. 96 (1992) 4412.

[10] A. Vibok and G.G. Balint-Kurti, J. Chem. Phys. 96 (1992) 7615.

[11] A. Vibok and G.G. Balint-Kurti, J. Chem. Phys. 96 (1992) 8712.

[12] D. Brown and J.C. Light, J. Chem. Phys. 97 (1992) 5465.

[13] M. Monnerville, P. Halvick and J.C. Rayez, Chem. Phys. 159 (1992) 227.

[14] S. Brouard, D. Macas and J.G. Muga, J. Phys A 27 (1994) L439.

[15] D. Macías, S. Brouard and J.G. Muga, Chem. Phys. Lett. 228 (1994) 672.

[16] U. Peskin and W.H. Miller, J. Chem. Phys. 102 (1995) 4084.

[17] D. Neuhauser, J. Chem. Phys. 103 (1995) 8513.

[18] U.V. Riss and H.D. Meyer, J. Phys. B 28 (1995) 1475.

[19] U.V. Riss and H.D. Meyer, J. Chem. Phys. 105 (1996) 1409.

[20] T. Peng and J.Z.H. Zhang, J. Chem. Phys. 105 (1996) 6072.

[21] W. Zhu, T. Peng and J.Z.H. Zhang, J. Chem. Phys. 106 (1997) 1742.

[22] N. Balakrishnan, C. Kalyanaraman and N. Sathyamurthy, Phys. Rep. 280 (1997) 79.

[23] J.Y. Ge and J.Z.H. Zhang, J. Chem. Phys. 108 (1998) 1429; J.Y. Ge and J.Z.H. Zhang, Chem. Phys. Lett. 292 (1998) 51.

[24] J.P Palao and J.G. Muga, Chem. Phys. Lett. 292 (1998) 1.

[25] Although the use of CAPs do really represent a step further in the absorbing potentials application, we still here use the simpler form, the NIPs, in order to keep the simplicity of the original formulation.

[26] V. Khare, D.J. Kouri and M. Baer, J. Chem. Phys., 1979, 71, 1188. J.M. Bowman and K.T. Lee, J. Chem. Phys., 1980, 72, 5071.

[27] H. Nakamura, A. Ohsaki and M. Baer, J. Phys. Chem. 90 (1986) 6176: A. Laganà, X. Giménez, E. García and O. Gervasi, Chem. Phys. Lett. 176 (1991) 280.

[28] A. Laganà, A. Aguilar, X. Giménez and J.M. Lucas, Chem. Phys. Lett. 189 (1992) 138; A. Aguilar, X. Gimnez, J.M. Lucas, O. Gervasi and A. Laganà, Theor. Chim. Acta 79 (1991) 191.

[29] A. Laganà, A. Aguilar, X. Giménez and J.M. Lucas, J. Chem. Phys. 95 (1991) 2218; A. Laganà, A. Aguilar, X. Giménez and J.M. Lucas, Faraday Discuss. Chem. Soc. 91 (1991) 121; A. Laganà, A. Aguilar, X. Giménez and J.M. Lucas, in: "Advances in Mol. Vibrations and Collision Dynamics: Quantum Reactive Scattering". Vol. IIA. J.M. Bowman (Ed.). JAI Press, Greenwich, 1994.

[30] X. Giménez, J.M. Lucas, A. Aguilar and A. Laganà, J. Phys. Chem. 97 (1993) 8578.

[31] M. Gilibert, X. Giménez, M. González, R. Sayós and A. Aguilar, Chem. Phys. 191 (1995) 1.

[32] A. Aguilar, M. Albertí, X. Giménez, X. Grande and A. Laganà, Chem. Phys. Lett. 233 (1995) 201.

[33] A. Aguilar, M. Gilibert, X. Giménez, M. González and R. Sayós, J. Chem. Phys. 103 (1995) 4496.

[34] A. Laganà, G. Ochoa de Aspuru, A. Aguilar, X. Giménez and J.M. Lucas, J. Phys. Chem. 99 (1995) 11696.

[35] M. González, R.M. Blasco, X. Giménez and A. Aguilar. Chem. Phys. 209 (1996) 355.

[36] F. Huarte-Larrañaga, X. Giménez, M. Albertí , A. Aguilar, A. Laganà and J.M. Alvariño, Chem. Phys. Lett. 282 (1998) 91.

[37] F. Huarte-Larrañaga, X. Giménez, M. Albertí, A. Aguilar, A. Laganà and J.M. Alvariño, Phys. Chem. Chem. Phys. 1 (1999) 1133.

[38] D.T. Colbert and W.H. Miller, J. Chem. Phys. 96 (1992) 1982.

[39] G.A. Parker, R.T. Pack and A. Lagan, Chem. Phys. Lett. 202 (1993) 75, and references therein.

[40] C.Y. Yang, S.J. Klippenstein, J.D. Kress, R.T. Pack, G.A. Parker and A. Laganà, J. Chem. Phys. 100 (1994) 4917.

[41] X. Giménez. Unpublished work.

[42] A. Laganà, M. Dini, E. García, J.M. Alvariño and M. Paniagua, J. Phys. Chem. 95 (1991) 8379.

[43] N. Jonathan, S. Okuda and D. Timlin, Mol. Phys. 24 (1972) 1143.

[44] J.N.L. Connor, A. Lagan, A.F. Turfa and J.C. Whitehead, J. Chem. Phys. 75 (1981) 3301.

[45] D.C. Clary and J.N.L. Connor, J. Chem. Phys. 75 (1981) 3329.

[46] X. Giménez, Ph.D. Thesis, Universitat de Barcelona, 1991.

[47] U. Fano, Phys. Rev. A 24 (1981) 2402.

[48] A. Ohsaki and H. Nakamura, Phys. Rep. 187 (1990) 1.

[49] V. Aquilanti, S. Cavalli and G. Grossi, Chem. Phys. Lett. 110 (1984) 43; V. Aquilanti and S. Cavalli, Chem. Phys. Lett. 141 (1987) 309; V. Aquilanti, S. Cavalli, G. Grossi, V. Pellizzari, M. Rossi, A. Sgamellotti and F. Tarantelli, Chem. Phys. Lett. 162 (1989) 179.